Methodologies for measuring the degree of reaction in Portland cement blends with supplementary cementitious materials by ^{29}Si and ^{27}Al MAS NMR spectroscopy

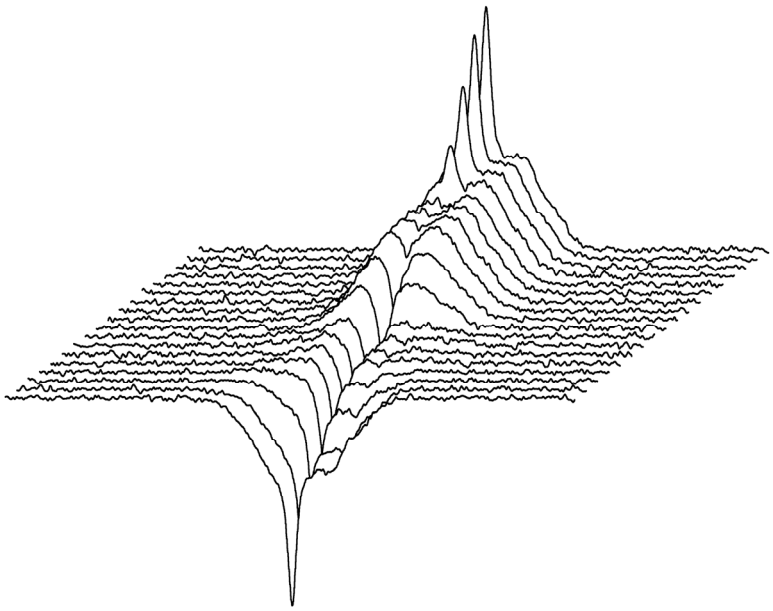

PhD Thesis

by

Søren Lundsted Poulsen

October 2009

Instrument Centre for Solid-State NMR Spectroscopy

Department of Chemistry and Interdisciplinary Nanoscience Center

Aarhus University, Denmark

nanocem

iNANO

AARHUS UNIVERSITET

Preface

This PhD thesis presents the results obtained during the time span of my three year PhD programme affiliated with the interdisciplinary Nanoscience Center (iNANO), Aarhus University. The work has been carried out in the period from October 2006 to September 2009 at the Instrument Centre for Solid-State NMR Spectroscopy, Department of Chemistry, Aarhus University, and the project was financed by Nanocem, a European consortium of industrial and academic partners concerned with fundamental cement and concrete research.

Acknowledgements

I would like to acknowledge a few people without whom the present work could not have been carried out. First and foremost, I wish to thank my supervisor Assoc. Prof. Jørgen Skibsted for his encouragement, support and excellent guidance during the past three years. He always took the time to answer the questions, trivial or complicated, I had to ask him. Furthermore, his enthusiasm for the project has been truly inspiring.

I would also like to express my gratitude to PhD Vanessa Kocaba for her willing collaboration on the project throughout the three years. The help and input from PhD Gween Le Saout, Prof. Karen Scrivener and chief scientist Duncan Herfort is also much appreciated. Prof. Hans J. Jakobsen is acknowledged for various discussions and the technicians Rigmor Johansen and Anne Birgitte Johansen for technical assistance with the acquisition of the experimental spectra. Assoc. Prof. Henrik Bildsøe is thanked for lending his assistance in sorting out several computer related problems.

MSc Thuan Thai Tran is thanked for numerous discussions on the subject “cement” and for helping me out when different software problems cropped up. MSc Tine Fly Sevelsted, MSc Maiken Rabøl Jørgensen, MSc Søren Sørensen and PhD Bavornpon Jansang are thanked as well for various inputs and for creating a nice working atmosphere at the Instrument Centre for Solid-State NMR Spectroscopy. Finally, NANOCEM is thanked for the financial support.

Table of contents

Preface i

Introduction 1

Chapter 1: Introduction to Portland cement 3
1.1 Definitions and historical aspects 3
1.2 Manufacture of Portland cement 5
1.2.1 Quarrying of raw materials 5
1.2.2 Preparation of raw materials 5
1.2.3 Clinkering 6
1.2.4 Cement milling 7
1.3 Main constituents of Portland cement 7
1.3.1 Alite 7
1.3.2 Belite 10
1.3.3 Tricalcium aluminate 12
1.3.4 Calcium alumino-ferrite 13

Chapter 2: Supplementary cementitious materials and types of cement 15
2.1 Introduction 15
2.2 Supplementary cementitious materials (SCMs) 17
2.2.1 Blastfurnace slag 18
2.2.2 Pulverised fly ash 19
2.2.3 Microsilica (silica fume) 20
2.2.4 Natural pozzolans 21
2.2.5 Other SCMs and mineral additions 22
2.3 Types of cement 23
2.3.1 Standardized common cements 23
2.3.2 Sulphate-resistant cement 25
2.3.3 Low alkali-cement 25
2.3.4 Calcium aluminate cement 26

Chapter 3: Hydration of plain and blended Portland cements 27
3.1 Introduction 27
3.2 Portland cement hydration 27
3.3 Hydration products 29
3.3.1 Calcium silicate hydrate (C-S-H) 29
3.3.2 Portlandite 30
3.3.3 AFm phases 30
3.3.4 AFt phases 31
3.3.5 Hydrogarnet 31
3.3.6 Brucite 31
3.3.7 Hydrotalcite and related phases 31
3.4 Microstructural development in Portland cement paste 32
3.4.1 Early period of hydration (0 – 3 h) 32
3.4.2 Middle period of hydration (3 – 24 h) 32

3.4.3. Late period of hydration (> 24 h) ... 33
3.5 Hydration of blended cements ... 33
3.5.1 Portland cement – slag blends ... 33
3.5.2 Portland cement – fly ash blends ... 34
3.5.3 Portland cement – natural pozzolan blends ... 34
3.5.4 Portland cement – microsilica blends ... 34

Chapter 4: Analytical techniques commonly used in cement research ... 35
4.1 Introduction ... 35
4.2 X-ray diffraction analysis ... 35
4.2.1 XRD with Rietveld analysis ... 37
4.3 Light microscopy ... 39
4.4 Scanning electron microscopy ... 39
4.5 Transmission electron microscopy ... 41
4.6 Isothermal calorimetry and thermal analysis (DTA/TGA) ... 41
4.7 Bogue calculations ... 43
4.8 Selective dissolution methods ... 44
4.9 Chemical shrinkage ... 45

Chapter 5: Introduction to solid-state NMR and its application in cement research ... 47
5.1 Introduction ... 47
5.2 Solid-state NMR ... 47
5.2.1 Spin interactions and magic angle spinning (MAS) ... 47
5.2.2 Chemical shielding anisotropy (CSA) ... 48
5.2.3 Cross-Polarization ... 49
5.2.4 ^{29}Si MAS NMR ... 50
5.2.5 ^{27}Al MAS NMR ... 52
5.2.6 Multiple-quantum MAS ... 53
5.3 Application of solid-state NMR in the study of cementitious materials ... 54
5.3.1 ^{29}Si MAS NMR applied to cementitious materials ... 55
5.3.2 ^{27}Al MAS NMR applied to cementitious materials ... 58
5.3.3 Other NMR active nuclei applied to cementitious materials ... 59

Chapter 6: Characterization of anhydrous materials ... 61
6.1 Introduction ... 61
6.2 Preliminary investigations of anhydrous materials ... 61
6.2.1 XRF analysis ... 62
6.2.2 Laser granulometry ... 62
6.2.3 XRD with Rietveld analysis ... 65
6.2.4 Backscattered electron images from SEM ... 67
6.2.5 Characteristics of selected materials ... 67
6.3 Characterization of anhydrous materials by solid-state NMR ... 68
6.3.1 ^{29}Si MAS NMR of anhydrous cements ... 68
6.3.2 Quantification of alite and belite from ^{29}Si MAS NMR ... 70
6.3.3 ^{27}Al MAS NMR of anhydrous cements ... 72
6.3.4 ^{29}Si MAS NMR of SCMs ... 74
6.3.5 ^{27}Al MAS NMR of SCMs ... 77

Chapter 7: ^{29}Si inversion-recovery and other MAS NMR experiments applied to anhydrous materials 79
7.1 Introduction 79
7.2 ^{29}Si inversion-recovery MAS NMR of anhydrous cements 79
7.3 NMR investigation of synthetic $Si_5O(PO_4)_6$ 83
7.4 Employment of very short relaxation delays for the acquisition of ^{29}Si MAS NMR spectra of anhydrous Portland cement 89

Chapter 8: Reactivity of SCMs in Portland cement blends investigated by ^{29}Si and ^{27}Al MAS NMR 93
8.1 Introduction 93
8.2 Studied cement systems 93
8.3 Hydration of pure cements 94
8.4 Hydration of cement – microsilica blends 101
8.5 Hydration of cement – fly ash blends 105
8.6 Hydration of cement – natural pozzolan blends 108
8.7 Comparison of data obtained from ^{29}Si MAS NMR 110
8.8 Hydration of cement – slag blends 116
8.8.1 ^{29}Si MAS NMR 116
8.8.2 ^{27}Al MAS NMR 118

Conclusions 127

Appendix I: Exp. conditions for acquisition of solid-state MAS NMR spectra 149

Appendix II: Procedures for paste mixing and hydrationstop 151

Paper I: *Improved quantification of alite and belite in anhydrous Portland cements by ^{29}Si MAS NMR: Effects of paramagnetic ions* 153

Paper II: *Incorporation of Phosphorus Guest Ions in the Calcium Silicate Phases of Portland Cement from ^{31}P MAS NMR Spectroscopy* 167

Paper III: *Methodologies for measuring the degree of reaction in Portland cement blends with supplementary cementitious materials by ^{27}Al and ^{29}Si MAS NMR spectroscopy* 197

Introduction

Portland cement is probably the most important construction material in todays society with an annual world-wide production of more that 2.5 billion tons. Despite the wide-spread use of this material, the fundamental micro- and nanoscale mechanisms, which determine the macroscopic performance of cementitious materials, are poorly understood. Traditionally, progress has been based largely on empirical knowledge and has a tendency to be incremental in nature. Since no company or academic institution alone can devote the resources needed to change this situation, NANOCEM – a European industrial/academic partnership for fundamental research on cementitious materials – was established in 2004. Currently, NANOCEM comprises 23 academic and 14 industrial partners.

The traditional use of Portland cement as the binder in concrete constructions is being increasingly replaced by blended cements, where part of the cement is substituted by supplementary cementitious materials (SCMs) such as blastfurnace slag, microsilica ("SiO_2"), natural pozzolans or fly ash from coal-fired power stations. This replacement is very important for increasing the sustainability of the cement production by reducing the consumption of raw materials, the energy demands, and the CO_2 emission. However, the level of substitution is limited by the ability to predict the physical and chemical performance of these blends, in particular when the reactivity of the SCM has not been characterized in detail.

The present PhD project is funded by NANOCEM and focuses on methodologies to follow the reaction of Portland cements blended with SCMs. Generally, the complexity of theses materials requires the use of complementary techniques such as powder X-ray diffraction (XRD), solid-state NMR spectroscopy, electron microscopy and thermal analysis. This PhD project is mainly focused on solid-state NMR studies, whereas investigations by powder XRD, electron microscopy and thermal analysis of the same materials has been conducted by another PhD student also funded by NANOCEM. The studied materials include 12 Portland cements, 9 blastfurnace slags, 3 fly ashes, 1 microsilica and 1 natural pozzolan ("volcanic rock"). The anhydrous Portland cements have been studied in detail with the aim of obtaining an improved ^{29}Si MAS NMR method for quantification of the alite and belite phases in Portland cements. This method has subsequently been employed in the studies of hydrated cement blends. The primary goal of

the project has been the development ^{29}Si and ^{27}Al MAS NMR methods for measuring the degree of reaction for the different phases in cement blends including the SCMs.

The main part of the thesis is divided into eight chapters with Chapter 1 giving a general introduction to Portland cement and its four main constituents, alite, belite, tricalcium aluminate, and ferrite. The most commonly used types of SCMs are presented in Chapter 2 and the motivational background for partially replacing Portland cement by SCMs in construction materials is treated here as well. In Chapter 3 the hydration of Portland cements, with and without SCMs, is introduced along with a description of the main hydration products and the development of microstructure in a hydrating cement paste. A range of the most commonly applied analytical tools in cement research is described in Chapter 4 with an emphasis on techniques that have been employed in connection with this project. The first part of Chapter 5 gives a brief introduction to solid-state NMR with particular focus on ^{29}Si and ^{27}Al MAS NMR, while the second part deals with the application of ^{29}Si and ^{27}Al MAS NMR in cement science. Chapter 6 introduces the selection of materials that has been studied in the project by presentation of results from XRD investigations with Rietveld analysis, solid-state NMR spectroscopy, and other analytical techniques. Results from ^{29}Si inversion-recovery MAS NMR studies of anhydrous materials are the main focus of Chapter 7, while the last chapter describes the use of ^{29}Si and ^{27}Al MAS NMR for measuring the degree of reaction in hydrated cement – SCMs blends.

Chapter 1

Introduction to Portland cement

1.1 Definitions and historical aspects

Portland cement is a fine-grained material with hydraulic properties, *i.e.*, it sets and hardens when mixed with water. It is produced by heating limestone, clay or other similar materials with the same reactivity to partial fusion, resulting in the formation of roughly spherical clinker nodules with a composition of approximately 67% CaO, 22% SiO_2, 5.5% Al_2O_3, 3% Fe_2O_3 and 3% of other components [1]. The nodules are principally composed of four major phases: alite, belite, aluminate and ferrite. A small amount of gypsum (typically 2 – 5 wt%) is interground with the clinker as the final step of the cement manufacture. The gypsum acts as a controlling agent on the rate of setting.

The literature provides several shorthand definitions of Portland cement (and clinker). For example, the renowned book *Lea's Chemistry of Cement and Concrete* [2] gives the following definition:

> *"Portland cement is a synthetic mixture of calcium silicates formed in a molten matrix from a suitably proportioned and homogenously prepared mixture of calcareous and argillaceous components".*

The Prestandard ENV 197-1 [3], a standard for common cements collectively developed by a large group of European countries, offers another definition of Portland cement clinker:

> *"[…] a hydraulic material which shall consist of at least two-thirds by mass of calcium silicates ($(CaO)_3 \cdot SiO_2$ and $(CaO)_2 \cdot SiO_2$), the reminder containing aluminium oxide (Al_2O_3), iron oxide (Fe_2O_3) and other oxides. The ratio by mass (CaO/SiO_2) shall be no less than 2.0. The content of magnesium oxide (MgO) shall not exceed 5.0 per cent by mass."*

The evolutionary road leading to our modern day Portland cement is long and may be traced back to the early civilizations of the Assyrians and Babylonians who used clay to

cement together building materials such as burnt bricks or slabs of alabaster [4]. The Egyptians developed lime and gypsum mortars which were employed as binding agents in the construction of such structures as the Pyramids. Further improvements were made by the Greeks and later the Romans who mixed slaked lime with volcanic ash, thus producing a type of cement capable of hardening under water.

John Smeaton [5] made an important contribution to the development of cement when he was commissioned to erect a new lighthouse on the Eddystone Rock, Falkland Islands in 1756. From his search for the optimum material to use for the construction work, he concluded that mortars made from slaked limestone containing a considerable amount of clay resulted in the strongest material. This was the first systematic investigation concerning the influence of clay content on the "hydraulicity" of the lime. In 1811 Edgar Dobbs [6] patented a type of cement prepared by calcining an intimate mixture of limestone (chalk) and clay which was ground together in a wet mill. This was a precursor of the method employed nowadays to manufacture Portland cement.

Joseph Aspdin coined the name 'Portland cement' in his 1824 patent [7] on a certain type of hydraulic cement. He attributed the name to the material's resemblance to a limestone from Dorset in Southern England called 'Portland'. However, the cement was very unlike the Portland cement we know today, primarily due to a much lower burning temperature which resulted in a completely different mineralogy. In the mid-1840s Joseph's son, William Aspdin, made the crucial discovery that clinkered ("overburnt") raw materials substantially increased the strength of his cement. He had accidentally synthesized the calcium silicates alite and belite [8].

An important technical breakthrough in the manufacture of Portland cement was the introduction of the rotary kiln at the beginning of the twentieth century [4]. Up to that time static dome-like kilns had been used which only facilitated a batch production process. The rotary kiln, on the other hand, allowed a cement production carried out in continuous mode.

In 1887 Le Chatelier [9] published his theories on setting and hardening of Portland cement which represent a major advance in the study of Portland cement from a scientific point of view. He also used optical microscopy to conclude that the essential component of Portland cement was Ca_3SiO_5 as one of four kinds of crystals [10]. A few years later Törnebohm [11] also identified four types of crystals which he named alite, belite, celite,

and felite. In 1915 Rankin and Wright [12] published the results of their pioneering research on the ternary system CaO-Al_2O_3-SiO_2 which formed the basis for numerous later studies on clinker formation.

1.2 Manufacture of Portland cement

Portland cement is basically manufactured in a four step process: (1) quarrying of raw materials, (2) preparation of raw materials, (3) clinkering, (4) cement milling [1,13,14]. The individual steps are outlined in detail below.

1.2.1 Quarrying of raw materials

In order to produce Portland cement two kinds of raw materials are required: a calcareous material (*e.g.*, limestone, chalk, or another type of $CaCO_3$-rich rock) making up roughly 80% of the raw materials and a lesser amount of an argillaceous material such as clay, sand or shale. The argillaceous matter acts as the source of SiO_2, Al_2O_3 and Fe_2O_3. Cement plants are usually located in close proximity to natural occurrences of these raw materials, thus minimizing the transport distance from the site of quarrying to the factory. One of the main reasons for the widespread use of Portland cement as a construction material is the plentiful abundance in Earth's continental crust of the main metal oxides constituting Portland cement [15] (Fig. 1.1).

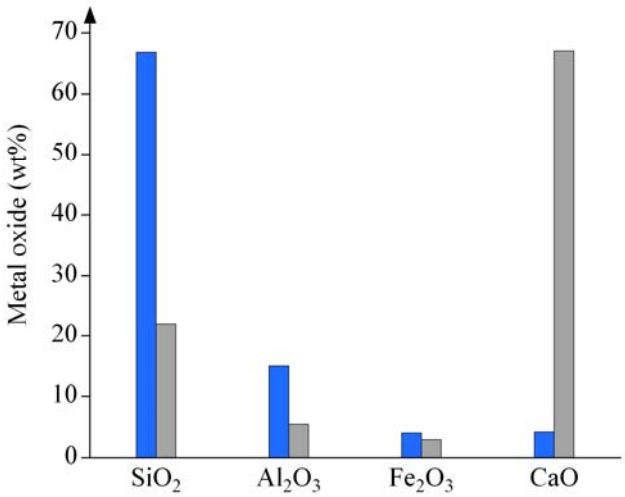

Fig. 1.1 Distribution of SiO_2, Al_2O_3, Fe_2O_3 and CaO in Earth's upper continental crust (blue bars) [15] and in normal Portland cement (grey bars) [1].

1.2.2 Preparation of raw materials

Once the raw materials have been quarried and transported to the cement production plant, further preparation is necessary before the actual formation of the cement clinker can take

place. The following steps depend on whether the wet or dry process is chosen. In the wet process the clay is mixed with water in a washmill resulting in a paste. Crushed limestone is subsequently added and the whole mixture is ground until a fine-grained slurry (the so-called raw meal) has been obtained. Initially the dry process involves separate crushing of the quarried limestone and clay in a dry state until nothing larger than a tennis ball remains. The limestone and clay is then fed together into a mill where the material is ground until more than 85% of the particles are < 90 μm in diameter. The resulting material is called the raw meal.

1.2.3 Clinkering

During this production step the raw meal is basically dried, heated (to partial fusion) and finally cooled down again. If the raw meal has been prepared using the dry process the fine-grained powder does not contain much moisture. This enables the use of a preheater tower. As the raw meal falls through the tower it is heated to approx. 800 °C which causes evaporation of the moisture. In addition, 90% of the limestone decarbonation (loss of CO_2) occurs in the preheater tower by reaction (1.1).

$$CaCO_3(s) \rightarrow CaO(s) + CO_2(g) \qquad (1.1)$$

The slurry resulting from the wet process contains too much moisture to be successfully dried in a preheater tower. Instead the raw meal is fed directly into the kiln which essentially is a long steel tube with an inside lining consisting of heat-resistant bricks. The kiln is inclined a few degrees to ensure the downward movement of the raw meal. The slurry is transformed into dry balls by the heat and rotation of the kiln and the wet process kilns are normally longer than the ones employed for dry process raw meals.

The kiln is usually heated by injecting pulverised coal dust into the discharge end where it ignites spontaneously due to the very high temperature. A number of reactions occur as the raw meal is gradually heated during the passage through the kiln. In the temperature range from 800 – 1000 °C the most important reactions are the decarbonation of limestone (1.1) and the formation of tricalcium aluminate ($Ca_3Al_2O_6$). As the temperature rises to 1100 – 1300 °C belite (Ca_2SiO_4) begins to form by the reaction of silica (SiO_2) with lime (CaO) (1.2):

$$2\ CaO(s) + SiO_2(s) \rightarrow Ca_2SiO_4(s) \quad (1.2)$$

Partial fusion (sintering) occurs as the temperature increases above 1300 °C which ultimately results in the formation of alite (Ca_3SiO_5) and ferrite ($Ca_4Al_2Fe_2O_{10}$) by reaction Eq. (1.3) and Eq. (1.4). Usually, the highest temperature reached in the kiln is approximately 1450 °C.

$$Ca_2SiO_4(s) + CaO(s) \rightarrow Ca_3SiO_5(s) \quad (1.3)$$

$$Ca_3Al_2O_6\ (s) + CaO\ (s) + Fe_2O_3\ (s) \rightarrow Ca_4Al_2Fe_2O_{10}\ (s) \quad (1.4)$$

The material leaving the kiln consists of roughly spherical nodules (typically 1 – 3 cm in diameter) which are referred to as clinkers. A cooling system follows directly after the kiln where the clinker is cooled by the means of air or, more rarely, by water.

1.2.4 Cement milling

To complete the manufacture of Portland cement the clinker nodules are ground in large tube mills with steel balls as grinding agents. During this production step a small amount of gypsum ($CaSO_4 \cdot 2H_2O$) is interground with the cement clinker. The gypsum acts as a set retarder when the Portland cement is mixed with water, thus preventing an undesired phenomenon known as 'flash setting'.

1.3 Main constituents of Portland cement

Portland cement clinkers are essentially composed of four phases, *i.e.*, alite, belite, tricalcium aluminate, and ferrite. The chemistry and structure of these phases are introduced below. It is noted that other phases such as lime (CaO), periclase (MgO), quartz (SiO_2), etc., may be present in Portland clinkers as well, though rarely in quantities exceeding 1 wt%.

1.3.1 Alite

The alite phase accounts for 50 – 70 wt% of normal Portland cement clinkers [1]. It is an impure form of tricalcium silicate (Ca_3SiO_5 or C_3S[1]) where 3 – 4 wt% of impurity oxides

[1] The following nomenclature is normally applied in the cement literature: C = CaO; S = SiO_2; A = Al_2O_3; F = Fe_2O_3; $\bar{S}$ = SO_3; H = H_2O. In this thesis the cement nomenclature is only used for the C-S-H phase and the four main clinker phases in their pure forms: C_3S, C_2S, C_3A, and C_4AF.

are incorporated into the crystal structure during the burning of the clinker in the kiln. It reacts rather quickly with water and in ordinary Portland cement it is the principal component for strength development; when considering ages up to 28 days, it is undoubtedly the most important phase.

Seven polymorphs of C_3S have been identified and upon heating/cooling pure C_3S undergoes a series of reversible phase transformations, which have been observed by a combination of high-temperature X-ray diffraction, high-temperature light microscopy and differential thermal analysis [16-23]:

$$T_1 \overset{620°C}{\longleftrightarrow} T_2 \overset{920°C}{\longleftrightarrow} T_3 \overset{980°C}{\longleftrightarrow} M_I \overset{990°C}{\longleftrightarrow} M_{II} \overset{1060°C}{\longleftrightarrow} M_{III} \overset{1070°C}{\longleftrightarrow} R$$

T = triclinic, M = monoclinic, R = rhombohedral.

However, ionic substitution may stabilize some of the high-temperature polymorphs at room-temperature. Normal Portland cement clinkers usually contain alite in the monoclinic M_I or M_{III} form, or a mixture of both [24]. A typical chemical composition of the alite phase in Portland cement clinker is presented in Table 1.1 along with representative phase compositions for belite, aluminate and ferrite.

The structure of the C_3S polymorphs are built from Ca^{2+} cations, O^{2-} anions and SiO_4 tetrahedra with the position of Ca^{2+} and O^{2-} ions and Si atoms essentially being the same for the different polymorphs, but with marked variations in the orientation of the tetrahedra, which exhibit different degrees of disorder [25]. Fig. 1.2 depicts the crystal structure for the triclinic T_1 C_3S polymorph [26]. The coordination of the Ca^{2+} ions to the O atoms in the SiO_4 units is affected by the structural differences between the polymorphs and several distinct crystallographic Ca^{2+} sites, having different coordination numbers, are present for each polymorph. Therefore, the mean coordination number of Ca^{2+} cations changes from 5.66 for the rhombohedral R-polymorph, to 6.15 and 6.21 for the monoclinic M_{III} and triclinic T_1 polymorphs, respectively [21].

Whether the M_I or M_{III} polymorph occurs in Portland cement is especially dependent on the contents of MgO and SO_3 [24]. A high content of MgO favours the formation of small crystals that invert to M_{III}, while high SO_3 concentrations promote the formation of large crystals that invert further to M_I. The cooling rate is also an important

factor, since a slow cooling will favour the transformation to M_I. If the cooling rate is particularly slow further transformation to the triclinic T_1 C_3S may occur, although this is only expected to take place if the alite phase is unusually low in substituent ions [24].

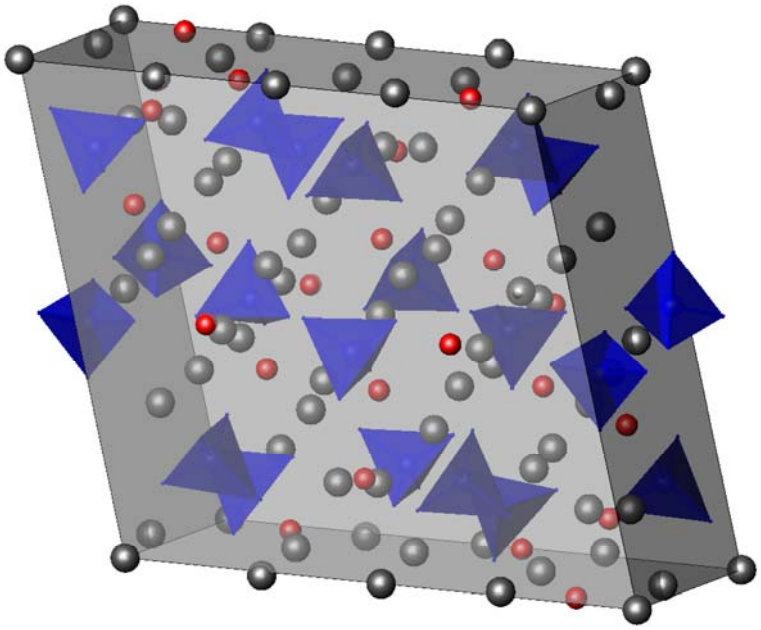

Fig. 1.2 Crystal structure of the triclinic T_1 polymorph of Ca_3SiO_5. SiO_4 units are displayed as blue tetrahedra, whereas the oxygen and calcium ions are shown as red and grey spheres, respectively. The figure is based on the crystal data by Golovastikov *et al.* [26].

The most important impurity oxides in alite are Al_2O_3, Fe_2O_3, MgO, SO_3, Na_2O, K_2O, and P_2O_5. The limit of substitution in C_3S of MgO, Al_2O_3 and Fe_2O_3, alone or in combination, was examined by Hahn *et al.* [27]. They found that Ca^{2+} could be partly replaced by Mg^{2+} and that Al^{3+} and Fe^{3+} could partly replace both Ca^{2+} and Si^{4+}. The limit of MgO incorporation into the C_3S structure was 2.0 wt% at 1550 °C and 1.5 wt% at 1420 °C, while the maximum contents of Al_2O_3 and Fe_2O_3 was reached at 1.0 wt% and 1.1 wt%, respectively. However, since Al^{3+} and Fe^{3+} compete for the same sites the limit of substitution for each was lowered if the other was also present. The substitution of Al^{3+} for Ca^{2+} was later queried by a ^{27}Al MAS NMR study [28], which showed that Al^{3+} was present almost entirely in tetrahedral sites, *i.e.*, a substitution of Si^{4+} by Al^{3+} ions. Woermann *et al.* [29] found that up to 1.4 wt% of either Na_2O or K_2O could be incorporated into C_3S at 1500 °C, however, observed contents of Na_2O and K_2O are much lower in alite of ordinary production clinkers. In a study on the influence of phosphorus on

the formation of C_3S, a limit of 1.1 wt% was detected by Gutt [30] for P_2O_5 inclusion in C_3S solid solution and it was suggested that P^{5+} was built into the C_3S structure by replacing Si^{4+}. To summarize, the most significant substitutions in the alite phase of Portland clinker are Na^+, K^+, Mg^{2+} and Fe^{3+} for Ca^{2+} and of Al^{3+}, P^{5+} and S^{6+} for Si^{4+}.

Besides affecting the structure of C_3S the presence of guest-ions in the crystal lattice also has an influence on the physical properties of the alite phase, *e.g.*, colour and grindability (measure of the ease with which a material can be ground). For instance, doping of C_3S with Fe^{3+} and Al^{3+} will decrease the grindability of C_3S [31]. Furthermore, the presence of guest ions can also affect the reactivity of the alite phase in a hydrating cement paste [32].

1.3.2 Belite

Belite is an impure form of dicalcium silicate (Ca_2SiO_4 or C_2S) and constitutes 5 – 30 wt% of ordinary Portland cement clinkers [1]. The belite phase is less important than alite when considering the strength development of Portland cement during the first 7 days of hydration, since belite reacts much slower with water than alite. However, belite contributes notably to the strength development at later stages. Ca_2SiO_4 also occurs naturally under the mineral name larnite [33]. Five polymorphs exist of pure C_2S [22,34-36]: one hexagonal (α), one monoclinic (β), and three orthorhombic (α'_H, α'_L, γ) forms. The transition temperatures between the different polymorphs are outlined below.

$$\gamma \xleftarrow{<500^\circ} \beta \xleftarrow{630\text{-}680^\circ C} \alpha'_L \xleftarrow{1160^\circ} \alpha'_H \xleftarrow{1425^\circ} \alpha$$

The crystal structures of the C_2S polymorphs are built from strings of alternating Ca^{2+} cations and isolated SiO_4 tetrahedra with the arrangement of these ions being very similar in the α, α'_H, α'_L and β forms (Fig. 1.3). The structure of γ-C_2S differs from that of the four other polymorphs in being much less dense. Normally, the high-temperature polymorphs cannot be preserved on cooling to room temperature if the C_2S structure is not stabilized by the incorporation of guest ions in the crystal lattice, but in all modern Portland cement clinkers the belite phase contains enough guest ions to prevent the transformation from β- to the γ-form of belite.

Table 1.1 Typical chemical compositions of the four constituent phases of Portland cement clinkers (wt%) [1].

	CaO	SiO_2	Al_2O_3	Fe_2O_3	MgO	Na_2O	K_2O	SO_3	P_2O_5	Mn_2O_3	TiO_2
Alite[1]	71.6	25.2	1.0	0.7	1.1	0.1	0.1	0.1	0.1	0.0	0.0
Belite[1]	63.5	31.5	2.1	0.9	0.5	0.1	0.9	0.2	0.1	0.0	0.2
Aluminate (cubic)[1]	56.6	3.7	31.3	5.1	1.4	1.0	0.7	0.0	0.0	0.0	0.2
Ferrite[1]	47.5	3.6	21.9	21.4	3.0	0.1	0.2	0.0	0.0	0.7	1.6
Aluminate (orthorhombic)[2]	53.9	4.3	28.9	6.6	1.2	0.6	4.0	0.0	0.0	0.0	0.5
Aluminate (low Fe)[3]	58.1	4.6	33.8	1.0	1.0	0.4	0.5	0.0	0.0	0.0	0.6
Ferrite (low Al)[4]	47.8	5.0	16.2	25.4	3.7	0.4	0.2	0.3	0.0	1.0	0.6

[1] Typical phase compositions for an ordinary Portland cement clinker with 1.65 wt% MgO and 3.1 wt% Fe_2O_3, and molar $SO_3/(K_2O + Na_2O) < 1.0$ wt%.
[2] Orthorhombic (or pseudotetragonal) polymorphs are sometimes present in clinkers high in alkalis.
[3] Typical composition for the aluminate phase in white cement clinkers.
[4] Composition for the ferrite phase in a typical sulphate-resistant clinker.

This phase transformation can cause the undesired phenomenon known as 'dusting' where crystals of β-belite crack and falls to a fine and more voluminous powdered material upon too slow cooling. Usually, belite is present in Portland cement clinker only as the β-polymorph, although the presence of some additional α and α'_L have been reported [17,22,23].

Typically, belite contains 4 – 6 wt% of substituent oxides, mostly Al_2O_3 and Fe_2O_3 [1]. A ^{27}Al MAS NMR study [28] has shown that Al^{3+} is located at the tetrahedral sites, *i.e.*, Al^{3+} substitutes for Si^{4+}. Belite, as compared to the alite phase, preferentially incorporates K_2O and SO_3 and Chan *et al.* [37] has reported an upper limit of K_2O substitution in belite of ~1.2 wt%. A typical belite composition is given in Table 1.1.

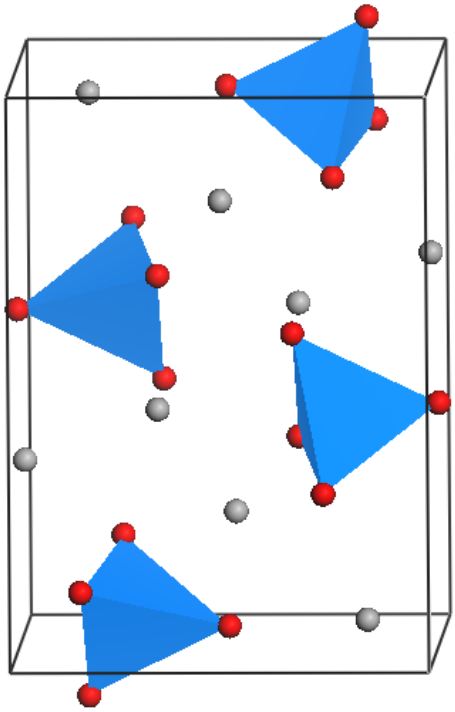

Fig. 1.3 Crystal structure of monoclinic β-$CaSiO_4$. Calcium and oxygen atoms are displayed as grey and red spheres, respectively. The blue polyhedra represent SiO_4 tetrahedra. The figure is based on the crystal data by Jost *et al*. [36].

1.3.3 Tricalcium aluminate

The tricalcium aluminate phase ($Ca_3Al_2O_6$ or C_3A) constitutes 5 – 10 % of normal Portland cement clinkers [1]. It reacts very rapidly when mixed with water, and can thus cause undesired fast setting of the cement. Therefore, a set-controlling agent, such as gypsum ($CaSO_4 \cdot 2H_2O$), is added to the clinker which retards the setting. In its pure form C_3A crystallizes in the cubic system and does not exhibit polymorphism [38]. The crystal structure is built from Ca^{2+} ions and rings consisting of six connected AlO_4 tetrahedra.

However, in the aluminate phase of production clinker extensive ionic substitution occurs, *e.g.*, replacement of Al^{3+} by Fe^{3+} or Si^{4+}, and Ca^{2+} by Na^{+}. Such modifications in composition can occasionally lead to changes in structure [39,40]. If the content of included Na_2O is below approximately 2.4 wt% the structure will remain cubic, but higher degrees of Na_2O incorporation leads to orthorhombic (2.4 – 4.6 wt%) or monoclinic structures (4.6 – 5.7 wt%) [39]. Lee *et al.* [41] reported ~2 wt% SiO_2 and ~3 – 4 wt% Fe_2O_3 as upper limits for Al^{3+} replacement. The total content of substituent oxides in the aluminate phase can be as high as ~13 wt% and ~20 wt% in the cubic and orthorhombic forms, respectively. For typical phase compositions of tricalcium aluminate in cement clinkers see Table 1.1.

In Portland clinkers the aluminate phase can occur either in the cubic or the orthorhombic modification, but mixtures of the two are seen as well. The monoclinic form has not been observed in production clinkers. Cubic aluminate is often finely grained and closely intermixed with dendritic (branched) ferrite crystals. Larger cubic aluminate crystals tend to be equidimensional while the orthorhombic form often exhibits a prismatic crystal habitus [42].

1.3.4 Calcium alumino-ferrite

The quantity of calcium alumino-ferrite ($Ca_2Al_xFe_{2-x}O_5$, $0 \leq x \leq 2$, or C_4AF for $x = 1$), commonly referred to simply as ferrite, is below 15 wt% and usually between 5 – 10 wt% in normal Portland cement clinkers [1]. The grey color of ordinary Portland cement is due to the presence of this iron-rich phase. Thus, the production of white Portland cement necessitates a minimization of the ferrite content in the clinkers. The hydration rate of ferrite is fairly variable, but considerably slower than the corresponding hydration rate of pure tricalcium aluminate [43].

C_4AF crystallizes in the orthorhombic system with each Ca^{2+} cation having seven oxygen neighbours [44]. The aluminium and iron atoms are both distributed between octahedral and tetrahedral sites, but with the greatest portion of the aluminium located at tetrahedral rather than octahedral sites. The typical composition of ferrite found in clinkers differs considerably from pure C_4AF (Table 1.1). Normally ferrite contains roughly 10 wt% of substituent oxides and has a composition close to $Ca_2AlFe_{0.6}Mg_{0.2}Si_{0.15}Ti_{0.05}O_5$. The Ca^{2+} cations exhibit very limited or no substitution, but Mg^{2+} can replace Fe^{3+} if the

substitution is accompanied by another Fe^{3+} being replaced by Si^{4+} or Ti^{4+} to maintain charge neutrality [45]. Mn^{3+} is capable of replacing all of the Fe^{3+} and 60 % of the Al^{3+} in pure C_4AF [46], which explains that small amounts of Mn_2O_3 are always present in clinker ferrite.

The composition of ferrite in sulphate-resistant cement clinkers differs somewhat from that observed in normal Portland clinkers. For instance, the ratio of Fe to Al is higher and there is a substantial substitution of Al^{3+} cations besides the replacement of Fe^{3+}.

Chapter 2

Supplementary cementitious materials and types of cement

This chapter is primarily devoted to the introduction of the so-called supplementary cementitious materials (SCMs) as they form an essential part of the present PhD project. In particular, attention is paid to the types of SCM which are employed in the hydration experiments presented in Chapter 8. Furthermore, a classification scheme for cements is presented, and a few specialized types of cement not included in the classification are briefly described as well.

2.1 Introduction

During the last six decades the global demand for Portland cement has exhibited a continued growth. This is illustrated in Fig. 2.1 which plots the world production of Portland cement from 1926 to 2007 [47]. The accelerated growth since the beginning of the 1990s is mainly attributable to a dramatically increased demand for cement in the developing countries. Humphreys and Mahasenan [48] have forecasted a 115 – 180 % increase from 1990 levels in global cement demand by 2020, with a four-fold increase by 2050 being likely.

Climate change is now widely recognized as one of the greatest challenges facing humanity and the discussion regarding its origin is a matter of considerable controversy. However, much scientific evidence links global warming to increased emissions of green house gasses (GHGs) of which carbon dioxide (CO_2) accounts for 82 % [49]. On average, the manufacture of 1 kg of Portland cement generates 0.87 kg of CO_2, but almost no other GHGs, and it is estimated that the cement industry produces approximately 5 % of the global manmade CO_2 emissions [48]. Portland cement manufacturing accounts for ~3 % of the global emission if all GHGs originating from human activities are considered as a whole.

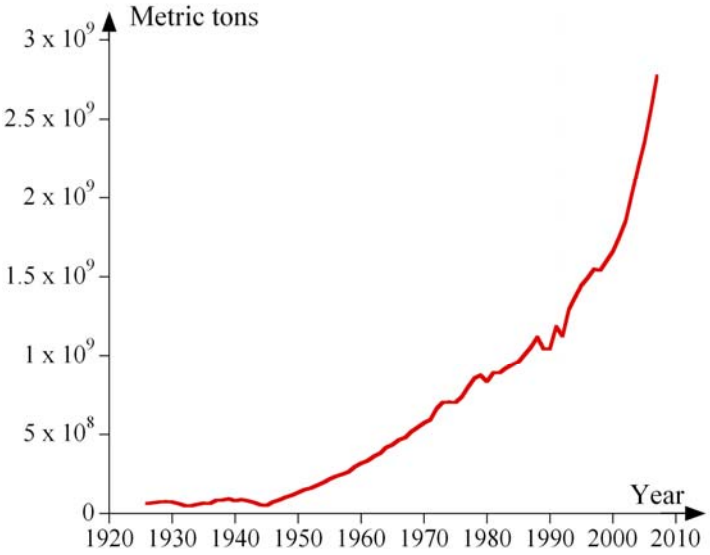

Fig. 2.1 World production of Portland cement from 1926 to 2007 [47].

Over the past decades the cement industry has taken an active part in seeking ways to cut back the CO_2 outlet associated with its activities. Essentially, the CO_2 emissions from Portland clinker production falls into two categories: those arising from the de-carbonation (calcination) of $CaCO_3$ in the raw material (Eq. (1.1)) and those derived from the burning of fuel in the kiln. The most commonly employed approaches to achieve CO_2 reductions include improvement of the thermal efficiency of kiln and cooler systems, replacement of conventional carbon based fuels by alternative fuels, use of alternative raw materials with high contents of calcium in a non-carbonated form, and partial replacement of clinker in cement by other inorganic materials such as SCMs.

Of all kiln fuels used in Europe, the alternative fuels account for 14 % based on calorific value and include materials like meat and bone meal, used tyres, solvents, plastics, paper, saw dust and a whole range of other waste materials [50]. However, not all of these alternative fuels are approved as carbon neutral, *i.e.*, fuels with no net release of CO_2. Materials such as animal waste, paper waste and biodegradable municipal waste may be regarded as carbon neutral since the CO_2 released by combustion and the amount absorbed by photosynthesis are at equilibrium, but waste material originating from fossil fuels, such as plastics, solvents and the rubber in used tyres, etc., are not approved as carbon neutral. The use of these non-carbon neutral waste materials as kiln fuels is, nevertheless, associated with a significant reduction in CO_2 emissions as the incineration plants, where the waste materials would otherwise be burned, are not as efficient in terms of energy recovery as the cement kiln. An additional advantage of using waste materials as

alternative fuels in the cement kiln is that no residues are produced, as all of the ash is incorporated in the cement clinker. Although improving kiln efficiency and using alternative fuels and raw materials can lead to substantial reductions in the CO_2 emission, the replacement of clinker in the cement by other suitable materials is probably the most effective approach for achieving CO_2 reductions. In the following, a group of such materials is introduced.

2.2 Supplementary cementitious materials (SCMs)

SCMs refer to a rather broad group of materials including ground granulated blastfurnace slags, fly ashes, microsilica (silica fume), natural and artificial pozzolans, calcined shales/clays, and rice husk ash. Before the individual SCMs types are considered, the terms 'pozzolanic' and 'latent hydraulic' are defined as they are crucial for the characterization of SCMs:

- A 'pozzolanic' material will harden in water when mixed with calcium hydroxide $Ca(OH)_2$, or with other materials that can release calcium hydroxide (*e.g.*, hydrating Portland cement clinker), by formation of calcium silicate hydrates. If the content of Al_2O_3 is high in the pozzolanic material calcium aluminate hydrates or aluminium silicate hydrates can form as well. Examples of pozzolanic materials include low-calcium fly ashes, microsilica, and natural pozzolans.

- 'Latent hydraulic' materials set and harden when mixed water, but only if a minimal amount of an activator/catalyst such as $Ca(OH)_2$ or alkali is present. They have chemical compositions roughly intermediate between those of pozzolanic materials and Portland cement. Blastfurnace slag is an example of a latent hydraulic material.

Collectively, SCMs can be described as finely grained inorganic materials with pozzolanic and/or latent hydraulic properties. As mentioned above, SCMs are often used to partially replace Portland clinker, thus producing what is often identified as 'blended cements'. The SCM can be mixed/interground with the Portland clinker at the cement production plant or added directly to the concrete mix as a separate material at the construction site. The

former approach is most commonly applied in Europe, as reflected by the European prestandard [3] (see Section 2.3.1), whereas the latter is the most commonly used approach in USA. When designing blended cements the proportion of a latent hydraulic material can be higher than that of a pozzolanic material. The addition of SCMs can have a positive effect on the properties of concrete, for instance, improved workability of the freshly mixed concrete and reduced heat generation from hydration which minimizes the potential risk of thermally induced cracking in construction elements. Furthermore, SCMs can contribute substantially to the strength development of concrete.

2.2.1 Blastfurnace slag

Blastfurnace slag is a by-product from the manufacture of pig iron and consists essentially of calcium- and alumino-silicates [51]. In the blastfurnace the iron oxide ore is reduced by the means of coke into metallic iron, while the silica and alumina constituents combine with lime and magnesia to form a molten slag which collects on top of the molten iron at the bottom of the furnace. The slag melt is exposed to rapid cooling from about 1350 – 1550 °C to a temperature below 800 °C, whereby a largely glassy material with latent hydraulic properties is formed. Often the cooling is achieved by spraying droplets of the liquid slag with a high-pressure jet of water, thus resulting in a wet and sandy material which is denoted ground granulated blastfurnace slag (GGBS) after it has been dried and ground. The typical glass content is above 95 % and the glassy nature of the slags is a necessity for its use as SCM in blended cements. If the molten slag is cooled more gradually it will crystallize and result in a material with practically no cementing properties [52].

Typical compositional ranges of the major metal oxides in slags are: CaO, 30 – 50 wt%; SiO_2, 27 – 42 wt%; Al_2O_3, 5 – 33 wt%; MgO, 0 – 21 wt% [53]. These substantial variations are primarily caused by differences in the chemical composition of the ore used for the iron production which vary between plants. On the other hand, the composition of a slag from one particular plant is not expected to vary much, unless the ore is changed.

GGBS are basically supercooled liquid silicates. The structure of the silicate glass is built from isolated or polymerised silica tetrahedra sharing oxygen atoms, while cations like Ca^{2+} and Mg^{2+} are located in the cavities of the network, thus neutralising the negatively charged anionic groups of silica tetrahedra [54]. Besides the glassy matrix, the

most commonly observed crystalline phases are merwinite ($Ca_3Mg[SiO_4]_2$), melilite ($(Ca,Na)_2[(Mg,Fe^{2+},Al,Si)_3O_7]$), calcite ($CaCO_3$), and quartz ($SiO_2$) [52].

When mixed with water Portland cement – slag blends give principally similar hydration products as the hydration of pure Portland cement [55], although the amount of $Ca(OH)_2$ is generally lower [56,57]. The literature provides widely differing data regarding the rate of slag reaction in Portland cement – slag pastes. Lumley *et al.* [58] reported that 30 – 55 wt% of the slag had reacted after 28 days in pastes of Portland cement blended with varying amounts of slag. After 1 – 2 years 45 – 75 wt% of the slag was consumed.

2.2.2 Pulverised fly ash

Fly ash is a by-product from the burning of pulverised coal at power plants and it is collected from the combustion gas by special mechanical devices or electrostatic precipitators [59]. The fly ash is formed when the mineral components of the coal melts and subsequently solidifies as small glassy droplets. The resulting material is highly dependent on which type of coal is burnt. The American Society for Testing and Materials (ASTM) classification distinguishes between four classes/ranks of coal – anthracite, bituminous, subbituminous and lignite – based on the content of fixed carbon and heating value [60]. Nowadays, anthracite is practically not used as fuel at power plants as it is too expensive for this application. The use of bituminous coal results in low-calcium fly ashes (corresponding roughly to Class F fly ash of the ASTM classification), whereas fly ashes with high calcium contents originate from the burning of subbituminious or lignite coal (also known as brown coal). The high-calcium fly ashes normally correspond to Class C fly ash of the ASTM system (*i.e.*, $SiO_2 + Al_2O_3 + Fe_2O_3 < 70$ wt%). However, this is not a general rule since lignite coal occasionally can be low in calcium. The fly ash particles are typically spherical and their sizes vary from < 1 μm to > 150 μm. Other particle shapes may be observed as well, depending on the burning process.

The bulk chemical composition of low-Ca fly ashes are dominated by silica and alumina, much like natural pozzolans, typically with 40 – 60 wt% SiO_2 and 20 – 30 wt% Al_2O_2. The content of Fe_2O_3 varies quite widely and the amount of CaO is low (2 – 5 wt%). Besides the prevailing glassy matrix only few crystalline phases are observed. In general, the only phases present in any appreciable amount are quartz (SiO_2), mullite ($3Al_2O_3{\cdot}2SiO_2$), hematite (Fe_2O_3), and magnetite (Fe_3O_4) [61].

High-Ca fly ashes show more variable chemical compositions than low-Ca ones. The higher calcium content is attributable to a significant quantity of limestone present in the coal gangue. The range of crystalline phases that can be observed is much broader in high-Ca than in low-Ca fly ashes as a consequence of the more variable bulk chemistry. Commonly observed phases include quartz, alkali sulfates, hematite, mullite, free lime (CaO), periclase (MgO), anhydrite ($CaSO_4$), ferrite (Ca_2AlFeO_5), spinel ($MgAl_2O_4$), merwinite, melilite, and sodalite ($Na_8[Al_6Si_6O_{24}]Cl_2$) [56].

The presence of fly ash affects the strength development in concrete. Compared to concrete made solely with Portland cement as the binding agent, the ones containing fly ash usually show a reduced early strength, but improved long-term strength [59]. The workability of fresh concrete is also enhanced by the addition of fly ash, an effect largely caused by the smoothness and spherical shape of the fly ash particles [62]. Several authors have studied the effect of fly ash on the hydration of Portland cement, but widely differing results have been obtained. Takemoto and Uchikawa [63] found that the presence of fly ash accelerates the reaction of alite at early stages, while Taylor and Mohan [64] observed accelerated alite reaction at all stages. In contrast, fly ash was found to retard the early hydration of alite in a number of other studies [65-68]. A quantitative X-ray diffraction study has demonstrated a faster reaction of the aluminate and ferrite phases in the presence of fly ash [69]. Generally, the hydration of blended cements containing fly ash is characterised by a lower $Ca(OH)_2$ content than observed for the hydration of pure Portland cement [55]. Quantitative studies on the rate of consumption of the fly ash itself are few and show rather inconsistent results.

2.2.3 Microsilica (silica fume)

Microsilica (also known as ‘silica fume’ or ‘condensed silica fume’) is a by-product from the silicon and ferrosilicon smelting industries and it is formed when high-purity quartz is reduced to produce silicon or ferrosilicon alloys [70]. The quartz is heated to 2000 °C with coal, coke or woodchips in an electric arc furnace, a process involving the formation of SiO vapour. In the upper part of the furnace the vapour oxidises and condenses to very small spheres of amorphous silica. It is an extremely fine-grained material with a mean particle size of 0.1 – 0.2 μm and very high specific surface area (15 – 20 m^2/g). The colour varies from nearly white to almost black.

Microsilica is composed of 94 – 98 wt% SiO_2 if it originates from the production of elementary silicon, whereas the content of SiO_2 typically is in the range 86 – 90 wt% if ferrosilicon alloys are manufactured [71]. Other components present in appreciable amounts (though rarely above 2 wt%) include MgO, K_2O, Na_2O, Fe_2O_3, and elementary carbon.

Microsilica exhibits a considerable pozzolanic activity when mixed with Portland cement due to its high content of reactive SiO_2 [72], and several authors have observed an accelerating effect of microsilica on the early reaction of the clinker phases [67,73-76]. Sun and Young [77] have reported degrees of reaction for microsilica in ultra-high strength cement pastes made from cement blends containing 18 – 48 wt% microsilica. Using solid-state ^{29}Si MAS NMR they found that 9 – 15 % had reacted after 1 day, increasing to 55 – 59 % at 180 days. In concrete mixes microsilica increases the water demand and results in reduced permeability of the hardened material by densifying the matrix of the concrete. The presence of microsilica can also increase the strength of concrete significantly [78].

2.2.4 Natural pozzolans

The term ‘pozzolan’ (or ‘pozzolana’) is derived from the name of the Italian city Pozzuoli which is located in an area rich in occurrences of largely glassy volcanic rocks [5]. The ancient Romans discovered the hydraulic properties of this material when it was mixed with burnt lime. Nowadays ‘pozzolan’ rather refers to a much broader range of inorganic materials, all having the common property of being able to harden in water when mixed with calcium hydroxide ($Ca(OH)_2$) or with a material that can release $Ca(OH)_2$ such as Portland cement. Pozzolans are classified as being of either natural or artificial origin, although the distinction between the two categories is not always clear. For instance, the diatomaceous earth from Denmark called ‘moler’ is composed essentially of a mixture of clay (montmorillonite) and amorphous SiO_2 (opal). While the amorphous SiO_2 exhibits pozzolanic properties without further treatment of the material, the clay will not show a clear pozzolanic character unless it is thermally activated.

The natural pozzolans can roughly be divided into two main categories based on the geological origin of the material: (1) pozzolans of volcanic or (2) sedimentary origin. The first group consists of so-called pyroclastic rocks resulting from explosive volcanic eruptions where liquid magma is ejected into the atmosphere thus causing the formation of

a glassy material by rapid quenching. The material can occur as incoherent deposits or appear as coherent, compact rocks (tuffs). A considerable variation of the chemical composition is observed for such materials, since the initial magma can be derived from a wide range of different sources, but generally the bulk chemistry of natural pozzolans of volcanic origin is dominated by SiO_2 (~50 – 70 wt%), Al_2O_3 (~10 – 20 wt%), CaO (~3 – 10 wt%), and Fe_2O_3 (~ 1 – 10 wt%). In addition to the glassy matrix these rocks normally contain a small amount of crystalline phases, the most commonly observed being quartz, feldspars, pyroxenes, and micas. Due to chemical weathering the volcanic pozzolans sometime show severe degrees of zeolitisation, *i.e.*, transformation of the glassy pozzolan into zeolitic minerals such as clinoptilolite ($(Na,K,Ca)_{2-3}Al_3(Al,Si)_2Si_{13}O_{36}\cdot 12H_2O$) or analcime ($NaAlSi_2O_6\cdot H_2O$). Such an alteration of the volcanic material can improve the pozzolanic properties. The natural pozzolans of sedimentary origin include a group of so-called diatomaceous earths which are soft, chalk-like materials consisting of the fossilized skeletons/shells of microorganisms collectively known as diatoms. Typical chemical compositions of the major oxides range from 60 – 85 wt% SiO_2, 2 – 16 wt% Al_2O_3, 2 – 7 wt% Fe_2O_3, 1 – 2 wt% CaO, and 1 – 2 wt% MgO.

When pozzolans, artificial or natural, are mixed with Portland cement and water they react with the $Ca(OH)_2$ formed by the hydration of the calcium silicates (alite and belite) in the cement clinker and form C-S-H. Therefore, the content of portlandite is always lower in the hydration products as compared to that found by the hydration of pure Portland cements [59]. Studies on the heat evolutions from hydration of C_3S blended with natural pozzolans have demonstrated an accelerating effect of the latter on the C_3S reaction [79]. Massazza and Testolin [80] reported that in pastes of C_3S with natural pozzolan, 16 – 29 % of the pozzolan had been consumed after 180 days.

2.2.5 Other SCMs and mineral additions

The burning of rice husks results in a strongly pozzolanic ash, if performed under controlled conditions, a material which has received much attention for its potential as a SCM [81,82]. It is characterised by a high content of amorphous SiO_2 and a high specific surface area. Khan *et al.* [83] have studied the hydration of pastes of C_3S blended with rice husk ash and found that C-S-H was formed with a mean Ca/Si ratio of 1.3. The content of

$Ca(OH)_2$ reached a maximum of ~3 wt% after 3 days of hydration and after 28 days only 1 wt% was left.

Artificial pozzolans can be produced by heating shale or clay to a temperature in the order of 600 – 900 °C [59]. The thermal treatment removes the chemically combined water and causes the crystalline network of the clay minerals to collapse which results in a largely amorphous material with pozzolanic properties. The chemistry is dominated by silica and alumina. Wild *et al.* [84] have investigated the effect of thermally activated clay (metakaolin) on the hydration of Portland cement in concrete and concluded that the reaction of the clinker phases in the cement was accelerated by the presence of metakaolin.

A small amount of limestone is often interground with the Portland cement clinker as it is a relatively inexpensive material compared to the clinker. However, it has only a little effect on the performance of hardened concrete if added in small amounts (0 – 5 wt%) [85]. Normally, limestone is not regarded as a true SCM, since it is lacking pozzolanic or latent hydraulic properties, but is instead referred to as a mineral addition. The limestone (essentially $CaCO_3$) does not merely act as a filler, but reacts chemically. For most cements the maximum quantity of $CaCO_3$ that can react seems to be ~2 – 3 wt%. It is well-known that the presence of limestone favours the formation of monocarbonate ($4CaO{\cdot}Al_2O_3{\cdot}CaCO_3{\cdot}11H_2O$) rather than monosulphate ($3CaO{\cdot}Al_2O_3{\cdot}CaSO_4{\cdot}12H_2O$) in hydrating Portland cement [85-88]. Furthermore, the reaction of alite and the aluminate phase is accelerated by limestone as it is the case with many other fine-grained materials such as silica fume and fly ash.

2.3 Types of cement

2.3.1 Standardized common cements

EN 197-1 is a harmonized European prestandard [3] which classifies cements made for general purposes, *i.e.*, cements with special properties, such as sulphate-resistant or calcium aluminate cements, are not included in the classification. A few of the most important types of these specialized cements are treated separately (see Sections 2.3.2-2.3.4). The EN 197-1 standard distinguishes between five different main types of cement:

CEM I:	Portland cement
CEM II (A/B):	Portland-composite cement

CEM III (A/B/C): Blastfurnace cement
CEM IV (A/B): Pozzolanic cement
CEM V (A/B): Composite cement

The classification operates with ten different constituents (Table 2.1) and the cements are classified as either CEM I, II, II, IV or V depending on the proportion of the individual constituents in the final anhydrous cement mix. Letters in the parentheses of Table 2.1 are abbreviations taken from the EN 197-1 standard. 'P' refers to natural pozzolans, whereas 'Q' denotes artificial pozzolans, *i.e.*, thermally activated clays and shales, and air-cooled slags from the extraction of elementary Pb, Cu and Zn. Fly ashes are subdivided into two categories: 'V' and 'W' are used for low- and high-calcium fly ashes, respectively. Constituents 1 to 7 are referred to as the 'main constituents'.

Table 2.1 Constituents of common cements in the EN 197-1 prestandard [3].

1. Portland cement clinker
2. Granulated blastfurnace slag
3. Pozzolanic material (P, Q)
4. Fly ash (V, W)
5. Burnt shale
6. Limestone
7. Silica fume (D)
8. Minor additional constituents
9. Calcium sulphate
10. Additives

CEM I is a Portland cement containing ≥ 95 wt% of clinker. CEM II's are all blended cements which contain 6 – 35 wt% of one or more main constituents besides clinker. CEM II cements are subdivided into the categories A or B indicating 6 – 20 and 21 – 35 wt% of clinker replacement, respectively. However, the content of silica fume is limited to 10 wt%. The category CEM III encompasses three types of blastfurnace slag cements with slag contents of 36 – 65 (A), 66 – 80 (B), and 81 – 95 wt% (C). CEM IV are pozzolanic cements with pozzolan (D, P, Q, or V) contents of 11 – 35 (A) or 36 – 55 wt% (B). In order to be classified as CEM IV, these cement blends must pass a specific pozzolanicity

test. CEM V's (A and B) are composite cements. Besides 40 – 64 wt% clinker, type A contains 18 – 30 wt% slag in addition to 18 – 30 of pozzolan (P, Q, V), while type B is a mixture of 20 – 39 wt% clinker, 31 – 50 wt% slag, and 31 – 50 wt% pozzolan (P, Q, V).

The widespread use of SCM as clinker replacements in cements is illustrated in Fig. 2.2 which shows the marked share of the five common cement types in the EU. The blended cements (CEM II-V) account roughly for two thirds of all common cements sold in the EU [89].

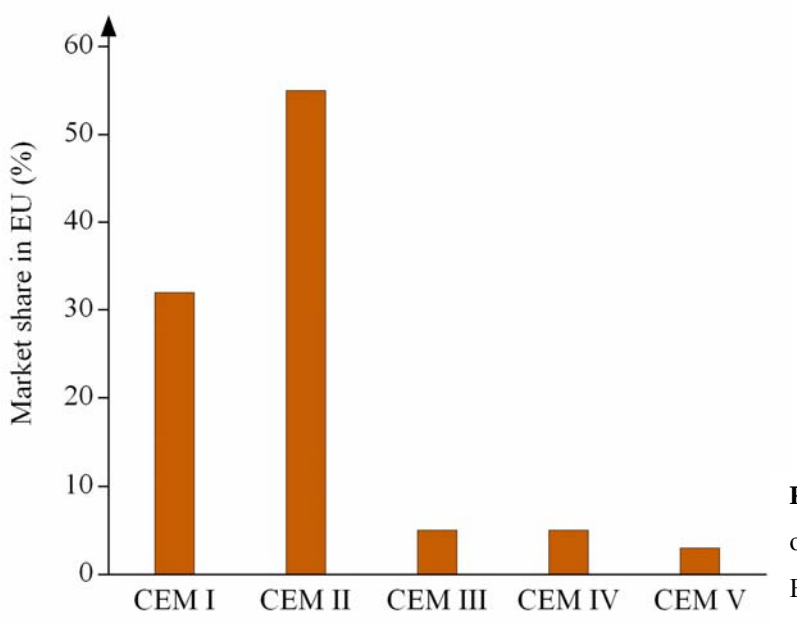

Fig. 2.2 The market share (%) of the different cement types in EU in 2003 [89].

2.3.2 Sulphate-resistant cement

Sulphate-resistant cement is a specialized type of cement to be used for concrete structures placed in environments where increased resistance to sulphate attack is required (*e.g.*, from sodium and magnesium sulphate in ground water). This type of cement has a reduced content of calcium aluminate (C_3A), typically less than 3 wt%, as this is the phase which specifically reacts with the sulphates ions. Cements with improved sulphate resistance can also be produced by replacing a high proportion of CEM I Portland cement by an appropriate amount of blastfurnace slag, thus resulting in a CEM III type cement.

2.3.3 Low alkali-cement

The American Standard ASTM 150-72 defines a low alkali-cement as one containing ≤ 0.6 wt% alkalis calculated as the Na_2O equivalent ($Na_2O + 0.658 \cdot K_2O$). This type of cement is

used in the production of concrete which is exposed to moist atmospheric conditions and contains aggregates with alkali-reactive constituents. The low content of alkalis prevents alkali-silica reaction (ASR), which can occur when hydroxide ions in the pore solution react with silica in the aggregates [1]. ASR can cause undesired expansion and cracking of the concrete.

2.3.4 Calcium aluminate cement

Calcium aluminate cements (CACs) refer to a range of cements with the common characteristic that the reactive phases and hydrates formed are calcium aluminates [90]. Compared to Portland cement the annual production of CACs is very limited, but due to several unique properties CACs are important in a number of applications where Portland cement does not suffice. These properties include rapid strength development, resistance to a wide range of chemically aggressive environments, and resistance to high temperatures.

Chapter 3

Hydration of plain and blended Portland cements

3.1 Introduction

This chapter introduces the hydration of Portland cement. First, a brief general description of Portland cement hydration is given, which is followed by a presentation of the structure and composition of the individual main hydration products. The subsequent section is devoted to the microstructural development of a hydrating cement paste, while the final part of the chapter discusses the hydration of cements blended with different types SCMs.

3.2 Portland cement hydration

Once water is mixed with Portland cement, several chemical processes and physical changes set off. Collectively, these changes are covered by the term 'hydration'. Taylor [1] defines 'hydration' as:

> *"The totality of the changes that occur when an anhydrous cement, or one of its constituent phases, is mixed with water".*

A mixture of water and Portland cement, in which setting and hardening occur, is called a 'cement paste'. This term also applies to the hardened material. Fig. 3.1 gives a schematic presentation of the hydration of the four principal clinker phases. The main products from hydration of alite and belite are the calcium silicate hydrate phase (C-S-H) and portlandite ($Ca(OH)_2$). C-S-H normally constitutes ~60 % of the hydration products and is by far the most important phase for strength development. It is an amorphous or poorly crystalline phase, which can exhibit a fairly wide range in composition as indicated by the dashes in the abbreviation C-S-H. The hydration of C_3S and C_2S can be formally represented by the following reactions:

$$\underset{\text{tricalcium silicate}}{Ca_3SiO_5} + (3 - x + y)\underset{\text{water}}{H_2O} \longrightarrow \underset{\text{C-S-H}}{Ca_xSi(H_2O)_y} + (3 - x)\underset{\text{portlandite}}{Ca(OH)_2} \qquad (4.1)$$

$$\underset{\text{dicalcium silicate}}{Ca_2SiO_4} + (2 - x + y)\underset{\text{water}}{H_2O} \longrightarrow \underset{\text{C-S-H}}{Ca_xSi(H_2O)_y} + (2 - x)\underset{\text{portlandite}}{Ca(OH)_2} \qquad (4.2)$$

In Eq. (4.1) and Eq. (4.2) x is often assumed to have a value of 1.7. The hydration of tricalcium aluminate ($Ca_3Al_2O_6$), calcium alumino-ferrite ($Ca_2Al_xFe_{2-x}O_5$, $0 \le x \le 2$) and gypsum ($CaSO_4 \cdot 2H_2O$) results in the remaining ~20% of the hydration products. These include a variety of calcium sulpho-aluminate and calcium sulpho-ferrite hydrates, with ettringite ($Ca_6[Al(OH)_6]_2(SO_4)_3 \cdot 26H_2O$) and monosulphate ($Ca_4[Al(OH)_6]_2SO_4 \cdot 6H_2O$), and their respective iron(III) analogues, as the main products [1].

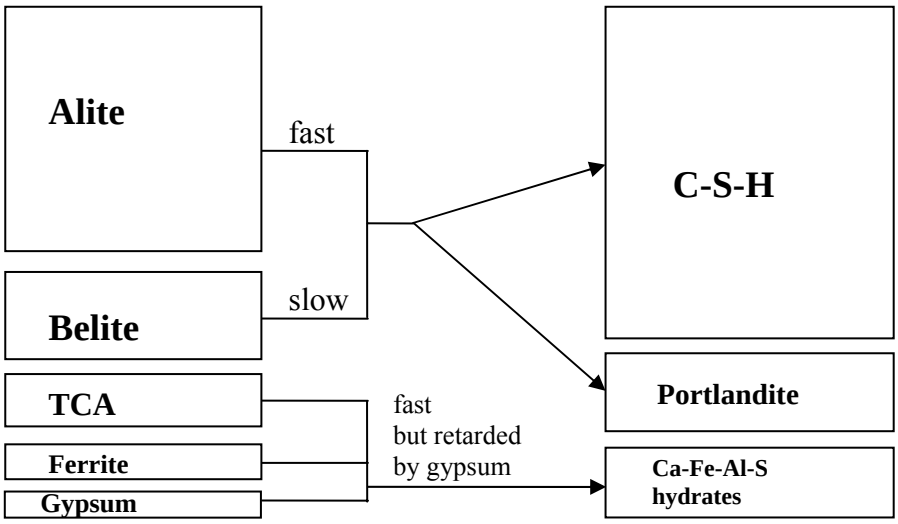

Fig. 3.1 Schematic representation of the hydration of the anhydrous components in Portland cement and the resulting hydration products. The areas of the boxes correspond roughly to the normal volume proportions of the phases as reported in Ref. [1]. TCA = tricalcium aluminate.

Hydrogarnet ($Ca_3[Al(OH)_6]_2$) may also form if a sufficient amount of gypsum is not added to the cement clinker. The formation of ettringite and monosulphate can be described by the following formal equations.

$$\underset{\text{tricalcium aluminate}}{Ca_3Al_2O_6} + 3\,\underset{\text{gypsum}}{CaSO_4 \cdot 2H_2O} + 26\,\underset{\text{water}}{H_2O} \longrightarrow$$

$$\underset{\text{ettringite}}{[Ca_3Al(OH)_6 \cdot 12H_2O]_2 \cdot (SO_4)_3 \cdot 2H_2O} \qquad (4.3)$$

$$\underset{\text{tricalcium aluminate}}{Ca_3Al_2O_6} + \underset{\text{ettringite}}{[Ca_3Al(OH)_6\cdot 12H_2O]_2\cdot(SO_4)_3\cdot 2H_2O} + 4\ \underset{\text{water}}{H_2O} \longrightarrow$$

$$3\ \underset{\text{monosulphate}}{Ca_4[Al(OH)_6]_2SO_4\cdot 6H_2O} \qquad (4.4)$$

3.3 Hydration products

3.3.1 Calcium silicate hydrate (C-S-H)

The most important product of Portland cement hydration is a calcium silicate hydrate, normally referred to simply as C-S-H. In cement pastes C-S-H occurs as an essentially amorphous phases, but more structurally ordered C-S-H may be formed in relatively pure systems. It is well-known that the C-S-H phase incorporates considerable quantities of alumina, sulphate, iron, alkalis, and possibly other species present in a cement paste, as guest ions [91-93]. Copeland and Kantro [92] have estimated that up to 50 % of the total amount of sulphate, alumina and iron in a cement paste eventually end up in the C-S-H. SEM [94,95] and TEM [96,97] studies combined with microanalysis have demonstrated a notable variability in composition of the C-S-H from one paste to another, but also from one reacted cement grain to the next within the same paste. Typically reported compositional ratios are [93]: Ca/Si = 1.7-2.1, Ca/Al = 20-30, Ca/S = ~25, which gives the C-S-H the approximate composition $C_{1.7\text{-}2.1}S(A_{0.04}\bar{S}_{0.04})H_x$.

The structure of C-S-H is a topic which has been, and still is, actively debated. Several structural models have been proposed over the years, but there seems to be some consensus that the C-S-H phase contains structural elements of both the minerals 14 Å tobermorite and jennite [98-100]. From chemical analysis [101] and ^{29}Si MAS NMR studies [102,103] it is known that the silica in C-S-H is organized in linear chains of silicate tetrahedra (SiO_4) of variable length, which represent fragments of so-called 'dreierketten' wherein bridging tetrahedra are randomly omitted (see Section 5.3.1 for further discussion). Richardson and Groves [103] have proposed a generalized formula for the composition of C-S-H: $[Ca_xSi_{(3n-1)}O_{(9n-2)}H_{(6n-2x)}]\cdot z Ca(OH)_2\cdot m H_2O$. The part of the formula in square brackets represents silicate chain fragments which are attached to a central Ca-O sheet, while the $Ca(OH)_2$ component can be interpreted as representing the occurrence of degenerate jennite elements, or solid solution with amorphous or

cryptocrystalline $Ca(OH)_2$. The 'amorphous $Ca(OH)_2$' may be regarded as regions in the C-S-H structure that are very low in silica.

3.3.2 Portlandite

$Ca(OH)_2$ exhibits a layered structure with two sheets of hydroxyl groups (OH^-) parallel to the basal plane and with a sheet of Ca^{2+} ions between them (Fig. 3.2). Calcium and oxygen are in octahedral and tetrahedral coordination, respectively [104]. The phase is generally identified by its mineral name, portlandite, and accounts for about 20 % of the hydration products in Portland cement pastes [1]. $Ca(OH)_2$ will grow as euhedral hexagonal crystals under ideal conditions of crystallization, but in pastes it often occurs as massive deposits.

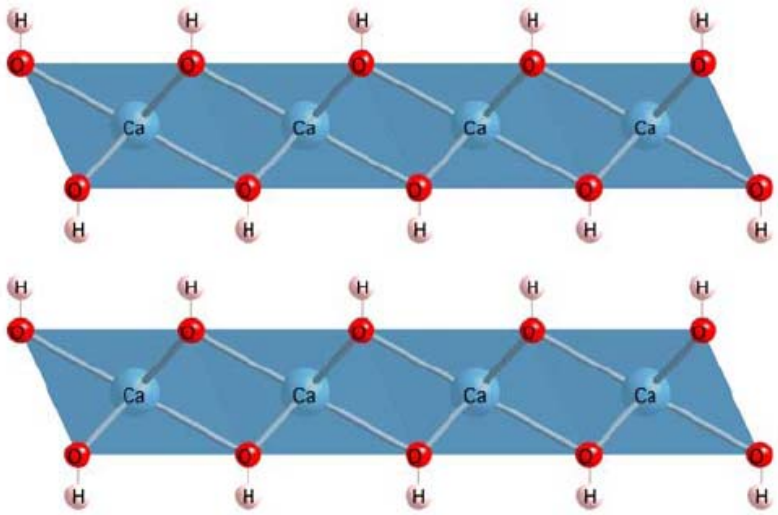

Fig. 3.2 Schematic representation of the layered crystal structure of portlandite ($Ca(OH)_2$). Each calcium ion is coordinated to six hydroxyl groups. The figure is adapted from Fig. 2 in Ref. [105].

3.3.3 AFm phases

The abbreviation 'AFm' (Al_2O_3-Fe_2O_3-mono) encompasses a group of phases all sharing the general formula $[Ca_2(Al,Fe)(OH)_6]\cdot X\cdot xH_2O$ [1]. Here X represents one formula unit of a single charged anion, or half a formula unit of a double charged anion. In Portland cement pastes these anions are most often OH^-, SO_4^{2-}, or CO_3^{2-}. More than one species of X can occur in the same AFm phase, *e.g.*, Kuzel's salt ($3CaO\cdot Al_2O_3\cdot 0.5CaCl_2\cdot 0.5CaSO_4\cdot 10H_2O$) [106,107].

The AFm phases have layered structures that can be derived from that of $Ca(OH)_2$ by ordered replacement of one third of the Ca^{2+} ions by Al^{3+} or Fe^{3+}. These principal layers

are alternating with interlayers containing the X anions and H_2O molecules. Since the Ca^{2+} ions are partially replaced by the smaller Al^{3+} or Fe^{3+} ions the structure is slightly distorted. Normally the AFm phases form platy, hexagonal crystals, but in cement pastes AFm can also occur in a poorly crystalline state where it is intimately mixed with the C-S-H phase [1,108].

3.3.4 AFt phases

'AFt' (Al_2O_3–Fe_2O_3-tri) denotes a group of phases all having the general formula $[Ca_3(Al,Fe)(OH)_6{\cdot}12H_2O]_2{\cdot}X_3{\cdot}xH_2O$, where $x \leq 2$ and X is either one formula unit of a doubly charged anion, or two formula units of a single charged anion. AFt phases form hexagonal prismatic or needle-shaped crystals. In Portland cement pastes the most important AFt phase is ettringite: $[Ca_3Al(OH)_6{\cdot}12H_2O]_2{\cdot}(SO_4)_3{\cdot}2H_2O$.

3.3.5 Hydrogarnet

Hydrogarnet, $Ca_3[Al(OH)_6]_2$, sometimes occurs as a minor hydration product in blended cement pastes, and in a poorly crystalline state in older Portland cement pastes. However, modern Portland cements, probably with exception of sulphate-resistant cement types [109], do normally not contain quantities of hydrogarnet detectable by XRD.

3.3.6 Brucite

Brucite ($Mg(OH)_2$), a phase with a layered structure similar to that of $Ca(OH)_2$ [33] (see Section 3.3.2), is sometimes formed in concrete that has been attacked by Mg salts [1]. It can also form in minor quantities by hydration of Portland cements high in MgO.

3.3.7 Hydrotalcite and related phases

Hydrotalcite occurs naturally as a mineral with composition $[Mg_{0.75}Al_{0.25}(OH)_2]$-$(CO_3)_{0.125}(H_2O)_{0.5}$. Numerous other phases of this type are known, as the Mg^{2+} and/or Al^{3+} can be replaced by other ions of similar size [110,111]. The CO_3^{2-} may also be substituted by other anions. These phases have layered structures which are related to that of brucite, *i.e.*, some of the Mg^{2+} ions in brucite are replaced by tripositive ions, such as Al^{3+} or Fe^{3+}, and charge neutrality is maintained by anions sited in the interlayer along with H_2O molecules. Such hydrotalcite-type phases are sometimes referred to as Mg-Al layered

double hydroxides and have been observed in hydrated cement – slag blends [112,113], but they may also form as a minor hydration product in Portland cement pastes [1].

3.4 Microstructural development in Portland cement paste

The following description of the microstructural development in hydrating Portland cement is largely based on Ref. [114] and the process is divided into three main stages, namely an early (0 to 3 h), middle (3 to 24 h) and late (> 24 h) period of hydration.

3.4.1 Early period of hydration (0 – 3 h)

As evidenced by high-voltage TEM, a thin gel layer or membrane forms on the surface of the cement grains soon after mixing with water [115,116]. This amorphous material has a composition which varies with that of the underlying surface, and is generally believed to be rich in alumina and silica, but significant amounts of calcium and sulphate are also present. Short rods of AFt phases, roughly 0.25 μm long and 0.1 μm thick, are observed within the first 10 min of hydration [117]. They occur both on the surface of the cement grains and at some distance away from these.

3.4.2 Middle period of hydration (3 – 24 h)

The middle period of hydration is characterized by a rapid formation of C-S-H and $Ca(OH)_2$ and is associated with a strong evolution of heat; roughly 30 % of the cement reacts during this period. The C-S-H forms a thickening shell around the cement grains which surrounds the AFt rods, and at ~12 h adjacent shells (about 0.5 – 1.0 μm thick) are beginning to merge. This is known as the cohesion point and corresponds to the completion of the setting. The morphology of the C-S-H phase is dependent on the space available for growth. If space is rather restricted honeycombs or networks of reticular C-S-H forms whereas fibres of C-S-H develop if space is freely available.

In the originally water-filled capillary pores between the cement grains portlandite forms massive crystals which may grow to enclose some of the smaller cement grains. Spaces filled with a highly concentrated solution develops between the inside wall of the shells and the anhydrous material which is approximately 0.5 μm wide at 12 h. The shells are sufficiently porous at this stage for ions to migrate readily through them. The existence of these spaces shows that reaction proceeds by dissolution and precipitation processes.

A renewed growth of the AFt phase is observed towards the end of this middle period. However, the AFt crystals are much longer (normally 1 – 2 μm, and sometimes up to 10 μm) than the ones formed in the early period. This growth is associated with a shoulder on the heat evolution curve (see Fig. 4.2).

3.4.3. Late period of hydration (> 24 h)

As the permeability of the shells decreases C-S-H begins to deposit on their inside surfaces and the space between the shells and the anhydrous core is gradually filled up. The deposition of C-S-H is proceeding at a faster rate than the dissolution of the anhydrous cores, and after about seven days the spaces have disappeared and the shells have a typical thickness of approximately 8 μm. Cement grains smaller than 5 μm have normally reacted completely before this period. Once the space between shell and core have filled up reaction is slow and probably occur by a topochemical mechanism [118].

In old cement pastes three different regions of C-S-H can be observed in the relicts of larger fully reacted cement grains: (1) an outer layer (~1 μm thick) that formed through solution in the originally water-filled space between cement grains, (2) a middle layer roughly 8 μm thick that was deposited on the inside of the shells, and (3) a central core that has transformed into C-S-H through a topochemical reaction. The terms “inner product” and “outer product” are often used to distinguish the types C-S-H that forms within the cement grains and in the water-filled space between the grains, respectively [119].

3.5 Hydration of blended cements

3.5.1 Portland cement – slag blends

The hydration of cement blends containing blastfurnace slag results in products essentially similar to those of plain Portland cements. However, magnesium from the slag enters a hydrolatcite-type phase [120-122]. Besides containing a smaller amount of portlandite, the microstructures of cement – slag blends are also fairly similar to those observed for plain Portland cement pastes. Layers/rims of gradually inward thickening hydration products form at the boundaries of the slag grains, as with the cement grains. Richardson and Groves [122] concluded from a TEM study that the C-S-H formed in the originally water-filled space between the anhydrous cement and slag grains show progressively less fibrillar and more foil-like morphologies as the content of slag increases in cement – slag blends. In

general, lower Ca/Si ratios are observed in the C-S-H phases of cement – slag pastes that in those of plain Portland cements [122-124]. Furthermore, the Ca/Si ratio has been reported to decrease with increasing proportion of slag in the blend [122]. A hydration product called strätlingite ($Ca_2Al_2SiO_2(OH)_{10}\cdot 2.25H_2O$) may form if the slag, or the blend as a whole, has a very high content of Al_2O_3 [121].

3.5.2 Portland cement – fly ash blends

Broadly similar hydration products form upon hydration of cement – fly ash blends and of Portland cement, but lower amounts of $Ca(OH)_2$ are formed in the former case. The presence of fly ash also results in C-S-H with lower Ca/Si and higher Al/Si ratios [1], and the content of alkalis is normally higher if fly ash is present [55,125]. Cement – fly ash pastes develop microstructures roughly similar to those of plain Portland cement [55,126]. In sufficiently old pastes reaction rims may be observed around the fly ash particles [1]. According to Mohan and Taylor [127] the polymerization of silicate tetrahedra in the C-S-H phase occurs at a quicker rate in C_3S pastes containing fly ash than in pure C_3S paste.

3.5.3 Portland cement – natural pozzolan blends

These blends give roughly the same products upon hydration as plain Portland cement, but since the overall composition of the cements blended with natural pozzolan are different from that of Portland cement, the hydration products occur in different percentages, *i.e.*, less $Ca(OH)_2$ and more C-H-S is formed in the cement – natural pozzolan blends [128]. The C-S-H phase generally has a lower Ca/Si ratio and higher alumina content than in plain Portland cement pastes. Depending on the composition of the natural pozzolan formation of additional minor hydration products like strätlingite, hydrogarnet or different C_4AH_x phases may occur [1]. The microstructure of hydrated cement – natural pozzolan blends does not differ significantly from that of Portland cement besides the lack of large $Ca(OH)_2$ crystals.

3.5.4 Portland cement – microsilica blends

As with the other SCMs the hydration products generated from cement – microsilica blends are similar to those of plain Portland cements, but again the formed C-S-H has a lower mean Ca/Si ratio. Furthermore, a higher degree of polymerization is observed for the chains of silicate tetrahedra in the C-S-H structure [75,76].

Chapter 4

Analytical techniques commonly used in cement research

4.1 Introduction

A wide range of analytical techniques have been used for the characterization of cementitious materials and concrete throughout the years. An attempt to treat them all is beyond the scope of the present thesis. Therefore, this chapter mainly concentrates on introducing techniques that have been employed during data acquisition in this project. Particular focus is addressed on how these techniques can be utilized to obtain quantitative information about the constituent phases of the studied systems, as this forms the basis for determining degrees of hydrations for the clinker phases and SCMs, which is a principal objective of the present project. An introduction to solid-state NMR and its application in cement research is given separately in Chapter 5.

4.2 X-ray diffraction analysis

Powder X-ray diffraction (XRD) is one of the most important techniques used in the characterization of cementitious materials [129]. It has been utilized for many years to identify and quantify the crystalline phases in Portland cement. XRD-based quantifications of the main constituents of cements have not always been successful, though. This is due to several well-recognized problems, some of which are briefly outline below.

Portland cements are multiphase systems and overlapping of peaks from different phases occurs in the XRD pattern. Especially the predominant alite phase tends to swamp the peaks of the other phases. For example, all the strong peaks from belite are overlapping to some extend with ones deriving from alite [1]. Another problem is the variability of the XRD peaks from Portland cements. Such effects are due to both compositional variations and peak broadening. In real Portland cement clinker C_3S, C_2S, C_3A and C_4AF do not exist as pure phases, but with a substantial amount of guest ions incorporated in their crystal lattices. Depending on which raw materials are used in the cement manufacture the amount of these guest ions will vary from one cement plant to another. For example, one plant may

use a raw feed particularly high in Mn, and a significant amount of the Mn may end up in the ferrite phase [130], which effectively will introduce changes the XRD pattern.

Crystals diffract X-rays and the amount of diffraction is dependent on the crystallinity. Amorphous materials are lacking the long-range order in the arrangement of its constituent atoms as compared to the high degree of order observed in well-crystallized substances. As a consequence, amorphous materials give rise to very diffuse and weak diffraction peaks, sometime referred to as 'amorphous humps'. This problem is encountered with the nearly amorphous C-S-H phase in hydrated cement pastes, as well as with many of the most commonly used SCMs in blended cements (*e.g.*, fly ash, slag, and microsilica). Broadening of the XRD peaks can also occur due to overgrinding, or compositional zoning of crystals.

The possible presence of amorphous matter is often an overlooked issue in XRD based determinations of the relative amounts of the constituent phases in anhydrous Portland cements, as the material has traditionally been believed to consist completely of crystalline phases [1]. However, this notion has been challenged by several authors. The combination of XRD with Rietveld analysis allows the content of amorphous material to be determined by the use of either an internal or external crystalline standard (*e.g.*, rutile (TiO_2)) [131-133]. In the internal standard method a defined quantity of crystalline standard material is mixed with the sample, which makes it possible to determine the ratio of crystalline material in the sample to crystalline standard and thus calculate the amount of amorphous material [134]. In the external standard method the XRD data are obtained separately (under identical conditions) for the sample and the standard, thereby avoiding complications that may be caused by grinding and mixing the sample with an internal standard [133].

Yang [135] determined the amorphous content in a number of synthesized clinker minerals and hydration products. He found 12 wt% in alite, 1 – 15 wt% in β-C_2S, 12 wt% in C_4AF, 7 wt% in C_3A, 25 – 35 wt% in ettringite, and 14 % in portlandite. A number of cement clinkers were studied by Suherman *et al.* [132] who reported total contents of amorphous materials varying between 6 wt% and 15 wt%, while De La Torre *et al.* found 7 wt% [136] and 19 wt% [137] of amorphous content in a cement clinker and a sample of monoclinic C_3S, respectively. If not taken into account, the presence of such significant

amounts of amorphous matter in the cement phases can lead to serious errors in the phase quantification.

Problems associated with preferred orientation can arise during loading of the specimen holder if platy or needle-shaped crystals are present in the powder under investigation. This phenomenon of particle packing in a preferred orientation can affect the peak intensities in the XRD pattern. In cementitious materials such effects are sometime seen with the alite and portlandite phases, and especially with the sulphate minerals gypsum, anhydrite and hemihydrate due to their characteristic cleavage and relative softness [138]. The problem with preferred orientation can practically be eliminated by grinding the sample material to a fineness < 1 μm and by using the so-called back-filling method when loading the sample holder [129].

Absorption contrast, also known as microabsorption, is a consequence of crystals variable ability to absorb X-rays. It is a phenomenon which causes reduced diffraction of the high absorbers relative to the low absorbers. The effect is diminished if sufficient grinding is carried out during sample preparation, ideally to a grain size below 1 μm. In Portland cements the phases all have fairly similar absorption coefficients except for the ferrite phase in which case the effect can be significant.

4.2.1 XRD with Rietveld analysis

In the late 1980s, XRD combined with Rietveld analysis was introduced as a method for quantifying the phase contents in anhydrous Portland cement and the approach has since become increasingly popular due to its speed and perceived simplicity [129,139-142]. The principle of the Rietveld analysis [143] is to iteratively minimize a function M, which represents the difference between an observed (experimental) XRD pattern and a pattern simulated (calculated) from crystal parameters and equipment parameters for a mixture of known phases. The accuracy of phase quantification by XRD with Rietveld analysis has improved considerably in recent years due to work on the input files ("control files") for the crystal structures used in the Rietveld refinement [131,144,145]. Maximum errors for the determination of major and minor phases in typical cementitious materials have been reported by Walenta *et al.* [145] and are presented in Table 4.1.

Table 4.1 Typical contents of the major and some minor phases in Portland cement along with accuracies for the phase quantification by XRD with Rietveld analysis [145].

Phase	Typical content (wt%)	Accuracy (± wt%)
Alite	60	2
Belite	15	1.5
Aluminate	4	0.6
Ferrite	4	0.6
Free lime	1	0.3
Gypsum	2	0.3
Calcite	1	0.3

In a Rietveld analysis the sum of the phases present in the sample is normalised to 100 %. Consequently, crystal data for all phases expected to be present must be entered into the analysis, which ultimately requires knowledge of the crystal structures of the cement phases. The presence of amorphous or unknown phases will result in too high estimates for the quantity of the crystalline phases. Such overestimations may be circumvented by adding a known amount of an internal standard to the sample [146], *e.g.*, rutile (TiO_2) or corundum (Al_2O_3). The phase quantities from the Rietveld analysis may then be corrected by dividing the overestimated values by the ratio of the measured to true amount of internal standard. The amorphous content can be calculated by subtracting the total of the corrected quantities of phases from 100 %.

Recently, the application of XRD with Rietveld analysis has been extended from anhydrous to hydrated cements. Scrivener *et al.* [147] followed the hydration of a typical Portland cement quantitatively using the Rietveld method and found a good agreement between the obtained results and independent measures for the same material from analysis of back-scattered electron images (BSE/IA). During the last decade the development of the Rietveld method for phase quantification has reached a level of such sophistication and speed that cement plants are beginning to implement this technique as a means for automated on-line quality control of the clinker production [138,148,149]. A XRD measurement can be performed in roughly 10 min which is very fast compared to, for example, phase quantification by SEM where a minimum of 5 hours is needed for sample polishing and the actual analysis [147].

4.3 Light microscopy

The use of light microscopy can provide information about the microstructure of clinkers and thereby on the conditions prevailing at different stages of the clinker formation [150]. The technique is therefore often used as a mean to find the cause of unsatisfactory clinker quality. Other applications include quantitative determination of phase composition [151] and prediction of strength development [152]. Most often polished or etched sections are examined in reflected light, but valuable information can also be obtained by studying thin sections in transmitted light. It is very important to work on a representative sample when using light microscopy. Otherwise, misleading conclusions about the investigated material can easily be drawn.

The combination of point counting and light microscopy can be utilized to quantify the phases in cement clinker. The determination is based on the principle that the areas of the phases on the polished section are proportional to their volumes in the sample. Sources of error include imperfect sampling, incorrect phase identification by the operator and the presence of inclusions too small to be observed. Errors can also arise from counting statistics, which depends on the number of points and the grain sizes of the phases. Hofmänner [151] has specified that quantifications based on 4000 points normally gives a reasonable precision. Another problem regularly encountered with light microscopy is difficulty in distinguishing tricalcium aluminate from ferrite since these phases tend to be mixed on a scale of a few micrometers with the ferrite forming dendrites or needles in a matrix of aluminate.

4.4 Scanning electron microscopy

Information essentially similar to that given by light microscopy can be obtained from backscattered electron (BSE) imaging acquired in a scanning electron microscope (SEM) [114,153-156]. In addition, the SEM often provides the possibility to attain chemical analyses of the phases on the micrometer scale by so-called energy dispersive X-ray spectroscopy (EDS). Another advantage is the opportunity to store the images electronically for various subsequent analyses.

Grey levels in the BSE images can be used to distinguish between the clinker phases as the intensity of the electron backscattered from a certain region of the sample depends approximately on the average atomic number of the material in that region [157].

Image analysis makes it possible to quantify the BSE image and thus determine the relative proportions of the anhydrous clinker phases by using the abovementioned grey level discrimination. The subjectivity of a quantification based on light microscopy is eliminated with this technique.

It is also possible to distinguish between the anhydrous (unreacted) clinker phases and the hydration products in a cement paste on the basis of grey levels [126,156,158], which allows a determination of the total degree of hydration (α_{SEM}) as defined by:

$$\alpha_{SEM} = \frac{V_{anhydrous}^{t=0} - V_{anhydrous}^{t}}{V_{anhydrous}^{t=0}} \tag{4.5}$$

where the total volume fraction (V) of the anhydrous phases of the cement paste before (t = 0) and after a certain time (t) of hydration are used for the calculation. The grey level differences between the various hydration products (C-S-H, ettringite, monosulphate, etc.) are too small for these to be distinguished individually, though [156]. Fig. 4.1 gives an example of a BSE image of a Portland cement paste.

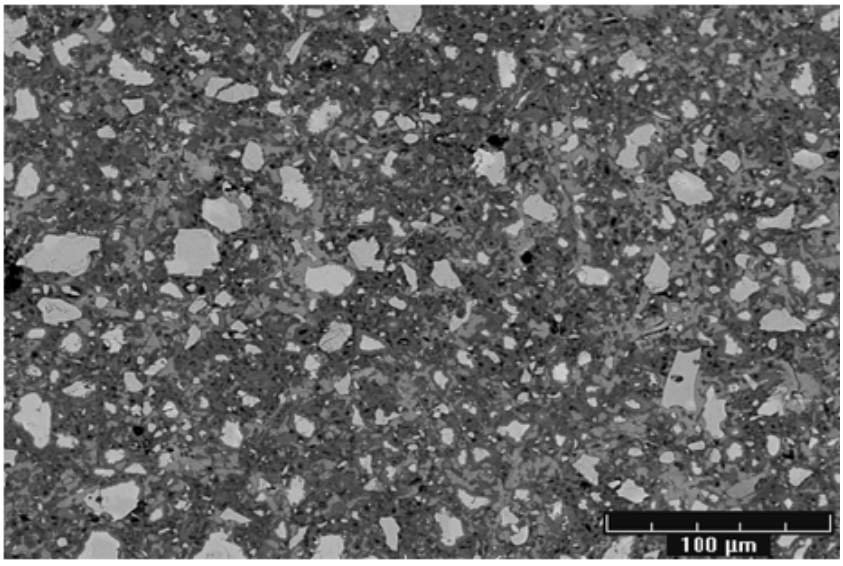

Fig. 4.1 Backscattered electron image of a white Portland cement paste (w/c = 0.4), aged three days. The brightest areas are of unreacted cement grains while the hydration products appear darker. The image was acquired at Laboratory of Construction Materials, EPFL, Switzerland using SEM and was kindly provided by Vanessa Kocaba. The sample is cement A of this project.

In recent years, this type of analysis has also been applied to blended cement pastes. Feng *et al.* [159] employed SEM combined with point-counting to study the hydration of cement blends containing either fly ash or blastfurnace slag. Besides the degree of cement hydration they were also able to determine the degree of reaction for the fly ash and slag.

Despite the fact that analysis of BSE images can provide valuable quantitative data a number of limitations are associated with this analytical technique [119]. These are mainly concerned with sample preparation and the position of different phases' thresholds on the grey scale. For example, transmission electron microscopy studies have shown that the hydrated remains of relatively small particles of Portland cement, fly ash or slag contain a less dense product, surrounded by a zone of denser C-S-H [119]. This denser zone can make it difficult for the resin used during the preparation of the specimen for BSE to penetrate the less dense interior. During the subsequent polishing this interior material may be removed. In the resulting BSE image such small grains will appear as isolated pores.

4.5 Transmission electron microscopy

Transmission electron microscopy (TEM) is a powerful tool for examining microstructural features of cement clinker and their hydration products [119]. Normally either dispersed or ion-beam-thinned specimens are studied with TEM. If equipped with an energy dispersive spectrometer (EDS), a major advantage of TEM is the possibility to combine the microstructural studies of images with analytical X-ray spectroscopy performed on very small sample regions. This allows an identification of phases and the chemical analysis obtained from the EDS is free from interfering contributions from neighbouring phases. TEM has been used in numerous studies on the morphology and chemical composition of the C-S-H phase [160-163], also in cement pastes containing different types of SCMs [97,164,165]. Various attempts to perform high-resolution TEM imaging have been unsuccessful due to thermal and irradiation damage of the specimens [119].

4.6 Isothermal calorimetry and thermal analysis (DTA/TGA)

The hydration of cement is an exothermic process and variations in the heat generation reflect the hydration reactions taking place. A typical heat evolution curve from isothermal

calorimetry is shown in Fig. 4.2. The degree of cement hydration α(t) at time t is often approximated with the amount of heat (Q(t)) liberated until that time:

$$\alpha(t) = \frac{Q(t)}{Q_{tot}} \qquad (4.6)$$

The total heat of hydration (Q_{tot}) liberated after complete hydration is estimated from the chemical composition of the cement using the Bogue calculation and the heat of hydration of the individual cement phases [166]. It is not possible to deduce the degree of hydration for the individual clinker phases using this approach.

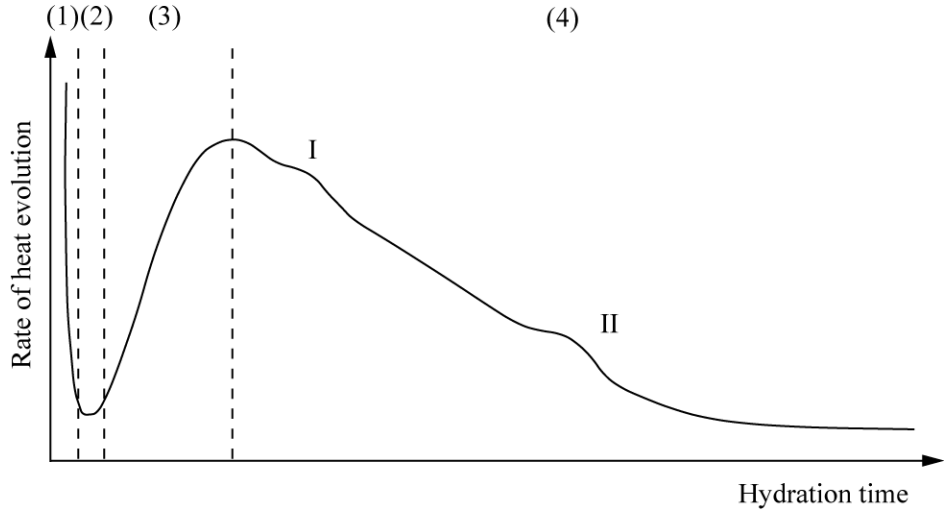

Fig. 4.2 Schematic rate of heat evolution curve illustrating the hydration of a typical Portland cement. The evolution is divided into four stages: (1) Pre-induction stage, (2) dormant stage, (3) acceleration stage, and (4) post-acceleration stage. Renewed formation of AFt and the conversion of AFt to AFm give the shoulders at I and II, respectively.

When considering blended cements the influence of the added SCM on the hydration can be followed by isothermal calorimetry [167]. For instance, the curve shape in Fig. 4.2 will change substantially if blastfurnace slag is added to the system [122,168] indicating the impact of the slag on heat liberation and thus on the hydration process. Pozzolanic reaction is known to occur in blended cement pastes also at later stages of the hydration process where the heat generation is low [166,167,169]. Consequently, isothermal calorimetry is not well-suited for hydration studies at later stages. Differential thermal analysis (DTA) combined with thermogravimetric analysis (TGA) is more appropriate for this purpose.

TGA/DTA have been employed in the study of cementitious materials for various purposes, *e.g.*, to study the hydration reactions in Portland cement pastes [170], for identification of phases formed upon hydration [171], and to investigate the effects of mineral additives (such as SCMs) on hydration [172], and to determine the content of $Ca(OH)_2$ in cement pastes.

Recently, Pane and Hansen [173] have quantified the overall degree of hydration for blended cements containing either fly ash, blastfurnace slag or microsilica by using a combination of DTA and TGA together with a so-called three-parameter hydration equation (TPE). Furthermore, they also quantified the degree of hydration for the individual SCMs by a method based on measurements of decomposition of $Ca(OH)_2$ combined with the abovementioned TPE.

4.7 Bogue calculations

The bulk chemical composition of a Portland cement clinker (*e.g.*, from a wet-chemical or X-ray Fluorescence (XRF) analysis) can be converted into a hypothetical quantitative phase composition by the Bogue equations [1,174]. For the calculation it is assumed that (*i*) the four major phases exist in their pure forms, *i.e.*, as C_3S, C_2S, C_3A and C_4AF, (*ii*) all Fe_2O_3 is allocated to C_4AF, (*iii*) the remaining Al_2O_3 occurs as C_3A, (*iv*) the amounts of CaO attributable to C_4AF, C_3A and free lime is subtracted from the total CaO content, and two simultaneous equations are solved to obtain the amounts of C_3S and C_2S. This gives the following four equations, in which the quantities of the components are given as weight percentages (wt%) and it is assumed that the CaO content has been corrected for free lime.

$$C_3S = 4.0710 \cdot CaO - 7.6024 \cdot SiO_2 - 6.7178 \cdot Al_2O_3 - 1.4297 \cdot Fe_2O_3 \quad (4.7)$$

$$C_2S = -3.0710 \cdot CaO + 8.6024 \cdot SiO_2 + 5.0683 \cdot Al_2O_3 + 1.0785 \cdot Fe_2O_3$$

$$= 2.8675 \cdot SiO_2 - 0.7544 \cdot C_3S \quad (4.8)$$

$$C_3A = 2.6504 \cdot Al_2O_3 - 1.6920 \cdot Fe_2O_3 \quad (4.9)$$

$$C_4AF = 3.0432 \cdot Fe_2O_3 \quad (4.10)$$

The calculation can be applied for cements as well as clinkers if the CaO content is further corrected by the amount attributable to the calcium sulphate phase ($0.7 \cdot SO_3$). Minor oxide

components like Na_2O, K_2O and P_2O_5 are ignored in the calculation, where it is also assumed that all Mg^{2+} occurs as periclase (MgO).

Nowadays, it is commonly agreed that the standard Bogue calculation gives rather unrealistic phase compositions. In comparison with other experimental quantification techniques, such as XRD or optical microscopy, the Bogue approach tends to under- and overestimate the alite and belite contents, respectively. The two main sources of error in the calculation are (*i*) the assumption that thermodynamic equilibrium is maintained during cooling of the clinker and (*ii*) that the chemical composition of the phases differs markedly from those of the pure phases.

Taylor has proposed a modified Bogue calculation which takes into account the significant incorporation of substituent ions observed in the major phases of industrially manufactured cement clinkers [1,175]. The compositions employed in such a Taylor-modified Bouge calculation are given in Table 1.1. If converted to stoichiometric formulas, Taylor compositions for alite and belite are $Ca_{2.91}Si_{0.96}Mg_{0.06}Al_{0.04}Fe_{0.02}Na_{0.01}O_5$ and $Ca_{1.94}Si_{0.9}Al_{0.07}K_{0.03}Fe_{0.02}Mg_{0.02}$-$Na_{0.01}S_{0.01}O_{3.93,}$ respectively. These compositions should be valid for Al_2O_3/Fe_2O_3 ratios (by weight) in the range 1.5 to 3.0. Compared to the standard Bogue calculation much more realistic quantities of the phases are estimated using Taylor's modified calculation.

Alternatively, chemical compositions obtained from SEM/EDS analysis of the individual phases can be used in a modified Bogue calculation, thus employing the actual compositions of the phases rather than the approximated ones of the Taylor-modified Bogue calculation.

4.8 Selective dissolution methods

Numerous dissolution methods have been proposed as means to physically separate the phases in Portland cement clinker. Such approaches are often combined with other analytical techniques, *e.g.*, XRD, microscopy or solid-state NMR, for phase identification and quantification. Takashima [176] introduced an effective method in which a solution of salicylic acid in methanol (SAM) is utilized to dissolve the silicate phases thus leaving a residue consisting of aluminate, ferrite and additional minor phases. The SAM reagent dissolves free lime, alite and belite at rates decreasing in that order and the composition of the reagent can be adjusted to dissolve all of the alite and belite, or to remove much of the

alite, to give a residue suitable for studies of the belite phase [177]. The silicate phases can also be dissolved by a solution of maleic acid in methanol [178]. This method is quicker than the SAM dissolution, but may involve problems with ettringite formation if the methanol contains water [179]. Gutteridge [180] has devised a method for separating the silicate phases by dissolution of the interstitial aluminate and ferrite phases. The extraction is achieved by using a solution of sucrose in aqueous potassium hydroxide, also known as KOSH reagent. A sample consisting mainly of belite can be obtained if the SAM and KOSH procedures are used in combination.

Various selective dissolution methods have been used to determine the amount of unreacted blastfurnace slag in hydrating cement – slag blends. Luke and Glasser [112,181] made comparative studies of such methods and concluded that the most satisfactory results were obtained by using a modified version of Demoulian *et al.*'s method [182], in which an alkaline solution of ethylenediaminetetraacetic acid (EDTA) in aqueous triethanolamine dissolves all constituents other than the unreacted slag. They also reported that this technique was less suitable for determining the content of unreacted fly ash in pastes of cement blends containing fly ash. In more recent studies, Lumley [58] and Escalante [183] used further modified versions of the method of Demoulian *et al.* with the purpose of measuring the degree of reaction for slag in cement – slag pastes, while Dyson *et al*. [113] used a combination of selective dissolution and ^{29}Si MAS NMR to quantify the slag reaction in a cement – slag blend. Coole [184] used HCl to dissolve all phases, except fly ash, in hydrated cement – fly ash blends to determine the amount of unreacted fly ash. Taylor *et al.* [125] used a similar approach, but exposed samples to salicylic acid in methanol in addition to HCl.

4.9 Chemical shrinkage

The reaction between cement and water in a hydrating cement paste is associated with a reduction in volume, since the hydration products occupy a smaller volume than the starting materials (anhydrous cement + water), a phenomenon known as chemical shrinkage. The hydration rate can be quantified in a convenient and rather inexpensive manner by measuring the chemical shrinkage of a hydrating paste [185]. The chemical shrinkage is directly proportional to the degree of hydration of the cement at early curing

ages [186]. However, this technique does not allow quantification of hydration degrees for the individual components of the hydrating cement.

Chapter 5

Introduction to solid-state NMR and its application in cement research

5.1 Introduction

Since the advent of high-resolution solid-state NMR spectroscopy in the early 1980s (facilitated by improvements in the magic angle spinning (MAS) technique), numerous applications of this analytical technique have been established the studies of anhydrous cementitious materials and their reaction products [187-190]. A range of different NMR nuclei can be used as probes with ^{1}H, ^{27}Al, and ^{29}Si being the most frequently used in cement research, but other nuclei have been employed as well, *e.g.* ^{17}O, ^{2}D, ^{23}Na and ^{35}Cl.

The NMR technique is most sensitive to the local ordering and structure around the observed NMR nucleus as opposed to X-ray diffraction measurements where the long-range ordering of crystalline materials is detected. Solid-state NMR is therefore well-suited for investigations of both crystalline and amorphous/poorly crystalline materials such as the C-S-H phase formed by cement hydration and different SCMs types characterised by a high content of largely amorphous matter. Furthermore, NMR makes it possible to study different phases separately by utilizing specific NMR active nuclei, for example for selective studies of the aluminate phases or of the calcium silicates by employment of the ^{27}Al and ^{29}Si nuclei, respectively.

The first part of this chapter gives a general introduction to solid-state NMR and a few of the most widely used experimental NMR techniques in cement research. Subsequently, the application of solid-state NMR in the study of cementitious materials is presented with the main emphasis on ^{29}Si and ^{27}Al NMR.

5.2 Solid-state NMR

5.2.1 Spin interactions and magic angle spinning (MAS)

Static-powder solid-state NMR spectra normally suffer from severe line broadening of resonances caused by various interactions between the spin nuclei, such as homo- and heteronuclear dipolar and indirect (J-coupling) spin-spin couplings, the chemical shielding

interaction, and for spin nuclei with $I > ½$, the quadrupole interaction. For these interactions the first-order Hamiltonian contains the geometric factor $(3\cos^2\theta - 1)$, where θ is the angle between a specific molecule-fixed vector and the static magnetic field. This geometric factor is averaged to zero in liquids by rapid molecular tumbling and the so-called magic-angle spinning (MAS) technique can be employed in solid-state NMR to mimic this molecular tumbling by rotating the sample around a fixed axis relative to the static magnetic field. If the rotation is performed around an axis that is inclined 54.736° (the 'magic' angle) relative to the static magnetic field the term $(3\cos^2\theta - 1)$ become equal to zero and the anisotropic interactions are thus eliminated or reduced significantly. This technique improves the resolution in the NMR spectra by narrowing the resonance lines. For a complete elimination of the line broadening effects, originating from the anisotropic interactions, the spinning speed needs (ν_R) to be larger than the width of the resonance in a static-powder experiment. A pattern of spinning sidebands will appear in the spectrum if this requirement is not fulfilled.

The dipolar and chemical shielding anisotropy (CSA) interactions can, in many cases, be eliminated completely by MAS with spinning speeds in the range 5 – 35 kHz [189]. Another experimental/technical means to improve the resolution of solid-state NMR spectra is the use high-power ^{1}H decoupling to remove the strong dipolar coupling between ^{1}H and the spin nucleus under detection.

5.2.2 Chemical shielding anisotropy (CSA)

The Hamiltonian for the chemical shielding and its anisotropy is given by $H_\sigma = \bar{I} \cdot \bar{\bar{\sigma}} \cdot \bar{B}$, where $\bar{\bar{\sigma}}$ is the CSA tensor describing the coupling of the spin ($\bar{I}$) with the external magnetic field $\bar{B} = (0, 0, B_0)$. In its principal axis system the CSA tensor takes the following form:

$$\bar{\bar{\sigma}} = \begin{pmatrix} \sigma_{xx} & 0 & 0 \\ 0 & \sigma_{yy} & 0 \\ 0 & 0 & \sigma_{zz} \end{pmatrix} = \begin{pmatrix} \sigma_{iso} - \frac{\delta_\sigma}{2}(1+\eta_\sigma) & 0 & 0 \\ 0 & \sigma_{iso} - \frac{\delta_\sigma}{2}(1-\eta_\sigma) & 0 \\ 0 & 0 & \sigma_{iso} + \delta_\sigma \end{pmatrix} \qquad (5.1)$$

where the principal elements are defined according to $|\sigma_{zz} - \sigma_{iso}| \geq |\sigma_{xx} - \sigma_{iso}| \geq |\sigma_{yy} - \sigma_{iso}|$ [191]. The trace of the tensor is the isotropic chemical shift: $\delta_{iso} = - \sigma_{iso} = -1/3(\sigma_{xx} + \sigma_{yy} + \sigma_{zz})$. At slow spinning speeds the intensity distribution in the pattern of spinning sidebands resembles the line profile of the corresponding static-powder NMR spectrum and the principal elements of the ^{29}Si CSA tensor can be determined from simulations of the spinning sideband intensities [192]. Hansen *et al.* [193] used such an approach for the determination of CSA parameters for a number of synthetic calcium silicates and calcium silicate hydrates from simulated spinning sidebands in ^{29}Si MAS NMR spectra recorded using slow-speed spinning (*i.e.*, $\nu_R \leq 1000$ Hz) at a relatively high magnetic field (14.1 T).

5.2.3 Cross-Polarization

Solid-state NMR spectra of dilute spin-½ nuclei (*e.g.*, ^{29}Si or ^{13}C) obtained using a single-pulse experiment frequently suffer from inherently low sensitivity and from the fact that very long recycle delays are often required due to long spin-lattice relaxation times (T_1). Application of the so-called Cross-Polarization (CP) technique can partly overcome these shortcomings [194].

If we assume we have a system with dipolar coupled spin pairs of *I* and *S*, where *I* is an abundant (or highly sensitive, *i.e.*, high gyromagnetic ratio γ) nucleus and *S* is a diluted spin (low natural abundance) then the principle of the CP technique is to transfer magnetization from the abundant to dilute nucleus to obtain a signal enhancement. The CP pulse sequence is schematically outlined in Fig. 5.1 for a ^{29}Si{^{1}H} CP/MAS NMR experiment, *i.e.*, where $I = {}^1$H and $S = {}^{29}$Si. In the CP experiment the *I* spins are first excited by a $(90°)_x$ pulse. Subsequently, the *I* magnetization is locked by a long *I* y-phase pulse. The *S* rf channel is switched on at this moment and the amplitude of this field (B_{1S}) is adjusted to meet the so-called Hartmann-Hahn matching condition ($\gamma_I B_{2I} = \gamma_S B_{1S}$) [195]. During the CP contact time (τ_{CP}) magnetization is transferred from *I* to *S* for spins that are dipolar coupled. The maximum signal enhancement obtainable from such a CP magnetization transfer is theoretically given by the ratio of the gyromagnetic ratios for the two spins. In the example with ^{1}H and ^{29}Si this ratio is $\gamma_H/\gamma_{Si} \approx 5$. However, in practice the factor of signal enhancement is usually somewhat lower. Besides the gain in signal intensity, the CP technique may also have the advantage of shortening the recycle delay

significantly, as this delay is determined by the spin-lattice relaxation time (T_1) of the abundant spin, which is often much shorter than T_1 for the dilute spin.

A third advantage is the ability to use the CP experiment as a sort of '^{1}H filter', since only dilute species (*e.g.*, ^{29}Si) having ^{1}H atoms in their nearest surroundings are observed, whereas dilute spins without protons in their close vicinity do not appear in the CP spectrum.

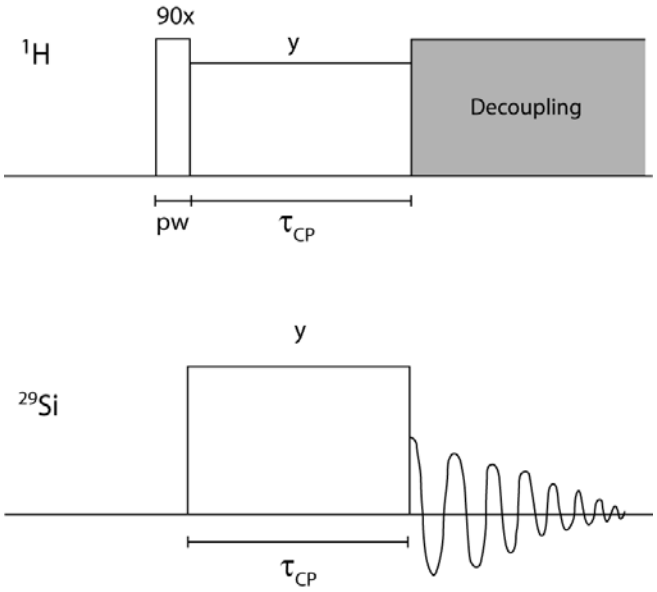

Fig. 5.1 The Cross-Polarization (CP) rf pulse sequence. τ_{CP} is the cross-polarization contact time and pw is the pulse width. During acquisition of the FID the ^{1}H atoms are decoupled. ^{1}H is the abundant spin (*I*) and ^{29}Si is the dilute spin (*S*).

5.2.4 ^{29}Si MAS NMR

Static-powder ^{29}Si NMR spectra of solid silicates give direct information regarding the anisotropy of the ^{29}Si chemical shift [196]. However, such spectra suffer from very broad and often overlapping resonances. The line broadening is mainly due to chemical shielding anisotropy, which can be removed by implementation of the MAS technique. MAS also provides the advantage of removing weak heteronuclear dipolar couplings to distant ^{1}H atoms or other NMR-active nuclei (*e.g.*, ^{27}Al). Stronger dipolar interactions of ^{29}Si with ^{1}H atoms in closer vicinity may be eliminated by the use of high-power ^{1}H decoupling.

For ^{29}Si (I = ½) the chemical shielding anisotropy (CSA) represents the dominant internal interaction, when dipolar couplings to ^{1}H are removed by ^{1}H high-power decoupling and/or MAS. Solid-state ^{29}Si MAS NMR offers the possibility to probe the

local structure around Si atoms in a very sensitive manner. Therefore, the technique is a valuable complement to X-ray and neutron diffraction techniques which give information concerning the long-range order of crystalline materials. ^{29}Si MAS NMR has also proven to be very useful in the study of amorphous or highly disordered solids, where the application of X-ray diffraction techniques is less informative [196].

Due to a low natural abundance (4.7 %) the acquisition of ^{29}Si NMR spectra are rather time consuming. Furthermore, long spin-lattice relaxation times T_1 of ^{29}Si (up to several thousand seconds) often necessitate long recycle delays. As mentioned above, the employment of the CP technique can significantly shorten the recycle delay between the individual scans, since the magnetization recovery is governed by the spin-lattice relaxation time T_{1H} rather than T_{1Si}, the former being generally much shorter. The CP technique can also be utilized to distinguish between ^{29}Si species having protons in their nearest surroundings and those without. In this manner, distinction between hydrated and anhydrous calcium-silicate phases in cementitious systems is possible (Fig. 5.2).

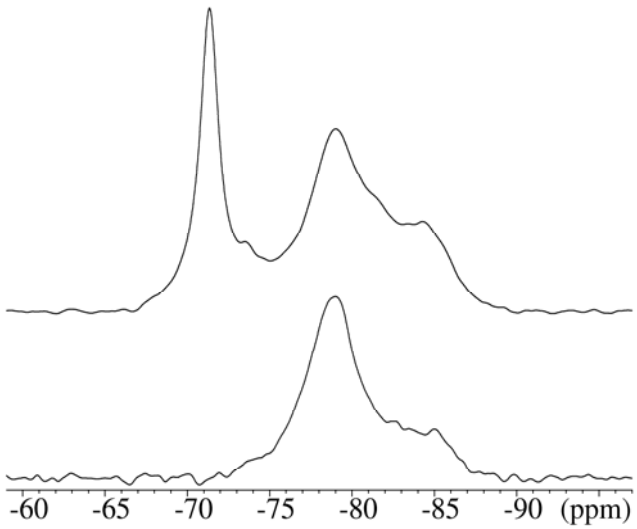

Fig. 5.2 Top spectrum: Single-pulse ^{29}Si MAS NMR spectrum of a Portland cement (cement C of this project) paste after two weeks of hydration. Both anhydrous and hydrated phases containing ^{29}Si species are observed. Bottom spectrum: ^{29}Si{^{1}H} CP/MAS NMR of the same sample. Only resonances from ^{29}Si in the hydrated phases appear in the spectrum.

^{29}Si MAS NMR spectroscopy has proven to be a valuable tool in the study of silicate structures [197]. This is due to the fact that the ^{29}Si isotropic chemical shift ($\delta(^{29}Si)$) of silicates mainly depends on the condensation (n) of SiO_4 tetrahedra (Q^n, $n = 0 – 4$). Increasing the degree of condensation has the effect of increasing the diamagnetic shielding of the ^{29}Si nucleus which leads to a shift of the resonances. A shift of approximately 10 ppm to lower frequency is generally observed for each newly formed Si-

O-Si connectivity in a given Q^n environment. On the other hand, each replacement of Si with Al in a $Q^n(m\text{Al})$ environment induces a shift of about 5 ppm towards higher frequency [198]. Here *m* equals the number of Al connected to a SiO_4 group via oxygen bridges. The ^{29}Si chemical shift is also very sensitive to the coordination number of the Si atom, since significant shifts towards lower resonance frequencies are observed on going from four- to five- to six-fold Si coordination to oxygen [199]. However, the majority of silicates contain fourfold coordinated Si, while the occurrence of five- and six-fold coordinated Si in silicates rarely is observed. Octahedral SiO_6 coordination has been reported for thaumasite ($CaSiO_3 \cdot CaCO_3 \cdot CaSO_4 \cdot 15H_2O$) and in a number of different high pressure silicate minerals (*e.g.*, the SiO_2 polymorph stishovite) [200], while five-coordinated SiO_5 has been found in quenched high-pressure alkali silicate glasses and crystalline $CaSiO_3$ samples [201].

5.2.5 ^{27}Al MAS NMR

^{27}Al (I = 5/2, 100 % natural abundance) results in much more complicated NMR spectra as compared to for example ^{29}Si (I = ½), since ^{27}Al has six non-degenerate spin-quantum energy levels (m = -5/2, -3/2 … 5/2). The transition with the highest probability is denoted the central transition (m = 1/2 ↔ m = -1/2), while transitions between the other energy levels are the so-called inner (m = ± 1/2 ↔ m = ±3/2) and outer satellite transitions (m = ±3/2 ↔ m = ± 5/2). The central transition is not affected by the first-order quadrupolar interaction ($H_Q^{(1)}$), which dominates for the satellite transitions. The effect of this first-order quadrupolar interaction can principally be removed by the employment of MAS NMR, however, the second-order quadrupolar interaction ($H_Q^{(2)}$) governing the central transition cannot be removed in this manner. ^{27}Al MAS NMR spectra are dominated by the quadrupole coupling interaction between the electric quadrupole moment (eQ) of the nucleus and the electric-field gradients (EFGs) at the site of the nucleus. The quadrupole interaction can be described by the Hamiltonian, $H_Q = \bar{I} \cdot \overline{\overline{Q}} \cdot \bar{I}$, where $\overline{\overline{Q}}$ is a second rank tensor which in its principal axis system may be expressed as:

$$\overline{\mathrm{Q}} = \frac{eQ}{2I(2I-1)h}\begin{pmatrix} \mathrm{V_{xx}} & 0 & 0 \\ 0 & \mathrm{V_{yy}} & 0 \\ 0 & 0 & \mathrm{V_{zz}} \end{pmatrix} = \frac{C_Q}{2I(2I-2)}\begin{pmatrix} -\frac{1}{2}(\eta_\sigma + 1) & 0 & 0 \\ 0 & -\frac{1}{2}(1\eta_\sigma - 1) & 0 \\ 0 & 0 & 1 \end{pmatrix} \quad (4.2)$$

employing the convention $|V_{zz}| \geq |V_{xx}| \geq |V_{yy}|$ for the traceless tensor (*i.e.*, $V_{xx} + V_{yy} + V_{zz} = 0$) [191]. The quadrupole interaction, which causes a severe anisotropic line broadening of the resonance, can be quantified by the quadrupolar coupling constant $C_Q = (eQ \cdot V_{zz}/h)$ and the EFG asymmetry parameter, $\eta_Q = (V_{yy} - V_{xx})/V_{zz}$; $0 \leq \eta_Q \leq 1$. C_Q and η_Q are sensitive structural probes and can be determined from the pattern of spinning side bands originating from the satellite transitions [202] (for small quadrupole couplings) or from a simulation of the second-order quadrupolar lineshape observed for the central transition [203]. Besides the line broadening effect, the quadrupole interaction also causes a shift for the resonances of the central and satellite transitions, which complicates a precise determination of the isotropic chemical shift (δ_{iso}).

The chemical shift of ^{27}Al is a reflection of the Al coordination state [204]. For aluminates resonances from tetrahedrally coordinated Al are observed in the region from 55 to 80 ppm, while Al in octahedral coordination results in chemical shifts from -5 to 20 ppm. The acquisition of ^{27}Al NMR spectra is generally much less time consuming than for example ^{29}Si spectra, primarily as a consequence of efficient spin-lattice relaxation and ^{27}Al having a natural abundance of 100 %.

5.2.6 Multiple-quantum MAS

The so-called multiple-quantum (MQ) MAS NMR experiment can be utilized to resolve overlapping resonances in NMR spectra of half-integer quadrupolar nuclei [205,206]. The experiment is a two-dimensional (2D) technique giving spectra with one dimension (isotropic) in which the line broadening effect from the second-order quadrupolar interaction has been removed, and an anisotropic dimension where the effect of this interaction still remains. The basic two-pulse sequence applied in the MQ MAS experiment is shown in Fig. 5.3. Triple-quantum coherences are created by the first rf pulse ($P_1(\beta_1)$) while the second rf pulse ($P_2(\beta_2)$) converts the triple-quantum coherences into observable single-quantum coherences by using appropriate phase cycling of the rf pulses

and the receiver. The temporal evolution of this single-quantum coherence will after a certain time (t_2) result in an echo signal, in which the effects from the second-order quadrupolar interaction have been refocused. The delay between the two pulses (t_1) is incremented and the free induction decay (FID) for each of the increments are accumulated to give a correlation spectrum (after 2D Fourier transformation) with an isotropic and an anisotropic dimension.

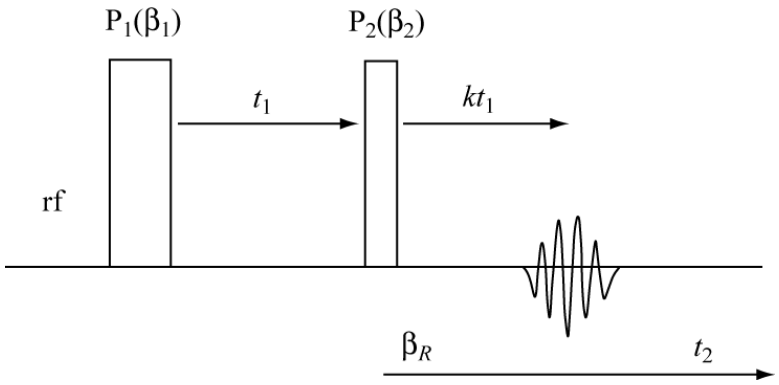

Fig. 5.3 Pulse sequence for the two-pulse triple-quantum MQ MAS NMR experiment. A six-step phase cycle of the two pulses (P_1 and P_2) and of the receiver (β_R) is used: β_1 = 0°, 60°, 120°, 180°, 240°, 300°; β_2 = 0°; β_R = 0°, 180°. After a certain time ($t_2 = kt_1$, where k depends on the spin-*I* quantum number) the evolution of single-quantum coherences results in an echo signal, where the effects from the second-order quadrupolar interaction have been refocused.

5.3 Application of solid-state NMR in the study of cementitious materials

In 1948, shortly after NMR had been discovered, Pake [207] studied the ^{1}H-^{1}H dipolar coupling in the water molecules of gypsum and thereby illustrated the potential of NMR as a research tool for studies of cementing minerals. He found that information regarding the distances between ^{1}H atoms may be derived from either ^{1}H single-crystals or powder NMR spectra.

During the following three decades NMR studies of cementitious materials were rather few. A number of researchers studied the reactions/kinetics of cement hydration by measuring variations in ^{1}H spin-lattice and spin-spin relaxation times [208-211]. The beginning of the 1980s marks a breakthrough in the application of solid-state NMR in the study of cementitious materials. This was facilitated by the new developments of high-field superconducting magnets in combination with instrumental improvements of MAS, which

made it possible to obtain high-resolution NMR spectra of spin nuclides such as ^{29}Si and ^{27}Al (see Sections 5.3.1 and 5.3.2).

Grimmer and Rosenberger [212,213] have measured ^{1}H isotropic shifts in hydrous silicates by using a combination of MAS and multi-pulse decoupling sequences to reduce the line broadening from ^{1}H-^{1}H dipolar couplings in ^{1}H NMR spectra. Subsequently, these results have been utilized to distinguish between different ^{1}H species in the C-S-H phase formed by Portland cement hydration.

Special NMR probes have been designed to facilitate high-temperature studies of clinker reactions and of the structure and dynamics of liquid silicates and calcium aluminates [214]. More recently, research groups at Ecole Polytechnique, France and University of Surrey, United Kingdom have used advanced ^{1}H NMR relaxation analysis to characterize water dynamics in the pore structure of cement pastes [215-217].

5.3.1 ^{29}Si MAS NMR applied to cementitious materials

Lippmaa *et al.* [218] carried out pioneering work on the application of ^{29}Si MAS NMR spectroscopy in the study of cementitious materials. They found that it was possible to follow the process of C-S-H formation, both qualitatively and semi-quantitatively, using ^{29}Si MAS NMR spectroscopy. This is based on the dependence of the ^{29}Si chemical shift ($\delta(^{29}Si)$) on the condensation of the SiO_4 tetrahedra (Fig. 5.4). With increasing condensation the chemical shift is displaced about 5 – 10 ppm to lower frequency for each successive degree of condensation [219-222].

The anhydrous calcium silicates of Portland cements contain isolated SiO_4 tetrahedra, which have ^{29}Si chemical shifts in the spectral region from -65 to -75 ppm. The ^{29}Si MAS NMR spectrum of pure C_3S in the triclinic form exhibits nine distinct resonances [222-224] (Fig. 5.5) in agreement with the nine distinct Si sites reported in the asymmetric unit for this phase [26]. The resonance lines appear in the range from -68.9 to -74.3 ppm and the small variation in chemical shifts between the individual resonances can be explained by minor differences in the mean Si-O bond lengths of the SiO_4 tetrahedra [223]. The ^{29}Si MAS NMR spectrum of β-C_2S, on the other hand, exhibits only one resonance, since all the Si atoms in the structure occupy equivalent crystallographic sites. However, there are small differences between the ^{29}Si chemical shifts of the α_L-, β- and γ-polymorphs

of C_2S [221,223] caused by small variations in the geometry of the SiO_4 tetrahedra in these polymorphs [223].

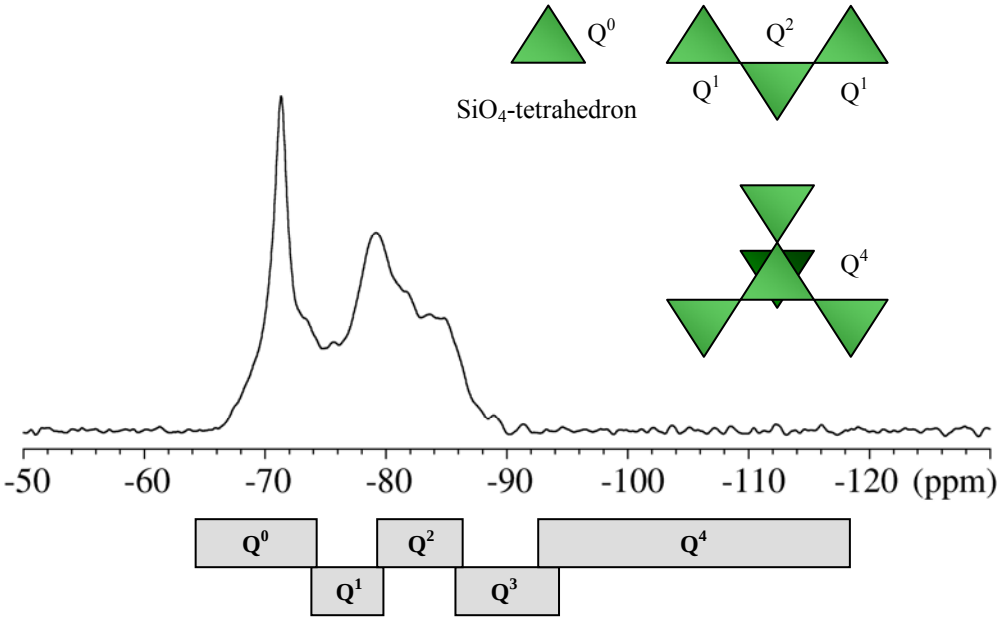

Fig. 5.4 ^{29}Si MAS NMR spectrum (9.4 T, ν_R = 12.0 kHz) of a Portland cement (cement C) after 28 days of hydration. Below the spectrum is shown the chemical shift regions for the different types of condensation of SiO_4 tetrahedra. Q represents the SiO_4 tetrahedron and the superscript gives the number of oxygen atoms in the tetrahedron involved in Si-O-Si bonding. The signal in the Q^0 region originates from ^{29}Si species in alite and belite in unreacted cement grains while the resonances in the Q^1 + Q^2 region originate from the C-S-H phase.

Fig. 5.5 ^{29}Si MAS NMR spectrum of triclinic C_3S acquired at 7.1 T using a spinning speed (ν_R) of 6.5 kHz. Nine resonances are included in the spectrum. The rather broad peak at -69 ppm includes two resonances (δ_{iso} = -68.93 ppm and δ_{iso} = 69.04 ppm) and the peak at δ_{iso} = 44.34 ppm exhibits two times the intensity relative to the other resonances.

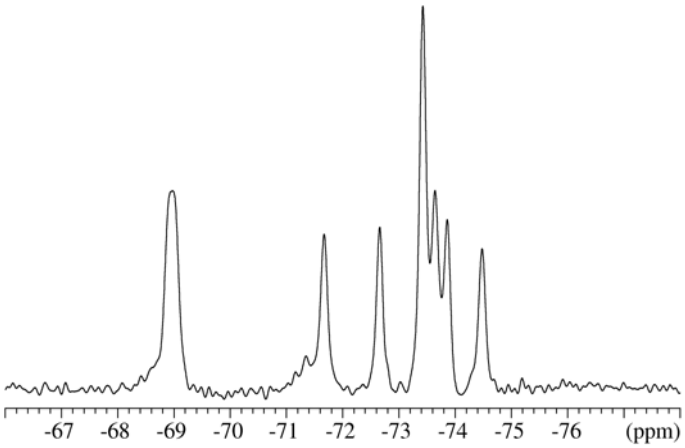

The alite phase of industrially produced cement clinkers always occurs with a significant amount of guest ions incorporated into the crystal lattice, which stabilizes either the monoclinic M_I or M_{III} forms of alite, or a mixture of the two [24]. The presence of these

impurity ions causes a slight distortion of the local environment of the SiO_4 tetrahedra which in effect broadens the individual resonances in the ^{29}Si MAS NMR spectrum. Therefore, M_I and M_{III} alite of production clinkers show complex line shapes in the ^{29}Si MAS NMR spectrum consisting of overlapping resonances. Nevertheless, Skibsted *et al.* [223] have shown that the M_I and M_{III} forms of alite can be distinguished on the basis of their characteristic ^{29}Si MAS NMR lineshapes, as illustrated by the ^{29}Si MAS NMR spectra of M_I and M_{III} alite in Fig. 5.6.

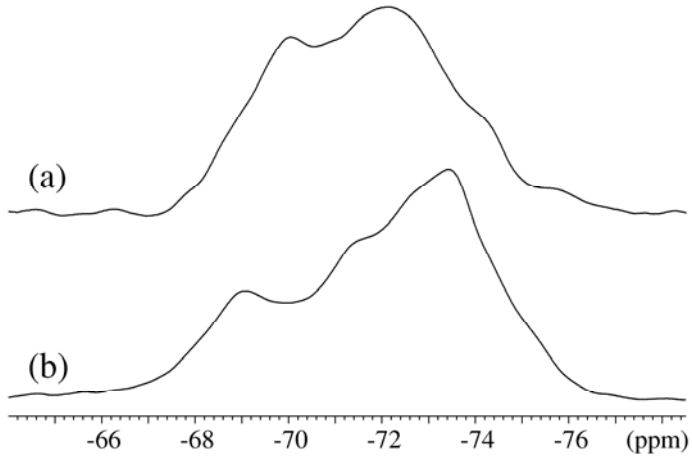

Fig. 5.6 ^{29}Si MAS NMR spectra of synthetic alite in the monoclinic M_{III} (a) and M_I (b) forms. The spectra were recorded at 7.1 T using a spinning speed (ν_R) of 7000 Hz.

^{29}Si MAS NMR spectroscopy has also been demonstrated as a valuable tool for the quantification of alite and belite in Portland cements [225]. As both alite and belite include isolated SiO_4 tetrahedra (*i.e.*, Q^0 units), the resonances from these phases occur as overlapping resonances in a ^{29}Si MAS NMR spectrum of an anhydrous cement. The determination of the alite and belite contents involves computer deconvolution of the ^{29}Si MAS NMR spectrum which gives the molar belite/alite ratio [225]. This ratio is subsequently combined with the bulk quantity of SiO_2 determined from an elemental analysis (X-ray fluorescence), thereby allowing a determination of the quantities of alite and belite. A modified version of this approach has been developed in this PhD project for quantification of alite and belite contents in various anhydrous Portland cements (see Section 6.3.2 and Paper I for further details).

As mentioned earlier, ^{29}Si MAS NMR provides a powerful analytical tool for studying the hydration of Portland cement, since the anhydrous phases (alite and belite) give resonances in the spectral region for Q^0 units, while the C-S-H formed upon hydration show resonances in the region for Q^1 ($\delta \approx -79$ ppm) and Q^2 units ($\delta \approx -85$ ppm). Q^3 and

Q^4 units are not observed in C-S-H formed at ambient temperatures and pressures, which indicate that the silica in C-S-H occurs in SiO_4 tetrahedra forming either dimers (Q^1 units) or longer chains of tetrahedra where dimers have been linked together by so-called bridging tetrahedra. The incorporation of an AlO_4 tetrahedron in the silicate chain results in a separate resonance ($\delta \approx$ -82 ppm) arising from SiO_4 tetrahedra bonded to the AlO_4 tetrahedron and a second SiO_4 unit, corresponding to a Q^2(1Al) site [226]. A determination of the relative intensities observed for the Q^1, Q^2(0Al) and Q^2(1Al) sites allows an estimation of the mean chain length of tetrahedra in the C-S-H as well as the Al/Si ratio for the C-S-H phase.

Solid-state ^{29}Si MAS NMR have also been used in many studies of different crystalline silicate hydrates. For example, Cong and Kirkpatrick [227] have investigated tobermorites and jennites using this technique. Blended cement systems containing slag, fly ash, microsilica, or other types of pozzolans can also be studied by ^{29}Si MAS NMR, as they all contain a significant amount of silicon. In the case with slag-containing blends quantitative evaluation of the spectra is normally complicated by the fact that the slag gives rise to a very broad and featureless resonance (due to its partly glassy nature), which overlaps severely with both the anhydrous silicate phases in the cement and with the C-S-H formed upon hydration [113]. High contents of iron in fly ashes can cause significant loss of signal intensities and broadening of resonances due to the presence of paramagnetic ions (Fe^{3+}), but generally the problems with overlapping signals that are encountered for cement – slag blends are less pronounced with fly ashes. The hydration of cement blends containing microsilica have successfully been investigated using ^{29}Si MAS NMR [75,76]. The broad signal from the amorphous microsilica is conveniently found in the ^{29}Si chemical shift region for Q^4 units, and thus well separated from the resonances originating from the anhydrous cement phases and from the C-S-H phase. Consequently, the extraction of quantitative information about microsilica (*e.g.*, degree of hydration) is more straight-forward from such spectra in comparison with the spectra obtained from slag and fly ash containing blends.

5.3.2 ^{27}Al MAS NMR applied to cementitious materials

Despite a typical content below 5 wt% Al_2O_3 in a Portland cement, ^{27}Al MAS NMR can be utilized to extract important information about both anhydrous and hydrated cements. For

example, ^{27}Al MAS NMR allows the hydration of tricalcium aluminate (C_3A) to be followed. This is mainly due to the fact that the reaction with water is accompanied by a transformation of Al in tetrahedral coordination into Al in octahedral coordination, which is manifested by a change in chemical shift of ^{27}Al [228].

The alite and belite phases in Portland cement clinkers invariably contain a significant amount of Al as guest ions. Skibsted *et al.* [28] reported that these Al species are observable and can be quantified even at rather low levels by ^{27}Al MAS NMR. Furthermore, they also demonstrated that Al only occupies tetrahedral sites in synthetic samples of C_3S and C_2S doped with Al, and in the calcium silicates of Portland cement, by replacement of Si^{4+}.

The ferrite phase (C_4AF), on the other hand, is generally not observed in Portland cements by ^{27}Al MAS NMR, since nuclear-electron dipolar couplings between ^{27}Al and the unpaired electron of the Fe^{3+} ions causes a severe line broadening of the ^{27}Al resonances [229].

^{27}Al MAS NMR spectra have been reported for a wide range of crystalline aluminate hydrates including phases such as ettringite, monosulphate, Fridel's salt and hydrotalcite. Quadrupole coupling parameters (C_Q and η_Q) and ^{27}Al isotropic chemical shifts have been determined for most of these phases from analysis of either the quadrupolar lineshape for the central transition, or the manifold of spinning sidebands originating from the satellite transitions. The extraction of these parameters has been valuable for the identification and quantification of ettringite and monosulphate in hydrated Portland cements [228,230].

5.3.3 Other NMR active nuclei applied to cementitious materials

NMR spectra of rare isotopes, that are practically unobservable under normal circumstances, can be made observable by isotopic enrichment. Examples include Klur *et al.*'s [231] use of the ^{43}Ca nucleus in a study of the structural evolution of C-S-H and Cong and Kirkpatrick's [227] use of ^{17}O in a structural study of some crystalline calcium silicate hydrates.

Potentially interesting NMR active nuclei in the study of cementitious materials, such as ^{2}D, ^{7}Li, ^{11}B, ^{13}C, ^{19}F and ^{31}P, have received a rather limited attention so far. However, in the present PhD project ^{31}P MAS NMR has been utilized to obtain

information about the incorporation of small amounts of phosphorus species in both anhydrous and hydrated cement phases (see Paper II).

Chapter 6

Characterization of anhydrous materials

6.1 Introduction

This chapter introduces the selection of materials studied in the project by presentation of results from XRF analysis, XRD investigations with Rietveld analysis, BSE images form SEM, granulometry, and solid-state NMR spectroscopy. The first part of the chapter concentrates on the utilization of preliminary data for choosing which materials to use for the subsequent SCM reactivity study, while the second part focuses on characterization of the anhydrous materials by ^{29}Si and ^{27}Al MAS NMR.

6.2 Preliminary investigations of anhydrous materials

An initial collection of materials (12 cements, 9 blastfurnace slags, 3 fly ashes, one natural pozzolan, and one microsilica) was considered with the purpose of selecting which cements and SCMs that should be investigated in detail in the study of SCM reactivity in blended cements. The materials were provided by different industrial manufacturers and were initially received in rather small quantities. Preliminary characterization of the materials by XRF analysis, XRD with Rietveld analysis, SEM and granulometry was mainly carried out by Vanessa Kocaba at École Polytechnique Fédérale Lausanne (EPFL), Lausanne, Switzerland. To avoid duplication of similar materials various parameters were used to choose among the initial range of cements, specifically the median grain size (d_{50}) and the contents of alite, tricalcium aluminate and alkalis (Na_2O + K_2O), as these parameters are all known to influence the reactivity of cements or SCM in cement – SCM blends. The choice of SCMs was based on criteria such as bulk chemical composition (*e.g.*, low content of Fe_2O_3), content of amorphous matter in the samples, and median grain size. The group of materials that was selected for the comprehensive series of hydration experiments was subsequently supplied in much larger quantities (approx. 1 tonne of each selected material) by the manufacturers.

The cements of the initial selection are denoted as cement 1 – 12, whereas the cements chosen for further investigations are identified by a capital letter rather than the original number, since the selected cements received in large quantities did not exhibit the

exact same bulk chemical and phase compositions as the initially received samples. Cements A, B and D correspond to cements 2, 5 and 11, respectively. Cement C was not included in the initial selection of materials, but added later to replace cement D, as this cement showed a significantly different phase composition in the large batch as compared to the originally received sample, *i.e.*, the content of tricalcium aluminate was much lower in the large batch. It is noted, that cements A and 2 are white Portland cements, while cement 8 is a sulphate-resistant cement.

6.2.1 XRF analysis

Bulk chemical compositions obtained by XRF analysis are presented for cements and SCMs in Table 6.1 and 6.2, respectively. The cements displays the following ranges in chemical composition for the main oxides (wt%): 57.7 – 69.2 CaO, 19.6 – 24.7 SiO_2, 2.1 – 5.6 Al_2O_3 and 0.3 – 4.6 Fe_2O_3, while the slags exhibit the ranges (wt%): 32.5 – 43.6 CaO, 31.9 – 40.5 SiO_2, 7.0 – 20.0 Al_2O_3, and 5.7 – 11.3 MgO. The three fly ash samples are dominated by SiO_2 (51.7 – 72.2 wt%) and Al_2O_3 (24.3 – 25.6 wt%), while the contents of CaO are low (0.1 – 5.7 wt%). These compositions corresponds to Class F fly ashes according to the ASTM classification (*i.e.*, $SiO_2 + Al_2O_3 + Fe_2O_3 > 70$ wt%). The natural pozzolan is also dominated by SiO_2 (64.2 wt%) and Al_2O_3 (13.5 wt%), while the microsilica sample is almost pure SiO_2 (98.5 wt%).

A high content of iron in a sample material can reduce the resolution and affect the quantitative reliability of the NMR spectra, as a result of strong dipolar interactions between the NMR-active nucleus under observation and the unpaired electrons of paramagnetic ions (*i.e.*, Fe^{3+}). Therefore, materials with low Fe_2O_3 contents are normally preferred from an NMR point of view. In this regard, fly ash 1, fly ash 3, and cement 8 immediately stands out with Fe_2O_3 contents of 4.6 wt%, 5.7 wt% , 8.3 wt%, respectively. This issue is discussed further in Section 6.3.1 and 6.3.4.

6.2.2 Laser granulometry

Particle-size distributions of the samples were obtained by laser granulometry. In Table 6.1 and 6.2 the median grain size (d_{50}) is displayed for cements and SCMs. d_{50} is the grain size at which 50 % of sample is finer. The cements can roughly be divided into two groups with cements A, D, 2, 9, and 10 having $d_{50} < 14$ μm and the remaining ones having $d_{50} > 14$ μm.

Table 6.1 Bulk chemical compositions of the Portland cements from XRF analysis (wt%) and median grain size d_{50} (μm) from laser granulometry.

Cement	SiO_2	Al_2O_3	Fe_2O_3	CaO	MgO	SO_3	K_2O	Na_2O	TiO_2	MnO	P_2O_5	LOI[1]	d_{50}[2]
A[3]	24.7	2.1	0.4	68.7	0.6	1.8	0.1	0.2	0.1	0.01	0.5	1.0	9
B	20.5	5.1	3.3	61.3	2.8	2.8	1.4	0.2	0.2	0.05	0.4	1.9	14
C	21.0	4.6	2.6	64.2	1.8	2.8	0.9	0.2	0.1	0.03	0.4	1.3	20
D	21.0	5.0	2.5	63.5	2.1	3.0	1.0	0.3	0.2	0.04	0.1	1.3	11
1	21.6	5.0	2.8	65.9	1.7	0.8	0.9	0.1	0.3	0.05[5]	0.4	2.7	~15
2[3]	24.5	2.1	0.3	69.2	0.6	2.2	0.2	0.1	-	-	-	-	~9
3	19.6	5.6	2.8	62.6	2.4	2.82	1.3	0.13	-	-	-	2.9	~15
4	19.4	4.5	2.9	64.1	1.2	2.7	0.8	0.1	-	-	-	3.4	~15
5	20.6	5.2	3.1	62.0	2.6	2.9	1.4	0.3	-	-	-	-	~15
6	19.6	5.5	3.3	62.5	1.6	3.1	1.4	0.2	-	-	-	2.7	~15
7	22.8	5.4	3.5	65.6	-	0.4	0.7	0.2	-	-	-	-	~15
8[4]	21.8	4.0	4.6	63.0	1.5	2.3	0.7	0.2	0.2	0.07[5]	-	1.0	~15
9	20.0	4.6	2.9	62.9	1.9	3.0	0.9	0.3	0.3	0.08	0.1	-	~9
10	21.8	5.3	2.9	57.7	2.0	2.1	1.0	0.3	0.3	0.1[5]	0.1	-	~9
11	20.7	4.7	2.3	62.5	2.6	3.2	1.0	0.3	0.2	0.1[5]	0.1	-	~15
12	20.1	4.3	2.5	60.9	1.4	3.1	0.9	0.1	0.3	-	0.2	-	~15

[1] LOI = loss on ignition. [2] d_{50} refers to the grain size at which 50 % of sample is finer. [3] White Portland cement.
[4] Sulphate-resisting cement. [5] The quantity corresponds to Mn_2O_3 rather than MnO.

Table 6.2 Bulk chemical compositions from XRF analysis (wt%), amorphous content (wt%) from XRD and median grain size d_{50} (μm) from laser granulometry for the SCMs.

Sample	SiO_2	Al_2O_3	Fe_2O_3	CaO	MgO	SO_3	K_2O	Na_2O	TiO_2	MnO	P_2O_5	Amorph.[1]	d_{50}[2]
slag 1	36.6	12.2	0.9	41.6	7.2	0.6	0.3	0.2	0.04	0.14	0.01	99.5 %	19
slag 2	36.6	12.2	0.9	41.6	7.2	0.6	0.3	0.2	0.04	0.14	0.01	99.5 %	8
slag 3	40.5	7.0	0.7	39.5	8.2	1.6	0.7	0.5	0.3	0.8[6]	-	83 %	15
slag 4	40.5	7.0	0.7	39.5	8.2	1.6	0.7	0.5	0.3	0.8[6]	-	83 %	10
slag 5	31.9	16.5	0.9	35.8	10.8	-	0.5	0.2	1.1	0.4	-	-	-
slag 6	34.9	12.2	0.6	37.1	11.3	-	0.3	0.1	0.5	0.2	-	-	-
slag 7	38.0	7.4	1.4	43.6	5.7	-	0.4	0.5	0.3	0.3	-	-	-
slag 8	34.6	20.0	0.5	32.5	9.2	2.0	0.8	0.2	0.67	0.06	0.01	94.2 %	15
slag 9	36.9	9.8	2.2	37.7	9.3	2.0	0.3	0.6	0.3	0.4[6]	-	95 %	20
FA 1[3]	51.7	25.5	5.7	3.1	2.7	0.8	4.1	1.3	0.9	0.1[6]	0.2	-	10
FA 2[3]	72.2	24.3	0.4	0.1	0.1	0.1	0.3	0.1	1.4	-	0.1	-	7
FA 3[3]	53.5	25.6	8.3	5.7	-	1.1	-	0.5	1.5	1.5[6]	-	-	19
NP[4]	64.2	13.5	2.6	3.0	1.1	-	-	0.1	-	0.1[6]	-	-	9
MS[5]	98.5	0.3	0.1	0.3	0.1	-	-	-	-	-	-	-	0.25

[1] Content of amorphous material in sample estimated by XRD with Rietveld analysis. [2] d_{50} is the grain size at which 50 % of sample is finer. [3] FA = fly ash. [4] NP = natural pozzolan. [5] MS = microsilica. [6] The quantity corresponds to Mn_2O_3 rather than MnO.

The slags and fly ashes display d_{50}-values in the ranges 8 – 20 μm and 7 – 19 μm, respectively, while the microsilica has a considerably smaller grain size (d_{50} = 0.25 μm). The natural pozzolan has d_{50} = 9 μm.

6.2.3 XRD with Rietveld analysis

Crystalline phases in the Portland cements have been identified and quantified using powder XRD in combination with Rietveld analysis (Table 6.3). This includes the following phases: alite, belite, tricalcium aluminate, ferrite, lime (CaO), periclase, sulphates (gypsum, hemihydrate, and anhydrite), quartz, calcite and portlandite.

Table 6.3 Phase contents (wt%) of the Portland cements determined by XRD with Rietveld analysis.

Sample	Alite	Belite	C_3A[1]	Ferrite	Lime	MgO[2]	Sulphates[3]	Quartz	Calcite	CH[4]
A[5]	68.9	23.4	3.9	-	-	-	3.2	-	-	0.6
B	49.0	23.7	5.6	12.6	1.4	1.9	2.7	-	0.6	-
C	61.8	16.9	6.8	9.5	-	-	2.8	-	-	0.4
D	66.2	14.1	3.7	10.6	-	0.7	2.8	-	-	-
1	66.9	10.3	4.5	8.8	-	0.5	4.2	-	4.9	-
2[5]	67.3	23.3	3.6	0.4	0.6	-	4.3	-	-	0.5
3	58.9	14.9	9.7	7.0	0.7	1.6	4.6	0.4	2.3	-
4	65.4	8.5	7.0	7.8	0.4	0.4	4.6	0.4	5.2	0.4
5	51.1	22.2	8.1	9.2	1.8	2.3	3.8	-	1.0	0.6
6	65.1	8.7	5.9	9.9	0.6	0.6	5.7	-	3.2	0.3
7	50.9	22.9	7.7	10.8	-	-	4.1	1.7	-	1.9
8[6]	58.7	17.9	2.3	16.0	-	0.5	2.1	-	0.7	-
9	66.2	10.3	6.6	6.9	0.9	1.0	3.9	0.4	3.9	-
10	58.6	7.9	5.8	5.8	-	0.7	4.4	2.6	14.3	-
11	70.1	8.0	7.9	6.4	-	1.3	5.2	-	1.2	-
12	70.0	14.3	3.7	9.2	-	0.5	2.5	-	-	-
SD[7]	2.23	1.41	0.74	0.95	0.4	0.32	0.58-0.81	0.4	0.5	0.4

[1] C_3A = tricalcium aluminate. [2] MgO = periclase. [3] Gypsum + hemihydrate + anhydrite. [4] CH = $Ca(OH)_2$. [5] White Portland cement. [6] Sulphate-resisting cement. [7] Standard deviations calculated from the analysis of cements A, B, C, D, and 8.

As expected, the samples are dominated by alite and belite, and to a lesser extent by tricalcium aluminate, ferrite, and sulphates. Some of the cements contain a small amount of

free lime which is a sign of insufficient burning of the clinker in the kiln during the manufacture. Half of the cements contains a small amount of portlandite which indicates that these samples have been exposed to a small degree of pre-hydration. However, the $Ca(OH)_2$ contents are $\leq$ 0.6 wt% for all cements except for cement 7 and therefore considered to be rather insignificant.

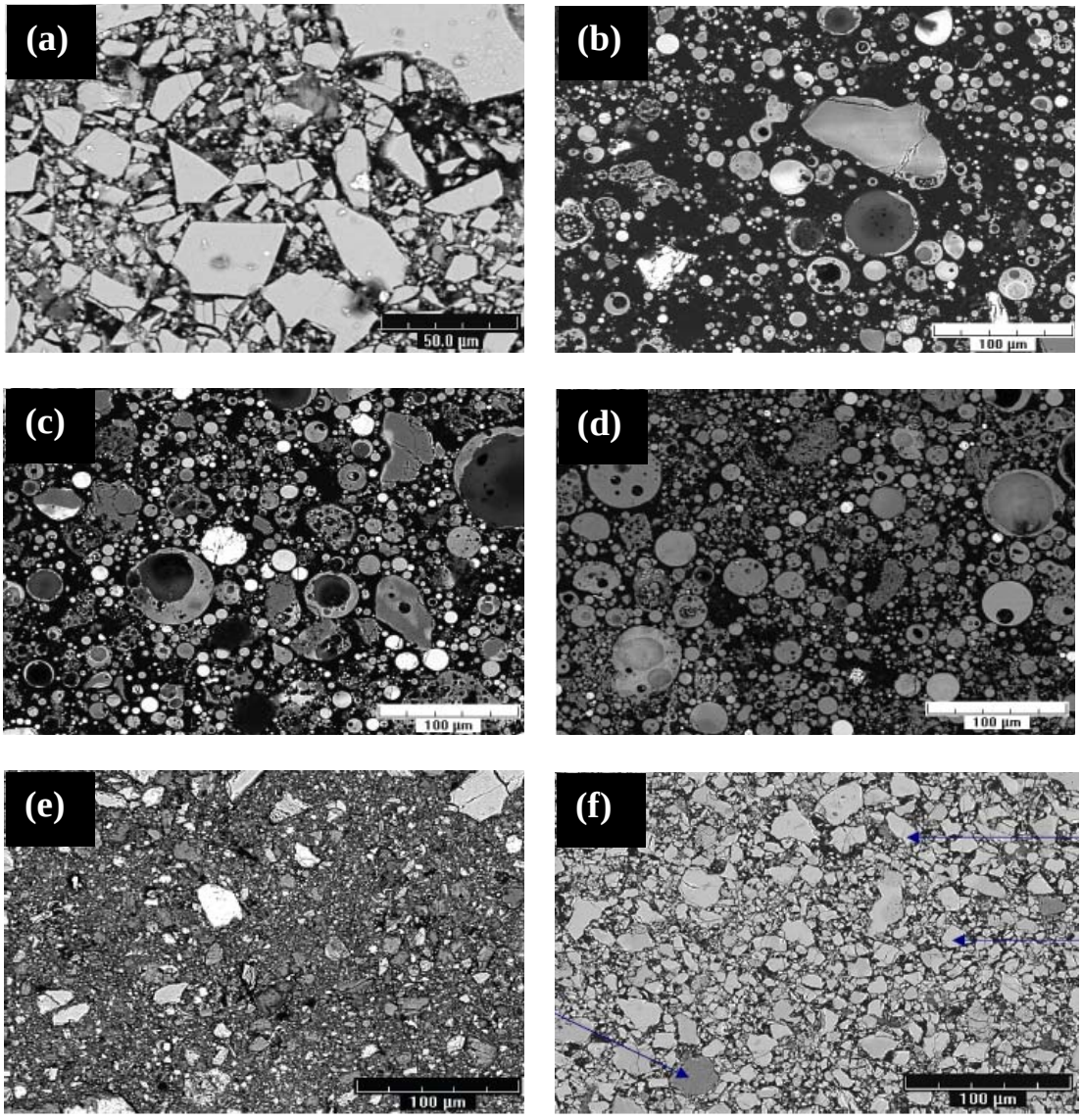

Fig. 6.1 Representative backscattered electron images of anhydrous samples of slag 1 (a), fly ash 1 (b), fly ash 2 (c), fly ash 3 (d), natural pozzolan (e), and cement A (f). The images were obtained at EPFL, Switzerland using SEM.

A few of the cements also contain minor quantities of quartz. All the cements are classified as CEM I according to the European pre-standard for common cements [3], with the

exception of cement 10, which is classified as CEM II due to the presence of approximately 15 wt% of limestone filler (calcite).

XRD have also been used to qualitatively identify phases in some of the SCMs. The phase melilite ($(Ca,Na)_2[(Mg,Fe^{2+},Al,Si)_3O_7]$) was identified in slag 8, and in the natural pozzolan clinoptilolite ($(Na,K)_6[Al_6Si_{30}O_{72}]24H_2O$), albite ($Na[AlSi_3O_8]$), sanidine ($(K,Na)[AlSi_3O_8]$), magnetite ($Fe_3O_4$) and silica were observed. The following phases were found in the fly ashes: mullite ($3Al_2O_3{\cdot}2SiO_2$), belite, anhydrite ($CaSO_4$) and hematite (Fe_2O_3) in fly ash 1; mullite, silica, anhydrite and hematite in fly ash 2; mullite and silica in fly ash 3. Crystalline phases were not detected in the microsilica sample.

6.2.4 Backscattered electron images from SEM

Backscattered electron (BSE) imaging from SEM in combination with EDS has been utilized to support the identification of phases present in the cements and SCMs. The BSE images also reveal the shapes and size distribution of the particles. Examples are given in Fig. 6.1 for some anhydrous SCMs and cement A. The images clearly demonstrate the spherical shape of the fly ash particles as compared to the angular slag fragments.

6.2.5 Characteristics of selected materials

Table 6.4 summarizes the selection of materials that was chosen for the subsequent hydration experiments involving cements blended with SCMs. The main characteristics on the basis of which the individual materials were chosen are outlined as well.

Table 6.4 Characteristics of selected materials

Sample	Characteristics
cement A	high alite content, low aluminate content, low bulk contents of alkalis and Fe_2O_3, d_{50} = 9 μm
cement B	low alite content, medium aluminate content, d_{50} = 14 μm
cement C	high alite content, medium aluminate content, d_{50} = 20 μm
slag 1	99.5 % amorphous material, typical bulk chemical composition for slags
slag 8	94.2 % amorphous material, high content of Al_2O_3
fly ash 2	low bulk contents of CaO and Fe_2O_3
natural pozzolan	high bulk contents of SiO_2 and Al_2O_3, low bulk content of CaO, d_{50} = 9 μm
microsilica	almost pure SiO_2, d_{50} = 0.25 μm

6.3 Characterization of anhydrous materials by solid-state NMR

6.3.1 ^{29}Si MAS NMR of anhydrous cements

Fig. 6.2 presents ^{29}Si MAS NMR spectra of all the 16 anhydrous cements studied in Core Project 4. The spectra were recorded at 9.4 T with a relatively high speed spinning (ν_R = 13.0 kHz). The acquisition of these spectra were rather time consuming, since typically 1000 – 2500 scans were required to obtain a satisfactory signal-to-noise ratio due to the low natural abundance of ^{29}Si (4.7 %). Furthermore, a recycle delay of 30 s was employed to insure full relaxation of the ^{29}Si spins between the individual scans, and consequently the total acquisition time for each spectrum was typically in the order of 24 h. Further details regarding the experimental conditions employed for acquisition of the spectra are given in Appendix I. All the ^{29}Si MAS NMR spectra in Fig 6.2 show overlapping signals from the two calcium silicates alite and belite. The rather narrow resonance at -71.3 ppm originates from β-C_2S (belite) in agreement with its crystal structure, where all Si atoms are in equivalent positions in the asymmetric unit [36]. On the other hand, alite exhibits broadened peaks which include a number of overlapping resonances in the spectral region from -66 to -78 ppm. This is a consequence of the large number of different SiO_4 tetrahedra in the monoclinic structures (M_I or M_{III}) of alite. Nishi *et al.* [232] have reported 18 different Si sites for the M_{III} form. It appears from a comparison of the overall lineshape of the alite peaks in Fig. 6.2 with the ^{29}Si MAS NMR spectra of synthetic samples of the M_I and M_{III} forms of alite (Fig. 5.6) that the studied cements are all dominated by alite in its monoclinic M_{III} form with the exception of cement 12, in which case alite appears to occur in the M_I form. These observations are in full accord with independent XRD investigations of the same cements performed by Vanessa Kocaba at EPFL.

The alite and belite contents have been quantified by deconvolution of the ^{29}Si MAS NMR spectra (see Section 6.3.2) utilizing that the relative quantities of alite and belite in the cements are clearly reflected by the overall lineshapes of the spectra. For example, the belite content of 20.0 wt% for cement A is reflected by the high intensity of the peak observed at -71.3 ppm, which is superimposed on the broadened resonances from alite. Correspondingly, the small belite peak observed for cement 6 reflects a very low belite content (4.9 wt%). The content of iron in the cements influences the overall lineshape of the ^{29}Si MAS NMR spectra. Cements 7 and 8 contain 3.5 and 4.6 wt% Fe_2O_3, respectively, which are the two highest iron contents among the studies samples. In the

spectra of these cements the distinction between the belite and alite resonances becomes less pronounced, because of linebroadening caused by interactions of the ^{29}Si spins with the unpaired electrons of the Fe^{3+} ions. This additional linebroadening tends to blur the spectra, thereby resulting in larger uncertainties on the ratio of alite and belite determined from computer deconvolution of the ^{29}Si MAS NMR spectra.

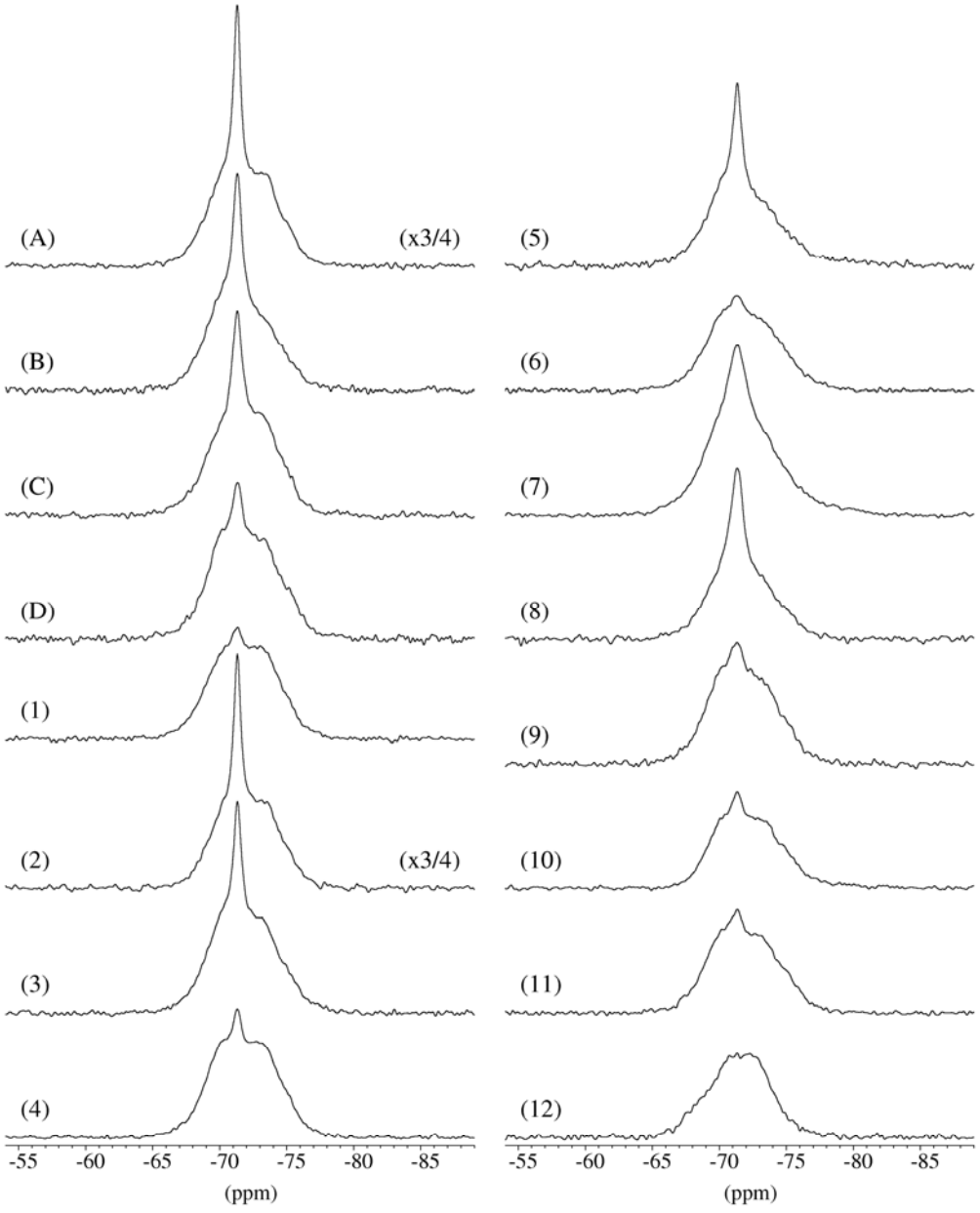

Fig. 6.2 ^{29}Si MAS NMR spectra (9.4 T, ν_R = 13 kHz) of anhydrous Portland cements A – D and 1 – 12. The spectra display a notable variation in signal intensity from the alite and belite phases. The intensity scale is identical for all the spectra except for cement A and 2 where the scale has been multiplied by a factor of ¾ relative to that for the others. The spectra were recorded with a 30 s relaxation delay and typically 1000 – 2500 scans.

The spectrum of cement 5 includes low-intensity Q^1 and Q^2 resonances ranging from approximately -78 to -85 ppm, which indicates a small degree of prehydration for this cement. Impurities of quartz and another silicate phase have been observed in cement 10 by a resonance at -107.4 ppm and a broad peak ranging from approx. -92 to -100 ppm (not seen in the spectral region displayed in Fig. 6.2). This is consistent with XRD investigations of this cement, which show a quartz content of 2.6 wt%. The broad peak probably originates from a clay mineral (*i.e.*, a phase containing Q^3 units).

6.3.2 Quantification of alite and belite from ^{29}Si MAS NMR

The contents of alite and belite have been determined for all anhydrous cements from the ^{29}Si MAS NMR spectra in Fig. 6.2 by employment of a procedure described in Paper I [233], which is a modified version of the procedure originally described in Ref. [225]. The main features of the refined quantification approach are briefly outlined in the following.

The determination involves computer deconvolution of the ^{29}Si MAS NMR spectra which gives the molar belite/alite ratio. Initially, a sub-spectrum of alite is created by deconvolution of the ^{29}Si MAS NMR spectra of the M_I or M_{III} forms of alite by the addition of a number of Gaussian and/or Lorentzian shaped peaks. Subsequently, a single peak corresponding to the isotropic chemical shift for belite is added, and finally the peaks from both alite and belite are optimized to the experimental spectrum by least-squares fitting (Fig. 6.3). In the fitting procedure the relative intensities of the peaks constituting the alite resonances are kept fixed and only manually scaled to fit the experimental spectrum. On the other hand, the intensity and linewidth of the single belite peak are allowed to vary freely in the fitting procedure. The molar ratio of belite/alite can subsequently be calculated from the resulting peak intensities, and combining this ratio with the total content of SiO_2 (determined from XRF analysis) allows calculation of the quantities of alite and belite in the stoichiometric forms C_3S and C_2S. It is assumed in this approach that all the SiO_2 present in the cement occurs only in the alite and belite phases.

Taylor [175] has proposed more realistic compositions of the major phases in construction industry cements which take into account the incorporation of different guest ions (see Section 4.7). These Taylor compositions have been employed along with the belite/alite molar ratios from the ^{29}Si MAS NMR spectra to give more realistic quantities of alite and belite. Table 6.5 presents the result of the ^{29}Si MAS NMR based quantification

along with the corresponding results from the XRD/Rietveld quantification. Generally, NMR gives slightly higher contents of alite than XRD whereas belite contents are consistently somewhat lower in the NMR quantification as compared to belite contents from XRD. This discrepancy between the NMR and XRD experiments is discussed in some detail in Paper I [233].

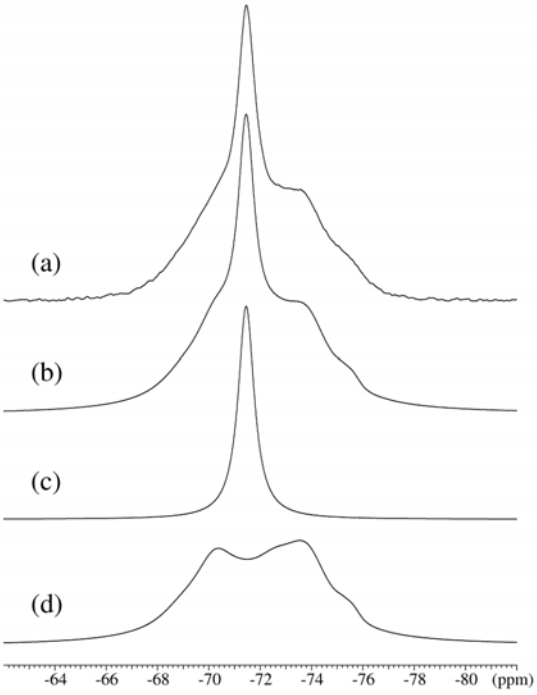

Fig. 6.3 Illustration of the deconvolution procedure employed for quantification of alite and belite from ^{29}Si MAS NMR spectra, here exemplified for cement A. (a) Experimental ^{29}Si MAS NMR spectrum of cement A (9.4 T, ν_R = 13 kHz). (b) Optimized simulation of ^{29}Si MAS NMR spectrum in (a). (c) Deconvolved belite sub-spectrum for the simulated spectrum in (b). (d) Deconvolved M_{III} alite sub-spectrum for the simulated spectrum in (b).

Besides using the abovementioned Taylor compositions in the quantification of alite and belite from ^{29}Si MAS NMR spectra, compositions obtained from EDS analyses (Table 6.6) have also been used for seven cements (A, B, C, D, 1, 4, and 8), thus employing the actual composition of the phases and taking into account the small amount of SiO_2 present in phases other than alite and belite. When comparing the results derived using the Taylor and EDS compositions, the differences in alite and belite content appear insignificant (Table 6.7). This reflects the fact that the EDS compositions for alite and belite are very close to those reported by Taylor and that the aluminate and ferrite phases only include very small amounts of the total SiO_2 content. Accordingly, these results justify the use of the Taylor compositions in the quantification procedure for alite and belite from the ^{29}Si MAS NMR spectra.

6.3.3 ^{27}Al MAS NMR of anhydrous cements

^{27}Al MAS NMR spectra have been recorded for six (A, B, C, D, 1, and 4) of the 16 anhydrous cements. Two representative spectra of cement A and C are shown in Fig. 6.4 which exhibit similar spectral features. The two overlapping peaks at ~81 and ~86 ppm originate from aluminium incorporated as guest ions in tetrahedral sites of the alite and belite phase, respectively. The broad resonance ranging from approx. 40 to 100 ppm, on which the two overlapping peaks are superimposed, originates from Al in tricalcium aluminate.

Table 6.5 Contents (wt%) of alite and belite in anhydrous cements from ^{29}Si MAS NMR and XRD with Rietveld analysis.

Cement	^{29}Si MAS NMR[1]			XRD with Rietveld analysis	
	***I*(belite)/*I*(alite)**	**alite**	**belite**	**alite**	**belite**
A[2]	0.3449	72.4	20.0	68.9	23.4
B	0.3676	59.1	17.4	49.0	23.7
C	0.3286	62.4	16.4	61.8	16.9
D	0.1805	70.3	10.2	66.2	14.1
1	0.1226	75.7	7.4	66.9	10.3
2[2]	0.3335	72.5	19.4	67.3	23.3
3	0.2559	60.1	12.3	58.9	14.9
4	0.0885	68.6	4.9	65.4	8.5
5	0.3376	60.7	16.5	51.1	22.2
6	0.0857	71.2	4.9	65.1	8.7
7	0.2918	64.4	15.1	50.9	22.9
8[3]	0.2540	67.7	13.7	58.7	17.9
9	0.1388	68.2	7.6	66.2	10.3
10	0.1427	66.6	7.6	58.6	7.9
11	0.0907	74.8	5.4	70.1	8.0
12	0.1907	66.6	10.2	70.0	14.3

[1] The quantification of alite and belite is based on deconvolution of the ^{29}Si MAS NMR spectra recorded at 9.4 T with a spinning speed of ν_R = 13.0 kHz. Compositions proposed by Taylor [175] are assumed for the alite and belite quantities determined from the ^{29}Si MAS NMR spectra. [2] White Portland cement. [2] Sulphate-resistant cement.

Tabel 6.6 Compositions of alite and belite in seven Portland cements obtained by SEM combined with EDS analysis[1].

cement	alite	belite
A	$Ca_{2.92}Mg_{0.04}Al_{0.07}Fe_{0.02}Si_{0.95}O_5$	$Ca_{1.99}Al_{0.08}Fe_{0.01}Si_{0.92}O_4$
B	$Ca_{2.84}Mg_{0.08}Al_{0.09}Fe_{0.04}Si_{0.93}O_5$	$Ca_{1.98}Mg_{0.02}Al_{0.07}Fe_{0.03}Si_{0.92}O_4$
C	$Ca_{2.93}Mg_{0.05}Al_{0.06}Fe_{0.04}Si_{0.93}O_5$	$Ca_{2.00}Al_{0.05}Fe_{0.03}Si_{0.91}O_4$
D	$Ca_{2.89}Mg_{0.08}Al_{0.09}Fe_{0.03}Si_{0.93}O_5$	$Ca_{1.98}Mg_{0.02}Al_{0.07}Fe_{0.02}Si_{0.91}O_4$
1	$Ca_{2.92}Mg_{0.05}Al_{0.05}Fe_{0.03}Si_{0.95}O_5$	$Ca_{2.00}Mg_{0.01}Al_{0.06}Fe_{0.02}Si_{0.93}O_4$
4	$Ca_{2.90}Mg_{0.04}Al_{0.06}Fe_{0.03}Si_{0.97}O_5$	$Ca_{1.97}Mg_{0.01}Al_{0.05}Fe_{0.02}Si_{0.95}O_4$
8	$Ca_{2.88}Mg_{0.06}Al_{0.06}Fe_{0.03}Si_{0.96}O_5$	$Ca_{1.97}Mg_{0.01}Al_{0.06}Fe_{0.03}Si_{0.93}O_4$
Taylor[2]	$Ca_{2.90}Mg_{0.06}Al_{0.04}Fe_{0.03}Si_{0.95}P_{0.01}Na_{0.01}O_5$	$Ca_{1.94}Mg_{0.02}Al_{0.07}Fe_{0.02}Si_{0.9}P_{0.01}Na_{0.01}K_{0.03}O_{3.93}$

[1] Metal ions corresponding to a molar content below 0.01 are not included in the formulas.

[2] Compositions proposed by Taylor [175]. Note that oxygen vacancies are included in belite.

Table 6.7 Content of the calcium silicate phases in seven Portland cements determined from ^{29}Si MAS NMR spectra (9.4 T, ν_R = 13.0 kHz). (Taylor) and (EDS) refer to the phase composition proposed by Taylor [175] and the compositions derived from EDS analysis, respectively, in the quantification procedure.

Cement	alite (Taylor)	belite (Taylor)	alite (EDS)	belite (EDS)
A[1]	72.4	20.0	72.5	19.5
B	59.1	17.4	58.8	16.7
C	62.4	16.4	62.8	15.9
D	70.3	10.2	70.2	9.8
1	75.7	7.4	74.9	7.1
4	68.6	4.9	66.1	4.5
8[2]	67.1	13.7	65.6	13.1

[1] White Portland cement. [2] Sulphate-resistant cement.

These assignments are based on an earlier study by Skibsted *et al.* [28] of aluminium guest ions in the silicate phases of cements. Well-defined quadrupolar lineshapes have been reported for the two non-equivalent Al_{IV} sites in synthetic $Ca_3Al_2O_6$ [228,234] which is in contrast to the rather featureless resonance observed for tricalcium aluminate in the ^{27}Al MAS NMR spectra of cements A and C. This difference is ascribed to the presence of

impurity ions in the crystal lattice of tricalcium aluminate in Portland cements which distort the local environment of the AlO_4 tetrahedra and thereby blur the distinct features of the quadrupolar lineshapes [28]. A visual comparison of the ^{27}Al MAS NMR spectra for cement A and C suggests that cement A has a higher content of tricalcium aluminate than cement C, since the intensity of the peak originating from this phase is higher for cement A than cement C. However, XRD investigations show that cement A and cement C contain 3.9 wt% and 6.8 wt% of tricalcium aluminate, respectively, which may seem to contradict the observations in the ^{27}Al MAS NMR. The lower intensity of the tricalcium aluminate peak in the spectra for cement C is probably a consequence of a significantly higher content of Fe_2O_3 (2.6 wt%) for this cement as compared to cement A (0.4 wt%), since strong dipolar interactions between the ^{27}Al spins and unpaired electrons of Fe^{3+} ions cause a broadening of resonances and distribution of a higher fraction of the intensity into the spinning sidebands, thus resulting in reduced intensity of the centerband. The aluminium in the ferrite phase is not observed in the ^{27}Al MAS NMR spectra of cement A and C due to effects of the abovementioned nucleus-electron dipolar interaction [229].

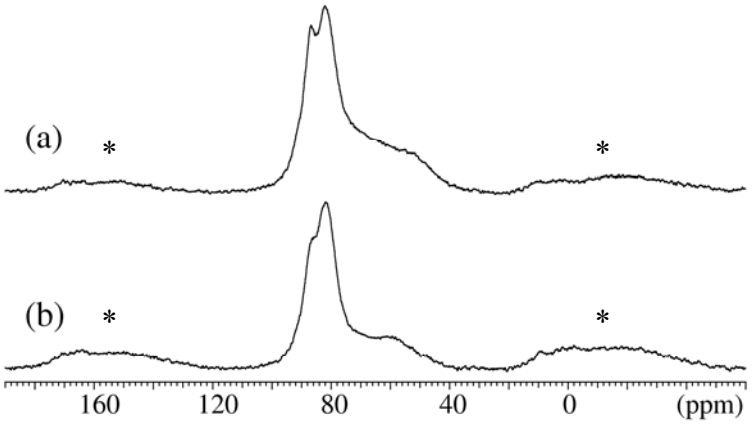

Fig. 6.4 Representative ^{27}Al MAS NMR spectra (14.1 T, ν_R = 13 kHz) of cement A (a) and cement C (b). The peaks indicated with asterisks (*) are spinning sidebands. The spectra a plotted on the same intensity scale.

6.3.4 ^{29}Si MAS NMR of SCMs

^{29}Si MAS NMR spectra of the five SCMs selected for the hydration experiments (see Table 6.4) are displayed in Fig. 6.5. A spectrum of cement A is included as well for comparison. The ^{29}Si MAS NMR spectrum of microsilica exhibits a broad resonance ranging from approx. -100 to -125 ppm in agreement with the amorphous nature of this material. The resonance is in the spectral region for fully condensed SiO_4 tetrahedra, *i.e.*, Q^4 sites. Similar silicate species as those observed for microsilica are also present in fly ash 2.

However, the ^{29}Si MAS NMR spectrum of the fly ash also contains low-intensity resonances from -90 to -102, which are assigned to ^{29}Si species in mullite based on the observation of this phase by XRD and on previously reported ^{29}Si chemical shifts for synthetic samples of mullite [235]. Four overlapping resonances are observed at -95, -101, -108 and -113 ppm in the ^{29}Si MAS NMR spectrum of the natural pozzolan in addition to a broadened low-intensity peak ranging from -85 to -95 ppm. As mentioned in Section 6.2.3, XRD investigations show that the natural pozzolan contains a mixture of the phases albite, clinoptilolite, sanidine, magnetite and silica. Based on ^{29}Si MAS NMR chemical shifts reported for these phases in the literature [236,237] and comparison with an earlier ^{29}Si MAS NMR study of similar natural pozzolans [238], the high-intensity peak at -101 ppm is assigned to contributions from silica, clinoptilolite, and albite, while the shoulder at -113 ppm is attributed to Q^4(0Al) sites in clinoptilolite.

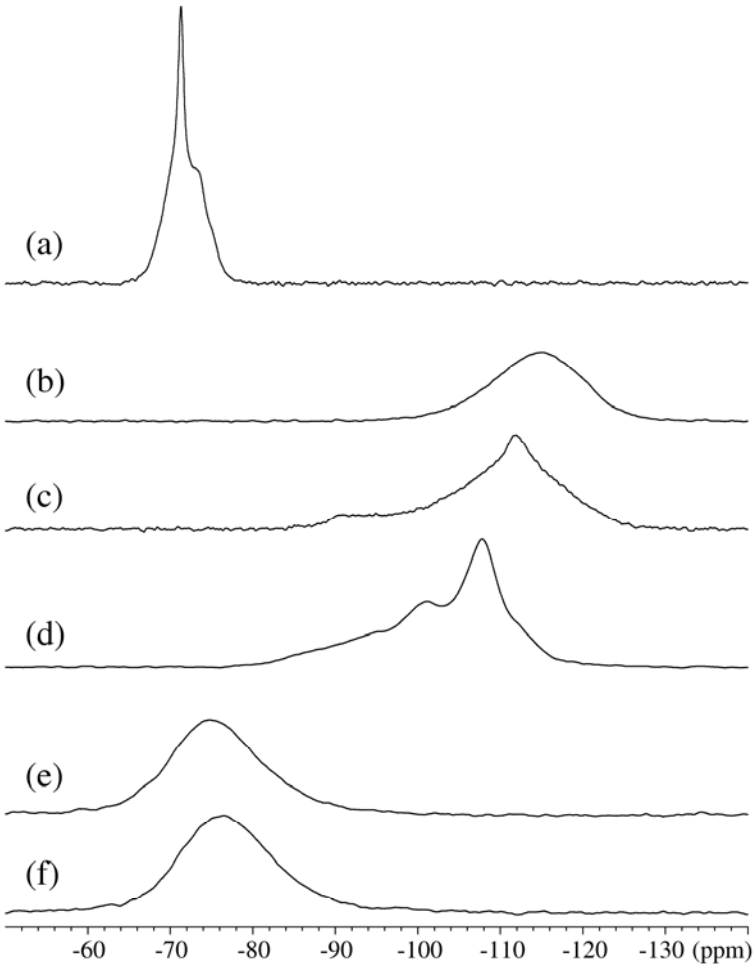

Fig. 6.5 ^{29}Si MAS NMR spectra (9.4 T, ν_R = 12 kHz) of microsilica (b), fly ash 2 (c), natural pozzolan (d), slag 1 (e), and slag 8 (f). The ^{29}Si MAS NMR spectrum of cement A (a) is included for comparison.

The peak at -101 ppm, as well as the low-intensity shoulder at -95 ppm, can be ascribed to a mixture of signals from albite, sanidine and clinoptilolite. The ^{29}Si MAS NMR spectra of slag 1 and slag 8 show very similar broad and featureless peaks ranging from approx. -65 to -95 ppm. Similar ^{29}Si MAS NMR spectra of slags have been reported earlier in the literature [239,240] and assigned to an amorphous glass-like phase containing a range of different Q^{0-3} species with different degrees of Al incorporation in the second-coordination sphere.

The strong influence of high iron contents on the acquisition of NMR spectra is illustrated in Fig. 6.7 where ^{29}Si MAS NMR spectra for fly ashes 1 – 3 are compared on a spectral width which includes the set of spinning sidebands occurring on the low- and high-frequency sides of the centerband at ~ -112 ppm. Evaluation of these spectra has given the data in Table 6.8.

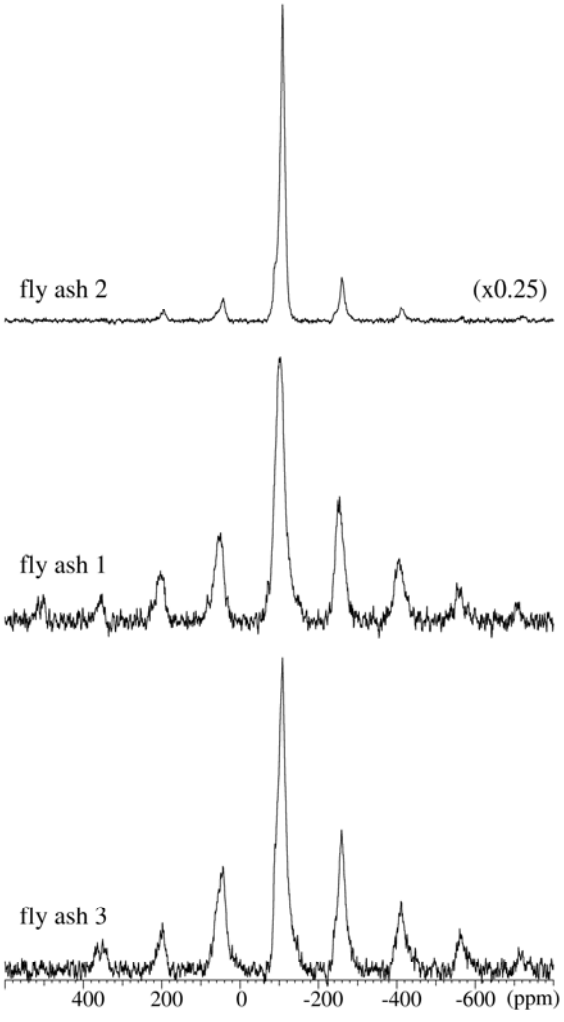

Fig. 6.6 ^{29}Si MAS NMR spectra (9.4 T, ν_R = 12 kHz) of fly ash 1 – 3. The spectra of fly ash 1 and 2 are shown on the same normalized intensity scale, whereas the intensity is reduced by a factor of 4 for fly ash 2. Contents of Fe_2O_3 are 0.43 wt% in fly ash 2, 5.72 wt% in fly ash 1, and 8.3 wt% in fly ash 3.

The spectrum of fly ash 2, which contains 0.4 wt% of Fe_2O_3, exhibits a much lower fraction of the total intensity in the spinning sidebands as compared to the spectra of the more iron-rich samples of fly ash 1 (5.7 wt% Fe_2O_3) and fly ash 3 (8.3 wt% Fe_2O_3) where a significant fraction of the total intensity occurs in the spinning sidebands. If I_{tot} is the combined intensity of the centerband and the spinning sidebands normalized by weight and $m(SiO_2)$ is the mass of SiO_2 in the sample, then the measure "$I_{tot}/m(SiO_2)$" should be equal for the three fly ashes, if Fe_2O_3 did not affect the detection of the ^{29}Si resonances. This is not the case, however, since $I_{tot}/m(SiO_2)$ is significantly lower for the iron-rich samples than for fly ash 2. Roughly 20 % of the ^{29}Si spins are not observed for fly ash 1 and 3 due to the strong interaction between the ^{29}Si nuclear spins and the unpaired electrons of the Fe^{3+} ions. Therefore, fly ashes low in iron are much preferred for the NMR studies.

Table 6.8 Bulk chemical contents (wt%) of SiO_2 and Fe_2O_3 from XRF analysis for fly ashes 1 – 3 and total signal intensities from centerband and spinning sidebands obtained from the evaluation of ^{29}Si MAS NMR spectra (9.4 T, ν_R = 12 kHz).

	Fly ash 1	Fly ash 2	Fly ash 3
SiO_2	51.7	72.2	53.5
Fe_2O_3	5.72	0.43	8.30
I_{tot} (normalized by weight)	0.729	1.281	0.756
$I_{tot}/m(SiO_2)$	1.41	1.77	1.42

6.3.5 ^{27}Al MAS NMR of SCMs

Fig. 6.7 presents ^{27}Al MAS NMR spectra of the SCMs selected for the hydration experiments with the exception of the microsilica, since this material contains only 0.3 wt% of Al_2O_3. The ^{27}Al MAS NMR spectrum of fly ash 2 displays a broad asymmetric peak ranging approx. from 36 to 78 ppm and a narrower peak at ~2 ppm. A previous ^{27}Al MAS NMR investigation of synthetic mullite revealed the presences of three distinct Al resonances originating from octahedral, tetrahedral, and distorted tetrahedral sites [235]. Mullite is the only Al-containing crystalline phase observed in fly ash 2 by XRD, and therefore, at least part of the intensity in the broad peak from 36 to 78 ppm is assigned to Al in tetrahedral or distorted tetrahedral sites of mullite, whereas octahedrally coordinated

Al in mullite most likely contributes to the resonance at ~2 ppm. In the ^{27}Al MAS NMR spectrum of the natural pozzolan a rather narrow line is observed at 55.9 ppm with a shoulder at 60.0 ppm. These two peaks are ascribed to tetrahedral Al sites in the phases clinoptilolite, albite, and sanidine. A limited amount of 6-fold coordinated Al is indicated as well by the low-intensity peak at ~4 ppm. The spectra of slag 1 and 8 are very similar, both exhibiting a broad asymmetric peak ranging from ~25 to ~85 ppm, which imply the presence of tetrahedrally, and possibly, a minor amount of penta-coordinated Al. A peak of very low intensity is observed around 11 ppm in the spectrum of slag 8 as well, thus indicating the presence of a small amount of octahedrally coordinated aluminium.

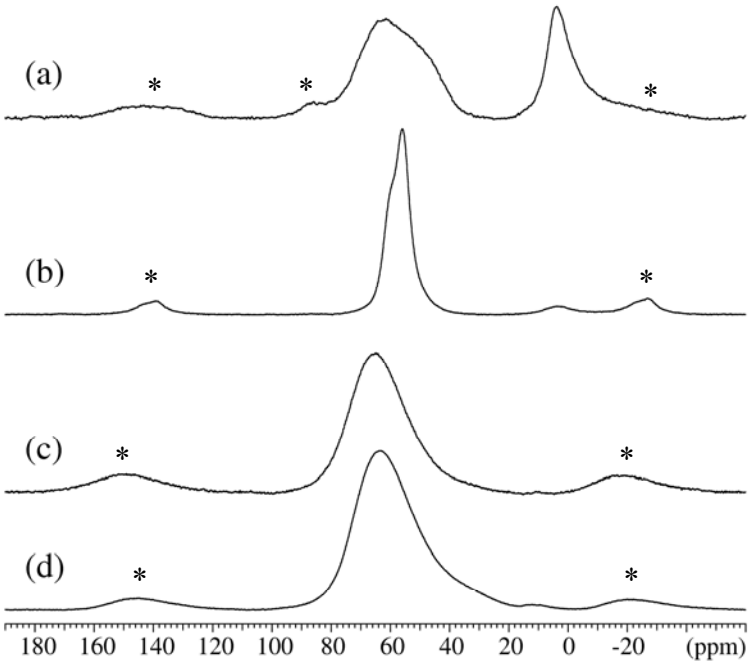

Fig. 6.7 ^{27}Al MAS NMR spectra (14.1 T, ν_R = 13 kHz) of fly ash 2 (a), natural pozzolan (b), slag 1 (c), and slag 8 (d). Peaks indicated with asterisks (*) are spinning sidebands.

Chapter 7

^{29}Si inversion-recovery and other MAS NMR experiments applied to anhydrous materials

7.1 Introduction

The determination of spin-lattice relaxation times for ^{29}Si spins in the alite and belite phases from ^{29}Si inversion-recovery MAS NMR is presented in this chapter, as well as the employment of the same technique as an alternative quantification tool for alite and belite in anhydrous Portland cements. Furthermore, NMR investigations of the synthetic reference material $Si_5O(PO_4)_6$ are presented. The final part of the chapter discusses the use of very short relaxation delays during acquisition of ^{29}Si MAS NMR spectra of Portland cements.

7.2 ^{29}Si inversion-recovery MAS NMR of anhydrous cements

^{29}Si MAS NMR based quantification of the alite and belite phases in Portland cements achieved using the deconvolution procedure outlined in Section 6.3.2 requires fully relaxed spectra in order to obtain reliable results. The belite phase generally exhibits much longer ^{29}Si spin-lattice relaxation times (T_1) than the alite phase. If sufficiently long relaxation delays (D1) are not employed between the individual scans of the single-pulse ^{29}Si MAS NMR experiments, the dissimilarity in T_1's for alite and belite will result in a quantitatively incorrect belite/alite intensity ratio. To ensure full relaxation between scans a relaxation delay of D1 > 5·T_1 is generally required for the different ^{29}Si spins in the cement sample (if a 90° excitation pulse is applied in a single-pulse experiment). Therefore, it is important to know the T_1-values for the ^{29}Si spins in alite and belite to guarantee a fulfilment of this requirement. Determination of T_1 for alite and belite can be achieved by employment of the inversion-recovery (IR) *rf* pulse experiment with the following pulse sequence: $180°_x$ – t – $90°_x$ – FID – D1 (Fig. 7.1). The recovery time (t) between the $180°_x$ and $90°_x$ pulses is incremented which results in a series of partially relaxed ^{29}Si IR MAS NMR spectra (Fig. 7.2(a)). By using the deconvolution procedure described in Section 6.3.2 for each of the IR spectra, a series of intensities for alite and belite as a function of the recovery time (t) can

be obtained. These intensities allow the determination of T_1 for alite and belite by least-squares fitting (three-parameter fit: T_1, M_0 and α) to the well-known equation describing the relationship between the observed intensity ($M_z(t)$) and the recovery time (t) [241]:

$$M_z(t) = M_0[1 - (1 + \alpha)\exp(-t/T_1)] \quad (7.1)$$

Here, M_0 is the equilibrium longitudinal magnetization (*i.e.*, for $t = \infty$) and α is a constant related to pulse imperfections. In the ideal case $\alpha = 1$ for a perfect 180º pulse.

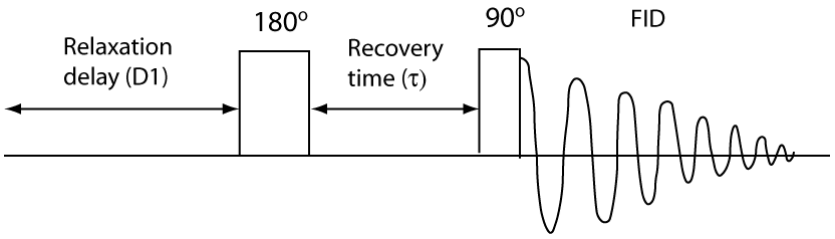

Fig. 7.1 Outline of the *rf* pulse sequence for the inversion-recovery (IR) MAS NMR experiment. The recovery time between the 180 and 90º pulses is incremented in order to obtain a series of partially relaxed IR MAS NMR spectra. FID (Free Induction Decay) is the recorded NMR signal. To ensure full relaxation between individual experiments a relaxation delay (D1) is inserted in the pulse sequence.

Alternatively, the series of intensities from the IR spectra can be fitted to an equation describing the relationship between $M_z(t)$ and t as a "stretched exponential" rather than the single-exponential relationship in Eq. (7.1):

$$M_z(t) = M_0[1 - (1 + \alpha)\exp(-(t/T_1')^{1/2})] \quad (7.2)$$

where the time constant for the spin-lattice relaxation is denoted T_1' instead of T_1. The stretched exponential relationship has previously been effectively applied in ^{29}Si MAS NMR studies of silicates containing small amounts of iron (*e.g.*, 0.1 – 5.0 wt% Fe_2O_3) [242,243] and was originally derived for spin relaxation (without spin diffusion) caused by the presence of paramagnetic impurities [244]. ^{29}Si IR MAS NMR spectra have been recorded and deconvolved for eight of the anhydrous cements (A, B, C, D, 1, 3, 4, and 8) in order to determine the ^{29}Si spin-lattice relaxation time constants for alite and belite. As reported in the enclosed Paper I [233], the best fits to the series of intensities for alite and belite from the IR spectra are achieved by employing Eq. (7.2) rather than Eq. (7.1). The

presence of paramagnetic ions (*e.g.*, Fe^{3+} in Fe_2O_3) can reduce the spin-lattice relaxation significantly for ^{29}Si species in cements [245-247]. Consequently, the longest relaxation times are expected for cements with a low content of Fe_2O_3, *e.g.*, white Portland cements. This is indeed confirmed by our ^{29}Si IR MAS NMR investigations which are presented thoroughly in Paper I. Furthermore, this study demonstrates that the relaxation of the ^{29}Si spins in alite and belite is overwhelmingly dominated by the Fe^{3+} ions incorporated as guest ions in these phases rather than by the Fe^{3+} sites in the ferrite phase as suggested by Edwards *et al.* [247] in a recent study.

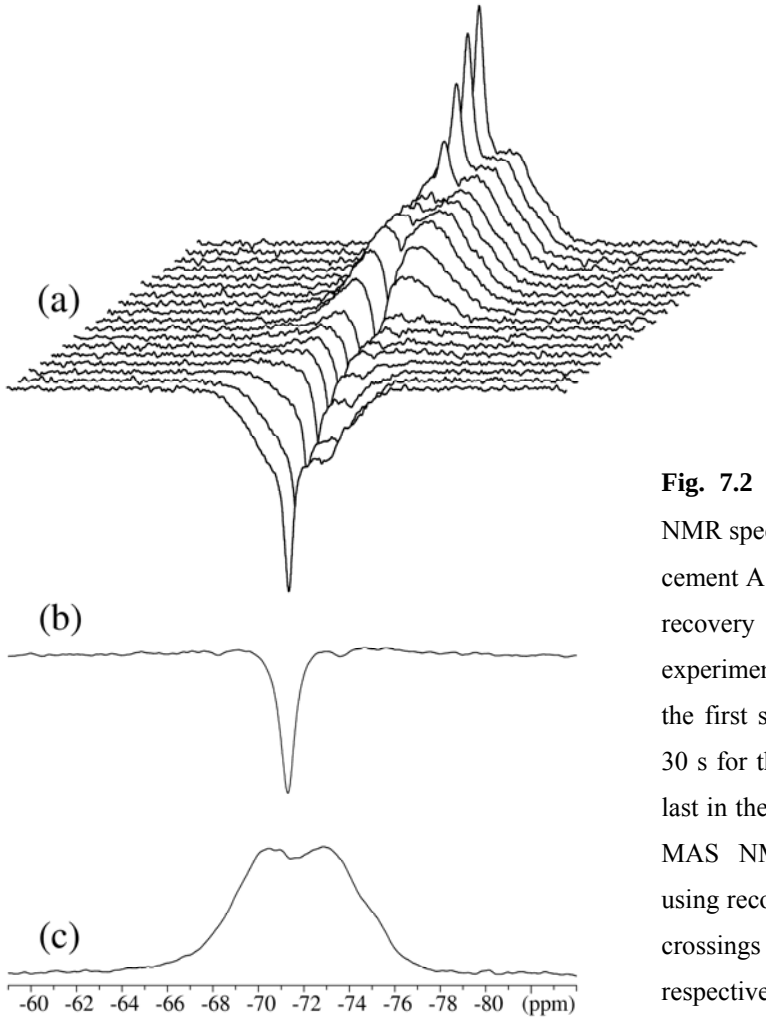

Fig. 7.2 (a) Series of ^{29}Si IR MAS NMR spectra (9.4 T, ν_R = 12.0 kHz) of cement A displayed in "3D" style. The recovery time employed in the IR experiments increases from 0.001 s for the first spectrum in the "3D" row to 30 s for the spectrum displayed as the last in the row. Two additional ^{29}Si IR MAS NMR spectra were recorded using recovery times close to the zero-crossings (t_0) for alite and belite, respectively: 0.14 s (b) and 2.5 s (c).

^{29}Si IR MAS NMR has also been utilized in the present project as an alternative tool for quantifying the calcium silicates in Portland cements. Fig. 7.2(a) shows a series of 18 ^{29}Si IR MAS NMR spectra for cement A (white Portland cement) recorded at 9.4 T using recovery times (t) ranging from 0.001 s to 30 s. It is observed that the ^{29}Si nuclei in

alite relax much faster than the ones in belite, *i.e.*, as the recovery time increases, the intensity of the alite resonances (approx. -66 to -77 ppm) increase at a faster rate than the intensity of the belite peak (-71.3 ppm).

The two additional ^{29}Si IR MAS NMR spectra of cement A, displayed in Fig. 7.2(b) and (c), have been recorded using t-values close to the zero-crossings (t_0) for alite and belite, respectively. Consequently, Fig. 7.2(b) and (c) must represent sub-spectra for the belite and alite phases in cement A, respectively, utilizing the difference in ^{29}Si spin-lattice relaxation times for these phases. By fitting the alite and belite intensities from the IR spectra to Eq. (7.2), the relaxation time constants $T_1' = 0.24$ s and $T_1' = 8.2$ s are obtained for alite and belite, respectively, in cement A. The fitting procedure also gives the M_0-values for alite and belite on the same arbitrary intensity scale: M_0(alite) = 27.142 and M_0(belite) = 10.479, giving the ratio M_0(belite)/M_0(alite) = 0.3861, which corresponds to the molar belite/alite ratio. Quantification of the alite and belite is thus possible by combining this ratio with the bulk content of SiO_2 from XRF analysis.

Alternatively, the recovery times (t) for the ^{29}Si IR MAS NMR spectra in Fig. 7.2(b) and (c) can be employed to calculate M_0 (on another arbitrary intensity scale) for alite and belite according to Eq. (7.2):

Alite: $M_z(2.5\text{ s}) = M_0[1 - 1.95\cdot\exp(-(2.5\text{ s}/0.24\text{ s})^{1/2}]$ => M_0(alite) = 27.523

Belite: $M_z(0.14\text{ s}) = M_0[1 - 1.71\cdot\exp(-(0.14\text{ s}/8.2\text{ s})^{1/2}]$ => M_0(belite) = 11.309

resulting in the ratio M_0(belite)/M_0(alite) = 0.4108. This ratio is close to M_0(belite)/M_0(alite) = 0.3861 from the results of the fitting to Eq. (7.2) for cement A, thus confirming the assumption that the recovery times (t) for the IR spectra in Fig. 7.2(b) and (c) are good approximations of zero-crossing times (t_0) for alite and belite.

The alite and belite contents determined on the basis of M_0(belite)/M_0(alite) ratios obtained from ^{29}Si IR MAS NMR spectra by the fitting of alite and belite intensities to Eq. (7.2) are presented in Table 7.1 for eight cements (A, B, C, D, 1, 3, 4, and 8). For comparison, the corresponding results obtained from the single-pulse ^{29}Si MAS NMR spectra are also given. A very good agreement is observed between the quantities of alite and belite derived by the two approaches for cements C, 1, 3, 4, while the agreement is considered fairly good for cements A and B. However, for cement D, and especially cement 8, the agreement is poor. In the case of cement 8 this may be due to the fact that

this cement has the highest content of Fe_2O_3 (4.6 wt%) among the studied samples, which makes the distinction between the alite and belite resonances less clear, thus inducing a greater uncertainty on the derivation of the alite/belite intensity ratio from the deconvolution.

Table 7.1 Contents (wt%) of alite and belite in eight Portland cements determined from single-pulse ^{29}Si MAS NMR spectra (9.4 T, ν_R = 13.0 kHz) and ^{29}Si inversion-recovery MAS NMR spectra (9.4 T, ν_R = 12.0 kHz), respectively. Compositions proposed by Taylor [175] are assumed for alite and belite.

Cement	Single-pulse ^{29}Si MAS NMR			^{29}Si IR MAS NMR		
	***I*(belite)/*I*(alite)**	**alite**	**belite**	***M*$_0$(belite)/*M*$_0$(alite)**	**alite**	**belite**
A	0.3449	72.4	20.0	0.3861	70.2	21.8
B	0.3676	59.1	17.4	0.3187	61.3	15.7
C	0.3286	62.4	16.4	0.3174	62.9	16.0
D	0.1805	70.3	10.2	0.1100	74.7	6.6
1	0.1226	75.7	7.4	0.1109	76.5	6.8
3	0.2559	60.1	12.3	0.2796	59.0	13.2
4	0.0885	68.6	4.9	0.0798	69.1	4.4
8	0.2540	67.7	13.7	0.4467	58.1	20.8

7.3 NMR investigation of synthetic $Si_5O(PO_4)_6$

The PhD project has involved an investigation of the incorporation of small amounts of phosphorus guest ions in the anhydrous cement phases and their hydration product using ^{31}P MAS NMR techniques. The results of this study are presented in the enclosed Paper II. As reference materials for this study samples of synthetic $Si_5O(PO_4)_6$ were prepared from an earlier reported procedure [248] using a mixture of TEOS ($Si(OCH_2CH_3)_4$), ethanol, distilled water (TEOS:EtOH:H_2O = 1:4:3) and the phosphorus precursor H_3PO_4 (85%) (Si/P = 1:1). The mixtures were stirred at 25 °C for 2 hours resulting in greenish wet gels. After a heat treatment at 1000 °C for 2 hours the final powders were obtained. In one sample 1% (molar ratio) of the paramagnetic complex $NiCl_2{\cdot}6H_2O$ was added with the purpose of shortening NMR relaxation times. The structure of $Si_5O(PO_4)_6$ (trigonal, $R\bar{3}$, a = 7.869 Å, c = 24.138 Å, JCPDS: 70-2071) is built of SiO_6 and SiO_4 groups linked by PO_4 tetrahedra and contains one unique P site and three inequivalent Si sites (one 4-fold

coordinated atom (Si_{IV}) and two 6-fold coordinated atoms (Si_{VI})) [249]. Each [PO_4] tetrahedron is surrounded by three Si_{VI} atoms and one Si_{IV} atom.

Fig. 7.3 presents a ^{29}Si MAS NMR spectrum of synthetic $Si_5O(PO_4)_6$ (with $NiCl_2{\cdot}6H_2O$) and a $^{29}Si\{^{31}P\}$ cross-polarization (CP) MAS NMR spectrum of the same sample. The ^{29}Si MAS NMR spectrum contains three distinct resonances at -119.8, -213.9 and -217.6 ppm, corresponding to the tetrahedrally coordinated Si site (Si(1)) and the two octahedrally coordinated Si sites (Si(2) and Si(3)), respectively. A broad resonance centered at approx. -115 ppm, originating from some amorphous silica (Q^4 sites) in the sample, is observed as well. The $^{29}Si\{^{31}P\}$ CP/MAS NMR spectrum was recorded using a triple-tuned Doty probe at 9.4 T, employing the pulse scheme shown in Fig. 7.4 (see Appendix I for further details). Only ^{29}Si nuclei in close vicinity to the ^{31}P species are detected by the $^{29}Si\{^{31}P\}$ CP/MAS NMR experiment, and therefore, the broad resonance from the amorphous SiO_2 is not observed in the recorded spectrum. On the other hand, the ^{29}Si resonances for Si(1), Si(2) and Si(3) appear in the spectrum, since these Si-sites all have a phosphorus atom in their second coordination sphere. The spectra in Fig. 7.3 are in excellent agreement with previously reported ^{29}Si MAS NMR and $^{29}Si\{^{31}P\}$ CP/MAS NMR studies of synthetic $Si_5O(PO_4)_6$ [248,250] and demonstrate the ability of the $^{29}Si\{^{31}P\}$ CP technique to obtain direct proof for the presence of ^{31}P species in silicates. It is the intention to utilize $^{29}Si\{^{31}P\}$ CP/MAS NMR to investigate the incorporation of phosphorus guest ions in the calcium silicates of Portland cements and work on this issue is currently being carried out in our laboratory.

The synthetic $Si_5O(PO_4)_6$ samples has also been used to study the effect of the paramagnetic complex $NiCl_2{\cdot}6H_2O$ (Ni^{2+} is paramagnetic) on the relaxation of the ^{29}Si spins. Initially, a series of six ^{29}Si MAS NMR spectra, in which the relaxation delay (D1) was incremented, was recorded for the $Si_5O(PO_4)_6$ sample prepared without the paramagnetic addition (Fig. 7.5(a)). The shortest D1-value was 30 s and the longest 360 s. Very low signal intensities are observed in all the spectra due to partial signal saturation, and the intensities do not seem to level off towards the longest D1 of 360 s, thus indicating very long relaxation times for the ^{29}Si species in this sample. A similar series of ^{29}Si MAS NMR spectra was also acquired for the sample containing the paramagnetic complex (Fig. 7.5(b)). In this case, 10 spectra were recorded with D1 values ranging from 2 s to 120 s.

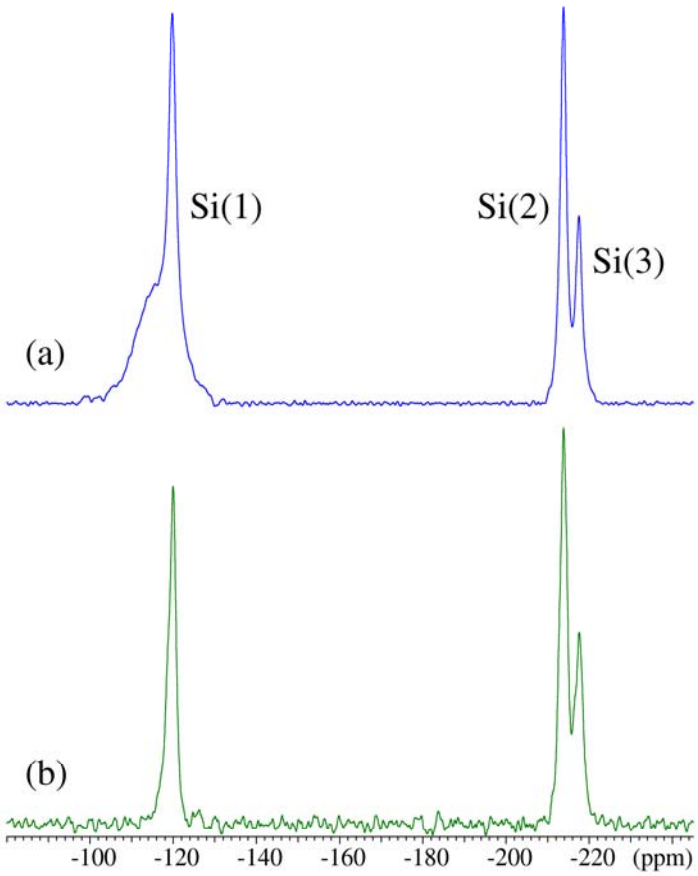

Fig. 7.3 (a) ^{29}Si MAS NMR spectrum of synthetic $Si_5O(PO_4)_6$ recorded at 7.1 T with ν_R = 7.0 kHz. Three distinct resonances are observed corresponding to the three Si sites S(1), S(2), and Si(3). The broadened resonance overlapping with the Si(1) peak is due to the presence of amorphous SiO_2 in the sample. (b) ^{29}Si{^{31}P} CP/MAS NMR spectrum of the same sample (9.4 T, ν_R = 7.0 kHz) recorded using the pulse scheme outlined in Fig. 7.4 (see Appendix I for experimental details).

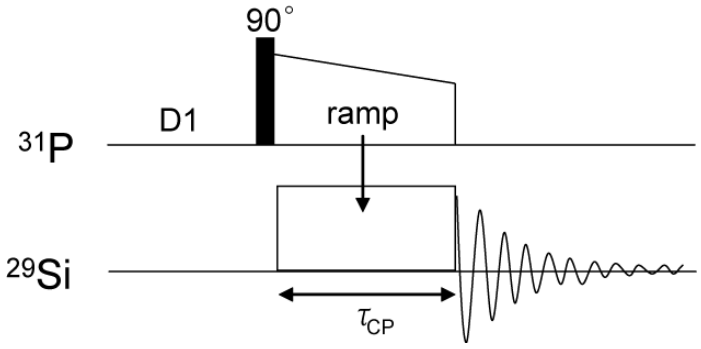

Fig. 7.4 Pulse scheme used for the ^{31}P → ^{29}Si CP magnetization transfer. On the ^{31}P channel a ramp scheme is applied (VACP) [274] and no ^{31}P decoupling is employed during the ^{29}Si acquisition. D1 is a relaxation delay and τ_{CP} is the contact time.

The ^{29}Si resonances exhibit much higher intensities in these spectra (on the same arbitrary intensity scale as in Fig. 7.5(a)) compared to the spectra of the sample without the paramagnetic complex. Also, the increase in signal intensities with increasing values of D1 seems to level of as D1 = 120 s is approached, indicating that quantitatively reliable ^{29}Si MAS NMR spectra of $Si_5O(PO_4)_6$ (with the paramagnetic complex) can be acquired using a relaxation delay of ~120 s. These results demonstrate how significant reductions in ^{29}Si

relaxation times can be achieved by addition of a paramagnetic material to the sample. The shortening of the ^{29}Si relaxation times is caused by the dipolar interaction of the unpaired electrons of the paramagnetic Ni^{2+} ions with the ^{29}Si nuclei. Similar reductions in ^{29}Si relaxation times, although caused by the presence of another paramagnetic ion (Fe^{3+}), have been reported for cementitious materials as well [247,251].

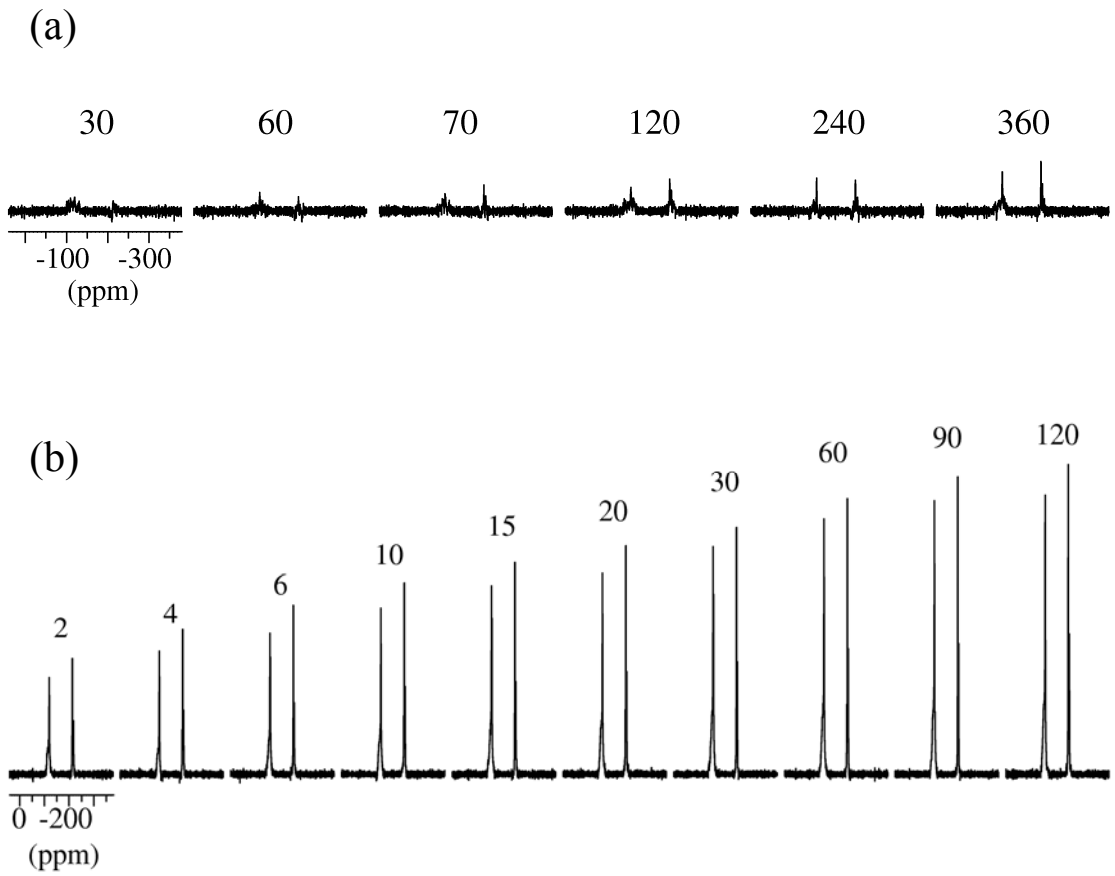

Fig. 7.5 ^{29}Si MAS NMR spectra (7.1 T, ν_R = 7.0 kHz) of synthetic $Si_5O(PO_4)_6$ recorded using different relaxation delays (D1). The employed D1-values (in seconds) are indicated above each spectrum. The spectra in (a) are of "pure" $Si_5O(PO_4)_6$, while the spectra in (b) are obtained for $Si_5O(PO_4)_6$ with a small amount of the paramagnetic complex $NiCl_2 \cdot 6H_2O$ added.

In Fig. 7.6 a series of ^{29}Si IR MAS NMR spectra of $Si_5O(PO_4)_6$ (with the paramagnetic complex) are displayed. Each of these spectra have been deconvolved to obtain three series of intensities, one series for each of the Si(1), Si(2), and Si(3) resonances. The deconvolution procedure involved three Gaussian shaped lines and was carried out using VNMR software. These resulting intensities were initially fitted to Eq. (7.1), which describes the relationship between the observed intensity ($M_Z(t)$) and the recovery time (t)

as a single-exponential process. However, much better fitting results were achieved using the equation for a stretched exponential relaxation process (Eq. (7.2)). This is illustrated in Fig. 7.7 by the plots of $[1 - M_z(t)/M_0]$ versus t and $\sqrt{t}$ for the three Si-sites. The fitting procedure gives the ^{29}Si spin-lattice relaxation time constants (T_1') presented in Table 7.2. As mentioned in the previous section, the stretched exponential relationship is also better suited for describing the spin-lattice relaxation of ^{29}Si spin in the (Fe^{3+}-containing) Portland cements than the single-exponential relationship and has previously been applied with success in ^{29}Si MAS NMR studies of silicates containing small amounts of paramagnetic of iron [242,243]. Therefore, the results presented here from the ^{29}Si IR MAS NMR studies of Portland cements and synthetic $Si_5O(PO_4)_6$ with a small amount of Ni^{2+} imply that ^{29}Si spin-lattice relaxation governed by a stretch exponential process is favoured in the presence paramagnetic species.

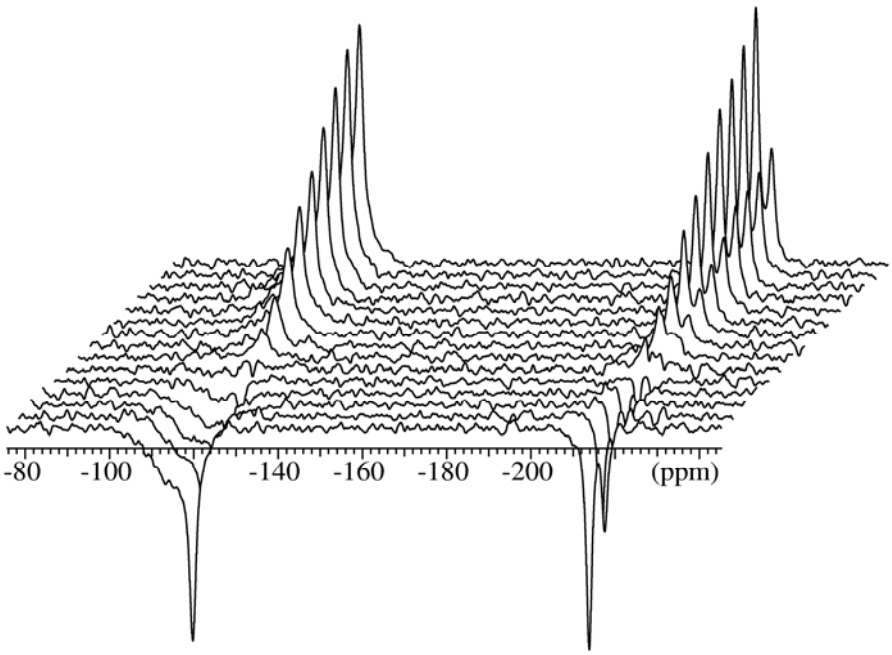

Fig. 7.6 ^{29}Si IR MAS NMR spectra (7.1 T, ν_R = 7.0 kHz) of synthetic $Si_5O(PO_4)_6$ containing a small amount of the paramagnetic complex $NiCl_2 \cdot 6H_2O$. The 15 spectra were recorded using a relaxation delay of 120 s and the recovery time (t) between the 180° and 90° pulses of the IR pulse sequence was ranging from 0.01 s ("nearest" spectrum in the "3D" row) to 120 s (most "distant" spectrum of the row).

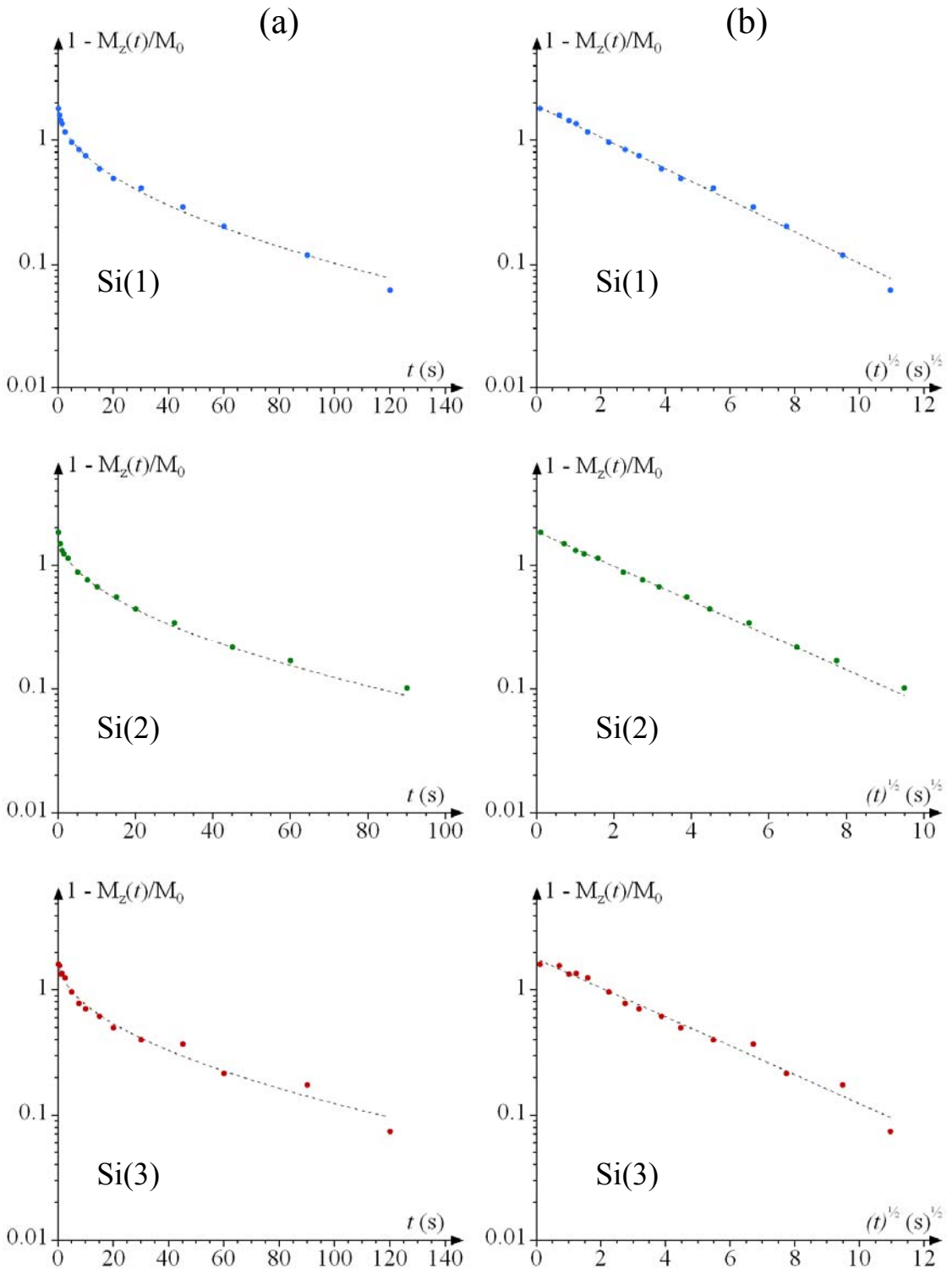

Fig. 7.7 Semilog plots of $[1 - M_z(t)/M_0]$ as a function of the recovery time, t (left column (a)) and $\sqrt{t}$ (right column (b)). Data for the Si(1), Si(2) and Si(3) sites of $Si_5O(PO_4)_6$ obtained from ^{29}Si IR MAS NMR spectra are plotted as blue, green and red circles, respectively. The plots in (a) would be linear if the spin-lattice relaxation was a single-exponential process. The convincing fitting to the straight lines in (b) demonstrates that the ^{29}Si spins follow a stretched exponential relaxation process.

Table 7.2 Time constants for the ^{29}Si spin-lattice relaxation (T_1') obtained from ^{29}Si IR MAS NMR for the three distinct silicon sites in synthetic $Si_5O(PO_4)_6$ prepared with the addition of 1% (molar ratio) of the paramagnetic complex $NiCl_2 \cdot 6H_2O$. The correlation coefficient R for the fit of experimental intensities to the "stretched exponential" equation $M_z(t) = M_0[1 - (1 + \alpha) \exp(-(t/T_1')^{½})]$ for the relaxation process is included as well.

	Si(1)	Si(3)	Si(3)
T_1' (s)	3.419 ± 0.065	3.088 ± 0.059	3.7545 ± 0.182
R	0.9989	0.9999	0.9929

7.4 Employment of very short relaxation delays for the acquisition of ^{29}Si MAS NMR spectra of anhydrous Portland cement

Edwards *et al.* [247] have recently proposed the use of very short relaxation delays (D1) in the acquisition of ^{29}Si MAS NMR spectra of Portland cements, which is facilitated by a suggested reduction in spin-lattice relaxation times for ^{29}Si spins in alite and belite caused by the intimate mixture with the Fe^{3+}-rich ferrite phase. This supposed effect of the ferrite phases is challenged by the ^{29}Si IR MAS NMR studies presented in Paper I, which strongly suggest that the spin-lattice relaxation of the ^{29}Si spins is overwhelmingly dominated by Fe^{3+} guest ions incorporated in the alite and belite phases, rather than Fe^{3+} ions in the ferrite phase. This was demonstrated by analysis of ^{29}Si IR MAS NMR spectra acquired before and after subjecting a sample of cement B to a selective dissolution method [180] where the ferrite and tricalcium aluminate phases are removed from the sample (Fig. 7.8).

Fig. 7.8 The exposure of cement B to selective dissolution (KOSH) was accompanied by a noticeable change in colour caused by removal of the ferrite phase. The brighter sample on the left has been exposed to KOSH selective dissolution, whereas the darker sample on the right is the original cement.

The spin-lattice relaxation times for ^{29}Si spins in the alite and belite phases obtained from the IR spectra were nearly identical for the samples before and after selective dissolution, thus confirming that the ^{29}Si spin-lattice relaxation is dominated by relaxation from Fe^{3+} ions incorporated in alite and belite as guest ions.

The use of very short relaxation delays for the acquisition of ^{29}Si MAS NMR spectra of Portland cements have been investigated for cement A and cement B (Fig. 7.9). Spectra were recorded with D1 = 50 ms, 100 ms and 1.0 s for both cements, as well as 30 s for cement A and 10 s for cement B, and the spectra illustrate how the intensity of the alite and belite signals for both cements are reduced significantly due to partial signal saturation, when the short relaxation delays are employed (D1 < 10 s).

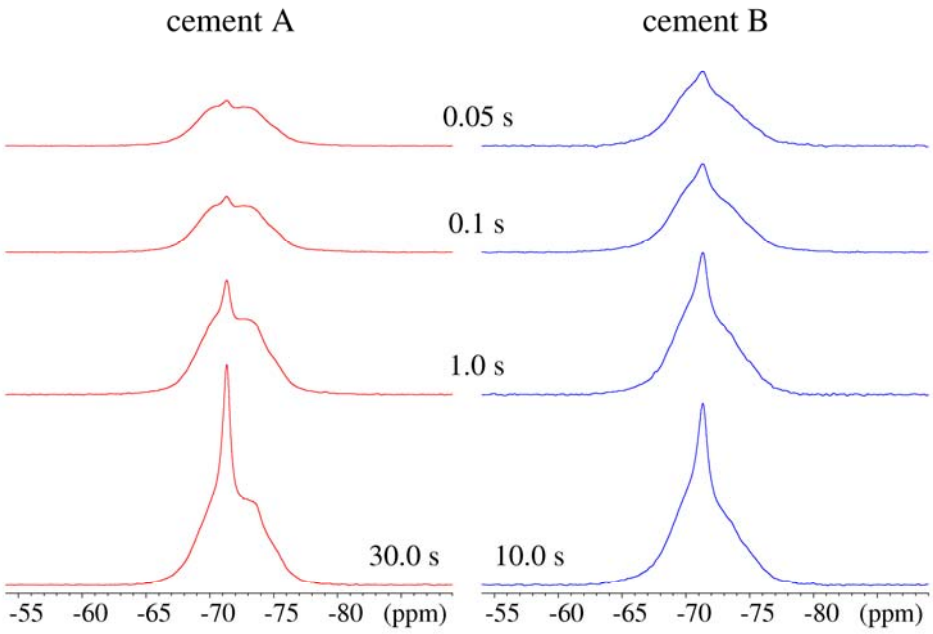

Fig. 7.9 ^{29}Si MAS NMR spectra (7.1 T, ν_R = 7.0 kHz) of anhydrous samples of cement A and B. The different relaxation delays employed for the acquisitions are indicated for each spectrum. The intensities of the belite and alite signals are reduced in the spectra recorded with a relaxation delay < 10 s due to insufficient relaxation of ^{29}Si species between individual scans. It is noted that the intensity of the belite resonance (-71.3 ppm) is reduced to a higher degree than that of the alite peak (approx. -66 to -77 ppm).

It is also noticed that the reduction of the intensity is more pronounced for belite than alite due to a much shorter ^{29}Si spin-lattice relaxation time for the latter phase. The spectra in Fig. 7.9 clearly demonstrate that quantitatively reliable belite/alite intensity ratios can not

be obtained using the short relaxation delays, not even for cement B, which contains a relatively high amount of iron (3.3 wt% Fe_2O_3, 12 wt% ferrite). However, the total acquisition time for the individual spectra obtained using relaxation delays of 50 or 100 ms between the scans (~10,000) were approx. 15 min or less. In contrast, the spectrum of cement A (~4000 scans) had a total acquisition time of about 24 h. These spectra show that a satisfactory signal to noise ratio can be achieved within 15 min or less, if the quantitative reliability of the ^{29}Si MAS NMR spectra is not an issue.

Chapter 8

Reactivity of SCMs in Portland cement blends investigated by ^{29}Si and ^{27}Al MAS NMR

8.1 Introduction

The main goal of this work is the quantification of SCM reaction in hydrating Portland cement blends by the application of solid-state NMR. This chapter presents the methodologies used to extract such data from either ^{29}Si or ^{27}Al MAS NMR spectra. The reactivity of SCMs have been studied in Portland cement blends with microsilica, fly ash, natural pozzolan and slag, and the degrees of hydration for SCMs and the calcium silicates of the cements have been determined from ^{29}Si MAS NMR spectra for the blends containing microsilica, fly ash, or natural pozzolan. Quantitative information about the Al/Si ratio and average chain length of alumino-silicate tetrahedra in the C-S-H phase has also been obtained from these spectra. The degree of hydration for slags cannot be determined directly from the ^{29}Si MAS NMR spectra due to severe overlap of the slag peak with the resonances from alite, belite, and the C-S-H phase of the hydrating cement. Therefore, a new method based on ^{27}Al MAS NMR has been used to obtain quantitative estimates for the degree of slag hydration. Results are presented and discussed for each type of cement blend separately, but a section of the chapter is also devoted to the comparison of results obtained for the different types of blends. Finally, the estimates for slag reaction derived from ^{27}Al MAS NMR are compared with similar results obtained for the same cement – slag blends using a SEM-BSE based quantification. The enclosed Paper III also discusses the use of ^{29}Si and ^{27}Al MAS NMR for measuring the degree of reaction in Portland cement blends with SCMs.

8.2 Studied cement systems

The different cement systems subjected to hydration experiments are listed in Table 8.1 along with the weight proportions of cement and SCM in the anhydrous blends, as well as the water/binder and water/cement ratios used in the pastes. The paste mixes are designed to keep the ratios by volume of water to binder at a constant value (V_{water}/V_{binder} = 0.4) for

all systems. The procedures employed for paste mixing, curing and stopping of hydration are given in Appendix II, while the experimental conditions employed for the acquisition of ^{29}Si and ^{27}Al MAS NMR spectra are found in Appendix I.

Table 8.1 Studied cement systems and their main characteristics in the mixed pastes[1].

Materials	Substitution ratio in paste	water/binder[2]	water/cement[2]
cement A	100 %	0.40	0.40
cement C	100 %	0.40	0.40
cement A – microsilica	90 %-10 %	0.41	0.45
cement C – microsilica	90 %-10 %	0.41	0.45
cement A – fly ash 2	70 %-30 %	0.45	0.64
cement C – fly ash 2	70 %-30 %	0.43	0.61
cement A – natural pozzolan	70 %-30 %	0.43	0.61
cement C – natural pozzolan	70 %-30 %	0.43	0.61
cement A – slag 1	60 %-40 %	0.41	0.69
cement C – slag 1	60 %-40 %	0.42	0.69
cement A – slag 8	60 %-40 %	0.42	0.69
cement C – slag 8	60 %-40 %	0.42	0.70

[1] It is noted that cement A is a white Portland cement. [2] The ratios water/binder and water/cement are by weight.

8.3 Hydration of pure cements

The hydration of pure pastes of cement A and cement C have been studied as reference systems and the result obtained for these two systems will be compared with similar results for the blended systems. The hydration was stopped after 1, 2, 3, 7, 14, 28, 90, 180, and 360 days. Fig. 8.1 illustrates the hydration of cement A and C followed by ^{29}Si MAS NMR. The spectra of the anhydrous cements (top spectra in Fig. 8.1(a) and (b)) only display the overlapping resonances from the alite and belite phases (Q^0 units) in the range from approx. -66 to -77 ppm. After one day of hydration new signals appear in the chemical shift range from -77 to -88 ppm, corresponding to Q^1 and Q^2 units. This is due to formation of the C-S-H phase from the reaction of the anhydrous calcium silicates with water. As the hydration proceeds, the intensity of the resonances from the C-S-H phase

increases while the intensities of the alite and belite signals are correspondingly reduced. It is evident from visual inspection of the spectra that the intensity of the broad peak from alite decreases at a faster rate compared to the narrow signal from belite (-71.3 ppm), thus demonstrating the difference in reaction rate for alite and belite. It also appears from the spectra, that a substantial amount of belite is still present in the pastes of both cement A and cement C even after 360 days of hydration.

The degrees of hydration (*H*) for alite and belite have been determined at each step of the hydration process by computer deconvolution of the ^{29}Si MAS NMR spectra. This is performed in much the same way as described in Section 6.3.2 for the deconvolution of ^{29}Si MAS NMR spectra of anhydrous cements, but with the additional employment of Q^1 and Q^2 resonances originating from the C-S-H phase. This is exemplified in Fig. 8.2 for the ^{29}Si MAS NMR spectrum of cement C hydrated for 14 days. Fig. 8.3 gives a schematic two dimensional representation of the C-S-H structure (14 Å tobermorite). A principal layer of composition CaO_2 is located between two silicate chains, with the upper part of the figure displaying an octameric silicate chain containing two bridging SiO_4 tetrahedra (Q_B^2), four paired SiO_4 sites (Q_P^2), and two SiO_4 chain-end groups (Q^1). Resonances from the SiO_4 Q^1 sites are observed at δ_{iso} = -78 ppm in the experimental spectrum of cement C hydrated for 14 days (Fig. 8.2 (a)). The Q_B^2 and Q_P^2 SiO_4 sites give rise to the peak observed at δ_{iso} = -84.5 ppm. Due to linebroadening it is not possible to distinguish between the resonances originating from the Q_B^2 and Q_P^2 SiO_4 sites in the C-S-H formed in hydrated Portland cements. However, these sites may be distinguished in ^{29}Si MAS NMR spectra of synthesized samples of C-S-H [252]. The assignment of the Q^1, Q_B^2, and Q_P^2 resonances are based on the early studies of solid silicates by Lippmaa and Mägi [219,253], which showed that the ^{29}Si isotropic chemical shift is mainly dependent on the degree of condensation of SiO_4 tetrahedra, and on later ^{29}Si MAS NMR studies of cementitious materials [76,188,254,255]. The incorporation of Al into a bridging site is illustrated in the lower part of Fig. 8.3. The electronic environments of the two neighboring SiO_4 sites (Q^2(1Al)) are slightly changed due to the presence of Al which results in a shift of the ^{29}Si resonances to higher frequency.

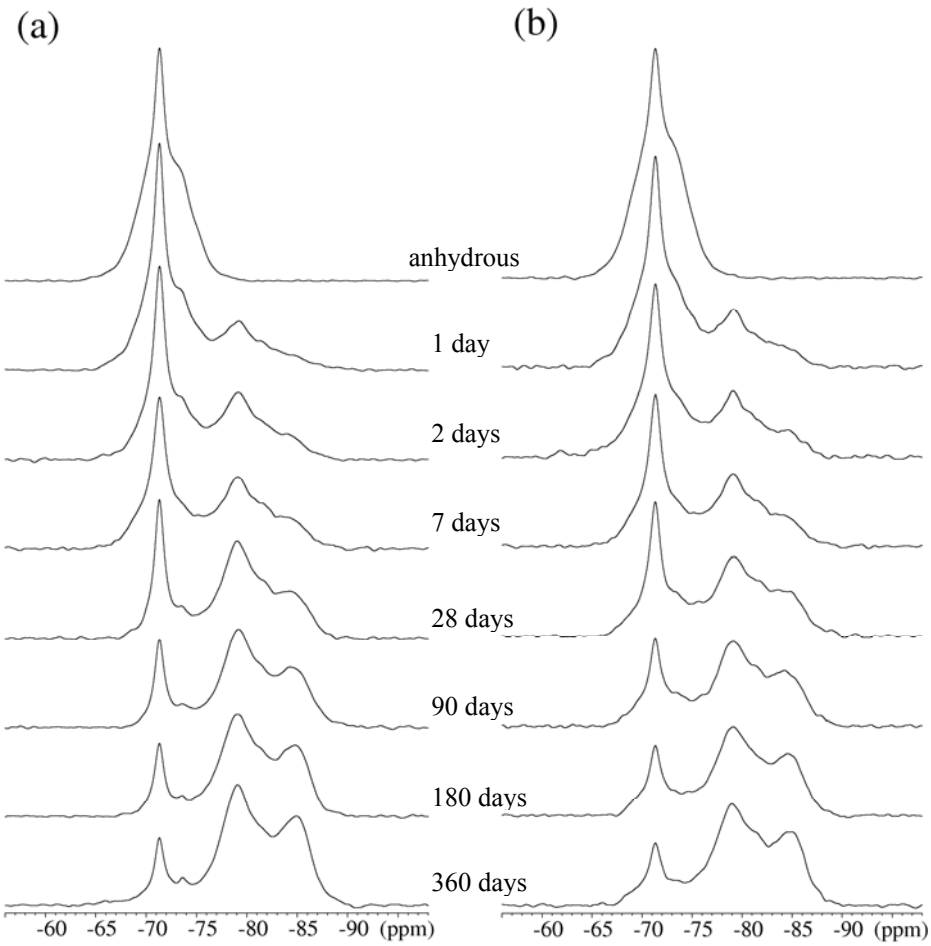

Fig. 8.1 ^{29}Si MAS NMR spectra (9.4 T, ν_R = 12.0 kHz) of (a) cement A and (b) cement C hydrated for 1, 2, 7, 28, 90, 180, and 360 days. Spectra of the anhydrous cements are also displayed for comparison.

A similar effect has been observed earlier for zeolites where the ^{29}Si chemical shift is changed by the incorporation of Al in tetrahedral Si sites [219,256]. In Fig. 8.2(a) the Q^2(1Al) resonance appears at δ_{iso} = -81.5 ppm between the peaks of Q^1 and Q^2. This assignment is originally based on the ^{29}Si and ^{27}Al MAS NMR and EELS investigations of a hydrated synthetic glass by Richardson *et al.* [226], an assignment which has later been supported by ^{29}Si and ^{27}Al MAS NMR studies by Andersen *et al.* [257] on the C-S-H formed in white Portland cement pastes. In the deconvolution of the Q^1, Q^2(1Al), Q^2 sites, the individual peaks are simulated using only one line for each site with the linewidths of the Q^1 and Q^2 resonances being allowed to vary freely, while the Lorentzian/Gaussian lineshape fraction is fixed at 0.5. For some of the samples, typically the ones hydrated for more than 7 days, the addition of an extra line at -77.0 ppm and -85.7 ppm is required for the simulation of the Q^1 and the Q^2 peaks, respectively. The linewidth of the Q^2(1Al)

resonance and the Lorentzian/Gaussian lineshape fraction is fixed at 200 Hz and 0.5, respectively, in accordance a with previous reported deconvolution procedure used for similar hydrated Portland cements [258].

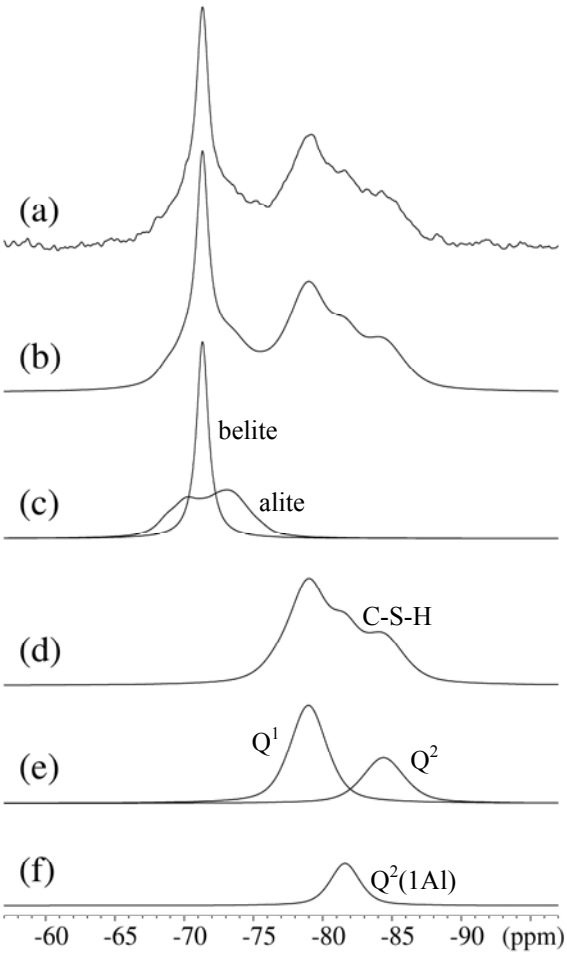

Fig. 8.2 Deconvolution of the ^{29}Si MAS NMR spectrum for cement C hydrated for 14 days. (a) Experimental ^{29}Si MAS NMR spectrum (9.4 T, ν_R = 12.0 kHz). (b) Optimized simulation of ^{29}Si MAS NMR spectrum in (a). (c) Deconvolved alite and belite sub-spectra for the simulated spectrum in (b). (d) Deconvolved C-S-H sub-spectrum for the simulated spectrum in (b). Part (e) and (f) illustrate the simulated resonances for Q^1, Q^2, and Q^2(1Al) sites in the C-S-H phase.

The type of information that can be extracted from the deconvolution of ^{29}Si MAS NMR spectra is the degrees of hydration for alite and belite, the average chain length of alumino-silicate tetrahedra in the C-S-H, and the Al/Si ratio for the C-S-H. The degree of hydration (H) for alite is calculated as:

$$H(\text{alite}) = \left(1 - \frac{I_{alite}^{hydrated}}{I_{alite}^{anhydrous}}\right) \times 100\ \% \qquad (8.1)$$

where $I_{alite}^{hydrated}$ is the normalised signal intensity originating from the unreacted alite in the ^{29}Si MAS NMR spectrum of a hydrated sample, and $I_{alite}^{anhydrous}$ is the normalised intensity

from alite in the corresponding anhydrous sample. The degree of hydration for belite is calculated using an analogous equation:

$$H(\text{belite}) = \left(1 - \frac{I_{belite}^{hydrated}}{I_{belite}^{anhydrous}}\right) \times 100\ \% \tag{8.2}$$

It is noted that the measures obtained from Eq. (8.1.) and (8.2) are independent of the chemical composition of the alite and belite phases. The deconvolution of the ^{29}Si MAS NMR spectra of the hydrated cements gives the intensity of the different Q^n-species as a function of hydration time. This information can be utilized to calculate the average silicate chain length in the structure of C-S-H (Fig. 8.3). The average length of chains containing both SiO_4 and AlO_4 tetrahedra ($\overline{CL}$) and of chains consisting purely of SiO_4 tetrahedra ($\overline{CL}_{Si}$) is derived by employment of the equations below, where the signal intensities of the different Q^n units in ^{29}Si MAS NMR spectra are used [259,260]:

$$\overline{CL} = \frac{I(\mathrm{Q}^1) + I(\mathrm{Q}^2) + \frac{3}{2} I(\mathrm{Q}^2(1\mathrm{Al}))}{\frac{1}{2} I(\mathrm{Q}^1)} \tag{8.3}$$

$$\overline{CL}_{\mathrm{Si}} = \frac{I(\mathrm{Q}^1) + I(\mathrm{Q}^2) + I(\mathrm{Q}^2(1\mathrm{Al}))}{\frac{1}{2} I(\mathrm{Q}^1 + \mathrm{Q}^2(1\mathrm{Al}))} \tag{8.4}$$

Furthermore, the Al_{IV}/Si ratio for the C-S-H phase can be obtained by [259]:

$$\mathrm{Al_{IV}/Si} = \frac{\frac{1}{2} I(\mathrm{Q}^2(1\mathrm{Al}))}{I(\mathrm{Q}^1) + I(\mathrm{Q}^2) + I(\mathrm{Q}^2(1\mathrm{Al}))} \tag{8.5}$$

where Al_{IV} is aluminium in tetrahedral coordination.

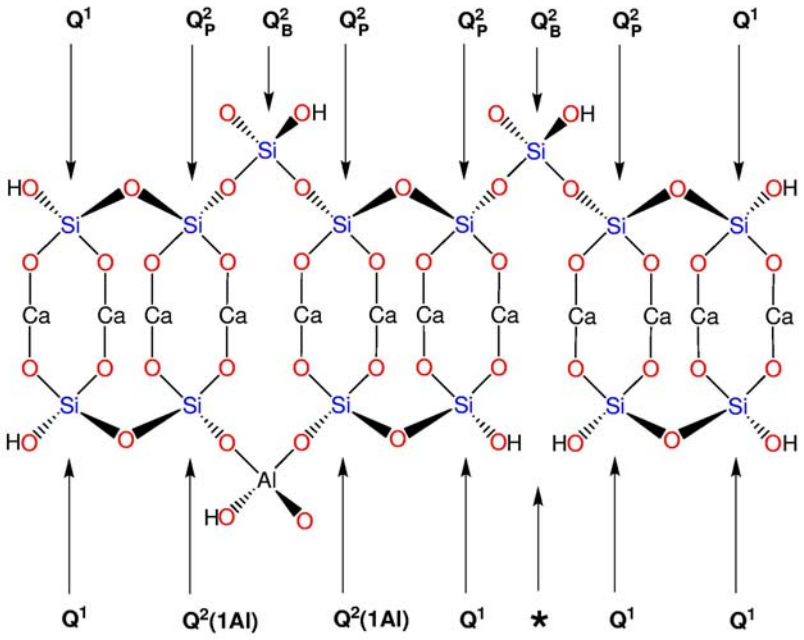

Fig. 8.3 Two dimensional schematic depiction of the main structural features of C-S-H in which a layer of composition CaO_2 is located between two silicate chains. The upper part shows an octameric chain with the characteristic features of the "dreierketten"-based models for the C-S-H phase. The incorporation of Al in a bridging site is illustrated in the lower part where a defect site (*) is also present, thus resulting in a pentameric chain and a dimer of SiO_4 tetrahedra. Interlayer Ca^{2+} ions and H_2O molecules are not included in this representation.

The results obtained from deconvolution of the ^{29}Si MAS NMR spectra of cement A and cement C are presented in Table 8.2 and Fig. 8.4. After one day of hydration roughly 40 wt% of the alite has reacted in both pastes, increasing to 91.9 wt% and 86.8 wt% for cement A and C, respectively, after 360 days. The belite is reacting at a much slower rate. For cement A the belite does not appear to react before at least 7 days of hydration, while approx. 10 wt% of the belite has reacted at 7 days for cement C. After 360 day some 30 wt% of unreacted belite still remains in both pastes. XRD investigations of the pure pastes of cement A and C [261] showed trends for the reaction of alite and belite similar to those derived here from NMR. The evolution of the average chain lengths in the C-S-H phase ($\overline{CL}$ and $\overline{CL}_{Si}$) with hydration time follows the same trend for cement A and cement C. The chains increase in length as the hydration proceeds, which is in good agreement with previously reported results from an ^{29}Si MAS NMR investigation of white Portland cement hydration [257]. In general, the chain lengths are rather similar for the two systems.

Table 8.2 Degrees of hydration (*H*) for alite and belite, as well as average chain lengths of alumino-silicate ($\overline{CL}$) and SiO_4 tetrahedra ($\overline{CL}_{Si}$) and Al/Si ratios for the C-S-H phase for pure pastes of cement A and cement C [1].

Hydration time (days)	cement A				
	H(alite)	*H*(belite)	$\overline{CL}$	$\overline{CL}_{Si}$	Al/Si ratio
1	39.2	0.0	3.55	2.48	0.095
2	58.7	0.0	3.73	2.46	0.109
3	65.3	0.0	3.74	2.46	0.110
7	75.2	0.0	3.69	2.45	0.108
14	80.9	16.8	3.85	2.78	0.079
28	84.6	24.1	4.02	2.86	0.080
90	91.1	44.0	4.35	3.01	0.083
180	91.7	61.1	4.35	3.07	0.078
360	91.9	69.5	4.70	3.21	0.081
Hydration time (days)	cement C				
	H(alite)	*H*(belite)	$\overline{CL}$	$\overline{CL}_{Si}$	Al/Si ratio
1	38.5	4.5	3.53	2.59	0.081
2	54.1	0.0	3.83	2.55	0.103
3	58.1	3.3	3.75	2.60	0.093
7	63.4	9.7	3.85	2.62	0.096
14	69.6	11.3	3.85	2.70	0.088
28	74.9	22.9	4.08	2.93	0.077
90	84.3	31.8	4.07	3.10	0.062
180	84.8	57.0	4.06	3.03	0.068
360	86.8	67.2	4.14	3.10	0.065

[1] Data were obtained from ^{29}Si MAS NMR spectra (9.4 T, ν_R = 12.0 kHz) acquired after nine different hydration times.

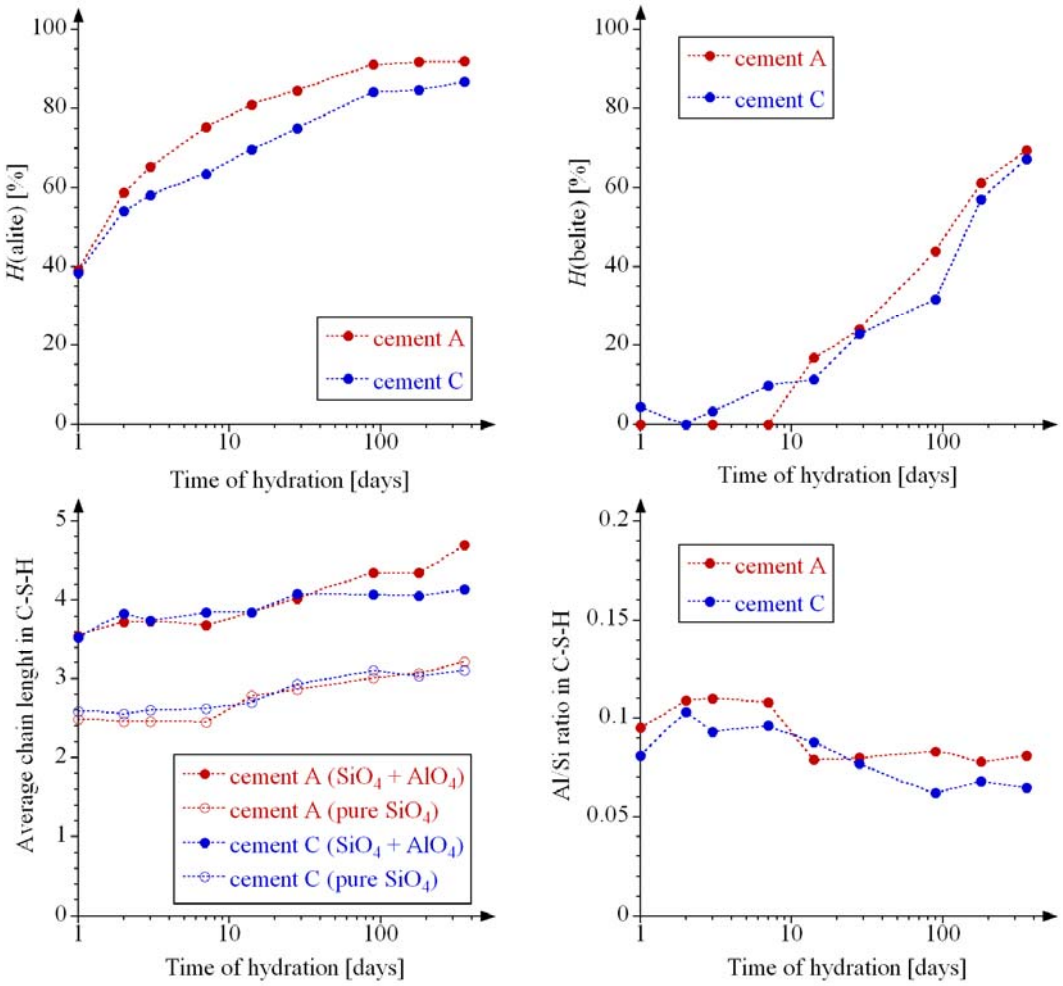

Fig. 8.4 Degrees of hydration (*H*) for alite and belite and average chain lengths and Al/Si ratios in the C-S-H phase for hydrated samples of cement A and cement C. Data were obtained from ^{29}Si MAS NMR spectra (9.4 T, ν_R = 12.0 kHz) and are found in Table 8.2.

8.4 Hydration of cement – microsilica blends

The hydration of cement A and cement C in blends with microsilica have been studied for hydration times up to 180 days. The mixing procedure for these pastes differs somewhat from the procedure employed for all other systems, as microsilica is added to the mix not as a dry powder, but in the form of a slurry (see Appendix II for details). This was done to secure a good dispersion of the very fine-grained microsilica in the paste. Representative ^{29}Si MAS NMR spectra for the two hydration series involving microsilica are displayed in Fig. 8.5. These spectra appear very similar to the ones recorded of the pure pastes of cement A and C, but with the addition of a broad peak ranging from approx. -100 to -125 ppm, which is due to the presence of the amorphous microsilica. The intensity of this peak

gradually decreases as microsilica reacts and contributes to the formation of the C-S-H phase.

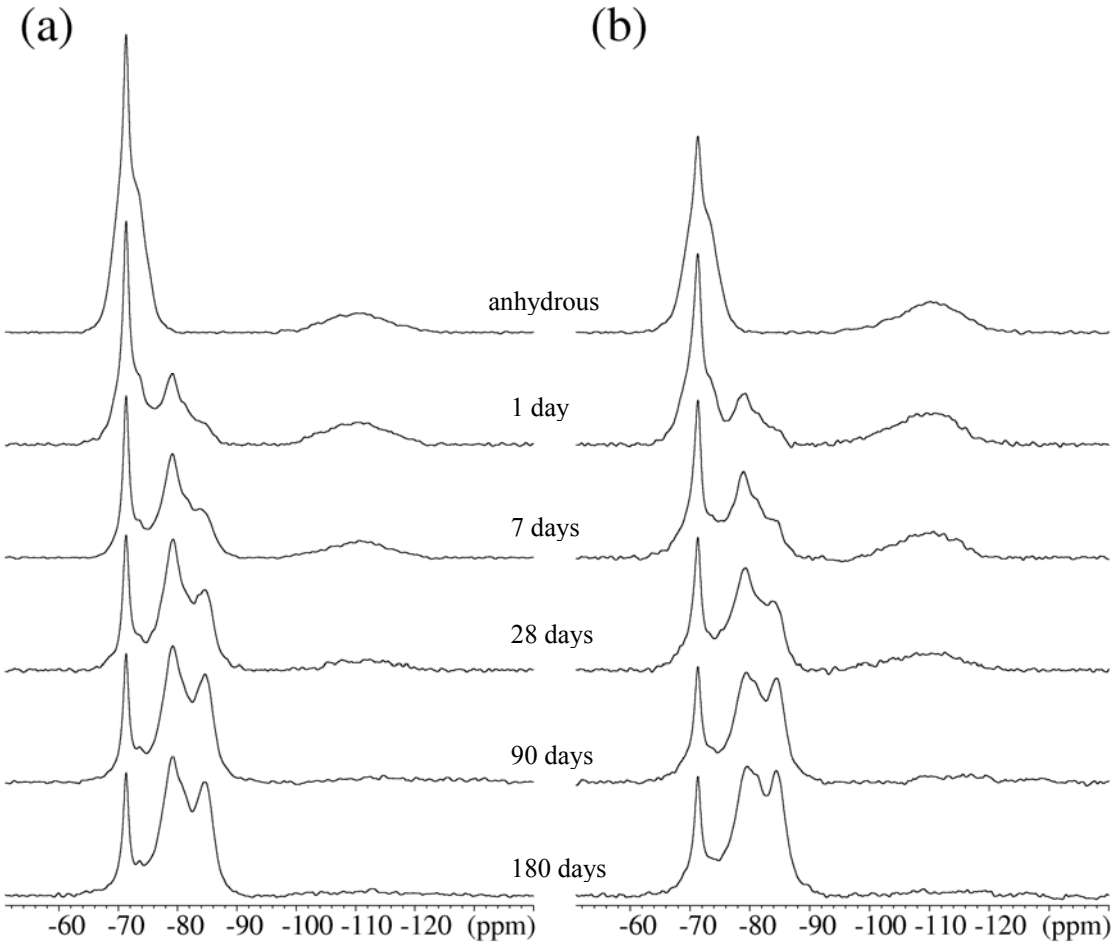

Fig. 8.5 ^{29}Si MAS NMR spectra (9.4 T, ν_R = 12.0 kHz) of (a) cement A – microsilica and (b) cement C – microsilica hydrated for 1, 7, 28, 90, and 180 days. Spectra of the anhydrous blends are displayed as well for comparison.

The broad signal from microsilica is conveniently separated from the other resonances in the spectra, which makes the deconvolution procedure rather straight-forward. The only difference to the procedure used for the pure Portland cement pastes is the addition of two resonances (-107.5 ppm and -112.0 ppm) for the simulation of the peak originating from microsilica. In the deconvolution of the ^{29}Si MAS NMR spectra the linewidth was fixed at 650 and 750 Hz for these two resonances, respectively, and the Lorentzian/Gaussian lineshape factor was fixed at 0.5. Fig. 8.6 gives an example of the simulated spectrum of

cement A – microsilica hydrated for 7 days. The results obtained from the deconvolution of the ^{29}Si MAS NMR spectra are listed in Table 8.3.

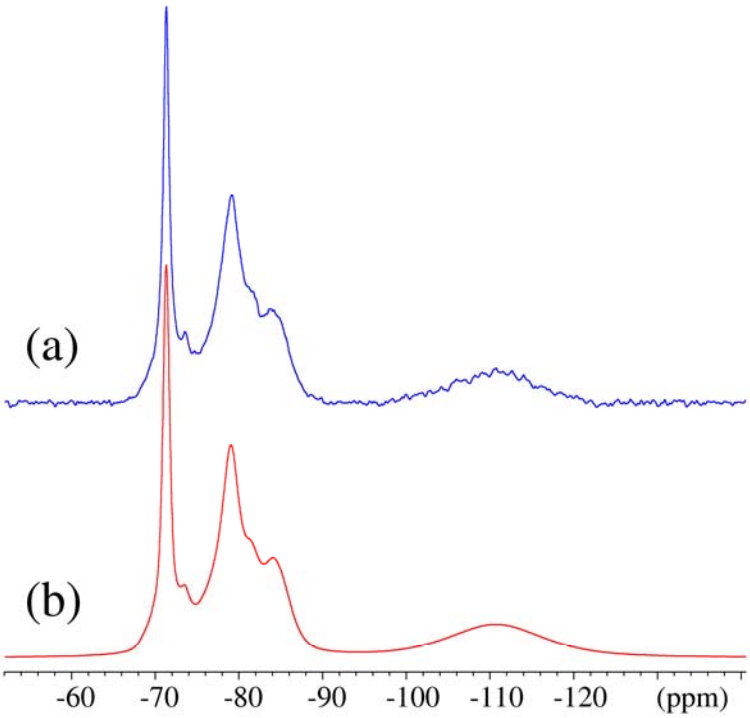

Fig. 8.6 (a) Experimental ^{29}Si MAS NMR spectrum (9.4 T, ν_R = 12.0 kHz) of cement A blended with microsilica after 7 days of hydration. (b) Optimized simulation of the spectrum in part (a).

The degree of hydration for the microsilica is lower in the blend with cement A as compared to the cement C blend after 1 and 2 days of hydration (Fig. 8.7). Hereafter, the situation is reversed with microsilica in the blend with cement A exhibiting the highest degree of hydration. At 180 days about 85 % of the microsilica has reacted in both systems. ^{29}Si MAS NMR has previously been utilized to follow the hydration of cement blends containing various proportions of microsilica [75,76]. For instance, Sun and Young [77] have reported degrees of reaction for microsilica in ultra-high strength cement pastes. They found that 9 – 15 % of the microsilica had reacted after 1 day, increasing to 55 – 59 % at 180 days. These results differ somewhat from the ones presented in Table 8.3, where less than 5 % of the microsilica has reacted after one day, and more than 84 % has reacted after 180 days. However, this discrepancy may be due to the fact that the cement pastes studied by Sun and Young contained 18 – 48 wt% of microsilica, whereas the ones investigated in this work contained only 10 wt%. The degrees of hydration for alite and belite, and the chain lengths and Al/Si ratio in C-S-H will be compared with similar results from the other cement systems ± SCMs in Section 8.7.

Table 8.3. Degrees of hydration (*H*) for alite, belite, and microsilica, as well as average chain lengths of alumino-silicate ($\overline{CL}$) and SiO_4 tetrahedra ($\overline{CL}_{Si}$) and Al/Si ratios for the C-S-H phase for hydrated mixtures of cement A and cement C with microsilica[1].

Hydration time (days)	cement A – microsilica					
	H(alite)	*H*(belite)	*H*(MS)	$\overline{CL}$	$\overline{CL}_{Si}$	Al/Si ratio
1	51.27	6.09	1.09	3.65	2.58	0.089
2	67.78	11.87	2.93	3.80	2.64	0.091
3	71.68	12.96	14.31	3.93	2.74	0.088
7	79.93	18.25	24.04	4.19	2.86	0.089
14	83.24	25.26	39.31	4.43	3.00	0.088
28	88.37	28.69	58.40	4.51	3.12	0.081
90	90.68	32.95	78.68	5.11	3.28	0.091
180	91.97	38.21	84.08	5.19	3.26	0.096
Hydration time (days)	cement C – microsilica					
	H(alite)	*H*(belite)	*H*(MS)	$\overline{CL}$	$\overline{CL}_{Si}$	Al/Si ratio
1	36.12	1.73	4.30	3.72	2.52	0.101
2	41.86	4.45	8.81	3.71	2.51	0.102
3	47.60	9.80	4.46	3.65	2.54	0.094
7	56.96	30.94	12.09	4.10	2.68	0.104
14	61.02	33.08	29.01	4.09	2.78	0.093
28	67.42	33.99	48.17	4.20	2.99	0.078
90	73.21	41.49	80.31	5.44	3.37	0.095
180	75.82	47.20	86.01	5.66	3.36	0.103

[1] Data obtained from deconvolved ^{29}Si MAS NMR spectra (9.4 T, ν_R = 12.0 kHz) acquired after eight different hydration times for cement A and cement C in blends with microsilica (MS)

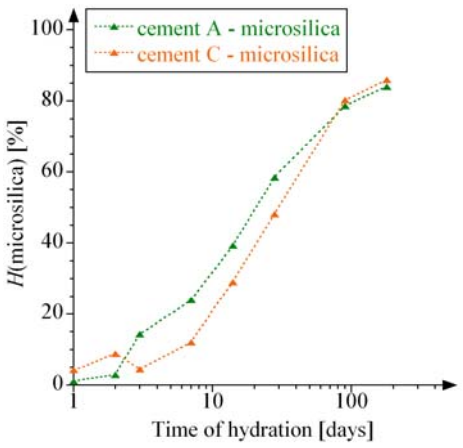

Fig. 8.7 Degrees of hydration (*H*) for microsilica in mixtures of cement A and cement C with microsilica. Data were obtained from ^{29}Si MAS NMR spectra acquired at 9.4 T using a spinning speed of ν_R = 12.0 kHz.

8.5 Hydration of cement – fly ash blends

The hydration of cement A and C blended with fly ash 2 has been studied for ages ranging from 1 to 180 days. Representative ^{29}Si MAS NMR spectra are given in Fig. 8.8, where the fly ash gives a broad asymmetric peak in the chemical shift region from -85 to -125 ppm. There is no overlap of resonances from the fly ash with the ones originating from the anhydrous calcium silicates in the anhydrous spectra, but as the hydration proceeds the peak from Q^2 sites in the C-S-H phase overlaps slightly with the low-intensity shoulder from the fly ash around -85 ppm. Visual inspection of the ^{29}Si MAS NMR spectra of the hydrated fly ash blends indicates that the overall lineshape of the fly ash peak do not change as the hydration proceeds. Therefore, it is assumed that no preferential hydration of parts of the fly ash material takes place during hydration. It also appears that the fly ash is almost non-reactive during the first 28 days of hydration in both systems.

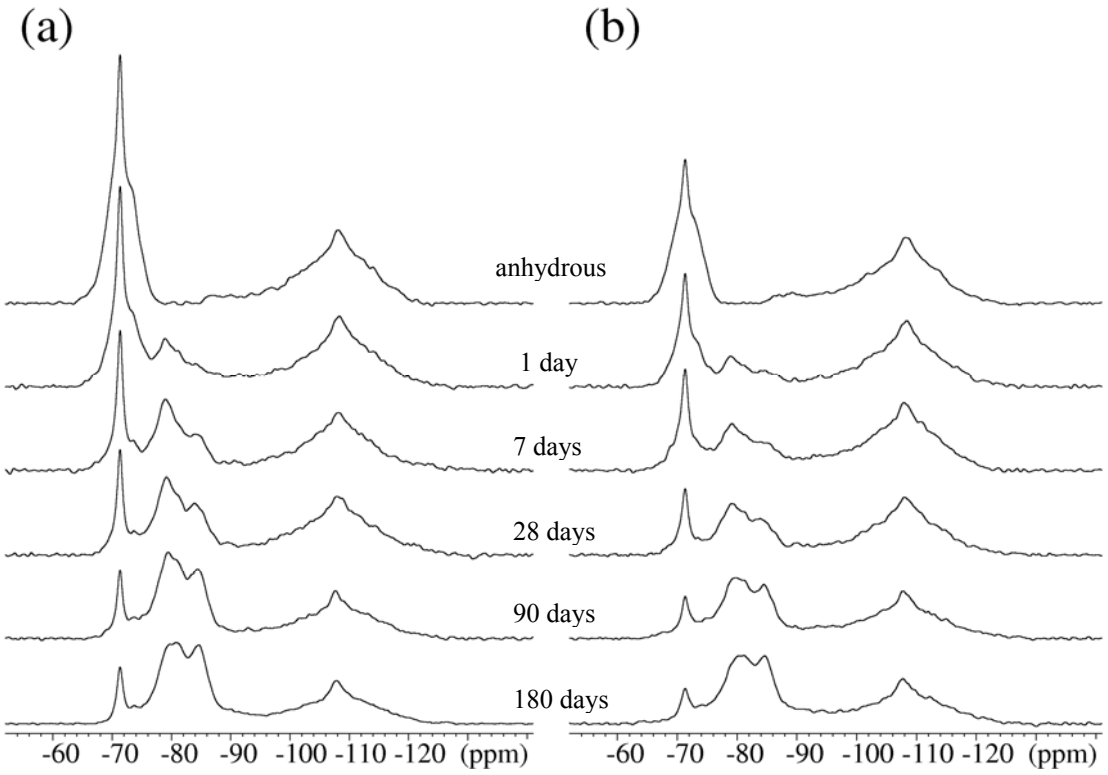

Fig. 8.8 ^{29}Si MAS NMR spectra (9.4 T, ν_R = 12.0 kHz) of (a) cement A – fly ash 2 and (b) cement C – fly ash 2 hydrated for 1, 7, 28, 90, 180 days. The top spectrum in each column is the ^{29}Si MAS NMR spectrum of the anhydrous blend.

For deconvolution of the ^{29}Si MAS NMR spectra of hydrated samples a sub-spectrum for the anhydrous fly ash 2 was initially created using nine lines with widths ranging from 300

to 575 Hz and Lorentzian/Gaussian lineshape fractions varying between 0 and 1. This fly ash sub-spectrum was subsequently employed as a fixed sub-spectrum in the devolution procedure, *i.e.*, intensities of the fly ash resonances were manually scaled to fit the experimental spectrum, while the relative intensities of the fly ash resonances were kept at a constant ratio. Fig. 8.9 illustrates the deconvolution of the ^{29}Si MAS NMR spectrum of cement C – fly ash 2 hydrated for 14 days.

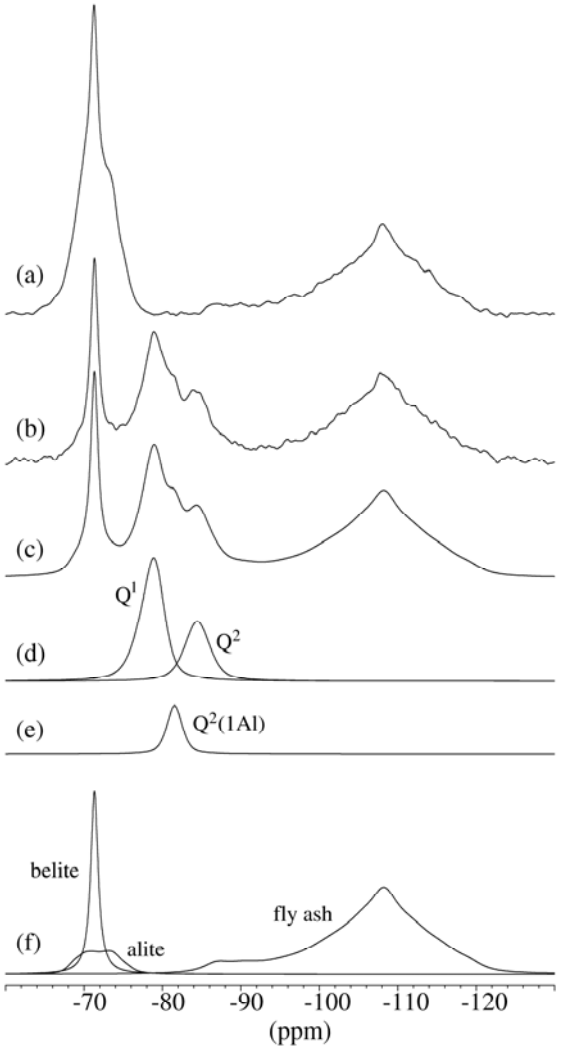

Fig. 8.9 Deconvolution of the ^{29}Si MAS NMR spectrum for cement C blended with fly ash 2 hydrated for 14 days. (a) Experimental ^{29}Si MAS NMR spectrum (9.4 T, ν_R = 12.0 kHz) of the anhydrous blend, which was used for creating the sub-spectrum for the fly ash. (b) Experimental ^{29}Si MAS NMR spectrum (9.4 T, ν_R = 12.0 kHz) of cement C – fly ash 2 hydrated for 14 days. (c) Optimized simulation of the ^{29}Si MAS NMR spectrum in part (b). Part (d) and (e) illustrate the simulated resonances for Q^1, Q^2, and Q^2(1Al) sites in the C-S-H phase, while the deconvolved sub-spectra for alite, belite and the fly ash are shown in part (f).

Table 8.4 presents the results obtained from deconvolutions of the ^{29}Si MAS NMR spectra. The fly ash in the cement A blend exhibits a notably low reactivity, at least for the first 28 days where less than 1 % of the fly ash has reacted, which is probably within the uncertainty of the determination. However, after 180 days of hydration ~20 % of the fly ash has reacted in this blend. The trend is the same for the blend with cement C where the degree of hydration is as low as 3.9 % after 28 day, rising to 26.7 % after 180 days. These

low degrees of fly ash reaction agree reasonably well with values reported earlier by Lam *et al.* [262]. They found, using a selective dissolution method, that after 7 days of hydration only 6 % of the fly ash had reacted in pastes containing 45 – 55 wt% fly ash, and that more than 80 % of the fly ash still remained unreacted after 90 days of hydration. Similarly, Feldman *et al.* [263] have reported that considerable amounts of fly ash remained as unreacted particles in cement – fly ash pastes after 91 days of hydration. This was based on electron microscopy and the content of unreacted fly ash was not quantified. Degrees of hydration for alite and belite as well as average chain lengths and Al/Si ratios for the C-S-H phase are discussed in Section 8.8.

Table 8.4 Degrees of hydration (*H*) for alite, belite, and fly ash as well as average chain lengths of alumino-silicate ($\overline{CL}$) and SiO_4 tetrahedra ($\overline{CL}_{Si}$) and Al/Si ratios for the C-S-H phase for hydrated mixtures of cement A and cement C with fly ash 2 [1].

Hydration time (days)	cement A – fly ash 2					
	H(alite)	*H*(belite)	*H*(FA2)	$\overline{CL}$	$\overline{CL}_{Si}$	Al/Si ratio
1	39.3	0.0	0.0	4.04	2.58	0.113
2	57.8	0.0	0.0	3.67	2.51	0.099
3	69.2	1.8	0.0	3.89	2.75	0.086
7	80.0	4.0	0.0	3.97	2.76	0.088
14	85.4	12.3	0.5	4.08	2.84	0.086
28	86.8	26.4	0.7	4.43	2.97	0.091
90	94.1	37.8	18.6	5.21	3.12	0.108
180	98.1	43.1	20.2	6.41	3.31	0.126
Hydration time (days)	cement C – fly ash 2					
	H(alite)	*H*(belite)	*H*(FA2)	$\overline{CL}$	$\overline{CL}_{Si}$	Al/Si ratio
1	44.9	0.1	1.2	4.75	2.90	0.111
2	53.7	0.0	0.5	4.61	2.89	0.106
3	58.2	1.1	0.0	4.78	2.94	0.108
7	72.0	1.1	0.0	4.77	2.95	0.107
14	77.2	4.5	2.7	4.68	2.95	0.103
28	81.8	22.8	3.9	4.88	3.05	0.102
90	86.5	49.7	18.6	5.89	3.12	0.129
180	87.9	63.3	26.7	6.82	3.42	0.127

[1] Data obtained from deconvolved ^{29}Si MAS NMR spectra (9.4 T, ν_R = 12.0 kHz) acquired after eight different hydration times for cement A and cement C in blends with fly ash 2 (FA2).

8.6 Hydration of cement – natural pozzolan blends

The hydration of cement A and cement C in blends with the natural pozzolan has been studied for ages of 1, 2, 3, 7, 14 and 28 days. In Fig. 8.10 representative ^{29}Si MAS NMR spectra for these hydration series are presented. The anhydrous spectra display resonances from alite and belite (-66 to -77 ppm) and from a number of overlapping peaks originating from the different components in the natural pozzolan (approx. -85 to -114 ppm). The intensity of the resonances from the alite and belite phases, as well as the natural pozzolan, decrease as the hydration proceeds with a corresponding increase of the intensity from the produced C-S-H. Around -85 ppm, part of the low-intensity shoulder of the natural pozzolan lineshape overlaps with the peak from the Q^2 sites of the C-S-H, which must be addressed in the deconvolution of the spectra. A sub-spectrum was initially created from the anhydrous ^{29}Si MAS NMR spectrum of the natural pozzolan, which involved six lines (-87, -90, -95, -101, -108, and -113 ppm) using linewidths of 200 Hz, 200 Hz, 350 Hz, 400 Hz, 365 Hz, and 400 Hz, respectively. The Lorentzian/Gaussian lineshape fraction varied between 0 and 0.5.

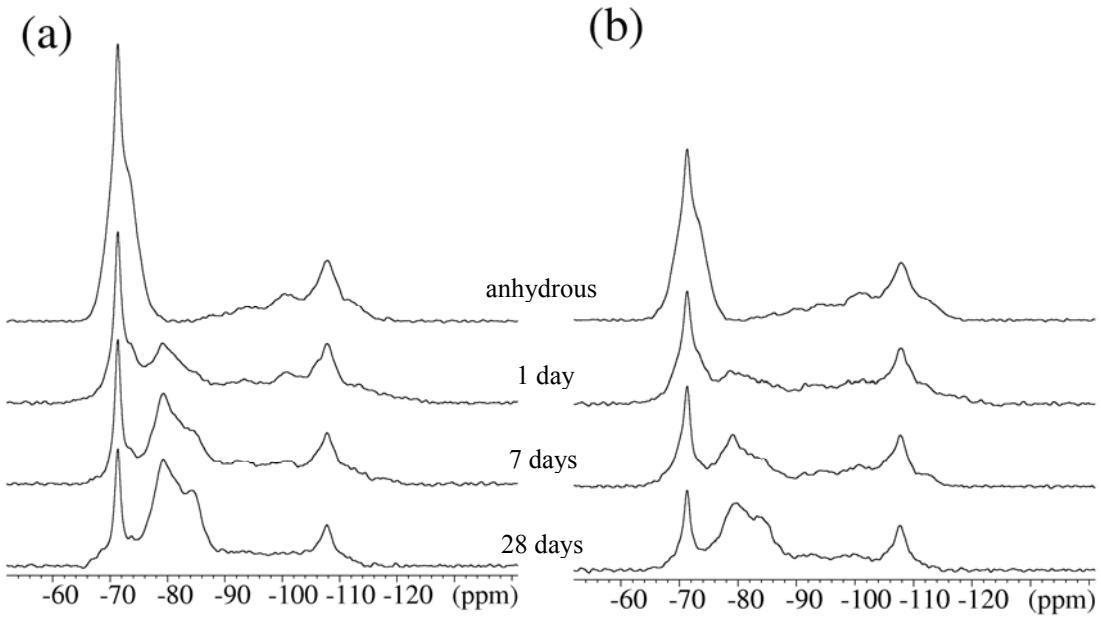

Fig. 8.10 ^{29}Si MAS NMR spectra (9.4 T, ν_R = 12.0 kHz) of (a) cement A – natural pozzolan and (b) cement C – natural pozzolan hydrated for 1, 7, and 28 days. The top spectrum in each column is the ^{29}Si MAS NMR spectrum of the anhydrous blend.

The overall lineshape of the overlapping resonances from the natural pozzolan appears almost constant in the different ^{29}Si MAS NMR spectra of the hydrated samples, which indicate roughly similar reaction rates for the different components in the pozzolan. Therefore, fixed relative intensities for the six resonances were used to simulate the lineshape of the pozzolan in the deconvolution of the spectra.

The deconvolution of the ^{29}Si MAS NMR spectra is illustrated in Fig. 8.11 for the cement A – natural pozzolan blend hydrated for 2 days and results from the deconvolutions are listed in Table 8.5. The degree of hydration is generally low for the pozzolan in both systems during the first three days of hydration (< 5 %). After 28 days ~35 % and ~31 % of the pozzolan have reacted in the blends with cement A and cement C, respectively. Low reactivity has previous been reported for natural pozzolan in pastes of C_3S. Massazza and Testolin [80] found that 16 – 29 % of the pozzolan had been consumed after 180 days.

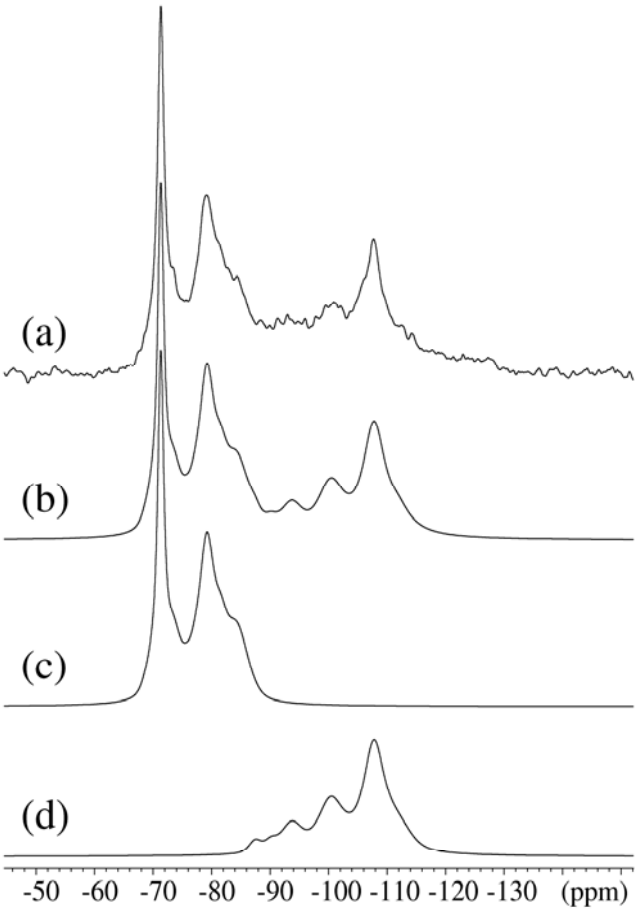

Fig. 8.11 Deconvolution of the ^{29}Si MAS NMR spectrum for the cement C – natural pozzolan blend hydrated for 2 days. (a) Experimental ^{29}Si MAS NMR spectrum (9.4 T, ν_R = 12.0 kHz). (b) Optimized simulation of the ^{29}Si MAS NMR spectrum in part (a). (c) Sub-spectrum containing contributions from alite, belite, and the C-S-H phase. (d) Deconvolved sub-spectrum for the natural pozzolan.

Table 8.5 Degrees of hydration (*H*) for alite, belite, and natural pozzolan (NP), as well as average chain lengths of alumino-silicate ($\overline{CL}$) and SiO_4 tetrahedra ($\overline{CL}_{Si}$) and Al/Si ratios for the C-S-H phase for cement A and cement C in blends with natural pozzolan [1].

Hydration time (days)	cement A – natural pozzolan					
	H(alite)	*H*(belite)	*H*(NP)	$\overline{CL}$	$\overline{CL}_{Si}$	Al/Si ratio
1	62.0	10.0	0.0	4.55	2.89	0.104
2	74.4	13.4	0.0	4.44	2.98	0.090
3	76.4	21.9	4.3	4.17	2.94	0.081
7	77.3	37.3	7.5	4.84	3.18	0.090
14	81.8	33.6	21.4	4.79	3.15	0.089
28	83.5	37.5	34.9	5.21	3.26	0.096
Hydration time (days)	cement C – natural pozzolan					
	H(alite)	*H*(belite)	*H*(NP)	$\overline{CL}$	$\overline{CL}_{Si}$	Al/Si ratio
1	43.9	0.0	0.8	4.47	2.72	0.117
2	53.5	0.0	0.9	4.13	2.59	0.115
3	56.5	0.0	2.8	3.61	2.44	0.103
7	60.6	0.0	13.3	4.49	2.77	0.113
14	68.1	4.5	23.6	4.22	2.80	0.098
28	80.4	11.1	31.4	4.85	3.08	0.099

[1] Data were obtained from deconvolved ^{29}Si MAS NMR spectra (9.4 T, ν_R = 12.0 kHz) recorded after 6 different hydration times.

8.7 Comparison of data obtained from ^{29}Si MAS NMR

The degree of hydration for alite, belite and SCMs (microsilica, fly ash 2, natural pozzolan) in the blends with cement A and cement C are compared in Fig. 8.12. Data for the pure pastes of cement A and C are included for comparison. The degree of hydration for alite is generally higher in the cement A – SCM blends than in the paste of pure cement A, especially during the first 7 days of hydration. At later ages the difference levels off. The accelerating effect of the SCM on the alite reaction is most pronounced for the blends with natural pozzolan and microsilica, *e.g.*, more than 60 % of the alite has reacted after 1 day for the cement A – natural pozzolan blend as compared to slightly less than 40 % in the pure paste. After 180 days more than 90 % of alite has reacted in the pastes (blends with natural pozzolan have not been studied beyond 28 days, as the hydration experiments

are still in progress). The acceleration of the alite reaction in less obvious for the cement C – SCM blends. The degree of hydration for alite in the blend with natural pozzolan is roughly similar to that of pure cement C, though slightly more alite has reacted after 1 day and 28 days for the blend. The fly ash containing blend generally exhibits accelerated alite reaction as compared to pure cement C, but the blend with microsilica shows a consistently lower degree of alite hydration. Such a retardation of the alite reaction is quite surprising and a similar behaviour in cement – microsilica blends has not been reported previously (to the author's knowledge). Therefore, additional investigations are planned for the cement C – microsilica blend. In general, the degree of hydration for alite is somewhat lower for the blends with cement C than for the corresponding blends with cement A, which may reflect the finer grain size of this cement (d_{50} = 9.4 μm) as compared to the coarser cement C (d_{50} = 20.1 μm). A possible explanation for the higher reactivity of alite in some of the SCM blends is the acting of the SCM particles as nucleation sites for C-S-H formation. Krøyer *et al.* [264] have previously proposed such a mechanism for the accelerated alite reaction in mixtures of Portland cement and kaolinite (clay mineral).

It is well-known that belite contributes less to the early strength development than alite. This is clearly reflected in Fig. 8.12 by the lower reactivity of belite as compared to that of alite. A very small amount of belite reacts in the pure pastes during the first 7 days, but hereafter the reactivity of belite increases. After 360 days ~70 % of the belite phase has reacted in both pastes. In the blends of cement A with microsilica and natural pozzolan the belite reaction is accelerated, at least during the first 28 days of hydration. The degree of hydration for belite is roughly the same in pure cement A and the blend containing fly ash. In the blend of cement C with microsilica the belite reaction is clearly accelerated as compared to pure cement C, whereas the reactivity of belite is very similar for the fly ash blend and the pure paste. The belite reaction seems to be slightly retarded in the cement C – natural pozzolan blend. The increased reactivity of belite in the blends containing microsilica (and the cement A – natural pozzolan blend) may be due to the consumption of the SCMs themselves, since the amount of available Ca^{2+} ions may be reduced by the reaction of the SCMs, thus leading to an increased dissolution of the belite phase.

The degree of hydration for the SCMs exhibits very similar trends in the blends with cement A and C. Microsilica is generally the most reactive SCM, reaching reaction

degrees of ~85 % at 180 days of hydration, which is corresponding well with previous ^{29}Si MAS NMR investigations of cement – microsilica blends [76,230], and with the fact that this SCM is characterized by having a markedly finer average grain size (d_{50} = 0.25 μm) than the other types of SCMs (d_{50} = 7 – 9 μm). The higher reactivity of microsilica may also reflect that only 10 wt% of microsilica was included in the blends as compared to 30 wt% for the fly ash and the natural pozzolan. It also appears from Fig. 8.12, that the fly ash reacts to a very limited degree during the first 28 days, and after 180 days only about 20 – 27 % of the fly ash has reacted, which is in good agreement with degrees of hydration for fly ash in high-volume (45 – 55 %) fly ash – cement pastes reported by Lam *et al.* [262]. The natural pozzolan generally shows degrees of hydration between those of microsilica and the fly ash.

The average chain lengths of SiO_4 + AlO_4 tetrahedra ($\overline{CL}$) and pure SiO_4 tetrahedra ($\overline{CL}_{Si}$), as well as the Al/Si ratios for the C-S-H phase are compared for the blends of cement A and C with microsilica, fly ash 2 and natural pozzolan in Fig. 8.13. Data for the pure cement pastes are also included. The average chain lengths are higher for the blends as compared to the pure cements, and $\overline{CL}$ (and to a lesser extent $\overline{CL}_{Si}$) generally increases for all systems as the hydration proceeds. Pure cement A exhibits $\overline{CL}$ ranging from 3.6 after 1 day to 4.7 after 360 days. By comparison, the C-S-H in the cement A – natural pozzolan blend shows $\overline{CL}$ of 4.6 after 1 day, rising to 5.2 after 28 days of hydration. $\overline{CL}$ is somewhat lower for pure cement C than cement A, with values increasing from 3.5 at 1 day to 4.1 after 360 days. The fly ash has the highest $\overline{CL}$ of the blends with cement C, reaching almost 7.0 after 180 days. The average chain lengths ($\overline{CL}$) determined for the pure cements in this work is somewhat higher than $\overline{CL}$ values reported by Roger *et al.* [265] for a paste of ordinary Portland cement. They observed an increase of $\overline{CL}$ from 2.0 to 3.1 over 12 months of hydration. In a ^{29}Si MAS NMR study of white Portland cement pastes, Andersen *et al.* [260] also obtained slightly shorter chain lengths for the C-S-H, with $\overline{CL}$ ranging from 2.7 – 3.9 over two years of hydration. However, the generally longer $\overline{CL}$ observed for C-S-H in the blended cements as compared the pure pastes is in accord with previously reported $\overline{CL}$ for pastes of Portland cement blended with different types of SCMs. For a paste of Portland cement blended with more than 50 wt% of microsilica, which had hydrated for 3 months at 40 °C, Groves *et al.* [266] have reported a

$\overline{CL}$ value of 8.5. Using ^{29}Si MAS NMR, Richardson and Groves [259] determined $\overline{CL}$ for C-S-H in pastes of white Portland cement in blends with different amounts of blastfurnace slag. For a water-activated blend with cement and slag in equal proportions they found a $\overline{CL}$ value of 4.05 after three weeks of hydration. They also demonstrated that $\overline{CL}$ increases with the proportion of slag added to the blend, thus giving $\overline{CL}$ = 6.45 for a mixture of 90 % slag and 10 % cement after three weeks of hydration.

The Al/Si ratio for pure cement A is almost constant (~0.11) during the first week, and then it drops to roughly 0.08 is observed for the remaining hydration times. The blends of cement A with microsilica and natural pozzolan exhibit nearly constant Al/Si ratios of ~0.09, which is also the case for the blend with fly ash until 180 days of hydration, where the Al/Si ratio has increased to ~0.13. A similar trend is observed for the fly ash blended with cement C. The Al/Si ratio of the C-S-H in pure cement C shows an essentially constant value (~0.09) during the first two weeks and then decreases to ~0.065 at later ages. The cement – SCM blends all display roughly constant Al/Si ratios at ~0.11, but with the fly ash blend showing an increase to ~0.13 at 90 and 180 days, a phenomenon also observed for the cement A – fly ash blend. This increase of Al/Si at later ages for the fly ash blends may reflect that the fly ash only reacts after prolonged hydration. The Al/Si ratio for the pure pastes is somewhat higher than the Al/Si ratios reported by Andersen *et al*. [260] for a white Portland cement paste. Using ^{29}Si MAS NMR they obtained Al/Si ratios showing an almost constant value of ~0.046 for hydration times ranging from 12 h to two years. However, a different preparation scheme (*e.g.*, water/cement = 0.5) and different curing conditions were applied, which may explain the difference in Al/Si ratios. Moreover, Andersen *et al.* [258] also reported an error limit of ±0.04 on the determination of the Al/Si ratio from the ^{29}Si MAS NMR spectra, which may also explain some of the discrepancy. The Al/Si ratios of this project agrees better with values reported by Famy *et al.* [267]. By the application of EDS analysis they found Al/Si ratios of 0.129 and 0.095 for an ordinary Portland cement paste after 20 and 300 days of hydration, respectively. It is noted however, that the EDS analysis does not distinguish between Al in tetrahedral, 5-fold, or octahedral coordination whereas the NMR approach includes only Al in tetrahedral coordination.

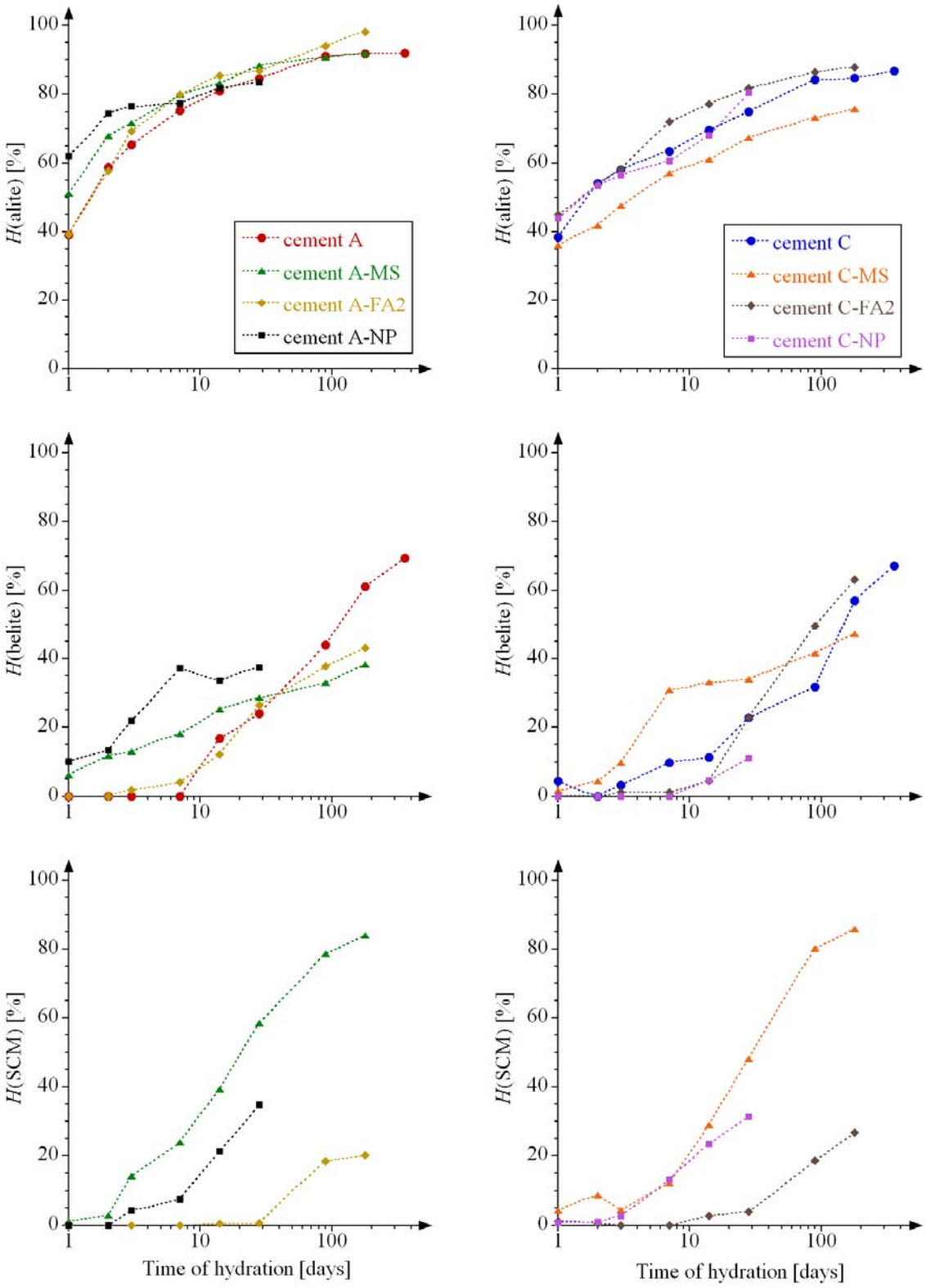

Fig. 8.12 Degrees of hydration (*H*) for alite, belite and SCMs (MS, FA2, NP) as a function of hydration time (logarithmic scale). The data (Tables 8.2 – 8.5) are obtained from deconvolved ^{29}Si MAS NMR spectra (9.4 T, ν_R = 12.0 kHz). MS = microsilica, FA2 = fly ash 2, NP = natural pozzolan.

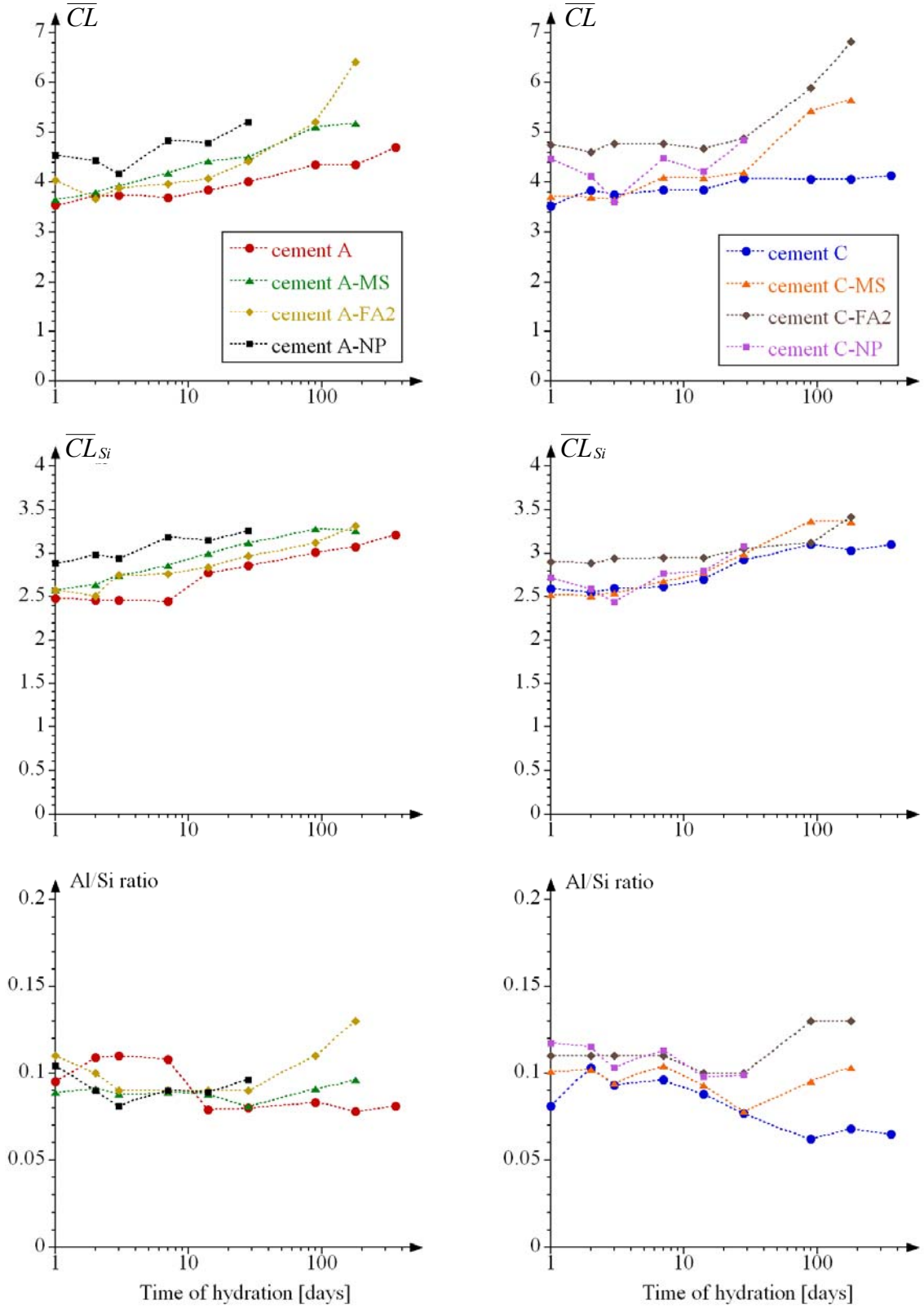

Fig. 8.13 Average chain lengths of alumino-silicate tetrahedra ($\overline{CL}$), pure silicate tetrahedra ($\overline{CL}_{Si}$) and Al/Si ratios for the C-S-H phase. The data (Tables 8.2 – 8.5) are obtained from deconvolved ^{29}Si MAS NMR spectra (9.4 T, ν_R = 12.0 kHz). MS = microsilica, FA2 = fly ash 2, NP = natural pozzolan.

8.8 Hydration of cement – slag blends

8.8.1 ^{29}Si MAS NMR

Two types of slags have been used for the hydration experiments of Portland cement – slag blends, specifically, slag 1 with a bulk chemical composition typical for blastfurnace slags used in cement blends, and slag 8 with a very high content of Al_2O_3 (20.0 wt%). The hydration has been followed by ^{29}Si MAS NMR for the four studied systems: cement A – slag 1, cement C – slag 1, cement A – slag 8, and cement C – slag 8. Representative ^{29}Si MAS NMR spectra are displayed in Fig. 8.14 and Fig. 8.15. A general feature for all spectra is the overlap of the resonances from alite and belite (-66 to -77 ppm) with the broad featureless peak originating from the amorphous slag (approx. -64 to -92 ppm), as illustrated in Fig. 8.16. Furthermore, the signals from Si in the C-S-H formed upon hydration of the cement phases and slag also overlap with the slag peak.

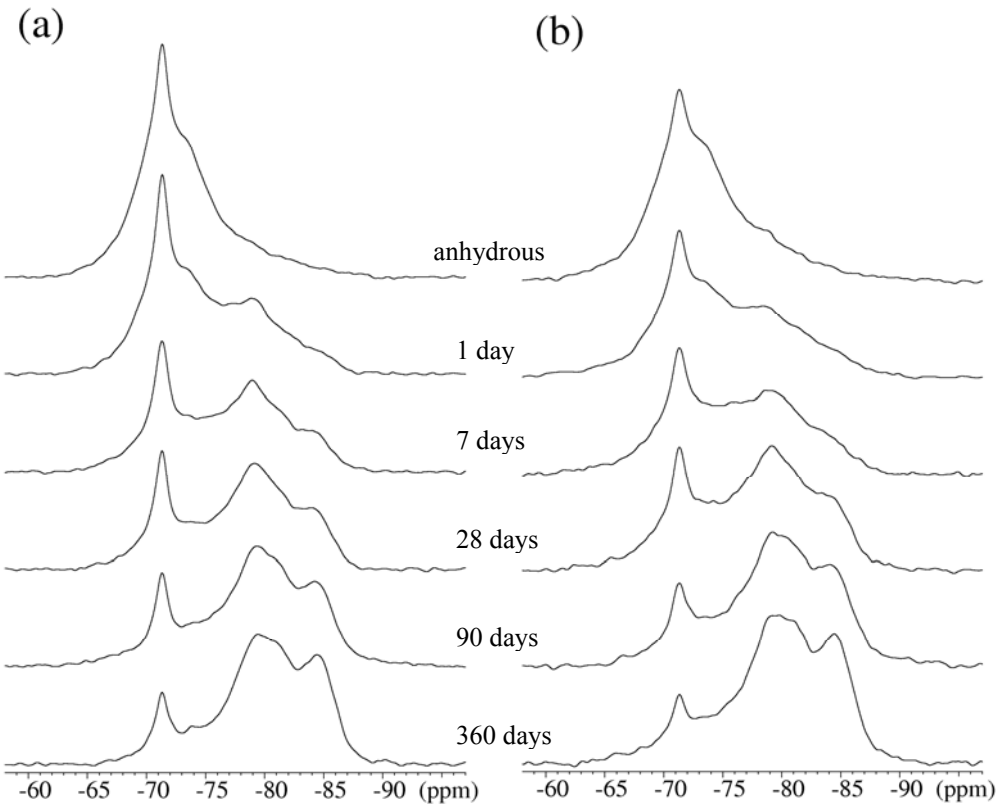

Fig. 8.14 ^{29}Si MAS NMR spectra (9.4 T, ν_R = 12.0 kHz) of (a) cement A – slag 1 and (b) cement C – slag 1 hydrated for 1, 7, 28, 90, 360 days. The top spectrum of each column is of the anhydrous blend.

These overlaps of resonances complicate the deconvolution of the ^{29}Si MAS NMR spectra of the hydrated cement – slag pastes. For instance, the overall lineshape for the slag peak may change during hydration due to a preferential reaction of certain constituents in the slag material, a phenomenon which cannot be deduced from the ^{29}Si MAS NMR spectra because of the severe overlaps of resonances. Consequently, the amount that the slag contributes to the intensity of a resonance, *e.g.*, the resonance for Q^1 sites in the C-S-H (-78 ppm), cannot be directly quantified by a deconvolution as the lineshape of the partly hydrated slag is unknown.

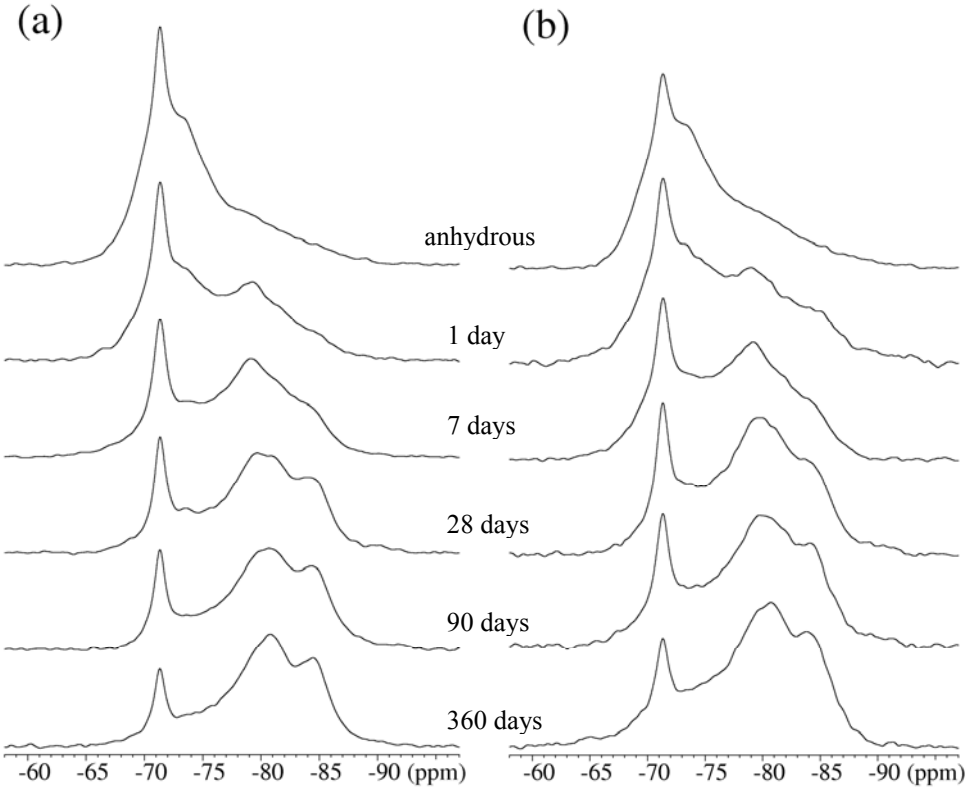

Fig. 8.15 ^{29}Si MAS NMR spectra (9.4 T, ν_R = 12.0 kHz) of (a) cement A – slag 8 and (b) cement C – slag 8 hydrated for 1, 7, 28, 90, 360 days. The top spectrum of each column is of the anhydrous blend.

The hydration can, however, be followed in a qualitative manner by the ^{29}Si MAS NMR spectra. Common for all four blends is the gradual decrease of the alite and belite intensities as the hydration proceeds with corresponding increase of the signals from the different Q^n sites in the C-S-H phase. Generally, the intensity of the Q^2(1Al) resonance (-81 ppm) relative to the resonance for the Q^1 and Q^2 sites is significantly higher for the slag

blends as compared to the pastes of pure cement A and cement C (see Fig. 8.1), especially after prolonged hydration. It is also noted that a considerable amount of belite (-71.3 ppm) is still present in the pastes even after 360 days of hydration.

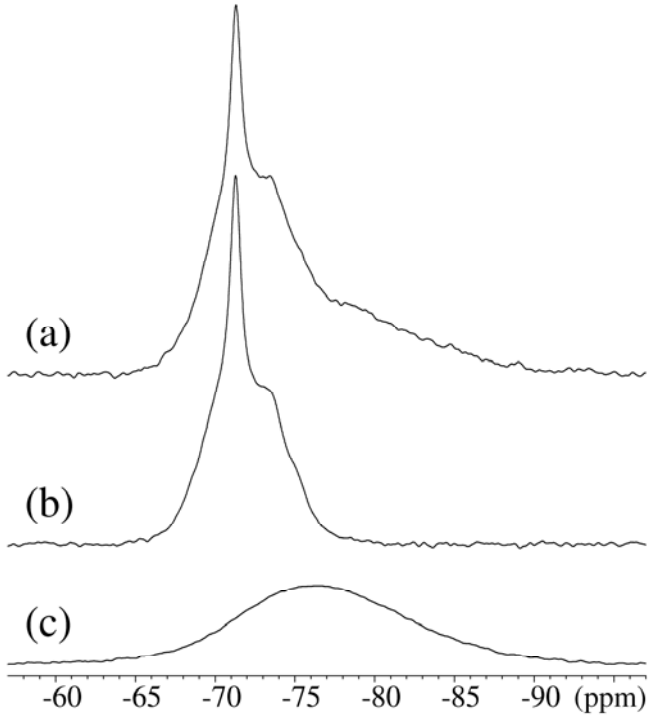

Fig. 8.16 ^{29}Si MAS NMR spectra (9.4 T, ν_R = 12.0 kHz) of the anhydrous cement A – slag 8 blend (a), anhydrous cement A (b), and anhydrous slag 8 (c), illustrating the severe overlap of resonances from the alite and belite phases in the cement with the broad peak from the slag.

8.8.2 ^{27}Al MAS NMR

The hydration of the cement – slag blends have also been studied using ^{27}Al MAS NMR. Resonances from aluminium in tetrahedral coordination (Al_{IV}) to oxygen atoms are generally observed in the range from 50 to 80 ppm, while those in octahedral coordination (Al_{VI}) are found in the range -10 to 20 ppm. Penta-coordinated aluminium (Al_V) displays chemical shifts between those of Al_{IV} and Al_{VI}. Fig. 8.17 display representative ^{27}Al MAS NMR spectra following the hydration of pure cement A and cement A blended with slag 8 (60:40 wt%). In the spectrum of anhydrous cement A overlapping resonances from Al_{IV} incorporated as guest ions in the alite and belite phases are observed at ~81 and ~86 ppm, respectively, and a broad peak originating from Al_{IV} in the tricalcium aluminate phase ranges from approximately 40 to 80 ppm [28]. The spectra of hydrated cement A reveal a gradual decrease of the intensities for Al in alite and belite corresponding to the continued reaction of alite and belite in the hydrating paste. The peak from the fast reacting tricalcium aluminate phase is strongly diminished after 1 day and has disappeared after 7

days of hydration in accord with XDR/Rietveld analysis carried out for the same hydration series of cement A [261]. The incorporation of Al_{IV} in the C-S-H phase is observed by the rather broad peak centred at ~72 ppm. As the hydration begins, three overlapping peaks at approx. 13, 9, and 5 ppm appear in the chemical shift region for octahedrally coordinated aluminium. These peaks are assigned to an AFt phase [228], an AFm phase [228] and a phase denoted the 'third aluminate hydrate' (TAH) [268], respectively. The TAH phase was characterized by Andersen *et al.* [268] using ^{27}Al and ^{29}Si MAS NMR and they described the phase as an amorphous/disordered aluminate hydroxide or a calcium aluminate hydroxide, which forms as a separate phase or as a surface precipitate on the C-S-H phase. The presence of a small amount of penta-coordinated Al in the C-S-H phase is indicated by the low-intensity resonance at ~38 ppm [269].

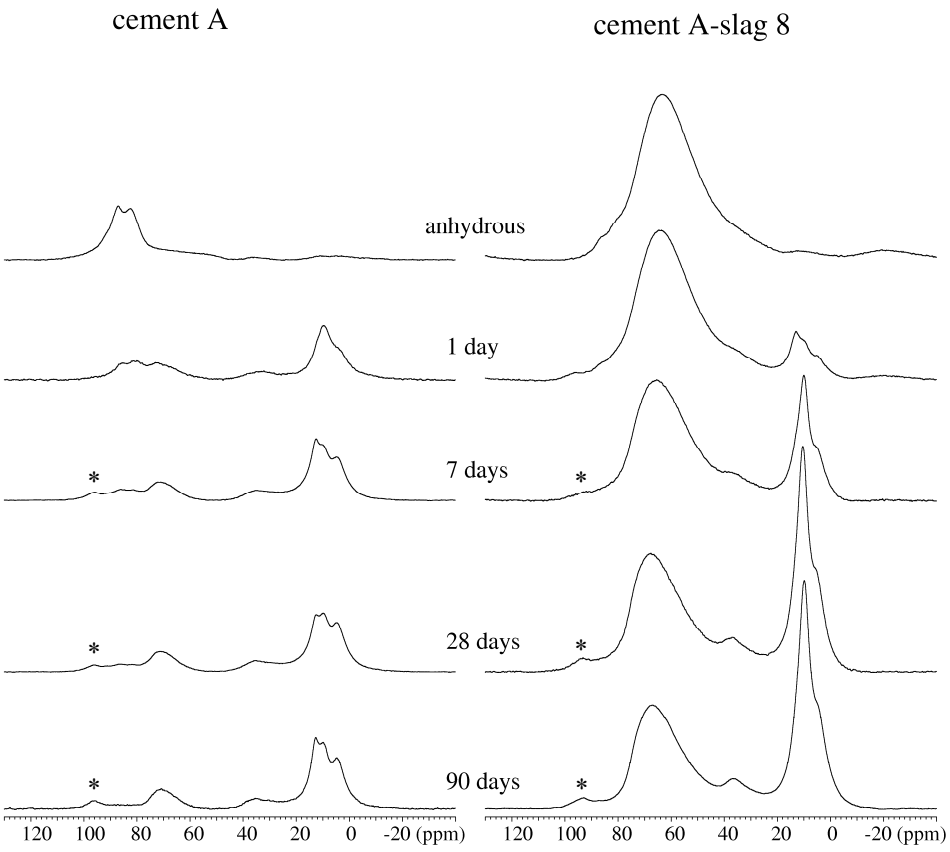

Fig. 8.17 ^{27}Al MAS NMR spectra (14.1 T, ν_R = 13.0 kHz) of pure cement A (left column) and cement A – slag 8 (right column) hydrated for 1, 7, 28, and 90 days. Spectra of the anhydrous samples are included as well. Peaks indicated by asterisks (*) are spinning sidebands. The spectra are all plotted on the same intensity scale.

The ^{27}Al MAS NMR spectrum of the anhydrous cement A – slag 8 blend is strongly dominated by a broad asymmetric peak centred at ~64 ppm, originating from 4-fold, and possibly 5-fold, coordinated aluminium in the amorphous slag, which overlaps with the resonances from Al_{IV} in alite and belite. The dominating appearance of the slag peak is due to the fact that this SCM contains 20.0 wt% Al_2O_3 compared to the much lower content of Al_2O_3 in the cement (2.1 wt%). It is noted that the spectra in Fig. 8.17 are plotted on the same intensity scale for both hydration series. In Fig. 8.18 the assignment of resonances in the spectra of hydrated samples is illustrated for cement A – slag 8 after 1 day of hydration. The higher intensity of the peaks in the chemical shift region for octahedrally coordinated Al in the spectra for the cement – slag blend is due to the higher content of Al_2O_3 in this system as compared to the pure cement. The peak at 13 ppm is assigned to an AFt phase [28], the presence of which was been confirmed by XRD [261]. TEM investigations carried out by Li and Richardson at University of Leeds have revealed that a Mg-Al layered double hydroxide (LDH) phase (hydrotalcite-type phase) occurs in the hydrated blend of cement A and slag 8. This type of phase has also been observed in earlier studies of Portland cement – slag pastes [112,113].

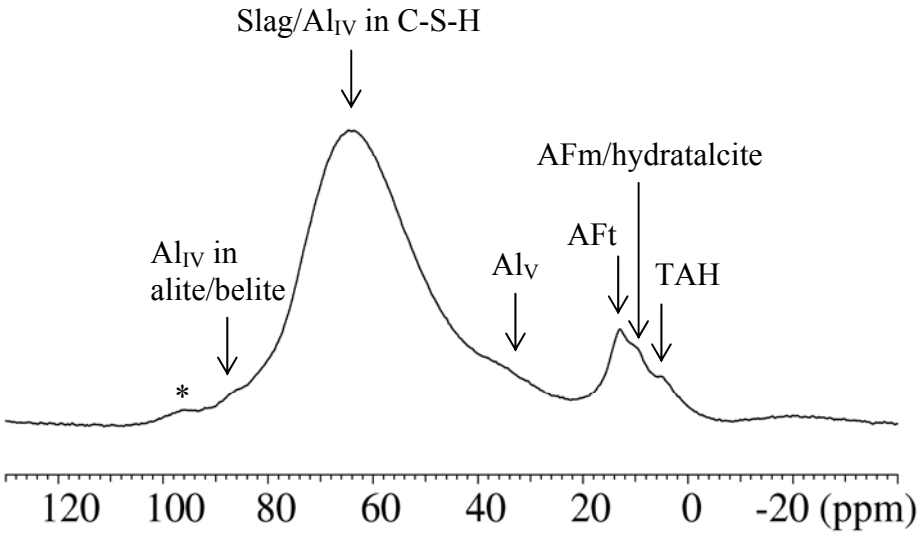

Fig. 8.18 ^{27}Al MAS NMR spectrum (14.1 T, ν_R = 13.0 kHz) of cement A – slag 8 hydrated for 1 day. The low-intensity peak at 98 ppm indicated with an asterisk (*) is a spinning sideband.

Aramendia *et al.* [111] and Takehira *et al.* [270] have reported chemical shifts close to 9 ppm for different hydrotalcite-type phases based on ^{27}Al MAS NMR spectra acquired at

9.4 T. As illustrated in Fig. 8.19, a similar chemical shift has been observed for a synthetic Mg-Al hydrotalcite (hycite® 713 from *Süd-Chemie AG*: $[Mg_{1-x}Al_x](CO_3)_{x/2}\cdot nH_2O$ ($0.25 < x < 0.33$)) in our laboratory.

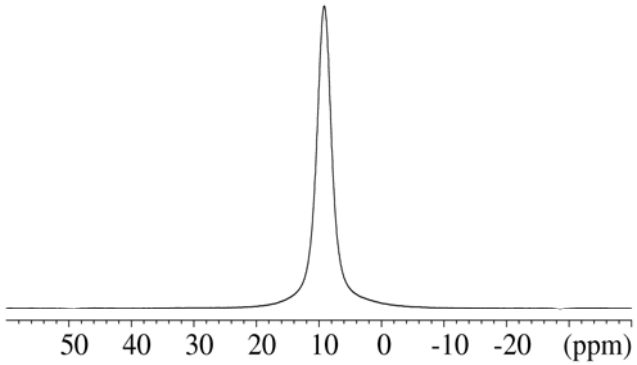

Fig. 8.19 ^{27}Al MAS NMR spectrum (9.4 T, ν_R = 12.0 kHz) of a synthetic Mg-Al hydrotalcite ($[Mg_{1-x}Al_x](CO_3)_{x/2}\cdot nH_2O$ ($0.25 < x < 0.33$). A single resonance is observed with a centre of gravity at 9.1 ppm.

Therefore, it seems probable that the peak at 9 ppm in the ^{27}Al MAS NMR spectra of hydrated cement A – slag 8 contains contributions from a Mg-Al LDH phase as well as from an AFm phase. The presence of AFm was confirmed by XRD/Rietveld analysis [261]. The peak at 5 ppm is attributed to the TAH phase [268], while the presence of a small amount of penta-coordinated Al in the C-S-H phase is indicated by the resonance centred at ~38 ppm. In contrast to the spectra of pure cement A paste, the peak originating from Al_{IV} incorporated in the C-S-H phase completely overlaps with the slag resonance in the spectra of the cement – slag blend, which complicates a clear distinction between the two signals.

As mentioned above, the extraction of degrees of hydration for the slags from deconvolution of ^{29}Si MAS NMR spectra is hindered by severe resonance overlaps. Instead, ^{27}Al MAS NMR spectra have been employed to quantify the slag reaction. In this approach it is assumed that no preferential hydration occurs for specific Al sites in the slag. This assumption is supported by SEM investigations of cement – slag pastes that reveal a clear boundary between the reacting slag grains and the formed hydration products [261]. Before acquisition of the ^{27}Al MAS NMR spectra the sample materials packed in the NMR rotors were weighed, both the samples of anhydrous cement – slag blends and the corresponding hydrated samples. The ^{27}Al MAS NMR based approach involves subtraction of the spectrum of the anhydrous blend from the spectrum of hydrated cement. The subtraction is carried out before baseline correction and is performed in an interactive

manner where the difference between the two spectra is displayed. The intensity of the spectrum for the anhydrous samples is thus manually scaled to precisely eliminate the contribution from the slag in the spectrum of the partially hydrated blend. The procedure is exemplified in Fig. 8.20 for the blend of cement A with slag 8 after 28 days of hydration. The spectrum resulting from the subtraction (Fig 8.20(c)) contains resonances from AFm/Mg-Al LDH (~9 ppm), the TAH phase (~5 ppm) as well as Al_{IV} (~72 ppm) and Al_V (~38 ppm) incorporated in the C-S-H phase, while the peak from the slag has been removed. The position of the resonance from Al_{IV} in the C-S-H at a higher frequency (~72 ppm) than the peak from the slag (~64 ppm) ensures that the subtraction can be performed in a reliable manner.

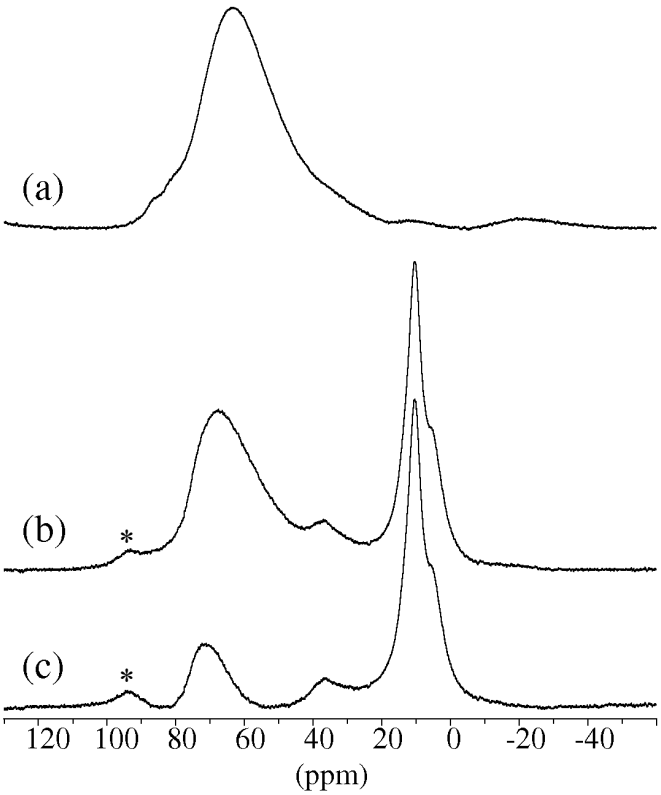

Fig. 8.20 ^{27}Al MAS NMR spectra (14.1 T, ν_R = 13.0 kHz) of (a) anhydrous cement A – slag 8 blend, (b) cement A – slag 8 blend after 28 days of hydration, and (c) the residual spectrum after subtraction of (a) from (b) where a scaling factor of 0.38 was applied to the spectrum in (a) in order to remove the peak from slag. Peaks indicated with asterisks (*) are spinning sidebands.

The scaled intensity of the anhydrous material subtracted from the hydrated material can be related to the quantity of unreacted slag in the blend if the amount of water bound in the sample during hydration, as well as the mass ratio for the samples involved in the subtraction, is taken into account. The content of bound water has been determined by measuring the loss on ignition for the individual hydrated samples.

The degree of hydration for the slags determined from ^{27}Al MAS NMR (or another method) can potentially be utilized to deconvolve the ^{29}Si MAS NMR spectra of the hydrated cement – slag blends, and thereby obtain information about the alumino-silicate chain length and Al/Si ratio of the C-S-H phase from the deconvolved resonances for the Q^1, Q^2(1Al) and Q^2 sites of the C-S-H. This may be achieved by subtracting an ^{29}Si MAS NMR spectrum of the anhydrous slag from a corresponding spectrum of a partially hydrated blend, where the ^{29}Si MAS NMR spectrum of the anhydrous slag has been scaled according to the degree of reaction obtain from ^{27}Al MAS NMR. The subtraction will thus result in a spectrum where the contribution from the slag has been removed.

The degree of hydration for the slags (for ages up to 90 days) has been estimated using the method based on ^{27}Al MAS NMR for three blends: cement A – slag 1, cement A – slag 8, and cement C – slag 8 (Table 8.6 and Fig. 8.21(a)). Slag 8 is generally more reactive than slag 1 according to the obtained results, which is in agreement with DTA studies of the same blends [261]. Furthermore, slag 8 exhibits higher degrees of hydration in the blend with cement A as compare to the blend with cement C.

Table 8.6 Degrees of hydration (%) estimated from ^{27}Al MAS NMR spectra (14.1 T, ν_R = 13.0 kHz) for slags in three cement – slag blends.

Time of hydration (days)	cement A – slag 1	cement A – slag 8	cement C – slag 8
1	0.0	15.5	0.0
2	3.4	27.5	1.5
3	8.0	32.3	7.3
7	12.6	40.9	21.2
14	23.8	51.5	36.9
28	32.0	56.9	48.3
90	47.3	65.2	60.5

The slag reaction has also been quantified by Vanessa Kocaba [261] using SEM/BSE with image analysis (IA) for the same blends. Fig. 8.21(b) and (c) compare the degree of hydration for the slags obtained by NMR and SEM/BSE-IA. For the cement A – slag 8 blend there is a good agreement of results, at least at early hydration times, while the NMR approach gives somewhat lower degrees of hydration for slag 1 in the blend with cement A as compared to SEM/BSE-IA. A good agreement is observed for the cement C – slag 8

blends for hydration times after 7 days of hydration whereas the degrees of hydration for slag 8 derived by SEM/BSE-IA are higher than the corresponding NMR results at earlier ages.

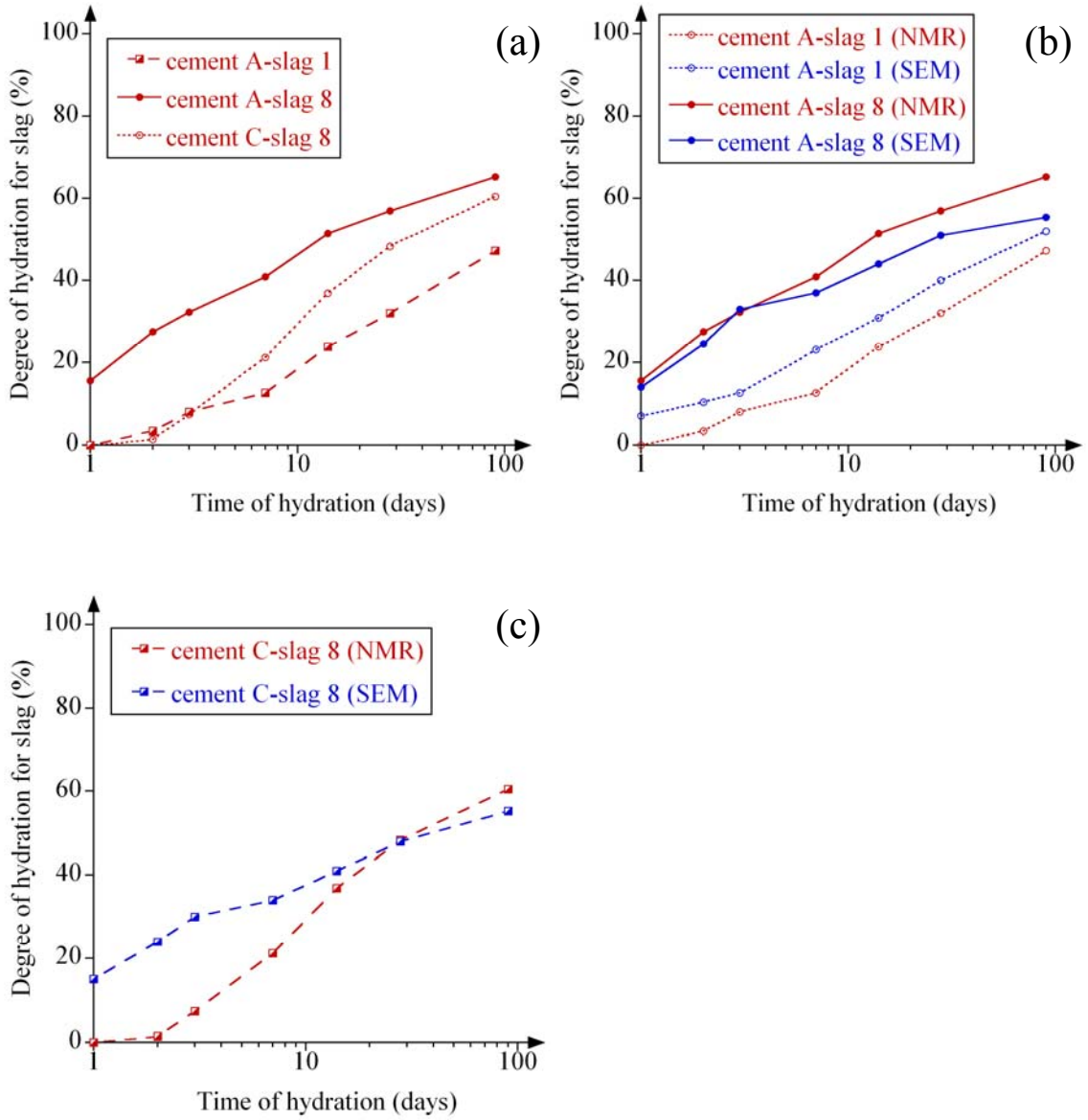

Fig. 8.21 Degrees of hydration (*H*) for slags in blends with cement A and C plotted as a function of hydration time (logarithmic scale). (a) Estimates for the slag reaction obtained from ^{27}Al MAS NMR (14.1 T, ν_R = 13.0 kHz). Comparison of degrees of hydration obtained from NMR and SEM/BSE-IA are displayed in (b) for cement A in blends with slag 1 and 8, and in (c) for cement C blended with slag 8.

Selective dissolution methods have been employed by a number of researchers to quantify the slag reaction in cement – slag blends [58,112,271-273], *e.g.*, Luke and Glasser [112]

reported that 40 – 40 % of the slag had reacted after one month of hydration, while Lumley *et al*. [58] found that 30 – 55 % of the slag had reacted within 28 days for cement – slag pastes employing water/cement ratios from 0.4 to 0.6. Dyson *et al.* [113] have recently used a combined ^{29}Si MAS NMR and selective dissolution technique to determine the degree of reaction for slag in a hydrated cement – slag blend (75: 25 wt%). The idea is to removes all silicate species from the anhydrous cement and the C-S-H by selective dissolution, thus enabling the acquisition of a ^{29}Si MAS NMR spectrum of the residue of slag, which is subsequently used as a sub-spectrum in the analysis of the ^{29}Si MAS NMR spectrum of the hydrated cement – slag blend. This allows quantification of the slag reaction and by employing this approach a degree of slag reaction of ~30 % was determined for the cement – slag paste after one month of hydration. However, TEM and ^{29}Si MAS NMR studies of the residue after selective dissolution indicated the presence of a small amount of an alumino-silicate gel in addition to the expected unreacted slag and aluminate phases. Whether this phase is a by-product for the dissolution process or a product formed during hydration of the slag cement could not be determined, which induces some uncertainty on the method. Some of the cement – slag blends studied in the present work have also been subjected to the selective dissolution method used by Dyson *et al*. [113] with subsequent investigations of the residues by XRD and SEM [261]. For both anhydrous and hydrated samples all examinations revealed that besides the expected slag phase a significant amount of undissolved cement phases was still present in the residue after the selective dissolution process. Furthermore, hydrotalcite was also observed in the residue of the hydrated cement – slag blends. The presence of a hydrotalcite-like phase in the residue of cement – slag pastes subjected to a similar selective dissolution method was also reported by Luke and Glasses [112].

Hinrichs and Odler [272] have determined the fraction of unreacted slag present in hydrated cement – slag blends with 25 wt%, 50 wt% or 70 wt% slag in the mixture using a DTA procedure. They found that the hydration of the slag was independent of its proportion in the anhydrous material and that approx. 38 – 69 % of the slag had reacted after 28 days of hydration for slags with a fineness (Blaine) of 300 m^2/kg. For more fine-grained slags (500 m^2/kg) the degree of hydration was somewhat higher at all hydration times (2 – 360 days).

In summary, rather diverse degrees of hydration for slags in cement – slag blends have been reported in the literature, which is probably a consequence of several issues. For instance, the reactivity of slags is dependent on such diverse factors as bulk chemical composition, content of amorphous material, fineness of the slag powder, curing conditions, water/binder ratio, etc. Therefore, comparison of degrees of reaction for slags can be dubious if the abovementioned factors differ from one study to another (which is most often the case). Moreover, uncertainties may also arise if different analytical techniques are employed for determining the slag reaction in comparative studies.

Conclusions

Solid-state magic-angle spinning (MAS) nuclear magnetic resonance (NMR) spectroscopy is generally recognized as an important and versatile analytical tool in the research of cementitious materials. The technique is well-suited for investigations of both crystalline and amorphous/poorly crystalline materials such as the C-S-H phase formed by cement hydration and different types of supplementary cementitious materials (SCMs) characterised by a high content of largely amorphous matter. Therefore, solid-state NMR represents an important complement to other techniques, *e.g.*, powder X-ray diffraction (XRD) where only the long-range ordering of crystalline materials is detected. Solid-state NMR also enables the study of different phases separately by utilizing specific NMR active nuclei, for example for selective studies of the aluminate phases or of the calcium silicates by employment of the ^{27}Al and ^{29}Si nuclei, respectively.

In this project solid-state ^{29}Si and ^{27}Al MAS NMR have been employed in studies of anhydrous and hydrated Portland cements blended with SCMs. The primary aim of the project is the development of methodologies for measuring the degree of reaction for SCMs, as well as cement phases, in hydrating cement – SCMs pastes. Initial investigations of anhydrous cements has led to an improved method for quantification of the calcium silicates alite and belite by deconvolution of ^{29}Si MAS NMR spectra recorded at 9.4 T with a relatively high spinning speed (ν_R = 13.0 kHz). Furthermore, the importance of employing fully relaxed ^{29}Si MAS NMR spectra for reliable quantification of alite and belite has been demonstrated.

The spin-lattice relaxation of ^{29}Si species in alite and belite has been studied by ^{29}Si inversion-recovery (IR) MAS NMR experiments. Analysis of the IR spectra show that the relaxation of the ^{29}Si spins is overwhelmingly dominated by the strong dipolar interaction of the ^{29}Si nuclei with unpaired electrons in paramagnetic Fe^{3+} ions incorporated in the alite and belite phases as guest ions. In addition, the analysis reveals that the spin-lattice relaxation follows a “stretched exponential” rather than a single-exponential decay process. Analysis of deconvolved ^{29}Si IR MAS NMR spectra has been shown to be a reliable alternative method for determination of alite and belite contents in Portland cements.

The hydration of two Portland cements, alone and in blends with microsilica, fly ash, natural pozzolan (volcanic rock) or blastfurnace slags, has been studied using ^{29}Si and ^{27}Al MAS NMR with the purpose of determining the degree of hydration for alite, belite

and the SCMs. This involves computer deconvolution of the ^{29}Si MAS NMR spectra to obtain the relative intensities for the different ^{29}Si species in the hydrated samples, which allows a quantification of the Si present in alite, belite, the hydration product C-S-H, and the SCM of the specific cement blend. The deconvolution procedure has successfully been employed for the cement blends including either microsilica, fly ash, or natural pozzolan, whereas the deconvolution of the ^{29}Si MAS NMR spectra for the cement – slag blends is impeded by severe overlap of resonances from the alite, belite and the C-S-H phase with the broad and featureless peak from the slag. Generally, the results from the deconvolutions reveal that the reaction of alite and belite is accelerated by the presence of microsilica, fly ash and natural pozzolan as compared to the rate of reaction in the corresponding pure Portland cements. Regarding the reaction of the SCMs themselves, microsilica exhibits the highest degrees of reaction among the studied SCMs. Much lower reactivity is observed for the fly ash. Clear indications of fly ash reaction are only detected for hydration times beyond 28 days and ~75 – 80 % of the fly ash has still not reacted after 180 days of hydration. The natural pozzolan displays degrees of hydration between those of the microsilica and the fly ash.

Deconvolution of the resonances form the different Si sites in the C-S-H phase (Q^1, Q^2, and $Q^2(1Al)$) in ^{29}Si MAS NMR spectra forms the basis for determination of the average alumino-silicate chain length ($\overline{CL}$) and the Al/Si ratio of the C-S-H phase. Generally, longer $\overline{CL}$ are observed for the cements blended with microsilica, fly ash and natural pozzolan as compared to the pastes of pure Portland cements, which is in accord with earlier ^{29}Si MAS NMR studies of blended cements.

Since the degree of reaction for slags can not be determined from deconvolution of the ^{29}Si MAS NMR spectra, a new method based on ^{27}Al MAS NMR has been developed to estimate the degree of slag reaction. The method involves subtraction of the ^{27}Al MAS NMR spectrum for the anhydrous cement – slag blend from a spectrum for a corresponding (partially) hydrated sample of the same blend. The intensity of the spectrum for the anhydrous blend is adjusted to give a residual ^{27}Al MAS NMR spectrum in which the contribution from the slag has been removed. This allows the degree of reaction for the slag to be estimated by taking into account the amount of water bound in the sample during hydration.

References

[1] H.F.W. Taylor. *Cement Chemistry, 2nd ed.* Thomas Telford Publishing, 1997, pp. 459.

[2] P.C. Hewlett (ed.). *Lea's chemistry of cement and concrete, 4th ed.,* Elsevier Ltd., 1998, pp. 1057.

[3] Harmonized European Standard EN 197-1: *Cement - Composition, specification and conformity criteria for common cements,* 2000.

[4] R.G. Blezard. *The History of Calcareous Cements.* In: P.C. Hewlett (ed.). *Lea's chemistry of cement and concrete, 4th ed.*, Elsevier Ltd., 1998, pp. 1-23.

[5] N. Davey. *A history of building materials.* Phoenix House, 1961, pp. 90.

[6] British Patent BP 3367: *Cement, mortar, stucco, etc.*, 1811.

[7] J. Aspdin. British Patent BP 5022: *Producing an artificial stone*, 1824.

[8] R.G. Blezard. *Technical aspects of Victorian cement.* Chemistry and Industry, 1981 pp. 631.

[9] H. Le Chatelier. *Experimental researches on the constitution of hydraulic mortars*, 1905. (Original doctoral thesis 1887)

[10] H. Le Chatelier. *Application des phénomènes de sursaturation à la théorie du durcissement de quelques ciments et mastics.* Comptes rendus hebdomadaries des Séances de l'Acadamie des Sciences 96 (1883) 1056-1059.

[11] A.E. Törnebohm. *Ueber die petrographie des Portland cements*, Stockholm: Verein Skandinavischer Portland Cement Fabrikanten, 1897, pp. 34.

[12] G.A. Rankin, F.E. Wright. *The ternary system CaO-Al_2O3-SiO_2.* American Journal of Science 39 (1915) 1-79.

[13] P.J. Jackson. *Portland cement: Classification and Manufacture,* In: P.C. Hewlett (ed.). *Lea's chemistry of cement and concrete, 4th ed.*, Elsevier Ltd., 1998, pp. 25-94.

[14] *The manufacture of Portland cement.* The Cement and Concrete Association of New Zealand, 1989.

[15] H. Wedepohl. *The composition of the continental crust.* Geochim. Cosmochim. Acta 59 (1995) 1217-1239.

[16] M. Bigaré, A. Guinier, C. Mazières, M. Regourd, N. Yannaquis, W. Eysel, T. Hahn, E. Woermann. *Polymorphism of Tricalcium Silicate and its Solid Solutions.* J. Am. Ceram. Soc. 50 (1967) 609-619.

[17] A. Gunier, M. Regourd. *Structure of Portland cement minerals.* Proceedings of the 5th ISCC, Vol. 1, 1969, pp. 1-41.

[18] I. Maki, S. Chromý. *Microscopic study on the polymorphism of Ca_3SiO_5.* Cem. Concr. Res. 8 (1978) 407-414.

[19] I. Maki, S. Chromý. *Characterisation of the alite phase in Portland cement clinker by microscopy.* Cemento 75 (1978) 247-252.

[20] I. Maki, S. Chromý. *Phase identification of alite in portland cement clinker.* Cem. Concr. Res. 12 (1982) 93-100.

[21] I. Maki. Proceedings of the 8th ICCC, Vol. 1, 1986, pp. 34-47.

[22] M. Regourd, A. Guinier. *Crystal chemistry of the components of Portland cement clinker.* Proceedings of the 6th ICCC, Vol. 1, 1976, pp. 25-51.

[23] G. Yamaguchi, S. Takagi. *The analysis of Portland cement clinker.* Proceedings of the 5th ISCC, Vol. 1, 1969, pp. 181-218.

[24] I. Maki, K. Goto. *Factors influencing the phase constitution of alite in Portland cement clinker.* Cem. Concr. Res. 12 (1982) 301-308.

[25] F. Dunstetter, M.-N.d. Noirfontaine, M. Courtial. *Polymorphism of tricalcium silicate, the major compound of Portland cement clinker: 1. Structural data: review and unified analysis.* Cem. Concr. Res. 36 (2006) 39-53.

[26] N.I. Golovastikov, R.G. Matveeva, N.V. Belov. *Crystal structure of the tricalcium silicate.* Kristallografiya 20 (1975) 721-729.

[27] T. Hahn, W. Eysel, E. Woermann. *Crystal chemistry of tricalcium silicate solid solutions.* Proceedings of the 5th ISCC, Vol. 1, 1969, pp. 61-66.

[28] J. Skibsted, H.J. Jakobsen, C. Hall. *Direct observation of aluminium guest ions in the silicate phases of cement minerals by ^{27}Al MAS NMR spectroscopy.* J. Chem. Soc. Faraday Trans. 90 (1994) 2095-2098.

[29] E. Woermann, T. Hahn, W. Eysel. *The substitution of alkalis in tricalcium silicate.* Cem. Concr. Res. 9 (1979) 701-711.

[30] W. Gutt. *The manufacture of Portland cement from phosphatic raw materials.* Proceedings of the 5th ICCC, Vol. 1, 1968, pp. 93-105.

[31] D. Stephan, S.N. Dikoundou, G. Raudaschl-Sieber. *Influence of combined doping of tricalcium silicate with MgO, Al_2O_3, Fe_2O_3: sythesis, grindability, X-ray diffraction and ^{29}Si NMR.* Materials and structures 41 (2008) 1729-1740.

[32] F.W. Locher, W. Richartz, S. Sprung. *Setting of cement, Part I. Reaction and development of structure.* Zement-Kalk-Gips 29 (1976) 435-442.

[33] W.A. Deer, R.A. Howie, J. Zussman. *An introduction to the rock-forming minerals, 2nd ed.*, Pearson Education Limited, 1992, pp. 696.

[34] P. Barnes, C.H. Fentiman, J.W. Jeffery. *Structurally related dicalcium silicate phases.* Acta Cryst. A36 (1980) 353-356.

[35] K. Niesel, P. Thormann. *The stability fields of dicalcium silicate modifications.* Tonind. Zeit. 91 (1967) 362-369.

[36] K.H. Jost, B. Ziemer, R. Seydel. *Redetermination of the Structure of β-Dicalcium Silicate.* Acta Cryst. B33 (1977) 1696-1700.

[37] C.J. Chan, W.M. Kriven, J.F. Young. *Analytical Electron Microscopic Studies of Doped Dicalcium Silicates.* J. Am. Ceram. Soc. 71 (1988) 713-719.

[38] P. Mondal, J.W. Jeffrey. *The crystal structure of tricalcium aluminate, $Ca_3Al_2O_6$.* Acta Cryst. B31 (1975) 689-697.

[39] Y. Takeuchi, F.M. Nishi. *Crystal-chemical characterization of the $3CaAl_2O_3$ solid-solution series.* Z. Kristallogr. 152 (1980) 259-307.

[40] L. Gobbo, L.S. Agostino. *C_3A polymorphs related to industrial clinker alkalis content.* Cem. Concr. Res. 34 (2004) 657-664.

[41] F.C. Lee, H.M. Banda, F.P. Glasser. *Substitution of Na, Fe, and Si in tricalcium aluminate and the polymorphism of solid solutions.* Cem. Concr. Res. 12 (1982) 237-246.

[42] I. Maki. *Nature of the prismatic dark interstilial material in Portland cement clinker.* Cem. Concr. Res. 3 (1973) 295-313.

[43] K.L. Scrivener, P.L. Pratt. *Microstructural studies of the hydration of C_3A and C_4AF independently and in cement paste.* Br. Ceram. Proc. 35 (1984) 207-219.

[44] A.A. Colville, S. Geller. *The crystal structure of brownmillerite, Ca_2FeAlO_5.* Acta Cryst. B27 (1971) 2311-2315.

[45] A.M. Harrisson, H.W.F. Taylor, N.B. Winter. *Electron-optical analyses of the phases in a portland cement clinker, with some observations on the calculation of quantitative phase composition.* Cem. Concr. Res. 15 (1985) 775-780.

[46] F. Puertas, M. Blanco Valera, R. Dominguez. *Characterization of Ca_2AlMnO_5. A comparative study between Ca_2AlMnO_5 and Ca_2AlFeO_5.* Cem. Concr. Res. 20 (1990) 429-438.

[47] United States Geological Survey. *Cement statistics, http://minerals.usgs.gov/ds-/2005/140/cement.pdf.*, 2008.

[48] K. Humphreys, M. Mahasenan. *Towards a sustainable cement industry. Sub-study 8: climate change,* An Independent Study Commissioned to Battelle by World Business Counsil for Sustainable Development, 2002.

[49] *Impacts of Europe's changing climate.* European Environment Agency Report no. 2, 2004.

[50] *Consumption of alternative fuels used in kiln*, Cembureau Internal Document, 2003.

[51] *Siliceous by-products for use in concrete.* Final Report of the 73 BSC RILEM Committee, 1988.

[52] M. Moranville-Regourd. *Cements made from blastfurnace slag.* In: P.C. Hewlett (ed.). *Lea's chemistry of cement and concrete, 4th ed.*, Elsevier Ltd., 1998, pp. 637-678.

[53] H.-G. Smolczyk. *Slag structure and identification of slag.* Proceedings of the 7th ICCC, Vol. 1, 1980, pp. 1-17.

[54] M. Regourd. *Characteristics and activation of additive products.* Proceedings of the 8th ICCC, Rio de Janeiro, Principal Report, Vol. 1, 1986, pp. 199-229.

[55] H. Uchikawa. *Effect of blending components on hydration and structure formation.* Proceedings of the 8th ICCC, Rio de Janeiro, Vol. 1, 1986, pp. 249-280.

[56] H. Smolczyk. *The hydration products of cements with high contents of blastfurnace slag.* Zement-Kalk-Gips Int. 18 (1965) 238-246.

[57] M. Regourd. Proceedings of the 7th ICCC, Paris Vol.1 , 1980, pp. III-2/10-III-2/24.

[58] J.S. Lumley, R.S. Gollop, G.K. Moir, H.F.W. Taylor. *Degrees of reaction of the slag in some blends with Portland cements.* Cem. Concr. Res. 26 (1996) 139-151.

[59] F. Massazza. *Pozzolana and pozzolanic cements.* In: P.C. Hewlett (ed.). *Lea's chemistry of cement and concrete, 4th ed.*, Elsevier Ltd., 1998, pp. 471-635.

[60] ASTM D388 – 05: *Standard Classification of Coals by Rank,* 2005.

[61] D.M. Roy, G.M. Idorn. *Developments of structure and properties of blastfurnace slag cements.* Journal of the American Concrete Institute 97 (1982) 444-457.

[62] M. Kokubu. Proceedings of the 5th ISCC, Vol. 4, 1969, pp. 75.

[63] K. Takemoto, H. Uchikawa. *Hydration of Pozzolanic Cements.* Proceedings of the 7th ICCC, Vol. 1, 1980, pp. IV-2/I-29.

[64] H.F.W. Taylor, K. Mohan. *Analytical study of pure and extended Portland cement pastes: II, Fly asg- and slag-cement pastes.* J. Am. Ceram. Soc. 68 (1985) 686-690.

[65] A. Ghose, P.L. Pratt. *Effects of Flyash Incorporation in Cement and Concrete (ed. S. Diamond).* Materials Reseach Society, University Park, PA, 1981, pp. 82.

[66] I. Jawed, J. Skalny. *Effects of Flyash Incorporation in Cement and Concrete (ed. S. Diamond).* Materials Reseach Society, University Park, 1981, pp. 60.

[67] Y. Halse, D.J. Goult, P.L. Pratt. *Calorimetry and Microscopy of flyash and silica fume cements blends.* Br. Ceram. Proc. 35 (1984) 403-417.

[68] F. Wei, M.W. Grutzeck, D.M. Roy. *The retarding effects of fly ash upon the hydration of cement pastes: the first 24 hours.* Cem. Concr. Res. 15 (1985) 174-184.

[69] J.A. Dalziell, W.A. Gutteridge. *The Influence of Pulverized-Fuell Ash upon the Hydration Characteristics and Certain Physical Properties of a Portland Cement Paste (Techn. Rpt. 560).* Cement and Concrete Association, Slough, 1986, pp. 28.

[70] P. Fidjestøl, R. Lewis. *Microsilica as an addition.* In: P.C. Hewlett (ed.). *Lea's chemistry of cement and concrete, 4th ed.*, Elsevier Ltd., 1998, pp. 679-712.

[71] L. Hjorth. *Microsilica in concrete.* Nordic Concrete Res. 1 (1982) 901-918.

[72] A. Traetteberg. *Silica fume as a pozzolanic material.* Cemento 75 (1978) 369-375.

[73] C. Huang, R.F. Feldman. *Influence of silica fume on the microstructural development in cement mortars.* Cem. Concr. Res. 15 (1985) 285-294.

[74] C. Huang, R.F. Feldman. *Hydration reactions in portland cement-silica fume blends.* Cem. Concr. Res. 15 (1985) 585-592.

[75] C.M. Dobson, D.G.S. Goberdhan, J.D.F. Ramsay, S.A. Rodger. *^{29}Si MAS NMR study of the hydration of tricalcium silicate in the presence of finely divided silica.* J. Mater. Sci. 23 (1988) 4108-4114.

[76] J. Hjorth, J. Skibsted, H.J. Jakobsen. *^{29}Si MAS NMR studies of Portland cement components and effects of microsilica on the hydration reaction.* Cem. Concr. Res. 18 (1988) 789-798.

[77] G. Sun, J.F. Young. *Quantitative determination of residual silica fume in DSP cement pastes by ^{29}Si NMR.* Cem. Concr. Res. (1993) 480-483.

[78] E.J. Sellevold, F.F. Radjy. *Condensed silica fume (microsilica) in concrete: water demand and strength development.* American Concrete Institute, Publication SP-79 11 (1983) 677-694.

[79] K. Ogawa, H. Uchikawa, K. Takemoto, I. Yasui. *The mechanism of the hydration in the system C_3S-pozzolana.* Cem. Concr. Res. 10 (1980) 683-696.

[80] F. Massazza, M. Testolin. *Trimethylsilylation in the study of pozzolana-containing pastes.* Cemento 80 (1983) 49-62.

[81] P.K. Mehta. *Rice husk ash - a unique supplementary cementing material.* Proceedings of the International Symposium on Advances in Concrete Technology, 1992, pp. 407-430.

[82] M. Nehdi, J. Duquette, A. El Damatty. *Performance of rice husk ash produced using a new technology as a mineral admixture in concrete.* Cem. Concr. Res. 33 (2003) 1203-1210.

[83] M.H. Khan, K. Mohan, H.F.W. Taylor. *Pastes of tricalcium silicate with rice husk ash.* Cem. Concr. Res. 15 (1985) 89-92.

[84] S. Wild, J.M. Khatib, A. Jones. *Relative strength, pozzolanic activity and cement hydration in superplasticised metakaolin concrete.* Cem. Concr. Res. 26 (1996) 1537-1544.

[85] B. Lothenbach, G. Le Saout, E. Gallucci, K. Scrivener. *Influence of limestone on the hydration of Portland cements.* Cem. Concr. Res. 38 (2008) 848-860.

[86] M. Regourd. *Characterization and activation of addition product (in French).* Proceedings of the 8th ICCC, Vol. 1, 1986, pp. 199-229.

[87] K.D. Ingram, K.E. Daugherty. *Limestone additions to Portland cement: uptake, chemistry and effect.* Proceedings of the 9th ICCC, Vol. 3, 1992, p. 180-186.

[88] G. Kakali, S. Tsivilis, E. Aggeli, M. Bati. *Hydration products of C_3A, C_3S and Portland cement in the presence of $CaCO_3$.* Cem. Concr. Res. 30 (2000) 1073-1077.

[89] C. Müller. *Cluster 2: Blended cements, European Construction in Service and Society (ECO-Serve),* Proceedings of Challenge for Sustainable Construction, Poland, 2006.

[90] K.L. Scrivener, A. Capmas. *Calcium Aluminate Cements.* In: P.C. Hewlett (ed.). *Lea's chemistry of cement and concrete, 4th ed.,* Elsevier Ltd., 1998, pp. 713-782.

[91] G.L. Kalousek. *Analyzing SO_3-bearing phases in hydrating cements.* Mater. Res Stand. 5 (1965) 292-304.

[92] L.E. Copeland, D.L. Kantro. *Hydration of Portland cement.* Proceeding of the 5th ISCC, Vol. 2, 1968, pp. 387-421.

[93] E.M. Gartner, J.F.D. Young D.A., I. Jawed. *Hydration of Portland cement.* In: J. Bensted, P. Barnes, (eds.). *Structure and Performance of Cements, 2nd ed.*, Spon Press, 2002, pp. 57-113.

[94] D. Bonen, D. Diamond. *Interpretation of compositional patterns found by quantitative dispersive energy X-ray analysis for cement paste constituents.* J. Am. Ceram. Soc. 77 (1994) 1875-1882.

[95] D.L. Rayment, A.J. Majumdar. *The composition of the C-S-H phase in Portland cement pastes.* Cem. Concr. Res. 12 (1982) 753-764.

[96] H.F.W. Taylor, K. Mohan, G.K. Moir. *Analytical study of pure and extended Portland cements: I, Pure Portland cement pastes.* J. Am. Ceram. Soc. 68 (1985) 680-684.

[97] I.G. Richardson. *The nature of C-S-H in hardened cements.* Cem. Concr. Res. 29 (1999) 1131-1147.

[98] H.F.W. Taylor. *Proposed structure for calcium silicate hydrate gel.* J. Am. Ceram. Soc. 69 (1986) 464-467.

[99] H.F.W. Taylor. *Nanostructure of C-S-H - current status.* Adv. Cem. Based Mater. 1 (1993) 38-46.

[100] Z. Xu, D. Viehland. *Observation of a microstructure in calcium silicate hydrate gels of Portland cement.* Phys. Rev. Lett. 77 (1996) 952-955.

[101] G.K. Sun, J.F. Young. *Silicate polymerization analysis.* In: V. S. Ramachandran, J. J. Beaudoin (eds.): *Handbook of Analytical Techniques in Concrete Science and Technology*, Noyes Publication, USA, 2000, pp. 657.

[102] P. Colombet and A. R. Grimmer (eds.). *Applications of NMR to Cement Science*, Gordon and Breach, London, 1994, pp. 484.

[103] I.G. Richardson, G.W. Groves. *Models for the composition and structure of calcium silicate hydrate (C-S-H) gel in hardened tricalcium silicate pastes.* Cem. Concr. Aggr. 22 (1992) 1001-1010.

[104] H.E. Petch. *The hydrogen positions in portlandite, $Ca(OH)_2$, as indicated by electron distribution.* Acta Cryst. 14 (1961) 950-957.

[105] I.G. Richardson. *Tobermorite/jennite- and tobermorite/calcium hydroxide-based models for the structure of C-S-H: applicability to hardened pastes of tricalcium silicate, h-dicalcium silicate, Portland cement, and blends of Portland cement with blast-furnace slag, metakaolin, or silica fume.* Cem. Concr. Res. 34 (2004) 1733-1777.

[106] H.-J. Kuzel. *Röntgenuntersuchung im System $3CaO{\cdot}Al_2O_3{\cdot}CaSO_4{\cdot}nH_2O$ – $3CaO{\cdot}Al_2O_3{\cdot}CaCl_2{\cdot}nH_2O$ – H_2O.* Neues Jahrbuch Mineralog. Monatsh. (1966) 193-200.

[107] F.P. Glasser, A. Kindness, S.A. Stronach. *Stability and solubility relationships in AFm phases: Part I. Chloride, sulfate and hydroxide.* Cem. Concr. Res. 29 (1999) 861-866.

[108] E. Henderson, X. Turrillas, P. Barnes. *Hydration behaviour of simulated high-performance concrete pastes using synchrotron energy-dispersive diffraction.* Adv. Cem. Res. 6 (1994) 173.

[109] R.S. Gollop, H.F.W. Taylor. *Microstructural and microanalytical studies of sulfate attack. II. Sulfate-resisting Portland cement: Ferrite composition and hydration chemistry.* Cem. Concr. Res. 24 (1994) 1347-1358.

[110] R. Allmann. *Doppelschichtstrukturen mit brucitähnlichen Schichtionen.* Chimia 24 (1970) 99-108.

[111] M.A. Aramendia, Y. Avilés, V. Borau, J.M. Luque, J.M. Marinas, J.R. Ruiz, F.J. Urbano. *Thermal decomposition of Mg/Al and Mg/Ga layered-double hydroxides: a spectroscopic study.* J. Mater. Chem. 9 (1999) 1603-1607.

[112] K. Luke, F.P. Glasser. *Selective dissolution of hydrated blast furnace slag cements.* Cem. Concr. Res. 17 (1987) 273-282.

[113] H.M. Dyson, I.G. Richardson, A.R. Brough. *A combined ^{29}Si MAS NMR and selective dissolution technique for the quantitative evaluation of hydrated blast furnace slag cement blends.* J. Am. Ceram. Soc. 90 (2007) 598-602.

[114] K.L. Scrivener. *The Microstructure of Concrete.* In: J.P. Skalny (ed.). *Materials Science of Concrete I*, American Ceramic Society, Waterville, 1989, pp. 127-140.

[115] D.D. Double, A. Hellawell, S.J. Perry. *Hydration of Portland cement.* Proceedings of the Royal Socciety London A359 (1978) 435-451.

[116] G.W. Groves. *Portland cement clinker viewed by transmission electron microscopy.* J. Mater. Sci. 16 (1981) 1063-1070.

[117] B.J. Dalgleish, A. Ghose, H.M. Jennings, P.L. Pratt. *The Correlation of Microstructure with Setting and Hardening in Cement Paste.* International Conference on Concrete of Early Ages [Proc. RILEM Colloq.], Paris, Vol. 1, 1982, pp. 137-143.

[118] H.F.W. Taylor. *Reactivity of Solids, Part A*. Mater. Sci. Monogr. 28A (1985) 39.

[119] I.G. Richardson. *Electron microscopy of cements.* In: J. Bensted, P. Barnes (eds.). *Structure and Performance of Cements, 2nd ed.*, Spon Press, 2002, pp. 500-556.

[120] Q.L. Feng, E.E. Lachowski, F.P. Glasser. *Densification and migration of ions in blast furnace slag-Portland cement pastes.* Mater. Res. Soc. Symp. Proc. 136 (1989) 263-272.

[121] R.S. Gollop, H.F.W. Taylor. *Microstructural and microanalytical studies of sulfate attack. V. Comparison of different slag blends.* Cem. Concr. Res. 26 (1996) 1029-1044.

[122] I.G. Richardson, G.W. Groves. *Microstructure and microanalysis of hardened cement pastes involving ground granulated blast-furnace slag.* J. Mater. Sci. 27 (1992) 6204-6212.

[123] A.M. Harrisson, N.B. Winter, H.F.W. Taylor. *An examination of some pure and composite Portland cement pastes using scanning electron microscopy with X-ray analytical capability.* Proceedings of the 8th ICCC, Vol. 4, 1986, pp. 170-175.

[124] H. Uchikawa, S. Uchida, K. Ogawa. Proceedings of the 8th ICCC, Vol. 4, 1986, pp. 251-256.

[125] H.F.W. Taylor, K. Mohan, G.K. Moir. *Analytical Study of Pure and Extended Portland Cement Pastes: II, Fly Ash- and Slag-Cement Pastes.* J. Am. Ceram. Soc. 68 (1985) 685-690.

[126] K.L. Scrivener, H.H. Patel, P.L. Pratt, L.J. Parrott. *Analysis of phases in cement paste using backscattered electron images, methanol adsorption and thermogravimetric analysis.* Mater. Res. Soc. Symp. Proc. 85 (1987) 67-76.

[127] K. Mohan, H.F.W. Taylor. *Effects of Flyash Incorporation in Cement and Concrete (ed. S. Diamond)*, Materials Research Society, University Park, 1981, pp. 54-59.

[128] F. Massazza. *Properties and applications of natural pozzolanas.* In: J. Bensted, P. Barnes (eds.). *Structure and Performance of Cements, 2nd ed.*, Spon Press, 2002, pp. 326-352.

[129] J.C. Taylor, L.P. Aldridge, C.E. Matulis, I. Hinczak. *X-ray powder diffraction analysis of cements.* In: J. Bensted, P. Barnes (eds.). *Structure and Performance of Cements, 2nd ed.*, Spon Press, 2002, pp. 420-441.

[130] R.A. Kennerley. *Composition of high manganese portland cement.* Cem. Concr. Res. 7 (1977) 565-574.

[131] T. Westphal, G. Walenta, T. Füllmann, M. Gimenez, E. Bermejo, K. Scrivener, H. Pöllmann. *Characterisation of cementitious materials - Part III.* Int. Cem. Rev. July 2002 (2002) 47-51.

[132] P.M. Suherman, A. Van Riessen, B. O'Conner, D. Bolton, H. Fairhurst. *Determination of amorphous phase levels in Portland cement clinker.* Powder Diffraction 17 (2002) 178.

[133] G. Le Saoût, T. Füllmann, V. Kocaba, K.L. Scrivener. *Quantitative study of cementitious materials by X-ray diffraction/ Rietveld analysis using an external standard.* Proceedings of the 12th International Congress on the Chemistry of Cement, Montréal, Canada, 2007, TH2-07.01.

[134] R. Jenkins, R.L. Snyder. *Introduction to X-ray Powder Diffractometry.* In: J.D. Winefordner (ed.). *Chemical Analysis: a series of monographs on chemistry and its applications*, Wiley, 1996, Vol. 138, pp. 432.

[135] R. Yang. *Crystallinity determination of pure phases used as standards for QXDA in cement chemistry.* Cem. Concr. Res. 26 (1996) 1451-1461.

[136] A.G. De la Torre, A. Cabeza, A. Calvente, S. Bruque, M.A.G. Aranda. *Full Phase Analysis of Portland Clinker by Penetrating Synchrotron Powder Diffraction.* Anal. Chem. 73 (2001) 151-156.

[137] A.G. De la Torre, S. Bruque, M.A.G. Aranda. *Rietveld Quantitative Amorphous Analysis.* J. Appl. Cryst. 34 (2001) 196-202.

[138] M. Enders. *Quantitative XRD-analysis in automated cement laboratories: requirementsr for sample preparation.* ZKG International 56 (2003) 54-62.

[139] D.L. Bish, S.A. Howard. *Quantitative phase analysis using the Rietveld method.* J. Appl. Cryst. 21 (1988) 86-91.

[140] R.A. Young. *The Rietveld Method. IUCR Monographs on Crystallogrphy 5.* Oxford University Pres, Oxford, UK, 1993.

[141] A.G. De la Torre, M.A.G. Aranda. *Accuracy in Rietveld quantitative phase analysis of Portland cements.* J. Appl. Cryst. 36 (2003) 1169-1176.

[142] V.K. Peterson, A.S. Ray, B.A. Hunter. *A comparative study of Rietveld phase analysis of cement clinker using neutron, laboratory X-ray, and synchrotron data.* Powder Diffraction 21 (2006) 12-18.

[143] H.M. Rietveld. *A Profile Refinement Method for Nuclear and Magnetic Structures.* J. Appl. Cryst. 2 (1969) 65-69.

[144] T. Füllmann, H. Pöllmann, G. Walenta, M. Gimenez, C. Lauzon, S.D. Hagopian-Babikian T., P. Noon. *Analytical Methods.* Int. Cem. Rev., January 2001, pp. 41-43.

[145] G. Walenta, T. Füllmann, M. Gimenez. *Quantitative Rietveld analysis of cement and clinker.* Int. Cem. Rev., June 2001, pp. 51-54.

[146] R.S. Winburn, D.G. Grier, G.J. McCarthy, R.B. Peterson. *Rietveld quantitative X-ray diffraction analysis of NIST fly ash standard reference materials.* Powder Diffraction 15 (2000) 163-172.

[147] K.L. Scrivener, T. Füllmann, E. Gallucci, G. Walenta, E. Bermejo. *Quantitative study of Portland cement hydration by X-ray diffraction/Rietveld analysis and independent methods.* Cem. Concr. Res. 34 (2004) 1541-1547.

[148] M. Enders, M. Berger. *Quantitative XRD (Rietveld-method) in cement plants: quality control of clinker production.* ZKG International 60 (2007) 50-59.

[149] M. Enders. *Quantitative Phase Analysis.* World Cement June 2007 (2007) 45-50.

[150] D.H. Campbell. *Microscopical Examination and Interpretation of Portland Cement and Clinker.* Construction Technology Laboratories, Skokie, IL, 1986, pp. 128.

[151] F. Hofmänner. *Microstructure of Portland Cement Clinker.* Rheintaler Druckerei un Verlag, Heerbrugg, Switzerland, 1975, pp. 48.

[152] Y. Ono. *Microscopical Observation of Clinker, For the Estimation of Burning Condition, Grindability, and Hydraulic Activity.* 3rd IC Cem. Microsc., 1981, pp. 198-210.

[153] K.L. Scrivener, P.L. Pratt. *Backscattered electron images of polished cement sections in the SEM.* 6th IC Cem. Microsc., 1984, pp.145-155.

[154] K.L. Scrivener. *The Microstructure of Anhydrous Cement and Its Effect on Hydration.* Mater. Res. Soc. Symp. Proc. 85 (1987) 39-46.

[155] P. Stutzman. *Scanning electron microscopy imaging of hydraulic cements microstructure.* Cement and concrete composites 26 (2004) 957-966.

[156] K.L. Scrivener. *Backscattered electron imaging of cementitious microstructures: understanding and quantification.* Cement and Concrete Composites 26 (2004) 935-945.

[157] J.I. Goldstein, D.E. Newbury, P. Echlin, D.C. Joy, C. Fiori, E. Lifshin. *Scanning Electron Microscopy and X-ray Microanalysis.* Plenum Press, New York, 1981, pp. 673.

[158] H. Zhao, D. Darwin. *Quantitative backscattered electron analysis of cement paste.* Cem. Concr. Res. 22 (1992) 695-706.

[159] X. Feng, E.J. Garboczi, D.P. Bentz, P.E. Stutzman, T.O. Mason. *Estimation of the degree of hydration of blended cement pastes by a scanning electron microscope point-counting procedure.* Cem. Concr. Res. 34 (2004) 1787-1793.

[160] Å. Grudemo. *Discussion following the paper by J. D. Bernal on 'The structure of cement hydratio compounds'.* Proceedings of the 3rd ISCC, 1954, pp. 247-253.

[161] H.M. Jennings, B.J. Dalgleish, P.L. Pratt. *Morphological development of hydrating tricalcium silicate as examined by electron microscopy techniques.* J. Am. Ceram. Soc. 64 (1981) 567-572.

[162] G.W. Groves, P.J. Le Seur, W. Sinclair. *Transmission electron microscopy and microanalytical studies of ion-beam-thinned sections of tricalcium silicate paste.* J. Am. Ceram. Soc. 69 (1986) 353-356.

[163] A.V. Girão, I.G. Richardson, C.B. Porteneuve, R.M.D. Brydson. *Composition, morphology and nanostructure of C–S–H in white Portland cement pastes hydrated at 55 °C.* Cem. Concr. Res. 37 (2007) 1571-1582.

[164] I.G. Richardson, J.G. Cabrera. *The nature of C-S-H in model slag-cements.* Cem. Concr. Comp. 22 (2000) 259-266.

[165] I.G. Richardson. *The nature of the hydration products in hardened cement pastes.* Cem. Concr. Comp. 22 (2000) 97-113.

[166] G. De Schutter. *Hydration and temperature development of concrete made with blast-furnace slag cement.* Cem. Concr. Res. 29 (1999) 143-149.

[167] B.W. Langan, K. Weng, M.A. Ward. *Effect of silica fume and fly ash on heat of hydration of Portland cement.* Cem. Concr. Res. 32 (2002) 1045-1051.

[168] J.-I. Escalante-Garcia, J.H. Sharp. *The chemical composition and microstructure of hydration products in blended cements.* Cem. Concr. Comp. 26 (2004) 967-976.

[169] Y. Zhang, W. Sun, S. Liu. *Study on the hydration heat of binder paste in high-performance concrete.* Cem. Concr. Res. 32 (2002) 1483-1488.

[170] C.J. Fordham, I.J. Smalley. *A simple thermogravimetric study of hydrated cement.* Cem. Concr. Res. 15 (1985) 141-144.

[171] A. Ray, E.R. Cantrill, M.G. Stevens, L. Aldridge. *Use of DTA to determine the effect of mineralizerson the cement-quartz hydrothermal reactions. Part 2. Clay addition.* Thermochimica acta 250 (1995) 189-195.

[172] V. Kasselouri, C. Ftikos, G. Parissakis. *DTA-TG study on the $Ca(OH)_2$ - pozzolan reaction in cement pastes hydrated up to three years.* Cem. Concr. Res. 13 (1983) 649-654.

[173] I. Pane, W. Hansen. *Investigation of blended cement hydration by isothermal calorimetry and thermal analysis.* Cem. Concr. Res. 35 (2005) 1155-1164.

[174] R.H. Bogue. *Calculation of the Compounds in Portland Cement.* Industrial and Engineering Chemistry (Analytical edition) 1 (1929) 192-197.

[175] H.F.W. Taylor. *Modification of the Bogue calculation.* Adv. Cem. Res. 2 (1989) 73-77.

[176] S. Takashima. *Systematic dissolution of calcium silicate.* Review of the 12th General Meeting, Cement Association of Japan, Tokyo, 1958, pp. 12-13.

[177] L. Hjorth, K.-. Laurén. *Belite in portland cement.* Cem. Concr. Res. 1 (1971) 27-40.

[178] A. Tabikh, R.J. Weth. *An X-ray analysis of portland cement.* Cem. Concr. Res. 1 (1971) 317-328.

[179] L. Struble. *The effect of water on maleic acid and salicylic aid extractions.* Cement and Concrete Research 15 (1985) 631-636.

[180] W.A. Gutteridge. *On the dissolution of the interstitial phases in Portland cement.* Cem. Concr. Res. 9 (1979) 319-324.

[181] K. Luke, F.P. Glasser. *Internal chemical evolution of the constitution of blended cements.* Cem. Concr. Res. 18 (1988) 495-502.

[182] E. Demoulian, C. Vernet, F. Hawthorn, P. Gourdin. *Slag content determination in cements by selective dissolution.* Proceedings of the 7th ICCC, 1980, Vol. 2, pp. III-151.

[183] J.I. Escalante, L.Y. Gómez, K.K. Johal, G. Mendoza, H. Mancha, J. Méndez. *Reactivity of blast-furnace slag in Portland cement blends hydrated under different conditions.* Cem. Concr. Res. 31 (2001) 1403-1409.

[184] M.J. Coole. *Calorimetric Studies of the Hydration Behaviour of Extended Cements.* Br. Ceram. Proc. 35 (1984) 385-401.

[185] T. Knudsen, M. Geiker. *Obtaining hydration data by measurement of chemical shrinkage with an archimeter.* Cem. Concr. Res. 15 (1985) 381-382.

[186] E. Tazawa, S. Miyazawa, T. Kasai. *Chemical shrinkage and autogenous shrinkage of hydrating cement paste.* Cem. Concr. Res. 25 (1995) 288-292.

[187] P. Colombet, A.-R. Grimmer (eds.). *Application of NMR Spectroscopy to Cement Science*, Gordon and Breach, Amsterdam, 1994, pp. 484.

[188] P. Colombet, A.R. Grimmer, H. Zanni, P. Sozzani (eds.). *Nuclear Magnetic Resonance Spectroscopy of Cement-Based Materials.* Springer-Verlag, Berlin and Heidelberg, 1998, pp. 302.

[189] J. Skibsted, C. Hall, H.J. Jakobsen. *Nuclear magnetic resonance spectroscopy and magnetic resonance imaging of cements and cement-based materials.* In: J. Bensted, P. Barnes (eds.). *Structure and Performance of Cements, 2nd ed.*, Spon Press, 2002, pp. 457-476.

[190] J. Skibsted, C. Hall. *Characterization of cement minerals, cements and their reaction products at the atomic and nano scale.* Cem. Concr. Res. 38 (2008) 205-225.

[191] H.W. Speiss. *NMR Basic Principles and Progress (Diehl, P., Fluck, E., Kosfeld, R. (eds.)),* Springer, Berlin, Vol. 15, 1978, pp. 55-214.

[192] J. Herzfeld, A.E. Berger. *Sideband intensities in NMR spectra of samples spinning at the magic angle.* J. Chem. Phys. 73 (1980) 6021-6030.

[193] M.R. Hansen, H.J. Jakobsen, J. Skibsted. *^{29}Si Chemical Shift Anisotropies in Calcium Silicates from High Field ^{29}Si MAS NMR Spectroscopy.* Inorg. Chem. 42 (2003) 2368-2377.

[194] A. Pines, G. Gibby, J.S. Waugh. *Proton-Enhanced Nuclear Induction Spectroscopy. A Method for High Resolution NMR of Dilute Spins in Solids.* J. Chem. Phys. 56 (1972) 1776-1777.

[195] S.R. Hartmann, E.L. Hahn. *Nuclear double resonance in the rotating frame.* Phys. Rev. 128 (1962) 2042-2053.

[196] G. Engelhardt. *Silicon-29 NMR of Solid Silicates.* In: D.M. Grant, R.K. Harris (eds.). *Encyclopedia of Magnetic Resonance*, John Wiley & Sons, Ltd., 1996, pp. 4398-4407.

[197] J.R. Kirkpatrick. *NMR Spectroscopy of Minerals and Glasses.* In: F.C. Hawthorne (ed.). *Spectroscopic Methods in Mineralogy and Geology*, Mineralogical Society of America, Washington, DC, 1988, pp. 341-403.

[198] G. Engelhardt, D. Michel. *High-resolution Solid-State NMR of Silicates and Zeolites.* John Wiley & Sons: Berlin, 1987, pp. 179.

[199] J.F. Stebbins. *Nuclear magnetic resonance spectroscopy of silicates and oxides in geochemistry and geophysics.* In: T.J. Ahrens (ed.). *Handbook of physical constants*, American Geophysical Union, Washington D.C., 1995, pp. 303-332.

[200] A.R. Grimmer, W. Wieker, F.v. Lampe, E. Fechner, R. Peter, G. Molgedey. *^{29}Si-NMR an festen Silicaten: anisotropie der chemischen Verschiebung im Thaumasit.* Z. Chem. 20 (1980) 453.

[201] J.F. Stebbins. *NMR evidence for five-coordinated silicon in a silicate glass at atmospheric pressure.* Nature (Lodon) 351 (1991) 638-639.

[202] E. Kundla, A. Samoson, E. Lippmaa. *High resolution NMR of quadrupolar nuclei in rotating solids.* Chem. Phys. Lett. 83 (1981) 229-232.

[203] J. Skibsted, N.C. Nielsen, H. Bildsøe, H.J. Jakobsen. *Satellite Transitions in MAS NMR Spectra og Quadrupolar Nuclei.* J. Mag. Reson. 95 (1991) 88-117.

[204] D. Müller, W. Gessner, H.J. Behrens, G.J. Scheler. *Determination of the aluminium coordination in aluminium-oxygen compounds by solid-state high-resolution ^{27}Al NMR.* Chem. Phys. Lett. 79 (1981) 59-62.

[205] L. Frydman, J.S. Harwood. *Isotropic spectra of half-integer quadropolar spins from bidimansional magic-angle spinning NMR.* J. Am. Chem. Soc. 117 (1995) 5367-5368.

[206] A. Medik, J.S. Harwood, L. Frydman. *Multiple-quantum magic-angle spinning NMR: A new method for the study of qudrupolar nuclei in solids.* J. Am. Chem. Soc. 117 (1995) 12779-12787.

[207] G.E. Pake. *Nuclear resonance absorption in hydrated crystals: fine structure of the proton line.* J. Chem. Phys. 16 (1948) 327-336.

[208] K. Kawachi, M. Murakami, E. Hirahara. *The hydration and hardening of cement: the nuclear magnetic resonance absorption of water molecules.* Bullitin of the Faculty of Engineering, Hiroshima University 4 (1955) 95-101.

[209] R.L. Blaine. *Proton magnetic resonance (N.M.R.) in hydrated portland cements.* National Bureau of Standards Monograph 43 (1960) 501-511.

[210] P. Seligmann. *Nuclear magnetic resonance studies of the water in hardened cement paste.* J. Portland Cem. Assoc. Res Dev. Lab. 1052-65.

[211] R. Blinc, M. Burgar, G. Lahajnar, M. Rozmarin, V. Rutar, I. Kocuvan, J. Ursic. *NMR relaxation study of adsorbed water in cement and C_3S paste.* J. Am. Ceram. Soc. 61 (1978) 35-37.

[212] A.-R. Grimmer, H. Rosenberger. *Proton solid-state NMR as a contrinution to the study of water-containing silicates.* Zeitschrift für Chmie 18 (1978) 378.

[213] H. Rosenberger, A.-R. Grimmer. *Studies on hydrogen-bonded compounds with high-resolution NMR spectroscopy in solids. The relation between the chemical shifts of protons and the character of hydroxyl groups in some crystalline silicates.* Z. Anorg. Allg. Chem. 448 (1979) 11-22.

[214] L. Bonafous, C. Bessada, D. Massiot, J.P. Coutures, B. Lerolland, P. Colombet. *^{29}Si MAS NMR study of dicalcium silicate: The structural influence of sulfate and alumina stabilizers.* J. Am. Ceram. Soc. 78 (1995) 2603-2608.

[215] P.J. McDonald, J.P. Korb, J. Mitchell, L. Monteilhet. *Surface relaxation and chemical exchange in hydrating cement pastes: A two-dimensional NMR relaxation study.* Phys. Rev. E 72 art. no. 011409 (2005)

[216] J.-. Korb, L. Monteilhet, P.J. McDonald, J. Mitchell. *Microstructure And Texture Of Hydrated Cement-Based Materials: A Proton Field-Cycling Relaxometry Approach.* Cem. Concr. Res. 37 (2007) 295-302.

[217] P.J. McDonald, J. Mitchell, M. Mulheron, P.S. Aptaker, J.-. Korb, L. Monteilhet. *2D Correlation Relaxometry Experiments of Cement Pastes Performed Using A New One-Sided NMR Magnet.* Cem. Concr. Res. 37 (2007) 303-309.

[218] E. Lippmaa, M. Mägi, M. Tarmak, W. Wieker, A.R. Grimmer. *A high resolution ^{29}Si NMR study of tricalcium-silicate.* Cem. Concr. Res. 12 (1982) 597-602.

[219] E. Lippmaa, M. Mägi, G. Engelhardt, A.-. Grimmer. *Structural studies of silicates by solid-state high-resolution silicon-29 NMR.* J. Am. Chem. Soc. 102 (1980) 4889-4993.

[220] A.R. Grimmer, F. von Lampe, M. Mägi, E. Lippmaa. *Solis-state high-resolution ^{29}Si NMR and Si-O-Si bond angle and chemical shift in disilicates.* Monatschrift für Chemie 114 (1983) 1053-1057.

[221] A.R. Grimmer, F. von Lampe, M. Mägi, E. Lippmaa. *High-resolution solid-state ^{29}Si NMR of polymorphs of Ca_2SiO_4.* Cem. Concr. Res. 15 (1985) 467-473.

[222] M. Mägi, E. Lippmaa, A. Samoson, G. Engelhardt, A.-. Grimmer. *Solid-state high-resolution ^{29}S chemical shifts in silicates.* J. Phys. Chem. 88 (1984) 1518-1522.

[223] J. Skibsted, J. Hjorth, H.J. Jakobsen. *Correlation between ^{29}Si NMR chemical shifts and mean Si-O bond lengths for calcium silicates.* Chem. Phys. Lett. 172 (1990) 279-283.

[224] A.-R. Grimmer, H. Zanni. *^{29}Si NMR of chemical shift tensor anisotropy of tricalcium silicate.* In: P. Colombet, A.-R. Grimmer, H. Zanni, (eds.). *Nuclear Magnetic Resonance Spectroscopy of Cement-Based Materials*, Springer Verlag, Berlin and Heidelberg, 1998, pp. 57-68.

[225] J. Skibsted, H.J. Jakobsen, C. Hall. *Quantification of Calcium Silicate Phases in Portland Cements by ^{29}Si MAS NMR Spectroscopy.* J. Chem. Soc. Faraday Trans. 91 (1995) 4423-4430.

[226] I.G. Richardson, A.R. Brough, R. Brydson, G.W. Groves, C.M. Dobson. *Location of aluminium in substituted calcium silicate hydrate (C-S-H) gels as determined by ^{29}Si and ^{27}Al NMR and EELS.* J. Am. Ceram. Soc. 76 (1993) 2285-2288.

[227] X.D. Cong, J.R. Kirkpatrick. *^{29}Si and ^{17}O NMR investigation of the structure of some crystalline silicate hydrated.* Adv. Cem. Based Mater. 3 (1996) 133-143.

[228] J. Skibsted, E. Henderson, H.J. Jakobsen. *Characterization of Calcium Aluminate Phases in Cements by ^{27}Al MAS NMR Spectroscopy.* Inorg. Chem. 32 (1993) 1013-1027.

[229] J. Skibsted, H.J. Jakobsen, C. Hall. *Quantitative Aspects of ^{27}Al MAS NMR of Calcium Aluminoferrites.* Adv. Cem. Based Mat. 7 (1998) 57-59.

[230] J. Skibsted, O. Mejlhede Jensen, H.J. Jakobsen. *Hydration kinetics for alite and belite, and calcium aluminate phases in Portland cements from ^{27}Al and ^{29}Si MAS NMR Spectroscopy.* Proc. 10th Int. Congr. Chem. of Cem., Gothenburg, Sweden, June 2-6, 1997, paper 2ii056.

[231] I. Klur, B. Pollet, J. Virlet, A. Nonat. *C-S-H structure evolution with calcium content by multinuclear NMR.* In: P. Colombet, A.-R. Grimmer, H. Zanni, P. Sozzani (eds.). *Nuclear Magnetic Resonance Spectroscopy of Cement-Based Materials*, Springer Verlag, Berlin and Heidelberg, 1998, pp. 119-141.

[232] F. Nishi, Y. Takéuchi, I. Maki. *Tricalcium silicate, the monoclinic superstructure. Z.* Kristallogr. 172 (1985) 297-314.

[233] S.L. Poulsen, V. Kocaba, G. Le Saoût, H.J. Jakobsen, K.L. Scrivener, J. Skibsted. *Improved quantification of alite and belite in anhydrous Portland cements by ^{29}Si MAS NMR: Effects of paramagnetic ions.* Solid State Nucl. Magn. Reson. 36 (2009) 32-44.

[234] J. Skibsted, H. Bildsøe, H.J. Jakobsen. *High-speed spinning versus high magnetic field in MAS NMR of quadrupolar nuclei. ^{27}Al MAS NMR of $3CaO{\cdot}Al_2O_3$.* J. Magn. Reson. 92 (1991) 669-676.

[235] L.H. Merwin, A. Sebald, H. Rager, H. Schneider. *^{29}Si and ^{27}Al MAS NMR Spectroscopy of Mullite.* Phys. Chem. Minerals 18 (1991) 47-52.

[236] J. Klinowski. *Nuclear magnetic resonance studies of zeolites.* Progress in NMR Spectroscopy 16 (1989) 237-309.

[237] J.R. Kirkpatrick, R.A. Kinsey, K.A. Smith, D.M. Henderson, E. Oldfield. *High resolution solid-state sodium-23, aluminium-27, and silicon-29 nuclear magnetic resonance spectroscopic reconnaissance of alkali and plagioclase feldspars.* American Mineralogist 70 (1985) 106-123.

[238] M.T. Blanco Varela, S. Martínez Ramírez, I.G. Ereña M., P. Carmona. *Characterization and pozzolanicity of zeolitic rocks from two Cuban deposits.* Applied Clay Science 33 (2006) 149-159.

[239] H.S. Pietersen, A.P.M. Kentgens, G.H. Nachtegaal, W.S. Veeman, J.M. Bijen. *The reaction mechanism of blended cements: A ^{29}Si NMR study.* 4th Canmet/ACI Conference on Fly Ash, Silica Fume, Slag, and Natural Pozzolans in Concrete, Vol. 1, 1992, pp.797-812.

[240] I.G. Richardson, A.R. Brough, G.W. Groves, C.M. Dobson. *The characterization of hardened alkali-activated blast-furnace slag pastes and the nature of the calcium silicate hydrate (C-S-H) phase.* Cem. Concr. Res. 24 (1994) 813-829.

[241] G.C. Levy, I.R. Peat. *The experimental approach to accurate carbon-13 spin-lattice relaxation measurements.* J. Magn.Reson. (1969) 18 (1975) 500-521.

[242] J.S. Hartman, B.L. Sherriff. *Silicon-29 MAS NMR of the aluminosilicate mineral kyanite: residual dipolar coupling to aluminum-27 and nonexponential spin-lattice relaxation.* J. Phys. Chem. 95 (1991) 7575-7579.

[243] J. Skibsted, L. Hjorth, H.J. Jakobsen. *Quantification of thaumasite in cementitious materials by $^{29}Si\{^1H\}$ cross-polarization mageic-angle spinning NMR spectroscopy.* Adv. Cem. Res. 7 (1995) 69-83.

[244] D. Tse, S.R. Hartmann. *Nuclear Spin-Lattice Relaxation Via Paramagnetic Centers Without Spin Diffusion.* Phys. Rev. Lett. 21 (1968) 511-514.

[245] J.A. Chudek, G. Hunter, G.W. McQuire, C.H. Rochester, T.F.S. Smith. *^{29}Si magic-angle spinning NMR study of Phillips catalysts: Multi-exponential spin-lattice*

relaxation resulting from adsorption of paramagnetic chromium species onto a silica surface. J. Chem. Soc., Faraday Trans. 92 (1996) 453-460.

[246] G.B. Furman, S.D. Goren. *Nuclear magnetic resonance detection of the nuclear spin near paramagnetic impurities in solids.* Phys. Condens. Matter 14 (2002) 873-881.

[247] C.L. Edwards, L.B. Alemany, A.R. Barron. *Solid-State ^{29}Si NMR Analysis of Cements: Comparing Different Methods of Relaxation Analysis for Determining Spin-Lattice Relaxation Times to Enable Determination of the C_3S/C_2S Ratio.* Ind. Eng. Chem. Res. 46 (2007) 5122-5130.

[248] C. Coelho, T. Azais, C. Bonhomme, L. Bonhomme-Coury, C. Boissiére, G. Laurent, D. Massiot. *Efficiency of dipolar and J-derived solid-state NMR techniques for a new pair of nuclei {^{31}P,^{29}Si}. Towards the characterization of Si-O-P mesoporous materials.* C. R. Chimie 11 (2008) 387-397.

[249] H. Mayer. *Die Kristallstruktur von $Si_5O[PO_4]_6$.* Monatshefte für Chemie 105 (1974) 46-54.

[250] C. Lejeune, C. Coelho, L. Bonhomme-Coury, T. Azaïs, J. Maquet, C. Bonhomme. *Studies of silicophosphate derivatives by $^{31}P \rightarrow ^{29}Si$ CP MAS NMR.* Solid State Nucl. Magn. Reson. 27 (2005) 242-246.

[251] H. Hilbig, F.H. Köhler, P. Schieβl. *Quantitative ^{29}Si MAS NMR spectroscopy of cement and silica fume containing paramagnetic impurities.* Cem. Concr. Res. 36 (2006) 326-329.

[252] P. Faucon, T. Charpentier, A. Nonat, J.C. Petit. *Triple-quantum two-dimensional ^{27}Al magic angle nuclear magnetic resonance study of the aluminum incorporation in calcium silicate hydrates.* J. Am. Chem. Soc. 120 (1998) 12075-12082.

[253] M. Mägi, A. Samoson, M. Tarmak, G. Engelhardt, E. Lachowski. *Study of the structure of silicates and zeolites by solid-state high-resolution ^{29}Si NMR spectroscopy.* Doklady Akedemii Nauk SSSR 261 (1981) 1169-1174.

[254] J.R. Barnes, A.D.H. Clague, N.J. Clayden, C.M. Dobson, C.J. Hayes, G.W. Groves, S.A. Rodger. *Hydration of of Portland cement followed by ^{29}Si solid-state NMR spectroscopy.* J. Mater. Sci. Lett. 4 (1985) 1293-1295.

[255] X. Cong, J.R. Kirkpatrick. *^{17}O and ^{29}Si MAS NMR study of β–C_2S hydration and the structure of calcium-silicate hydrates.* Cem. Concr. Res. 23 (1993) 1065-1077.

[256] E. Lippmaa, M. Magi, A. Samoson, M. Tarmark, J. Engelhardt. *Investigation of the structure of zeolites by solid-state high-resolution ^{29}Si MAS NMR spectroscopy.* J. Am. Chem. Soc. 103 (1981) 4992-4996.

[257] M.D. Andersen, H.J. Jakobsen, J. Skibsted. *Incorporation of Aluminium in Calcium Silicate Hydrate (C-S-H) of Hydrated Portland Cements: A High-Field ^{27}Al and ^{29}Si MAS NMR Investigation.* Inorg. Chem. 42 (2003) 2280-2287.

[258] M.D. Andersen. *Structural Investigations of Portland Cement-Based Materials by Solid-State NMR Spectroscopy.* PhD thesis, Aarhus University, Denmark, 2004, pp.172.

[259] I.G. Richardson, G.W. Groves. *The structure of the calciumsilicate hydrate phases present in hardened pastes of white Portland cement/blast-furnace slag blends.* J. Mater. Sci. 32 (1997) 4793-4802.

[260] M.D. Andersen, H.J. Jakobsen, J. Skibsted. *Characterization of white Portland cement hydration and the C-S-H structure in the presence of sodium aluminate by ^{27}Al and ^{29}Si MAS NMR spectroscopy.* Cem. Concr. Res. 34 (2004) 857-868.

[261] V. Kocaba. *Development and evaluation of methods to follow microstructural development of cementitious systems including slags.* PhD thesis No. 4523, École Polytechnique Fédérale de Lausanne, Switzerland, 2009, pp. 239.

[262] L. Lam, Y.L. Wong, C.S. Poon. *Degree of hydration and gel/space ratio of high-volume fly ash/cement systems.* Cem. Concr. Res. 30 (2000) 747-756.

[263] R.F. Feldman, G.G. Carette, V.M. Malhotra. *Studies on mechanics of development of physical and mechanical properties of high-volume fly ash-cement pastes.* Cem. Concr. Comp. 12 (1990) 245-251.

[264] H. Krøyer, H. Lindgreen, H.J. Jacobsen, J. Skibsted. *Hydration of Portland cement in the presence of clay minerals studied by ^{29}Si and ^{27}Al MAS NMR spectroscopy.* Adv. Cem. Res. 15 (2003) 103-112.

[265] S.A. Rodger, G.W. Groves, N.J. Clayden, C.M. Dobson. *Hydration of tricalcium silicate followed by ^{29}Si NMR with cross-polarization.* J. Am. Ceram. Soc. 71 (1988) 91-96.

[266] G.W. Groves, S.A. Rodger. *The hydration of C_3S and ordinary Portland cement with relatively large additions of microsilica.* Adv. Cem. Res. 2 (1989) 135-140.

[267] C. Famy, K.L. Scrivener, A. Atkinson, A.R. Brough. *Effects of an early or a late heat treatment on the microstructure and composition of inner C-S-H products of Portland cement mortars.* Cem. Concr. Res. 32 (2002) 269-278.

[268] M.D. Andersen, H.J. Jakobsen, J. Skibsted. *A new aluminium-hydrate species in hydrated Portland cements characterized by ^{27}Al and ^{29}Si MAS NMR spectroscopy.* Cem. Concr. Res. 36 (2006) 3-17.

[269] P. Faucon, A. Delagrave, J.C. Petit, C. Richet, J.M. Marchand, H. Zanni. *Aluminum incorporation in calcium silicate hydrates (C-S-H) depending on their Ca/Si ratio.* J. Phys. Chem. B 103 (1999) 103 (1999) 7796-7802.

[270] K. Takehira, T. Kawabata, T. Shishido, K. Murakami, T. Ohi, D. Shoro, M. Honda, K. Takaki. *Mechanism of reconstitution of hydrotalcite leading to eggshell-type Ni loading on Mg–Al mixed oxide.* Journal of Catalysis 231 (2005) 92-104.

[271] H.C. Erntroy. *Determination of Clinker Content of Composite Cements.* ZKG Int. 40 (1987) 270-272.

[272] W. Hinrichs, I. Odler. *Investigation of the hydration of Portland blasfurnace slag cement: hydration kinetics.* Adv. Cem. Res. 2 (1989) 9-13.

[273] R. Goquel. *A New Consecutive Dissolution Method for the Analysis of Slag Cements.* Cem. Concr. Agg. 17 (1995) 84-91.

[274] O.B. Peerson, X. Wu, I. Kustanovich, S.O. Smith. *Variable-Amplitude Cross-Polarization MAS NMR*. J. Magn. Reson. 104 (1993) 334-339.

Appendix I

Experimental conditions for acquisition of solid-state MAS NMR spectra

All experimental solid-state MAS NMR spectra in the thesis were obtained from powder samples. Prior to acquisition of the spectra the magic angle was set by minimizing the linewidths of the spinning sidebands from the satellite transitions in the ^{23}Na MAS NMR spectrum of $NaNO_3$.

^{29}Si MAS NMR experiments

The solid-state ^{29}Si MAS NMR spectra were recorded at two different magnetic field strengths (7.1 T and 9.4 T) on Varian Unity INOVA-300 and -400 spectrometers, using home-built CP/MAS probes designed for 7, 5, or 4 mm o.d. rotors with sample volumes of 220, 110, and 80 μL, respectively. The single-pulse experiments employed 45° excitation pulses (τ_{pw} = 2.5 – 3.0 μs) and relaxation delays of 30 s to ensure full relaxation of the ^{29}Si spins between the individual acquisitions. Spinning speeds (ν_R) of 7.0, 12.0 and 13.0 kHz were used for the 7, 5, and 4 mm rotors of PSZ (Partially Stabilized Ziconia), respectively. Typically, 1000 – 3000 scans were recorded for each spectrum. The individual probes employed for the two spectrometers used radio-frequency (rf) field strengths in the range: $\gamma B_1/2\pi$ = 40 – 60 kHz. The rf field strengths were calibrated using a sample of Na_2SiF_6 (δ_{iso} = -188.9 ppm) due to the short spin-lattice relaxation time for this compound (T_1 = 0.5 s at 7.1 T). ^{1}H decoupling was not employed in the ^{29}Si MAS NMR experiments, since MAS at spinning speeds above ~5 kHz efficiently averages out the ^{1}H – ^{29}Si dipolar couplings. The ^{29}Si chemical shifts in the ^{29}Si MAS NMR spectra are reported in ppm (parts per million) relative to an external sample of neat tetramethylsilane (TMS), using a sample of β-Ca_2SiO_4 (δ_{iso} = -71.33 ppm) as a secondary reference material.

^{27}Al MAS NMR experiments

The solid-state ^{27}Al MAS NMR spectra were acquired at 14.1 T on a Varian Unity INOVA-600 spectrometer equipped with a home-built CP/MAS probe for 4 mm o.d. rotors

(80 μL sample volume). For the acquisition of the single-pulse spectra, a pulse width of 0.5 μs (15° flip angle for ^{27}Al, I = 5/2, in a solid) was used to ensure quantitative reliability of the intensities observed for the ^{27}Al central transition for sites experiencing different quadrupole couplings. Furthermore, rf field strengths of $\gamma B_1/2\pi \approx 60$ kHz and a relaxation delay of 2.0 s were employed, while high-power ^{1}H decoupling was applied during acquisition of the FIDs. The rotors (PSZ) were spun at ν_R = 13.0 kHz and typically 5000 – 35000 scans were recorded for each spectrum. The ^{27}Al isotropic chemical shifts are reported in ppm relative to an external sample of 1.0 M $AlCl_3 \cdot 6H_2O$.

^{29}Si{^{31}P} Cross-Polarization/MAS NMR experiments

The ^{29}Si{^{31}P} Cross-Polarization (CP) MAS NMR spectrum displayed in Fig. 7.3(b) was acquired at 9.4 T using a Varian Unity INOVA-400 spectrometer equipped with a triple-tuned MAS probe for 5 mm rotors from Doty Scientific Inc. The sample was spun in a PSZ rotor at a moderate spinning speed (ν_R = 3.0 kHz). The experiment employed a rf field strength of $\gamma_P B_{2P}/2\pi$ = 36 kHz for the initial 90° pulse and $\gamma_P B_{2P}/2\pi \approx 25$ kHz and $\gamma_{Si} B_{1Si}/2\pi \approx 20$ kHz for the Hartmann-Hahn match. A linear ramp from $\gamma_{Si} B_{1Si}/2\pi$ = 25 kHz to $\gamma_{Si} B_{1Si}/2\pi$ = 16 kHz was employed for the Si channel during the CP contact time. A relaxation delay of 30 s was inserted between each of the 1952 recorded scans and no ^{31}P decoupling was applied during the acquisition.

Appendix II

Procedures for paste mixing and hydration stop

Mixing procedure for cement pastes

A motorized stirrer (IKA RW 20 digital) equipped with a custom made paddle is used for the mixing procedure for pure cement pastes and cement – SCM pastes:

1. Water is added to the cement (±SCM) and the paste is mixed at a rotational speed of 500 rpm for 3 minutes.
2. Mixing is stopped for 2 minutes.
3. The paste is mixed at a rotational speed of 2000 rpm for 2 minutes.
4. The paste is cast in a capped cylindrical plastic container (50 mL). In order to ensure proper compaction the plastic container is tapped against a table until air bubbles no longer emerges form the surface of the paste.
5. The sample is demoulded after 24 hours and subsequently placed in a closed plastic container (500 mL) filled with tap water.

The mixing procedure employed for the pastes containing microsilica differs somewhat from the five steps outlined above, since the microsilica is added to the mix not as a powder, but in the form of a slurry. The microsilica slurry is prepared from equal amounts (by weight) of distilled water and microsilica by mixing for 3 minutes with a Phillips (HR1364, 600 W) immersion stick blender, which results in a dense fluid. The slurry is subsequently left quiet for 2 – 3 hours before the paste mixing is carried out using the motorized stirrer:

1. Water is added to the cement and the paste is mixed at a rotational speed of 500 rpm for 2 minutes.
2. The microsilica slurry is added.
3. The paste is mixed at a rotational speed of 500 rpm for 3 minutes
4. Mixing is stopped for 2 minutes
5. The paste is mixed at a rotational speed of 2000 rpm for 2 minutes.

6. Hereafter the procedure is the same as for the other types of paste.

The water to binder volume ratio is kept constant for the pastes, thus resulting in w/c ratios from 0.40 to 0.45 depending on which binder (cement ± SCM) is used in the mix. For the long-term curing the plastic container is stored in a temperature-controlled laboratory at 21 ± 2°C.

Hydration stop

The procedure outlined below is employed for stopping the hydration of cement paste and is applied both to plain and blended cement pastes. The principle of the method is that the water in the sample is exchanged with isopropyl alcohol which only to a limited degree reacts with cement [1]. The alcohol is subsequently evaporated.

1. A small piece (~5 g) is knocked off the cylinder of cement paste using the pestle of a ceramic mortar.
2. Grinding in ceramic mortar until the sample is a fine powder.
3. The powder is mixed with 50 mL of isopropyl alcohol (min. 99%) in a conical flask (250 mL) for 1 hour using a magnetic stirrer. The flask is sealed with a rubber cork during the mixing to prevent ingression of atmospheric air.
4. The sample material is separated from the isopropyl alcohol using a filter paper.
5. The powder on the filter paper is dried in a desiccator over silica gel for 24 hours and subsequently stored in a small sealed glass container.

References

[1] Zhang, Z. *Quantitative microstructural characterisation of concrete cured under realistic temperature conditions*. PhD thesis No. 3725 EPFL, Suisse (2007)

Paper I

Improved quantification of alite and belite in anhydrous Portland cements by ^{29}Si MAS NMR: Effects of paramagnetic ions

Søren L. Poulsen, Vanessa Kocaba, Gwenn Le Saout, Hans J. Jakobsen, Karen L. Scrivener, Jørgen Skibsted

Solid State Nuclear Magnetic Resonance 36 (2009) 32-44

Solid State Nuclear Magnetic Resonance 36 (2009) 32–44

Contents lists available at ScienceDirect

Solid State Nuclear Magnetic Resonance

journal homepage: www.elsevier.com/locate/ssnmr

Improved quantification of alite and belite in anhydrous Portland cements by ^{29}Si MAS NMR: Effects of paramagnetic ions

Søren L. Poulsen [a], Vanessa Kocaba [b], Gwenn Le Saoût [b], Hans J. Jakobsen [a], Karen L. Scrivener [b], Jørgen Skibsted [a,*]

[a] Instrument Centre for Solid-State NMR Spectroscopy, Department of Chemistry and Interdisciplinary Nanoscience Center (iNANO), Aarhus University, DK-8000 Aarhus C, Denmark
[b] Laboratory of Construction Materials, IMX, Ecole Polytechnique Fédérale de Lausanne, 1015 Lausanne, Switzerland

ARTICLE INFO

Article history:
Received 18 December 2008
Received in revised form
17 March 2009
Available online 12 May 2009

Keywords:
Portland cement
Alite (Ca_3SiO_5)
Belite (Ca_2SiO_4)
^{29}Si MAS NMR
High-speed spinning
Paramagnetic ions (Fe^{3+})
Spin-lattice relaxation
Guest-ion substitution
XRD-Rietveld refinement
Taylor–Bogue calculation

ABSTRACT

The applicability, reliability, and repeatability of ^{29}Si MAS NMR for determination of the quantities of alite (Ca_3SiO_5) and belite (Ca_2SiO_4) in anhydrous Portland cement was investigated in detail for 11 commercial Portland cements and the results compared with phase quantifications based on powder X-ray diffraction combined with Rietveld analysis and with Taylor–Bogue calculations. The effects from paramagnetic ions (Fe^{3+}) on the spinning sideband intensities, originating from dipolar couplings between ^{29}Si and the spins of the paramagnetic electrons, were considered and analyzed in spectra recorded at four magnetic fields (4.7–14.1 T) and this has led to an improved quantification of alite and belite from ^{29}Si MAS NMR spectra recorded at "high" spinning speeds of $\nu_R = 12.0–13.0$ kHz using 4 or 5 mm rotors. Furthermore, the impact of Fe^{3+} ions on the spin-lattice relaxation was studied by inversion-recovery experiments and it was found that the relaxation is overwhelmingly dominated by the Fe^{3+} ions incorporated as guest-ions in alite and belite rather than the Fe^{3+} sites present in the intimately mixed ferrite phase ($Ca_2Al_xFe_{2-x}O_5$).

1. Introduction

Portland cement is the principal binding component in concrete, used in a wide range of constructions. The durability and low production costs of Portland cement lead to it being the most important building material in the World. The hydraulic properties of Portland cement are mainly related to alite and belite which are impure forms of the calcium silicates Ca_3SiO_5 (C_3S) and Ca_2SiO_4 (C_2S), respectively. Portland cement contains typically 50–70 wt% alite, 5–30 wt% belite along with 5–10 wt% calcium aluminate ($Ca_3Al_2O_6$) and 5–15 wt% ferrite ($Ca_2Al_xFe_{2-x}O_5$) which are denoted the four principal clinker phases. In addition, typically 2–5 wt% gypsum is added to the clinkers during the grinding stage. The chemical and physical properties of Portland cements are determined largely by their mineral composition and thus, it is of high importance in the cement industry and academic research that the quantities of the four clinker phases can be determined with good precision.

The most commonly employed method in industry for estimating the content of the four clinker phases in Portland cements is the so-called Bogue calculation [1] which transforms the elemental oxide composition, determined from wet chemical analysis or X-ray fluorescence (XRF), into the mineral composition, assuming stoichiometric phase compositions and that thermal equilibrium is achieved in the cement kiln during manufacture. A refined version of this approach, the Taylor–Bogue calculation [2], considers the significant amounts of guest-ions incorporated in the principal phases, employing average values for the individual phases based on X-ray microprobe analysis for a range of conventional Portland cements. The standard Bogue calculation tends to overestimate the belite content and underestimate the quantity of alite [3–5] whereas an improved quantitative prediction of these phases is achieved by the Taylor–Bogue calculation [2,5,6].

The commonly applied experimental methods for quantitative phase analysis are powder X-ray diffraction (XRD) combined with Rietveld analysis [7–10] and point counting based on optical microscopy data [11,12]. A clear advantage of the XRD—Rietveld method is that it can be performed in a very short time (less than 10 min), allowing the mineralogical composition of cement clinkers to be followed on-line in cement plants [13]. However, the determination of alite and belite by this approach is complicated by the severe overlap of high intensity reflections from alite and belite and the approximated pseudo structure of

* Corresponding author. Fax: +45 8619 6199.
E-mail address: jskib@chem.au.dk (J. Skibsted).

alite used in the Rietveld refinement. Moreover, the method requires careful sample preparation and consideration of experimental factors such as particle size distribution, preferred orientation, microabsorption, and the content of amorphous phases in the specific sample as discussed in recent reviews of the Rietveld method for quantitative phase analysis of anhydrous Portland cements [14,15]. Point counting techniques are more tedious and the accuracy depends partly on the skills of the microscopist in preparing representative etched polished sections, in particular in cases of rather heterogenenous grain-size distributions, and in identifying the individual phases [16].

Considering the importance of the phase composition for the physical properties of Portland cement, it is of general interest to develop independent tools for quantitative analysis, although their applications in practise may be most relevant for academic research and materials development. In this context, ^{29}Si MAS NMR represents an alternative tool for quantitative studies of the silicate phases. As it depends on local structural order it can detect equally amorphous and crystalline phases. However, this method requires significantly longer instrument times as compared to quantitative XRD due to the low natural abundance of ^{29}Si (4.7%) and its potentially long relaxation times. Earlier, it has been shown that ^{29}Si MAS NMR spectra of anhydrous Portland cements reflect the molar ratio of alite and belite [5,17] and that this ratio, determined from deconvolution of the overlapping resonances from alite and belite, can provide a valuable estimate of the quantities of alite and belite when combined with the bulk SiO_2 content from an elemental analysis. Employing this approach, quantities of alite and belite have been determined by ^{29}Si MAS NMR for different Portland cements and compared with Bogue and Taylor–Bogue calculations [5]. It was found that an improved agreement is achieved using the Taylor–Bogue calculation and the corresponding compositions of the impure forms of alite and belite in the quantitative evaluation of the ^{29}Si NMR data.

In this work we have refined this approach with the aim of improving the quantitative reliability and reproducibility of ^{29}Si MAS NMR for determination of alite and belite in anhydrous Portland cement. The main focus is on the effects of paramagnetic ions (i.e., Fe^{3+}), which may cause severe line-broadening of the ^{29}Si NMR resonances, thereby lowering the precision in the deconvolutions of the ^{29}Si MAS NMR spectra. These studies concern mainly effects from Fe^{3+} ions, since Portland cements generally contain 0.5–5 wt% Fe_2O_3, although minor traces (in the ppm range) of paramagnetic ions such as Cr^{3+}, Mn^{3+}, and Ni^{2+} may also be present. Furthermore, the influence of the Fe^{3+} ions on the spin-lattice relaxation for the ^{29}Si spins in alite and belite is investigated, providing new information on the location of the Fe^{3+} ions dominating the relaxation. This involves experiments on a sample exposed to selective dissolution of the calcium aluminate ($Ca_3Al_2O_6$) and ferrite ($Ca_2Al_xFe_{2-x}O_5$) phases.

The present study includes 11 different Portland cements and the amounts of alite and belite from ^{29}Si MAS NMR are compared with quantitative phase analyses from XRD—Rietveld refinement and Taylor–Bogue calculations. Moreover, elemental analyses of the alite and belite grains in the different cements, obtained by scanning electron microscopy (SEM) combined with energy-dispersive X-ray spectroscopy (EDS) microanalysis, are used to shed light on discrepancies between the individual methods and to investigate guest-ion substitutions into the silicate phases in detail.

2. Experimental

2.1. Materials

Eleven different commercial Portland cements (A–I) and ground clinkers (J, K, i.e., no addition of gypsum or small amounts of other additives such as limestone filler), obtained from different cement manufacturers in Europe, were investigated as received. Samples A and J are white Portland cements/clinkers (i.e., low Fe_2O_3 content) while cement F is a sulphate-resisting Portland cement, the others are standard grey Portland cements. The metal-oxide compositions, determined by XRF analysis, are summarized in Table 1. Selective dissolution of the calcium aluminate and ferrite phases was carried out for cement B following the procedure by Gutteridge [18]. 10.0 g of cement was added to a solution of 30.0 g KOH and 30.0 g sucrose in 300 mL of water at 95 °C and stirred for about 1 min. The solution was then filtered and the residue washed with 50 ml of water, followed by 100 ml of ethanol, and dried overnight in a closed desiccator over silica gel. Fractions with different grain sizes in the range from <20 to 112–315 μm were obtained by sifting, using analytical test sieves (Retsch, Haan, Germany, DIN/ISO 3310-1) positioned on an automated shaking apparatus. These grain-size experiments were performed for clinker nodules of cement J and K which were either ground by hand in a mortar or provided as a ground powder by the manufacturer.

Table 1
Bulk metal-oxide composition (wt%) for the Portland cements (A–I) and clinkers (J, K) from XRF analysis.

Cement	CaO	SiO_2	Al_2O_3	Fe_2O_3	MgO	SO_3	K_2O	Na_2O	TiO_2	P_2O_5	LOI[a]	CO_2[b]	Free lime[c]
A	68.67	24.68	2.11	0.43	0.58	1.82	0.06	0.17	0.05	0.45	0.97	0.4	0.0
B	61.29	20.51	5.10	3.33	2.82	2.78	1.40	0.24	0.19	0.37	1.94	0.8	1.4
C	64.18	21.01	4.63	2.60	1.82	2.78	0.94	0.20	0.14	0.40	1.26	0.7	0.0
D	63.45	21.03	5.01	2.54	2.05	3.01	1.02	0.26	0.16	0.08	1.34	0.5	0.0
E	65.86	21.55	5.03	2.82	1.73	0.76	0.91	0.12	0.30	0.43	2.72	2.2	0.0
F	63.62	21.33	4.13	4.96	1.61	2.13	0.74	0.25	0.15	0.06	0.97	0.2	0.0
G	62.6	19.6[d]	5.6	2.8	2.4	2.82	1.25	0.13	–	–	2.90	1.0	0.8
H	64.1	19.4[d]	4.5	2.9	1.2	2.65	0.84	0.10	–	–	3.42	2.3	0.4
I	62.5	19.6	5.5	3.3	1.6	3.10	1.40	0.20	–	–	2.73	1.5	0.6
J	69.73	25.57	2.05	0.46	0.59	0.10	0.04	0.18	0.05	0.48	0.74	0.0	0.0
K	67.05	24.68	4.09	1.48	0.71	0.38	0.82	0.14	0.13	0.16	0.34	0.2	0.0
SD[e]	0.40	0.40	0.20	0.10	0.10	0.10	0.04	0.03	0.01	0.01	0.10	0.2	0.4

[a] Loss on ignition.
[b] CO_2 content determined from thermal gravimetric analysis or calculated from the bulk content of calcite ($CaCO_3$) provided by the XRD/Rietveld analysis.
[c] Free lime content (CaO) determined from the XRD/Rietveld analysis.
[d] Cement G and H include both an impurity of 0.5 wt% quartz (SiO_2) according to the XRD-Rietveld analysis.
[e] Standard deviations on the metal-oxide contents from XRF.

2.2. NMR measurements

Solid-state ^{29}Si MAS NMR spectra were recorded at four different magnetic field strengths (4.7, 7.1, 9.4, and 14.1 T) on Varian Unity-*plus*-200, Unity INOVA-300, -400, and -600 spectrometers, using homebuilt CP/MAS NMR probes for either 7, 5, or 4 mm o.d. rotors with sample volumes of 220, 110, and 80 μL, respectively. The samples were spun in zirconia (PSZ) rotors using spinning speeds of $\nu_R = 6.0$, 12.0, and 13.0 kHz which are considered safe for this rotor material for the 7, 5, and 4 mm probes, respectively. The actual sample temperatures at these spinning speeds are approx. 37 °C (7 mm), 40 °C (5 mm) and 38 °C (4 mm) with an inlet temperature of 21 °C for the drive and bearing gas. The individual probes for the four spectrometers employed rf field strengths in the range $\gamma B_1/2\pi = 40$–65 kHz, which were calibrated in each case using ^{29}Si MAS NMR of Na_2SiF_6 ($\delta_{iso} = -188.9$ ppm) since this compound exhibits a short spin-lattice relaxation time ($T_1 = 0.5$ s at 7.1 T). The single-pulse experiments employed a 45° excitation pulse and a relaxation delay corresponding to full spin-lattice relaxation for ^{29}Si in the alite and belite phases (e.g., 10–30 s). The spectra shown in the figures and isotropic ^{29}Si chemical shifts are reported in ppm relative to an external sample of neat tetramethylsilane (TMS), using a sample of β-Ca_2SiO_4 ($\delta_{iso} = -71.33$ ppm) as a secondary reference material. The linewidths of the resonances in the ^{29}Si MAS NMR spectra of the cement samples were found to be sensitive to exact magic-angle setting and thus, the magic-angle was regularly adjusted by minimization of the linewidths observed for the satellite transitions in ^{23}Na MAS NMR spectra of $NaNO_3$. The deconvolutions of the ^{29}Si MAS NMR spectra were performed using the Varian Vnmr software which allows least-squares fitting of the experimental spectra for a series of peaks each composed of a linear combination of Gaussian and Lorentzian functions.

2.3. XRD-Rietveld analysis and Taylor–Bogue calculations

The powder X-ray diffraction (XRD) data were collected using a PANalytical X'Pert Pro MPD diffractometer in a θ–θ configuration, employing CuK_α radiation ($\lambda = 1.54$ Å) with a fixed divergence slit size of 0.5° and a rotating sample stage. The samples were scanned between 7 and 75° with the X'Celerator detector. The sample preparation (e.g., particle-size reduction to ~1 μm grains) and the procedure for the Rietveld refinement have been described in detail elsewhere in a study of the XRD-Rietveld methodology for quantitative phase analysis of anhydrous Portland cements [15]. The Taylor–Bogue calculations employed a homemade Java programme based on the approach by Taylor [2] and using the average compositions for alite, belite, calcium aluminate, and ferrite proposed in that work. The bulk metal-oxide composition, the loss on ignition, and the contents of CO_2 and free lime (CaO) are used as input (Table 1) and quantitative estimates of the four main clinker phases [2] as well as the quantities of sulphates (Na_2SO_4, K_2SO_4, and $CaSO_4$) [19], gypsum ($CaSO_4 \cdot 2H_2O$), free lime (CaO), and periclase (MgO) are provided by the calculations. The amount of Mg^{2+} and Fe^{3+} in alite is modified according to the bulk contents of MgO and Fe_2O_3, following the considerations by Taylor, and the Fe-rich composition for ferrite [2] is used for sulphate-resisting cements and the Al-rich composition of calcium aluminate [2] for white Portland cements.

3. Results and discussion

From preliminary studies of 16 different Portland cements/clinkers, nine cements and two clinkers were selected for the present detailed analysis, disregarding cements subjected to a minor degree of prehydration and cements including quartz or clay impurities as revealed by ^{29}Si MAS NMR and XRD measurements. The bulk metal-oxide compositions from XRF analysis are listed in Table 1 for the 11 cements whereas representative ^{29}Si MAS NMR spectra are shown in Fig. 1. These spectra include a rather narrow resonance at −71.3 ppm from the unique Si site of β-Ca_2SiO_4 (belite) [20] superimposed on a sum of overlapping resonances from alite. Following an earlier ^{29}Si MAS NMR study of synthetic samples of the M_I and M_{III} forms of alite [5], it is apparent from the overall lineshape of the overlapping resonances from alite that the studied Portland cements are dominated by alite in its monoclinic M_{III} form, which includes 18 different Si sites in the asymmetric unit [21]. This observation is in full agreement with the corresponding XRD patterns which are all refined using alite in its M_{III} form only.

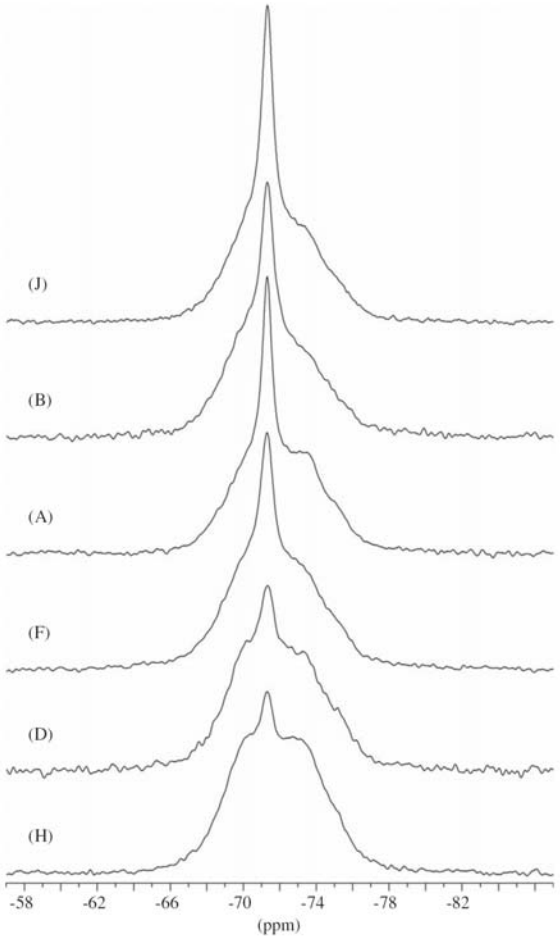

Fig. 1. ^{29}Si MAS NMR spectra for six of the studied Portland cements, reflecting their variation in alite and belite and shown in the order of decreasing belite/alite ratio, i.e., cement samples J, B, A, F, D, and H. The spectra have been recorded at 9.4 T with a spinning speed of $\nu_R = 13.0$ kHz, a 30 s relaxation delay, and 1000–2500 scans.

3.1. Deconvolution of ^{29}Si MAS NMR spectra

The quantification of alite and belite was obtained from their relative ^{29}Si intensities, determined from a deconvolution of the ^{29}Si MAS NMR spectrum, combined with the bulk SiO_2 content from an elemental (XRF) analysis. This approach assumes that the compositions for alite and belite are known and that the total amount of Si is present in alite and belite, although small quantities of Si may be incorporated as guest-ions in the calcium aluminate and ferrite phases. However, the inaccuracy caused by these assumptions is below the errors resulting from the repeatability tests as discussed in the final section. The ^{29}Si NMR intensity on an absolute scale could in principle be obtained from the total intensity of the spectrum employing an external intensity reference. However, this procedure would give a less precise quantification of the total SiO_2 content as compared to XRF analysis that can provide the SiO_2 content with a precision of typically $\pm$0.4wt% [15]. The deconvolution procedure for the ^{29}Si MAS NMR spectra largely follows the approach reported earlier [5] but includes a few improvements. A simulated sub-spectrum for alite is generated by deconvolution of the ^{29}Si MAS NMR spectrum for a synthetic sample of monoclinic M_{III} alite using nine peaks, with each being composed of a linear combination of Gaussian and Lorentzian lineshapes. The use of nine peaks was found to be sufficient to reproduce all spectral details of the ^{29}Si MAS NMR spectrum for synthetic M_{III} alite, although this polymorph includes 18 Si atoms in the asymmetric unit according to X-ray diffraction [21]. The individual peak intensities and fractions of Gaussian/Lorentzian lineshapes constituting the alite sub-spectrum are initially used as fixed parameters in least-squares optimizations to the ^{29}Si MAS NMR spectrum, where the relative alite–belite intensities and overall linewidths are optimized for the alite and belite peaks. In the final step, minor adjustments (approx. $\pm$10%) of the individual peak intensities and fractions of Gaussian/Lorentzian lineshapes for the alite sub-spectrum are allowed to account for minor intensity distortions on the low- or high-frequency side of the belite resonance when compared to the ideal alite sub-spectrum. These intensity variations in the sub-spectrum for alite may originate from minor distortions of the alite structure, for example as a result of different degrees of guest-ion incorporation (i.e., Mg^{2+}, Al^{3+}, Fe^{3+}, P^{5+}, S^{6+}, F^{-}). The result of the deconvolution procedure is illustrated in Fig. 2 for cement H where the deconvolution gives the intensity ratio $C_2S/C_3S = 0.0885$. Combining this ratio with the bulk SiO_2 content (18.9 wt%, Table 1) gives the formal quantities of the stoichiometric phases, i.e., 4.4 wt% C_2S and 66.1 wt% C_3S. However, more realistic phase compositions for alite and belite in conventional production Portland cements have been proposed by Taylor, $Ca_{2.9}Si_{0.95}Mg_{0.06}Al_{0.04}Fe_{0.03}P_{0.01}Na_{0.01}O_5$ and $Ca_{1.94}Si_{0.9}Al_{0.07}K_{0.03}Fe_{0.02}Mg_{0.02}P_{0.01}Na_{0.01}O_{3.93}$ [2], respectively, resulting in the quantities of 4.9 wt% belite and 68.6 wt% alite when combined with the belite/alite intensity ratio for cement H.

The individual cements were initially studied at 9.4 T using a spinning speed of $\nu_R = 6.0$ kHz and a 7 mm CP/MAS probe to attain the largest sample volume. However, at this spinning speed the $\pm$1 and $\pm$2 spinning sidebands (ssbs) are observed with a significant fraction of the overall intensity as illustrated in Fig. 3c for cement F. Although, the belite/alite intensity distribution of the ssbs may resemble that for the centerband, we find that a more reliable determination of the belite/alite ratio is achieved from deconvolution of ^{29}Si MAS NMR spectra recorded at relatively high spinning speeds where nearly all intensity is present in the centerband. This is illustrated by the results from deconvolution of ^{29}Si MAS NMR spectra recorded at $\nu_R = 6.0$ and 13.0 kHz for the 11 Portland cements (Fig. 4) which show slightly lower quantities of alite and correspondingly higher values for belite from the analysis of the high-speed spinning spectra. This change in quantities of alite and belite points towards a better agreement with the XRD-Rietveld phase analysis (*vide infra*) and indicates that the ssbs at $\nu_R = 6.0$ kHz contain a relatively larger fraction of intensity from belite compared to alite. Alternatively, the intensity contribution from alite and belite to the $\pm$1 and $\pm$2 ssbs in the spectra recorded at $\nu_R = 6.0$ kHz may be included in the deconvolution procedure. However, the spectral features from these phases are somewhat blurred in the ssbs due to their lower *S/N* ratios, as compared to the centerband. Thus, consideration of additionally variable alite/belite intensities in these peaks will hardly improve the precision of the overall deconvolution. Thereby we find that the optimum belite/alite ratios, and the corresponding quantities of alite and belite summarized in Table 2 for the 11 Portland cements, are all obtained from deconvolutions of the centerbands observed in ^{29}Si MAS NMR spectra using the high-speed spinning ($\nu_R = 13.0$ kHz).

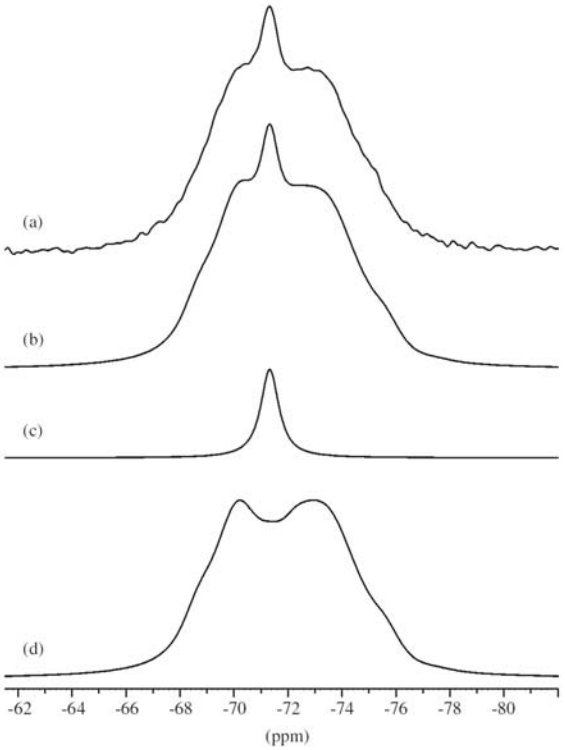

Fig. 2. ^{29}Si MAS NMR spectrum (9.4 T, $\nu_R = 13.0$ kHz) of (a) cement H and (b) its optimized deconvolution, which is composed of the sub-spectra for belite and alite shown in (c) and (d), respectively.

3.2. Effects from paramagnetic ions on the ssb intensities

Earlier ^{29}Si MAS NMR studies of synthetic samples of alite (Ca_3SiO_5–T1) [22] and belite (β-Ca_2SiO_4) [23], employing slow-speed spinning ($\nu_R = 270$ and 700 Hz) at 9.4 and 14.1 T magnetic fields, respectively, showed that the isolated SiO_4 tetrahedra in these silicates exhibit rather small chemical shift anisotropies (CSAs), $|\delta_\sigma| < 30$ ppm ($\delta_\sigma = \delta_{iso} - \delta_{zz}$, where δ_{zz} is the principal element of the CSA tensor). This implies that the CSA interaction is almost completely removed in ^{29}Si MAS NMR spectra recorded with spinning speeds above 6.0 kHz, even at relatively high

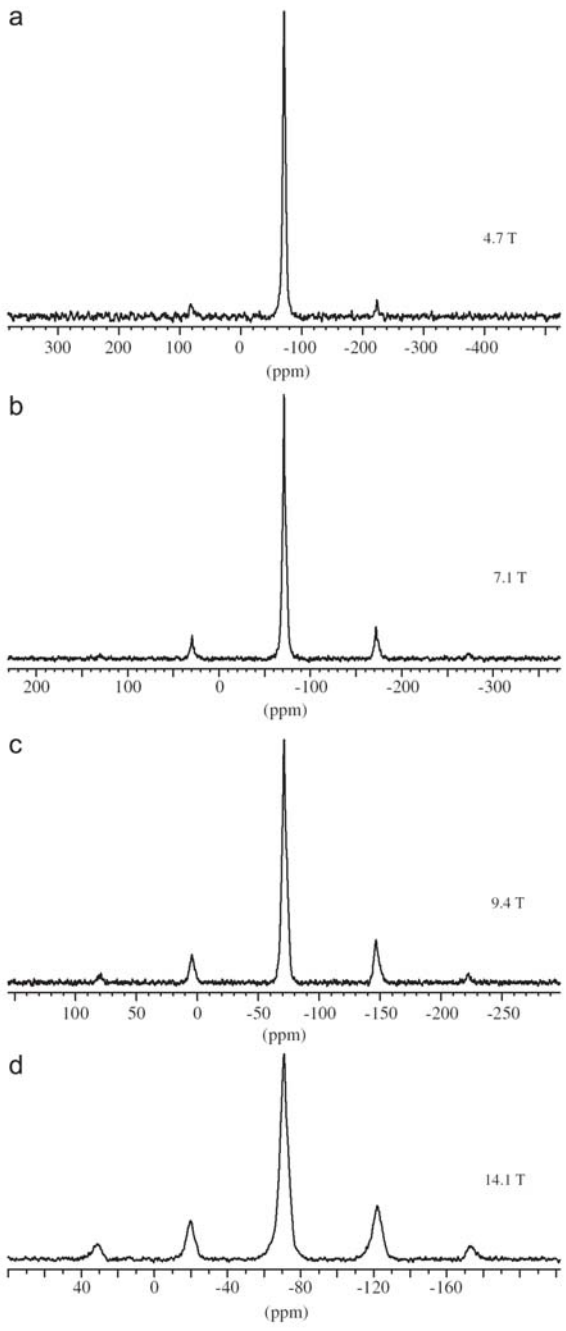

Fig. 3. ^{29}Si MAS NMR spectra of cement F recorded at four different magnetic fields, employing a spinning speed of $\nu_R = 6.0$ kHz, and illustrating the increase in ssb intensity with increasing magnetic field. The spectra are shown on the same scale in Hz for the four different magnetic fields.

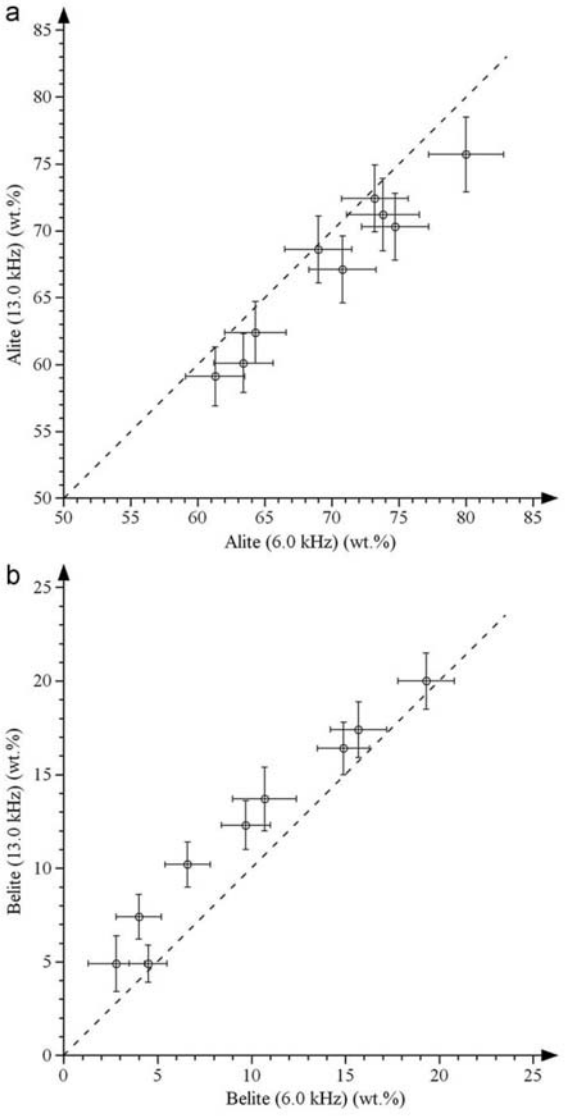

Fig. 4. Comparison of the quantities of (a) alite and (b) belite for the Portland cements (A–I) determined from deconvolutions of ^{29}Si MAS NMR spectra (9.4 T) recorded at spinning speeds of $\nu_R = 6.0$ kHz and $\nu_R = 13.0$ kHz. The dashed lines illustrate the 1:1 correlations.

magnetic fields (e.g., 14.1 T). Thus, the significant increase of the intensities for the ssbs in Fig. 3 originates from another type of line-broadening mechanism. To investigate this effect in more detail, Fig. 5a illustrates the fraction of ssb intensity as a function of the bulk Fe_2O_3 content observed in ^{29}Si MAS NMR spectra recorded with spinning speeds of $\nu_R = 6.0$ and 13.0 kHz for the 11 cements. This plot reveals a roughly linear increase in ssb intensity with increasing Fe_2O_3 content, indicating a significant interaction between the ^{29}Si spins and the unpaired electron spins of the Fe^{3+} ions. However, the application of the spinning speed of $\nu_R = 13.0$ kHz gives a substantial reduction in the fraction of ssb intensity where a level below 8% of the total intensity is generally achieved for $\nu_R = 13.0$ kHz at 9.4 T. A comparison of the ssb intensity fractions at $\nu_R = 6.0$ and 13.0 kHz clearly shows that an improved quantitative reliability of spectra for centerband analysis is achieved using relatively high spinning speeds, which

Table 2
Calcium silicate compositions for the Portland cements from ^{29}Si MAS NMR, XRD-Rietveld analysis, and Taylor–Bogue calculations.

Cement	^{29}Si MAS NMR[a]			XRD-Rietveld[b]		Taylor–Bogue[c]	
	I(belite)/*I*(alite)	alite	belite	alite	belite	alite	belite
A	0.3449	72.4±2.5	20.0±1.5	68.9	23.4	73.3	18.6
B	0.3676	59.1±2.2	17.4±1.5	49.0	23.7	49.1	23.1
C	0.3286	62.4±2.3	16.4±1.4	61.8	16.9	64.1	13.0
D	0.1805	70.3±2.5	10.2±1.2	66.2	14.1	58.5	17.4
E	0.1226	75.7±2.8	7.4±1.2	66.8	10.6	63.5	15.0
F	0.2540	67.1±2.5	13.7±1.7	58.7	17.9	61.5	16.0
G	0.2560	60.1±2.2	12.3±1.3	57.3	14.8	60.4	11.0
H	0.0885	68.6±2.5	4.9±1.0	63.1	8.9	67.3	5.3
I	0.0857	71.2±2.7	4.9±1.5	64.7	7.7	54.4	15.8
J	0.4749	68.4±2.5	26.1±1.7	65.2	29.6	79.5	16.6
K	0.3141	74.1±2.8	18.7±1.7	65.7	21.1	59.7	28.6

[a] Determined from ^{29}Si MAS NMR spectra recorded at 9.4 T using a spinning speed of $\nu_R = 13.0$ kHz. The quantities of alite and belite correspond to the compositions proposed by Taylor [2] and the error limits are calculated from the uncertainties on the *I*(belite)/*I*(alite) intensity ratio and the bulk SiO_2 content from XRF analysis. The uncertainties for the *I*(belite)/*I*(alite) intensity ratios are estimated from comparisons of the experimental spectra with simulated lineshapes corresponding to the alite in belite intensities used mainly in the final steps of the optimization procedure (i.e., the optimizations where minor adjustments of the alite lineshape are performed, see text).
[b] The standard deviations are ±2.2 and ±1.4 wt% for alite and belite, respectively, from the XRD-Rietveld analyses [15].
[c] The Taylor–Bogue calculations employ the data from bulk chemical analysis in Table 1 and assume the Taylor compositions for alite and belite [2].

is in contrast to the traditional practise over the past two decades to use low spinning speeds (e.g., $\nu_R = 3$–6 kHz) and large rotors in ^{29}Si MAS NMR studies of Portland cement-based materials.

The effect of the Fe_2O_3 content on the ssb intensities was also investigated for a fixed spinning speed ($\nu_R = 6.0$ kHz) at different magnetic fields for five of the cements studied (Fig. 5b), including cement F (Fig. 3) with the highest Fe_2O_3 content. Nearly linear relationships between ssb intensity and magnetic field strength are observed for all cements, which indicate that the line-broadening mechanism is proportional to the magnetic field strength. Moreover, it is observed that the linebroadening effect is much less pronounced for the white Portland cement (A), reflecting its low Fe_2O_3 content.

The interaction between an electron spin (S) of the paramagnetic ion and the spin (I) of the ^{29}Si nucleus in an external magnetic field includes contributions from the hyperfine (Fermi-contact) interaction ($\mathscr{H}_{hf}$) and the dipolar interaction between the magnetic moments of the electron and the nuclear spin ($\mathscr{H}_{D,e}$). The hyperfine interaction includes an isotropic contribution, which results in characteristic paramagnetic shifts of the spin–I resonances, whereas the dipolar term is anisotropic and can be expressed as [24]:

$$\mathscr{H}_{D,e} = -\gamma_I \langle \mu_e \rangle \hat{D}\vec{I}\frac{1}{r^3} \quad (1)$$

where γ_I is the gyromagnetic ratio of the nucleus, $\langle \mu_e \rangle$ the time averaged magnetic moment of the electron spin, $\hat{D}$ the axially symmetric dipolar coupling tensor, and r the distance between the nuclear spin and the electron of the paramagnetic centre. The time averaged magnetic moment of the electron spin is given by

$$\langle \mu_e \rangle = \frac{\beta_e^2 S(S+1)}{3kT}\hat{g}\hat{g}\vec{B}_0 \quad (2)$$

where β_e is the Bohr magneton and $\hat{g}$ is the electron g tensor. From these two equations, it is apparent that the dipolar coupling between the nuclear spin and the electron of the paramagnetic ion takes the same form as an axially symmetric chemical shift tensor (i.e., $\mathscr{H}_\sigma = -\gamma_I \vec{I}\cdot\hat{\sigma}\cdot\vec{B}_0$) with a linear magnetic field dependence. Qualitatively, this may explain the variation in ssb intensities with increasing magnetic field observed in Fig. 3 for cement F and in Fig. 5b for six cements. However, the spectra in Fig. 3 do not allow a straightforward estimation of the dipolar coupling tensor, since the paramagnetic centres are most likely distributed randomly in the calcium silicate phases, resulting in a number of different I–S interactions for the individual ^{29}Si spins. Furthermore, the ^{29}Si–e dipolar interactions are additive and thus, determination of the total dipolar coupling tensor requires summation over the dipolar coupling tensors for the individual Si–e couplings within a sphere of ~10 nm for a particular nuclear site [25], i.e., considering the $1/r^3$ dependency for $\mathscr{H}_{D,e}$.

3.3. Spin-lattice relaxation for ^{29}Si in alite and belite

The effects from paramagnetic ions (Fe^{3+}) was further investigated by ^{29}Si inversion-recovery (IR) MAS NMR experiments for alite and belite in cements A–H as illustrated in Figs. 6 and 7a for cement A and B. From these spectra it is apparent that the different ^{29}Si sites in alite exhibit nearly identical spin-lattice relaxation times (c.f., the spectra corresponding to the zero-crossings for alite and belite, Fig. 6), reflecting that these sites are influenced by the same source of relaxation. Thus, the relative alite and belite intensities in the individual ^{29}Si IR NMR spectra may be determined from the same kind of spectral deconvolutions as used for the single-pulse spectra, i.e., belite is simulated by a single peak at −71.3 ppm whereas 9 overlapping resonances (with the same relaxation time) constitute the alite sub-spectrum that covers a spectral range from −66 to −77 ppm. The resulting intensities are analyzed using the well-known relationship between observed intensity ($M_z(t)$) and recovery time (t) for a single-exponential relaxation process as well as the expression for a "stretched exponential"

$$M_z(t) = M_0[1 - (1+\alpha)\exp(-(t/T_1')^{1/2})] \quad (3)$$

where M_0 is the equilibrium longitudinal magnetization, α a constant related to pulse imperfections (i.e., $\alpha = 1$ for ideal pulses), and T_1' the time constant for the spin-lattice relaxation. The stretched exponential relationship has been derived for spin relaxation caused by paramagnetic impurities in the absence of spin diffusion [26] and successfully employed in ^{29}Si MAS NMR studies of silicates containing small amounts of iron (e.g., 0.1–5 wt% Fe_2O_3) [27–30]. For all cements the best fits to the experimental intensities for alite and belite are obtained by a

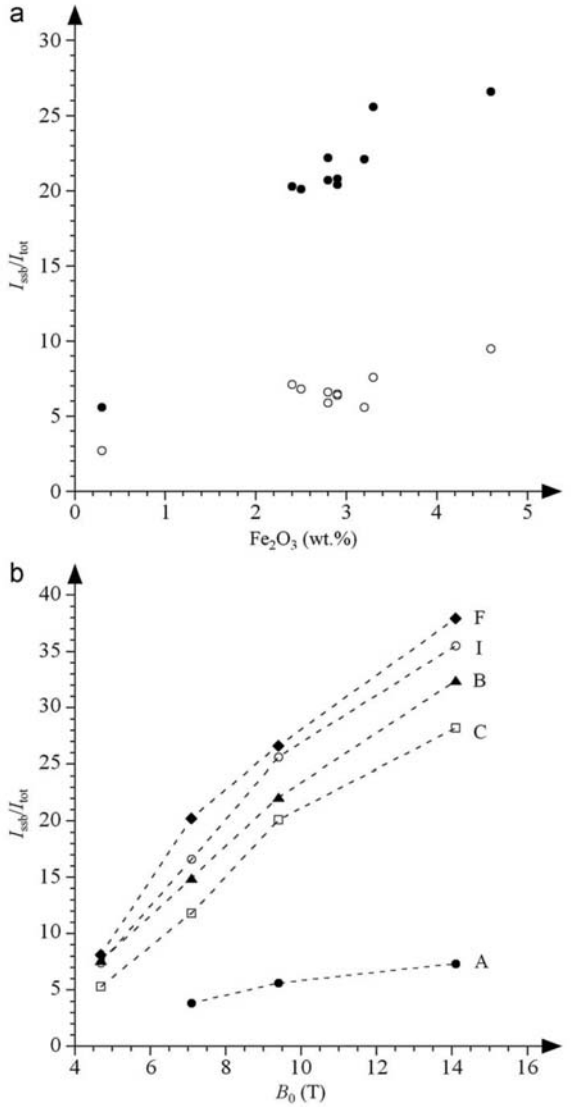

Fig. 5. (a) Fraction of intensity in the ssbs for the 10 cements as a function of their bulk Fe_2O_3 contents (Table 1) obtained from ^{29}Si MAS NMR spectra recorded at 9.4 T using spinning speeds of $\nu_R = 6.0$ kHz (filled circles) and $\nu_R = 13.0$ kHz (open circles). (b) Fraction of intensity in the ssbs for cements A, B, C, F, and I as a function of the magnetic field from ^{29}Si MAS NMR spectra recorded at 4.7, 7.1, 9.4, and 14.1 T using $\nu_R = 6.0$ kHz.

stretched exponential rather than a single-exponential decay of magnetization. This is illustrated by the plots of $[1-M_z(t)/M_0]$ versus t and $\sqrt{t}$ in Fig. 8 where the straight lines observed in the latter case correspond to the stretched exponential relationship (Eq. (3)). For relatively low concentrations of paramagnetic ions (N_p) and a direct relaxation of the I spins caused by the dipolar interaction with the electron spin (S) of the paramagnetic ions, the relaxation rate ($1/T_1'$) may be expressed as [30,31]:

$$1/T_1' = \frac{16}{9}\pi^3 N_p^2 C_I, \quad C_I = \frac{2}{5}\gamma_I^2\gamma_S^2\hbar^2 S(S+1)\frac{\tau_e}{1+\omega_I^2\tau_e^2} \qquad (4)$$

where τ_e is the relaxation time of the electron spin, ω_I the I-spin Larmor frequency, and γ_I, γ_S the gyromagnetic ratios for the I spin and the electron S spin. In agreement with this expression, the T_1' time constants for alite and belite in cements A–H (Table 3) tend to decrease with the bulk Fe_2O_3 content of the cements (Table 1) and thereby the amount of Fe^{3+} ions in alite and belite. Furthermore, it is observed that T_1' for alite is about an order of magnitude smaller than T_1' for belite for the individual cements (Table 3). This observation reflects the generally lower concentration of Fe^{3+} ions in belite as compared to the amount of Fe^{3+} guest-ions in alite, in accordance with the phase compositions derived from SEM combined with EDS analysis for six of the studied cements (Table 4) and the Fe^{3+} contents in Taylors average alite and belite compositions [2]. Finally, the T_1' values determined for alite and belite in cement A at four different magnetic fields (Table 3) show that the relaxation rate ($1/T_1'$) decreases with increasing magnetic field for ^{29}Si in both phases. This dependency is in accord with Eq. [4], if τ_e is assumed to be independent of B_0, and implies that longer repetition times are required at higher magnetic fields to obtain quantitative reliable ^{29}Si MAS NMR spectra.

3.4. Selective dissolution of the ferrite phase

The effect of paramagnetic species on the ^{29}Si spin-lattice relaxation for alite and belite in Portland cement has recently been investigated by Edwards et al. using inversion-recovery, variable-delay Bloch decay, and saturation-recovery experiments [32]. Of these techniques, they claimed that the saturation-recovery experiment offers the best combination of accuracy, speed, and ease of processing and proposed a method for determination of the belite/alite intensity ratio based on deconvolutions of saturation-recovery NMR spectra. Furthermore, in their investigation on the effect of paramagnetic species they concluded that the ^{29}Si spin-lattice relaxation for alite and belite is overwhelmed by the presence of Fe^{3+} ions in the ferrite ($Ca_2Al_xFe_{2-x}O_5$) phase which makes intimate contact with both the alite and belite phases [32]. This statement is examined in more detail in Fig. 7 by ^{29}Si IR NMR experiments on cement B (as received) and after selective dissolution of the aluminate and ferrite phases. The recipe for removing these phases from a cement powder [18] is generally accepted in cement chemistry and its validity for the specific sample of cement B is confirmed by an XRF analysis, which reveals that the bulk Fe_2O_3 content is reduced from 3.33 to 1.37 wt% and the quantity of Al_2O_3 from 5.10 to 2.15 wt% after the selective dissolution experiment. Moreover, it is not possible to detect the ferrite and aluminate phases by XRD-Rietveld analysis after selective dissolution whereas the quantities of these phases for the as-received cement B are 12.6 wt% ferrite and 5.6 wt% aluminate. These observations suggest that iron and aluminium are mainly present as guest-ions in the alite and belite phases of cement B after selective dissolution. The alite and belite intensities in the ^{29}Si IR NMR spectra recorded for cement B before and after selective dissolution (Figs. 7a and b, respectively) are nearly identical, demonstrating only rather small differences in ^{29}Si spin-lattice relaxation for these phases. Deconvolution of the individual spectra combined with least-squares fitting to Eq. (3) results in the T_1' values listed in Table 3 for the two samples of cement B, again demonstrating only a slight increase in T_1' for alite and belite in the sample exposed to selective dissolution. Thus, the ferrite phase has only a minor impact on the ^{29}Si spin-lattice relaxation for alite and belite and the present analysis, including the results from the preceding section, show that the relaxation process is overwhelmingly dominated by the Fe^{3+} ions

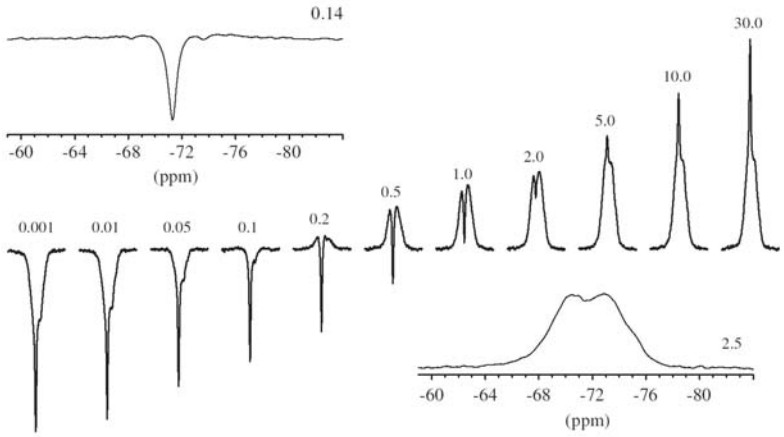

Fig. 6. Inversion-recovery ^{29}Si MAS NMR spectra (9.4 T, $\nu_R = 12.0$ kHz) of cement A, illustrating the differences in spin-lattice relaxation for alite and belite. The left- and right-hand expansions show sub-spectra of belite and alite obtained at the zero-crossings for ^{29}Si in alite and belite, respectively. The recovery times in seconds are indicated for the individual spectra.

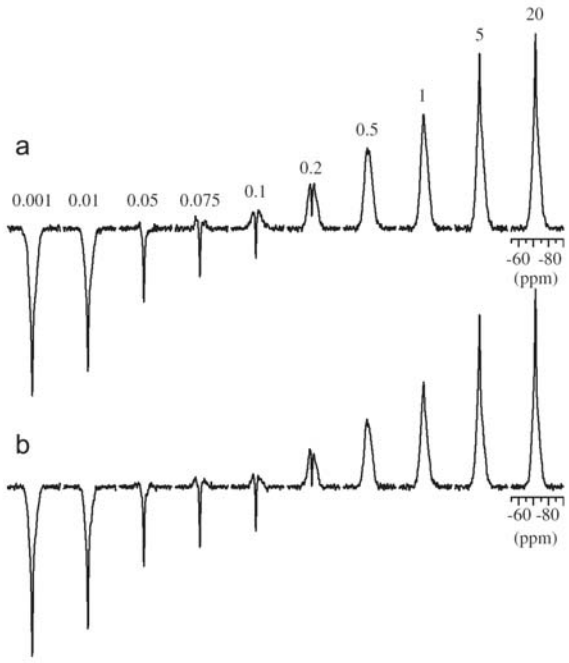

Fig. 7. Inversion-recovery ^{29}Si MAS NMR spectra (9.4 T, $\nu_R = 12.0$ kHz) of cement B (a) as-received and (b) after selective dissolution of the aluminate and ferrite phases. Each series of experiments employ the same recovery times which are indicated in seconds above the spectra in part (a).

incorporated as guest-ions in alite and belite. This conclusion contrasts the study by Edwards et al. [32] who proposed the relaxation to be governed by the Fe^{3+} ions in the separate ferrite phase. However, for special cements such as oil-well cements with high bulk iron contents (e.g., above 5 wt% Fe_2O_3), we cannot exclude that the Fe^{3+} species in ferrite may have a larger effect on the ^{29}Si relaxation.

3.5. Variation in alite and belite content with the grain-size fraction

In compositional studies of Portland cements, attention should obviously be paid to the selection procedure for the amount of sample used in the particular analysis. Generally, the fineness of Portland cement allows direct packing of the powder into the NMR rotors which in the present NMR experiments correspond to a sample volume of 110 μL (approx. 0.20 g cement) for the 5 mm o.d. PSZ rotors. For this amount of sample the ^{29}Si MAS spectrum reflects the average molar quantities of ^{29}Si in alite and belite with no preferential detection of small or large particles in the NMR rotor. However, such effects may influence the result of other experimental tools that primarily detect the "surface composition" for a stamped powder in the sample holder or require extensive sample preparation (e.g., polishing) in the setup for the specific experiment. To investigate the significance of such effects, we have separated powder fractions with different particle sizes by sifting powders of cements J and K made by grinding randomly picked clinker nodules for these two cements. Fig. 9 compares the ^{29}Si MAS NMR spectra for cement J before sifting with those of the fractions corresponding to grain sizes in the ranges 45–63 μm, 20–45 μm, and below 20 μm. Clearly, these spectra show that the molar belite/alite ratio decreases significantly when the grain size is reduced to these ranges. A similar effect is observed for cement K where deconvolution of the ^{29}Si MAS NMR spectra (not shown) shows a decrease in belite/alite ratio from 0.294 to 0.188 on going from grains in the range 63–112 μm to grains below 20 μm. The same grain-size fractions of cement J, as investigated by ^{29}Si MAS NMR (Fig. 9), have also been studied by XRF and XRD-Rietveld analysis and comparison of the quantities of alite and belite from these measurements (Fig. 10, Table 5) results in the same conclusion that the fraction of belite strongly depends on the particular grain size in the cement powder. It is noted that the NMR analysis generally gives a slightly higher quantity of alite and a lower quantity of belite as compared to the XRD-Rietveld analysis (*vide infra*). A lower belite and higher alite content in grains below 45 μm as compared to those in the range 106–150 μm has earlier been reported in a quantitative X-ray diffraction study of a Portland cement [33]. The variation in quantities of alite and belite shown in Fig. 10 is associated with the grinding process of the cement clinkers since the finer fractions are rich in the softest components while

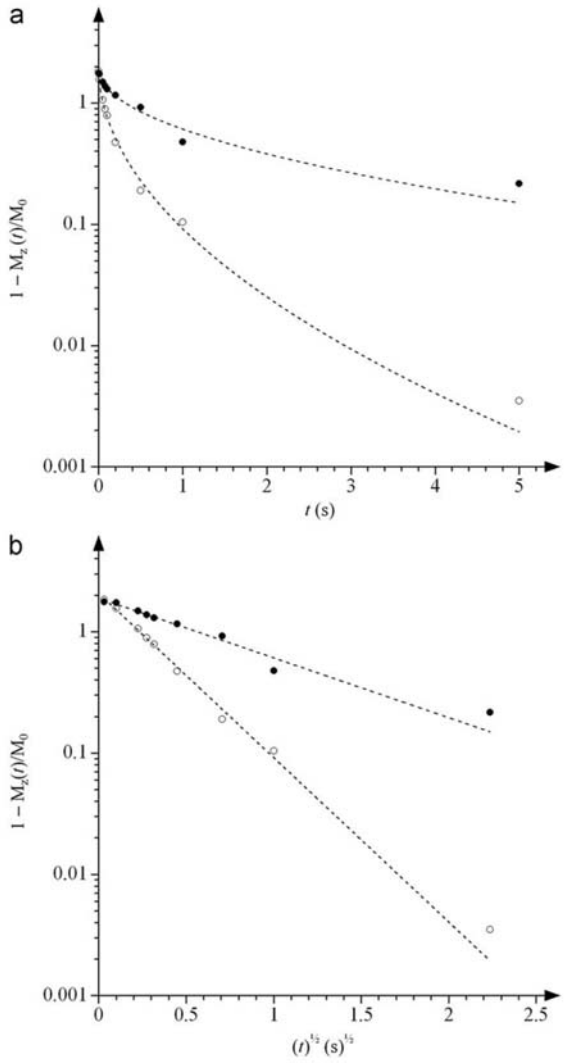

Fig. 8. Semilog plots of $(1-M_z(t)/M_0)$ as a function of the recovery time, t (a) and $\sqrt{t}$ (b), which should result in linear relationships for single-exponential and a stretched exponential spin-lattice relaxation processes, respectively. The graphs include data for alite (open circles) and belite (filled circles) from inversion-recovery ^{29}Si MAS NMR spectra of cement B recorded at 9.4 T (c.f., Fig. 7a).

coarse fractions are dominated by the harder phases. This observation is in disagreement with hardness of alite and belite according to Moh's scale, which indicate that alite (5.5) is slightly harder than belite (5.0) [34]. However, in industrial Portland cement clinkers a part of the belite grains aggregate, forming larger clusters in the inner part of the clinkers, which considerably reduce the grindability of the clinkers [35]. Moreover, microcracks (which increase the grindability) may be preferentially found in the alite crystals as a result of the volume shrinkage during crystallization with a frequency that depends on the cooling procedure and rate [36].

Table 3
Time constants for the ^{29}Si spin-lattice relaxation (T_1') for alite and belite in selected Portland cements from ^{29}Siinversion-recovery MAS NMR spectra.

Cement	B_0 (Tesla)	T_1' (alite)[a] (s)	T_1' (belite)[a] (s)
A	4.7	0.13	4.4
A	7.1	0.19	6.5
A	9.4	0.24	8.2
A	14.1	0.48	15.3
B	9.4	0.11	0.80
B, sel. diss.[b]	–	0.12	1.22
C	–	0.086	1.89
D	–	0.19	0.78
E	–	0.11	0.62
F	–	0.067	1.21
G	–	0.11	1.77
H	–	0.091	0.56

[a] Spin-lattice relaxation time corresponding to a stretched exponential relationship (c.f. Eq. (3)).
[b] Data obtained for cement B after selective dissolution of the calcium aluminate and ferrite phases (see text and Fig. 7b).

Table 4
Phase composition for alite and belite in selected Portland cements from SEM combined with EDS analyses.[a]

Cement	Alite	Belite
A	$Ca_{2.92}Mg_{0.04}Al_{0.07}Fe_{0.02}Si_{0.95}O_5$	$Ca_{1.99}Al_{0.08}Si_{0.92}O_4$
B	$Ca_{2.84}Mg_{0.08}Al_{0.09}Fe_{0.04}Si_{0.93}O_5$	$Ca_{1.98}Mg_{0.02}Al_{0.07}Fe_{0.03}Si_{0.92}O_4$
C	$Ca_{2.93}Mg_{0.05}Al_{0.06}Fe_{0.04}Si_{0.93}O_5$	$Ca_{2.00}Al_{0.05}Fe_{0.03}Si_{0.91}O_4$
D	$Ca_{2.89}Mg_{0.08}Al_{0.09}Fe_{0.03}Si_{0.93}O_5$	$Ca_{1.98}Mg_{0.02}Al_{0.07}Fe_{0.02}Si_{0.91}O_4$
F	$Ca_{2.88}Mg_{0.06}Al_{0.06}Fe_{0.03}Si_{0.96}O_5$	$Ca_{1.97}Mg_{0.01}Al_{0.06}Fe_{0.03}Si_{0.93}O_4$
E	$Ca_{2.92}Mg_{0.05}Al_{0.05}Fe_{0.03}Si_{0.95}O_5$	$Ca_{2.00}Mg_{0.01}Al_{0.06}Fe_{0.02}Si_{0.93}O_4$
H	$Ca_{2.90}Mg_{0.04}Al_{0.06}Fe_{0.03}Si_{0.97}O_5$-	$Ca_{1.97}Mg_{0.01}Al_{0.05}Fe_{0.02}Si_{0.95}O_4$-
Taylor[b]	$Ca_{2.90}Mg_{0.06}Al_{0.04}Fe_{0.03}Si_{0.95}$- $P_{0.01}Na_{0.01}O_5$	$Ca_{1.94}Mg_{0.02}Al_{0.07}Fe_{0.02}Si_{0.9}$- $P_{0.01}Na_{0.01}K_{0.03}O_{3.93}$

[a] Metal ions corresponding to a molar content below 0.01 are not included in the formulas.
[b] Compositions of alite and belite proposed by Taylor [2]. Note that oxygen vacancies are included in belite.

3.6. *Repeatability in the quantification of alite and belite from ^{29}Si MAS NMR*

The precision and repeatability of the ^{29}Si MAS NMR method for determination of the belite/alite ratio are examined by several experiments for selected cements. The effect of chemical shift dispersion on the reflection of the alite and belite resonances was investigated for cements A, C, and H by ^{29}Si MAS NMR spectra recorded at four magnetic field strengths (4.7–14.1 T) under identical conditions. Thus, each cement was packed once in a 5 mm PSZ rotor which was used for the four experiments at the different magnetic fields, all employing home-built CP/MAS probes for 5 mm o.d. rotors, a spinning speed of $\nu_R = 12.0$ kHz, and relaxation delays corresponding to full spin-lattice relaxation. ^{29}Si MAS NMR spectra at the four magnetic fields are illustrated for cement A in Fig. 11, which also includes similar spectra recorded for a synthetic sample of belite (β-Ca_2SiO_4). The observed linewidths (FWHM) for the resonance from synthetic belite are 0.51 ppm (4.7 T), 0.39 ppm (7.1 T), 0.33 ppm (9.4 T), and 0.28 ppm (14.1 T) and this decrease with increasing magnetic field serves to demonstrate that the theoretically expected increase in chemical shift dispersion is not blurred by a similar increase in magnetic field inhomogeneity. This is also apparent from the spectra of cement A (Fig. 11) which clearly reveal an improved reflection of the spectral features for the overlapping resonances

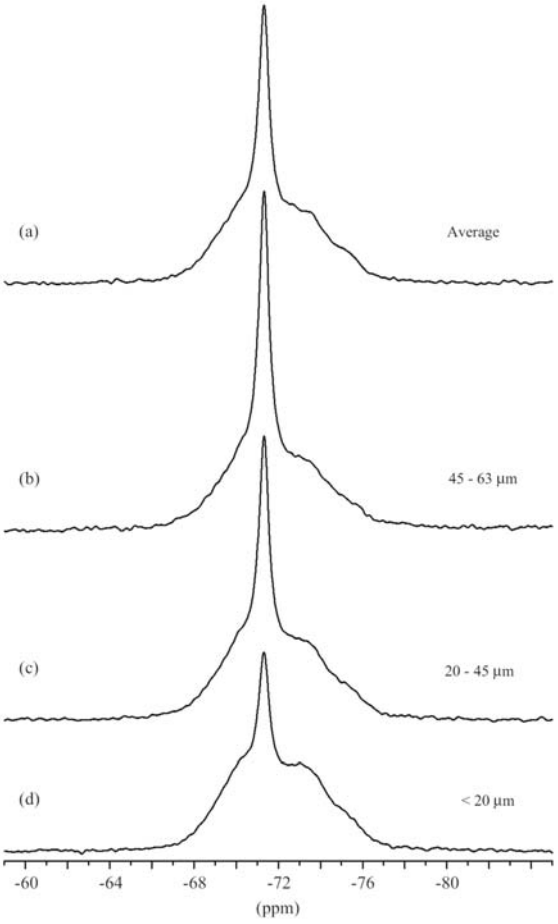

Fig. 9. ^{29}Si MAS NMR spectra (9.4 T, $\nu_R = 12.0$ kHz) of different grain-size fractions of cement J obtained by sifting ground clinkers using analytical test sieves. The spectra correspond to (a) the ground clinker before sifting, grain sizes in the range (b) 45–63 µm, (c) 20–45 µm, and (d) below 20 µm.

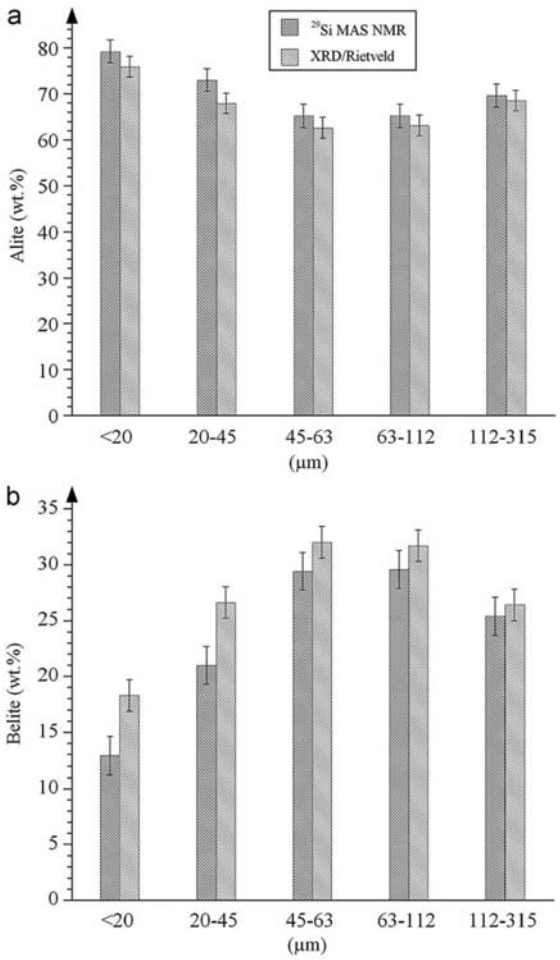

Fig. 10. Quantities of alite and belite in different grain-size fractions of cement J determined from ^{29}Si MAS NMR and XRD-Rietveld refinements (c.f., Table 5).

from alite on going from 4.7 to 14.1 T. Deconvolution of the ^{29}Si MAS NMR spectra for cements A, C, and H recorded at the four magnetic fields results in the quantities of alite and belite illustrated in Fig. 12, employing the Taylor composition for these phases and the bulk SiO_2 content from elemental analysis (Table 1). These plots strongly indicate that a precise determination of the belite/alite ratio is achieved from the ^{29}Si MAS NMR spectra and for cements with rather different belite/alite ratios. The largest difference between the lowest and highest quantity of alite is found for cement A (1.2 wt%) while the variations in belite content from the spectra at different magnetic fields are below 1.0 wt% for the three cements. Furthermore, this analysis, supported by the spectral appearance for cement A in Fig. 11, suggests that valuable ^{29}Si MAS NMR spectra of Portland cements for quantitative analysis can be achieved at moderate magnetic fields, i.e., 7.1 and 9.4 T, as employed in earlier ^{29}Si MAS NMR studies that involve quantification of alite and belite in anhydrous and hydrated Portland cements [5,17,37,38].

The repeatability has been tested by two types of experiments for cement B. The first type involved the sequential acquisition of five ^{29}Si MAS NMR spectra (9.4 T, $\nu_R = 12.0$ kHz, a 10 s relaxation delay, 6528 scans, 18.2 h spectrometer time) of the same sample of cement B. Evaluation of the total ^{29}Si signal intensity for the overlapping centerbands from alite and belite reveals that the difference between the largest and smallest intensity value, observed in the five ^{29}Si MAS NMR spectra, is 1.7% which demonstrates a high stability of the spectrometer over the total acquisition period of five days. Furthermore, deconvolution of the individual spectra results in quantities of alite and belite in the ranges 57.48–57.70 and 16.26–16.44 wt%, respectively, indicating a high repeatability in the analysis of exactly the same sample. The second type of experiments involved selection of five samples of ~5 g cement from randomly chosen places in the cement bag. For each of these samples a 5 mm PSZ rotor was packed, requiring approx. 0.20 g to fill the rotor, and ^{29}Si MAS NMR spectra were acquired, using the same experimental conditions as mentioned above. The corresponding analysis of the five spectra reveals quantities of alite and belite in the ranges 56.9–58.4 and 15.8–16.9 wt%, respectively. The somewhat larger variation in these quantities, as compared to the abovementioned analysis of

Table 5
Variation in bulk SiO_2 content and in the quantities of alite and belite (wt%) from ^{29}Si MAS NMR and XRD-Rietveld analysis for different grain-size fractions of cement J.[a]

Grain-size	SiO_2[b]	^{29}Si MAS NMR[c]			XRD-Rietveld[d]	
(μm)	(wt%)	*I*(belite)/*I*(alite)	alite	belite	alite	belite
< 20	24.17	0.2033	79.2	12.9	75.9	18.3
20–45	25.14	0.3580	73.0	21.0	67.9	26.6
45–63	25.82	0.5623	65.2	29.6	62.6	32.0
63–112	25.88	0.5651	65.2	29.6	63.1	31.7
112–315	25.67	0.4543	69.6	25.4	68.5	26.4
Average[e]	25.50	0.4157	68.2	26.0	65.2	29.6

[a] All experiments are performed on the same samples of sifted cements (c.f., experimental section).
[b] Bulk SiO_2 content from XRF analysis.
[c] *I*(belite)/*I*(alite) ratios from deconvolutions of ^{29}Si MAS NMR spectra recorded at 9.4 T and $\nu_R = 12.0$ kHz. The quantities of alite and belite assume the compositions for these phases proposed by Taylor [2]. The standard deviations are estimated to ±2.5 and ±1.7 wt% for alite and belite, respectively.
[d] The standard deviations are ±2.2 and ±1.4 wt% for alite and belite, respectively, from the XRD-Rietveld analyses [15].
[e] Data for the ground cement clinkers before sifting.

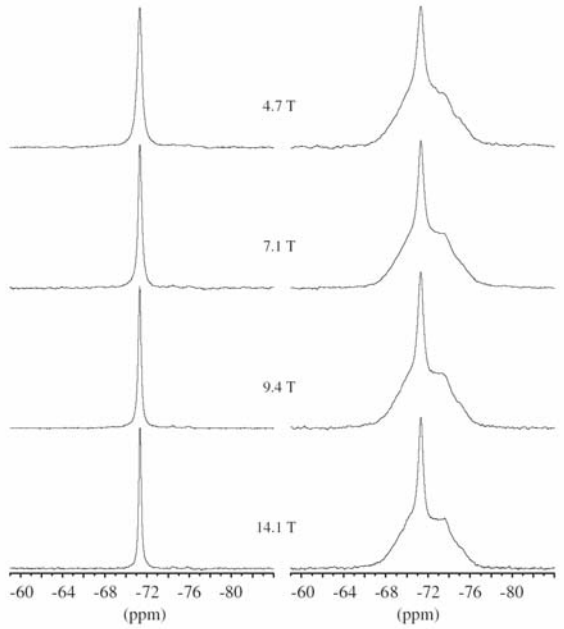

Fig. 11. ^{29}Si MAS NMR spectra ($\nu_R = 12.0$ kHz) of exactly the same samples of synthetic belite (β-Ca_2SiO_4) and cement A (packed once in 5 mm PSZ rotors), recorded under identical conditions at magnetic fields of 4.7, 7.1, 9.4, and 14.1 T. All spectra are obtained with a 45° excitation pulse and relaxation delays of 60 s and 30 s for belite and cement A, respectively.

the same sample, is ascribed to the precision of the method and a minor degree of heterogeneity of the cement powder in the bag.

3.7. Comparison of data from ^{29}Si MAS NMR, XRD-Rietveld, and Taylor–Bogue calculations

The quantities of alite and belite, determined from ^{29}Si MAS NMR spectra for the 11 Portland cements (Table 2), are compared with the results from XRD-Rietveld analysis [15] (Fig. 13a) and the phase compositions estimated from Taylor–Bogue calculations (Fig. 13b). Moreover, a comparison of the alite and belite contents

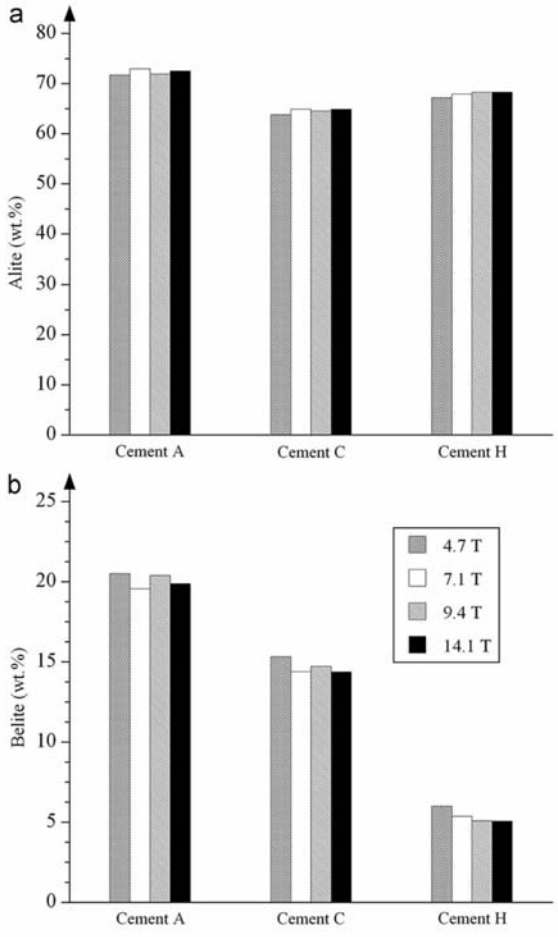

Fig. 12. Graphical representation of the quantities of (a) alite and (b) belite in cement A, C, and H determined from ^{29}Si MAS NMR spectra at 4.7, 7.1, 9.4, and 14.1 T. The spectra were recorded under identical conditions for each cement using the same packed 5 mm rotor at the different magnetic fields.

ı XRD-Rietveld analysis and the Taylor–Bogue calculations is trated in Fig. 13c. These plots show the best agreement for the erimental methods of ^{29}Si MAS NMR and XRD-Rietveld, ough some systematic deviations are also apparent between

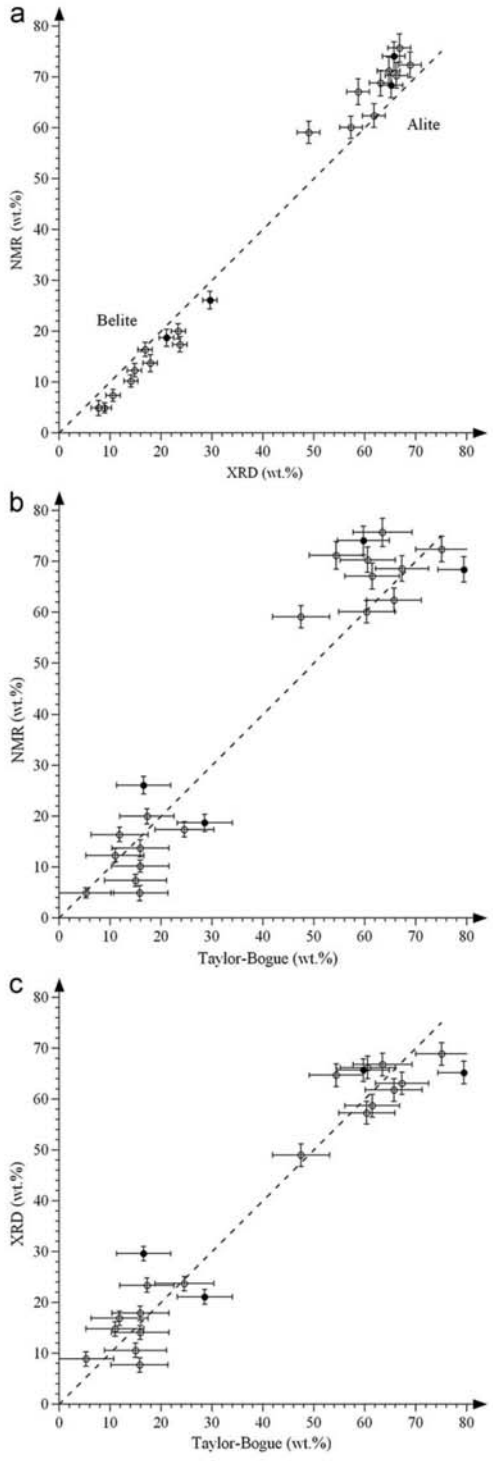

these two techniques. The mean deviations between the alite and belite contents from ^{29}Si NMR and XRD-Rietveld are 5.6 and 3.3 wt%, respectively, whereas the corresponding deviations between ^{29}Si NMR and Taylor–Bogue calculations are 7.7 and 5.4 wt%. The best agreement for alite is observed between XRD-Rietveld and the Taylor–Bogue calculations (mean deviation of 4.8 wt%, Fig. 13c), however, with a somewhat larger mean deviation for belite (5.0 wt%) as compared to the ^{29}Si NMR and XRD-Rietveld data. Some of the largest discrepancies are observed for the Portland clinkers (J and K) between the Taylor–Bogue calculations and the NMR data as well as the XRD results, whereas these two experimental techniques agree well for the two clinkers. On the other hand, systematic deviations between the results from NMR/XRD-Rietveld analysis and the Taylor–Bogue calculations are not apparent from the present data (Figs. 13b and c). Obviously, a major disadvantage of the Taylor–Bogue approach is its bulk-oxide to mineral transformation that assumes fixed compositions for the main phases (although depending on the type of cement). The compositions of the alite and belite phases, determined by EDS combined with SEM for seven cements (Table 4), do not appear to differ significantly from the average compositions proposed by Taylor [2] and used in the Taylor–Bogue calculations. However, small errors in the bulk-oxide composition are magnified in the Bogue calculation, as pointed out in a recent comparison of XRD-Rietveld analysis with Taylor–Bogue calculations [15]. For example, a typical standard deviation for the bulk CaO and SiO_2 content from XRF analysis is 0.4 wt% for both oxides. Assuming a change in the CaO and SiO_2 contents by +0.4 and −0.4 wt%, respectively, for cement A results in an increase in the alite content of 5.1 wt% and a decrease in belite of 5.3 wt% in the Taylor–Bogue composition when the values for the other elements remain unchanged. Thus, such inaccuracies in the elemental composition may account for some of the discrepancies between the Taylor–Bogue data and those derived from ^{29}Si NMR (Fig. 13b) and XRD-Rietveld analysis (Fig. 13c).

Although the best agreement is observed between the data from ^{29}Si NMR and XRD-Rietveld analysis, it is apparent from these data (Fig. 13a) as well as the graphical representation in Fig. 10 that the ^{29}Si NMR method underestimates the belite content and overestimates the alite content as compared to the XRD-Rietveld analysis. Although, the present work has coped with experimental parameters and effects that need consideration in the ^{29}Si MAS NMR method and that a similar study has recently been performed for the XRD-Rietveld technique [15], the background for this discrepancy is not immediately apparent and may not originate from a single parameter/effect. However, the systematic variations may reflect the difference in nature of the NMR and XRD experiments, which primarily depend on the local and long-range order in the materials, respectively.

A potential source of error could be an extensive substitution of the Si atoms in the belite structure, resulting in an underestimation of the quantity of this phase by ^{29}Si MAS NMR. However, calculation of the contents of alite and belite from ^{29}Si MAS NMR for cements A–F and H using the actual phase composition for these phases from EDS analysis (Table 4) and

Fig. 13. Comparison of the quantities of alite and belite determined from ^{29}Si MAS NMR with the data from (a) XRD-Rietveld analysis and (b) the phase compositions from Taylor–Bogue calculations. Part (c) illustrates the data from XRD-Rietveld refinement as a function of the quantities of alite and belite from the Taylor–Bogue calculations. The plots employ the values listed in Table 2 where open circles correspond to the cements and the filled circles to the Portland clinkers (J and K). The dashed lines show the 1:1 correlations. The uncertainty limits for alite and belite from the Taylor–Bogue calculations were estimated from calculations considering the standard deviations of the metal oxides from the XRF analyses only.

with correction of the bulk SiO_2 content for the amount of Si incorporated in the aluminate and ferrite phases (again according to EDS) results in only a minor, systematic decrease for the belite content (on average by 0.4 wt%) and similarly small variations in the alite content (an average deviation of 0.8 wt%). These deviations are below the variations found in the repeatability test and thus, should not lead to any modifications of the ^{29}Si MAS NMR method presented in this work.

Another explanation for the discrepancy could be that the fraction of amorphous alite is higher than the corresponding quantity of less-ordered belite in the cements, leading to an underestimation of this phase by XRD. This possible difference in amorphous contents may reflect that the monoclinic form of alite is metastable at room temperature and thereby more affected by the quenching of the clinkers when they leave the high-temperature zone of the cement kiln. Furthermore, as previously discussed, fracture takes place preferentially through the alite phase and grinding is well known to produce a small amount of amorphous material on the grain surfaces.

4. Conclusions

^{29}Si MAS NMR spectroscopy represents a valuable tool for quantification of alite and belite in anhydrous Portland cement containing low and moderate levels of iron (i.e., $Fe_2O_3 < 5$ wt%). An improved determination of the molar belite/alite ratio is achieved from high-speed spinning ($\nu_R = 12–13$ kHz) ^{29}Si MAS NMR spectra as compared to ratios derived from spectra at lower spinning frequencies, traditionally used in ^{29}Si MAS NMR studies of cementitious materials (e.g., $\nu_R = 3–6$ kHz). The investigations of the precision and repeatability have shown a high precision in the analysis of a sample at the same and at different magnetic fields. From this study it is concluded that moderate magnetic fields (e.g., 9.4 T) are suitable for this kind of spectral analysis. For different samples taken from the same source of cement, repeatability experiments have shown variations in the alite and belite contents of 1.5–2.0 wt%, in agreement with the results from similar XRD-Rietveld phase analyses [15]. Furthermore, it is observed that different grain-size fractions (in the range <20 to $\sim$150 μm) exhibit different belite/alite ratios.

The studies of effects from paramagnetic ions (i.e., Fe^{3+}) on the spectral appearance and spin-lattice relaxation for alite and belite have shown that the spinning sideband intensities increase almost linearly with the bulk Fe_2O_3 content of the cements and with the magnetic field strength, reflecting that they originate from dipolar interactions between the ^{29}Si spin and the unpaired electron spins of the Fe^{3+} ions. Moreover, it has been observed that the spin-lattice relaxation for ^{29}Si in alite and belite exhibit a non-exponential relationship (i.e., a stretched exponential), in agreement with spin relaxation caused by paramagnetic ions being the dominating relaxation mechanism. Finally, ^{29}Si spin-lattice relaxation studies of a cement, which has been exposed to selective dissolution of the calcium aluminate ($Ca_3Al_2O_6$) and ferrite ($Ca_2Al_xFe_{2-x}O_5$) phases, have shown that the ^{29}Si spin-lattice relaxation for alite and belite is dominated by relaxation from Fe^{3+} ions incorporated as guest-ions in these phases. Thus, relaxation from the Fe^{3+} ions of the ferrite phase, which may be intimately mixed with alite and belite, plays a less significant role at least for Portland cements with bulk Fe_2O_3 contents below $\sim$5 wt%.

The comparison of the quantities of alite and belite from ^{29}Si MAS NMR analyses of 11 commercial Portland cements with XRD-Rietveld phase analyses and Taylor–Bogue calculations has shown the best agreement between ^{29}Si MAS NMR and the XRD-Rietveld refinements. However, the quantities of alite and belite from ^{29}Si NMR are generally slightly higher and lower, respectively, as compared to the XRD-Rietveld method. These systematic discrepancies may be associated with effects such as differences in guest-ion replacement for Si in the lattices of alite and belite, which is not considered in the ^{29}Si MAS NMR approach, and the amount of amorphous material in the cement which may affect the quantities reported by the XRD-Rietveld analysis.

Acknowledgments

The use of the facilities at the Instrument Centre for Solid-State NMR Spectroscopy, Aarhus University, sponsored by the Danish Natural Science Research Council, the Danish Technical Science Research Council, Teknologistyrelsen, Carlsbergfondet, and Direktør Ib Henriksens Fond, is acknowledged. S.L. Poulsen and V. Kocaba would like to thank NANOCEM, a European industrial/academic partnership for fundamental research on cementitious materials, for financial support.

References

[1] R.H. Bogue, Ind. Eng. Chem. 1 (1929) 192–197.
[2] H.F.W. Taylor, Adv. Cem. Res. 2 (1989) 73–77.
[3] M. Kristmann, Cem. Concr. Res. 7 (1977) 649–658.
[4] W.A. Gutteridge, Proc. Br. Ceram. Soc. 35 (1984) 11–23.
[5] J. Skibsted, H.J. Jakobsen, C. Hall, J. Chem. Soc. Faraday. Trans. 91 (1995) 4423–4430.
[6] C. Hall, K.L. Scrivener, Adv. Cem. Bas. Mater. 7 (1998) 28–38.
[7] J. Neubauer, H. Pöllmann, H.W. Meyer, Quantitative X-ray analysis of OPC clinker by Rietveld refinement, in: Proceedings of the 10th International Congress on the Chemistry of Cement, vol. 3 paper 3v007, 1997.
[8] J.C. Taylor, I. Hinczak, C.E. Matulis, Powder Diffr. 15 (2000) 7–18.
[9] A.G. De la Torre, M.G. Aranda, J. Appl. Crystallogr. 36 (2003) 1169–1176.
[10] K.L. Scrivener, T. Füllmann, E. Gallucci, G. Walenta, E. Bermejo, Cem. Concr. Res. 34 (2004) 1541–1547.
[11] D.H. Campbell, Microscopic Examination and Interpretation of Portland Cement and Clinker, Portland Cement Association, Skokie, Illinois, 1999.
[12] A. Crumbie, G. Walenta, T. Füllmann, Cem. Concr. Res. 36 (2006) 1542–1547.
[13] N.V.Y. Scarlett, I.C. Madsen, C. Manias, D. Retallack, Powder Diffr. 16 (2001) 71–80.
[14] M. Enders, Zement-Kalk-Gips Int. 58 (4) (2005) 28–37.
[15] G. Le Saoût, V. Kocaba, K.L. Scrivener, Application of the Rietveld method to the analysis of anhydrous cement, Cem. Concr. Res. (to be submitted).
[16] D. Sorrentino, F. Sorrentino, E. Gartner, Prediction of a Portland cements's properties from its chemical and mineralogical composition, in: F. Young, J. Skalny (Eds.), Materials Science of Concrete VII, The American Ceramic Society, 2005, pp. 1–35.
[17] J. Hjorth, J. Skibsted, H.J. Jakobsen, Cem. Concr. Res. 18 (1988) 789–798.
[18] W.A. Gutteridge, Cem. Concr. Res. 9 (1979) 319–324.
[19] H.F.W. Taylor, Cem. Concr. Res. 29 (1999) 1173–1179.
[20] K.H. Jost, B. Ziemer, R. Seydal, Acta Crystallogr. B 33 (1977) 1696–1700.
[21] F. Nishi, Y. Takéuchi, I. Maki, Z. Kristallogr. 172 (1985) 297–314.
[22] A.-R. Grimmer, H. Zanni, ^{29}Si NMR study of chemical shift tensor anisotropy of tricalcium silicate, in: P. Colombet, A.-R. Grimmer, H. Zanni, P. Sozzani (Eds.), Nuclear Magnetic Resonance Spectroscopy of Cement-based Materials, Springer, Berlin, 1998, pp. 57–68.
[23] M.R. Hansen, H.J. Jakobsen, J. Skibsted, Inorg. Chem. 42 (2003) 2368–2377.
[24] A. Nayeem, J.P. Yesinowski, J. Chem. Phys. 89 (1988) 4600–4608.
[25] A.R. Brough, C.P. Grey, C.M. Dobson, J. Am. Chem. Soc. 115 (1993) 7318–7327.
[26] D. Tse, S.R. Hartmann, Phys. Rev. Lett. 21 (1968) 511–514.
[27] A. Thangaraj, S. Ganapathy, Ind. J. Chem. 29A (1990) 1080–1082.
[28] J.S. Hartman, B.L. Sherriff, J. Phys. Chem. 95 (1991) 7575–7579.
[29] J. Skibsted, L. Hjorth, H.J. Jakobsen, Adv. Cem. Res. 7 (1995) 69–83.
[30] S. Hayashi, E. Akiba, Solid-State Nucl. Magn. Reson. 4 (1995) 331–340.
[31] M.R. McHenry, B.G. Silbernagel, J.H. Wernick, Phys. Rev. B 5 (1972) 2958–2972.
[32] C.L. Edwards, L.B. Alemany, A.R. Barron, Ind. Eng. Res. 46 (2007) 5122–5130.
[33] W.A. Gutteridge, Brit. Ceram. Proc. 35 (1984) 11–23.
[34] M. Enders, World Cem. 38 (6) (2007) 45–50.
[35] I. Maki, S. Ito, T. Tanioka, Y. Ohno, K. Fukuda, Cem. Concr. Res. 23 (1993) 1078–1084.
[36] E.O. Viggh, World Cem. 25 (10) (1994) 44–48.
[37] M.D. Andersen, H.J. Jakobsen, J. Skibsted, Inorg. Chem. 42 (2003) 2280–2287.
[38] M.D. Andersen, H.J. Jakobsen, J. Skibsted, Cem. Concr. Res. 34 (2004) 857–868.

Paper II

Incorporation of Phosphorus Guest Ions in the Calcium Silicate Phases of Portland Cement from ^{31}P MAS NMR Spectroscopy

Søren L. Poulsen, Hans J. Jakobsen, Jørgen Skibsted

Submitted to Inorganic Chemistry

Abstract

Portland cements may contain small quantities of phosphorus (typically below 0.5 wt.% P_2O_5), originating from either the raw materials or alternative sources of fuel used to heat the cement kilns. This work reports the first ^{31}P MAS NMR study of anhydrous and hydrated Portland cements which focuses on the phase and site preferences of the $(PO_4)^{3-}$ guest ions in the main clinker phases and hydration products. The observed ^{31}P chemical shifts (10 ppm to –2 ppm), the ^{31}P chemical shift anisotropy, and the resemblance of the lineshapes in the ^{31}P and ^{29}Si MAS NMR spectra strongly suggest that $(PO_4)^{3-}$ units are incorporated in the calcium silicate phases, alite (Ca_3SiO_5) and belite (Ca_2SiO_4), by substitution for $(SiO_4)^{4-}$ tetrahedra. This assignment is further supported by a determination of the spin-lattice relaxation times for ^{31}P in alite and belite which exhibit the same ratio as observed for the corresponding ^{29}Si relaxation times. From simulations of the intensities, observed in inversion-recovery spectra for a white Portland cement, it is deduced that 1.3% and 2.1% of the Si sites in alite and belite, respectively, are replaced by phosphorus. Charge-balance may partly be achieved by a coupled substitution mechanism where Ca^{2+} is replaced by Fe^{3+} ions, which may account for the strong interaction of the ^{31}P spins with paramagnetic Fe^{3+} ions as observed for the ordinary Portland cements. $^{31}P\{^1H\}$ CP/MAS NMR spectra following the hydration of a white Portland cement show that the resonances from the hydrous phosphate species fall in the same spectral range as observed for $(PO_4)^{3-}$ incorporated in alite. This similarity and the absence of a large ^{31}P chemical shift ansitropy indicate that the hydrous $(PO_4)^{3-}$ species are incorporated in the interlayers of the calcium-silicate-hydrate (C-S-H) phase, the principal phase formed upon hydration of alite and belite.

Introduction

The global consumption of Portland cement has more than doubled during the past two decades, reflecting its vital role in the house-building industry and the improvement of infrastructures, and it is forecasted that todays cement production will at least double again by the year 2050 to more than 6 billion tonnes per year.[1,2] Roughly 800 kg CO_2 is emitted for every tonne Portland cement produced by todays technologies, amounting to more than two billion tonnes per year, and resulting in cement production being responsible for about 5% of the global anthropogenic CO_2 emission. Thus, the cement industry faces an urgent and serious challenge in increasing its production capacity and at the same time reducing the total CO_2 emission to meet World community's regulations.

Roughly 40% of the CO_2 emitted by cement production results from the fuel used to heat the cement kilns and drive the mills whilst 60% originates from the decarbonation of limestone, required to form the main cement clinker phases, *i.e.*, impure forms of alite (Ca_3SiO_5), belite (Ca_2SiO_4), tricalcium aluminate ($Ca_3Al_2O_6$) and calcium alumino-ferrite ($Ca_2Al_xFe_{2-x}O_5$). A direct approach to reduce the CO_2 emission is the partial replacement of Portland cement by supplementary cementitious materials, for example fly ashes from coal burning, slags from pig iron production, silica fume from the production of ferrosilicon or natural pozzolans such as volcanic rocks and heat-treated clay minerals. Another approach utilizes biofuels to heat the cement kilns, thereby partly replacing the traditional kiln fuels of gas, oil, and coal. Alternative fuels also include meat and bone meal, sewage sludge, used oils, waste tyres, solvents, and a range of other industrial by-products.[3,4] However, such waste materials may introduce trace elements in the cement which can affect the grindability of the clinkers, the reactivity (hydration reactions), and the durability of the resulting cement.[5,6] Thus, it is important to study the chemical impact of these guest ions on the main Portland clinker phases in relation to applications of alternative fuels. For example, the use of meat and bone meal or sewage sludge as alternative fuels may result in the incorporation of a significant amount of phosphorus in the

cement, corresponding to a bulk content roughly in the range 0.1 – 0.6 wt.% P_2O_5.[7]

Earlier studies have shown that phosphorus (P^{5+} in $(PO_4)^{3-}$ ions) mainly enters the calcium silicate phases with a preferential formation of a phosphatic belite solid solution for phosphorus concentrations above 1 wt.% P_2O_5.[8,9] The upper limit for incorporation of phosphate ions in alite has been reported to be 1.1 wt.% P_2O_5,[9] corresponding to a molar P/Si ratio of 0.036. Furthermore, incremental additions of P_2O_5 results in a progressive reduction in the alite content, corresponding to 9.9 wt.% per added 1 wt.% of P_2O_5,[8] which significantly reduces the mechanical strength of the resulting hydrated Portland cement. Phosphate contents above 1.0 wt.% P_2O_5 are only found in cements produced from phosphatic limestone deposits in certain parts of the World. Thus, more recent research has focussed on effects from small amounts of phosphate on the cement clinkering processes and hydraulic reactivities,[7,10-14] which are more realistic conditions for the clinker burning in an industrial kiln where a significant (*e.g.*, 20%) part of the conventional fuel is replaced by meat and bone meal. For a laboratory-made clinker containing 0.6 wt.% P_2O_5, X-ray microanalysis indicated that a maximum of 2.3% and 3.3% of the silicon sites can be replaced by phosphorus in alite and belite, respectively.[7] Other studies have investigated the coupled incorporation of $(PO_4)^{3-}$ and a tri-valent metal ion (Al^{3+}, Mn^{3+}, Fe^{3+}, Cr^{3+}) for synthetic phases of alite[10,14] and belite[11-13] with the principal aim of identifying polymorphic changes and transformations from alite to belite and CaO phases.

In this work we report the first application of solid-state ^{31}P Magic-Angle Spinning (MAS) Nuclear Magnetic Resonance (NMR) spectroscopy in cement chemistry by the detection of phosphorus guest ions in anhydrous and hydrated production Portland cements containing bulk phosphorus contents in the range 0.08 – 0.45 wt.% P_2O_5. Generally, the local environment of $(PO_4)^{3-}$ ions in cement minerals is difficult to characterize by conventional analytical techniques, such as powder X-ray diffraction, as a result of the low concentration and presumed random distribution over several lattice sites. The present work utilizes the very favourable NMR properties of the ^{31}P spin, *i.e.*, nuclear spin I = ½, high Larmor frequency, and 100% natural

abundance, as well as results from earlier studies of inorganic phosphates which have revealed that the phosphate ^{31}P NMR chemical shifts primarily depend on the local structural environments of the PO_4 species.[15,16] The observed ^{31}P chemical shifts, chemical shift anisotropies, and spin-lattice relaxation times, along with $^{31}P\{^1H\}$ cross polarization (CP) MAS NMR experiments for the hydrated samples, provide structural information about phase and site preferences of the phosphorus guest ions. ^{31}P MAS NMR has been widely used in inorganic chemistry, including applications that focus on small quantities of phosphate such as phosphor-modified alumina supports for heterogeneous catalysts[17] and phosphorus incorporated in silicious ZSM-5 zeolites[18,19] and the SiO_2 polymorph stishovite.[20] In cases where these materials contain significant amounts of phosphorus (> 2 wt.% P_2O_5), heteronuclear correlation NMR experiments such as ^{31}P – ^{27}Al REDOR/TRAPDOR[21] and ^{27}Al – ^{31}P CP-HECTOR[22] have been utilized to obtain further information on the local environments of the $(PO_4)^{3-}$ ions.

Experimental Section

Materials. Four commercial Portland cements (A – D) obtained from four European cement manufacturers were studied as received. Bulk chemical compositions were obtained by X-ray fluorescence (XRF) analysis and are summarized in Table 1 along with the quantities of alite and belite, determined recently by ^{29}Si MAS NMR in a study including the same cements.[23]

A series of hydrated samples were prepared for cement A using a water/cement ratio of 0.4. The cement and water were mixed at 500 rpm for 3 min (motorized stirrer), followed by a rest period of 2 min and then stirring at 2000 rpm for 3 min. The resulting paste was cast in a capped plastic container (50 mL) and after 24 hours the paste was demoulded and immersed in a closed plastic container (500 mL) filled with tap water. The container was stored in a temperature-controlled room at 21 ± 2°C. At appropriate time intervals ~5 g of sample was ground to a fine powder and the hydration was stopped by mixing the material with 50 mL isopropyl alcohol (99%) for 1 hour using a magnetic stirrer. Finally, the powder was dried over

silica gel in a desiccator for 24 hours.

NMR Measurements. Solid-state ^{31}P MAS, ^{31}P{^{1}H} CP/MAS, and ^{29}Si{^{31}P} CP/MAS NMR experiments were performed on a Varian INOVA-400 spectrometer (9.4 T), using a home-built CP/MAS probe for 5 mm o.d. zirconia (PSZ) rotors (110 μL sample volume), or on a Varian Direct Drive VNMRS-600 spectrometer (14.1 T), employing a Varian/Chemagnetics triple-resonance T3® MAS probe for 4 mm o.d. PSZ rotors (82 μL sample volume). The single-pulse and inversion-recovery ^{31}P MAS NMR spectra acquired at 9.4 T used an rf field strength of $\gamma B_1/2\pi$ = 60 kHz, the spinning speed ν_R = 12.0 kHz, a relaxation delay of 60 s, and typically 1000 scans. The ^{31}P{^{1}H} CP/MAS experiments (9.4 T) were performed at a moderate spinning speed (ν_R = 5 kHz), using rf field strengths of $\gamma B_2/2\pi$ = 52 kHz for the initial ^{1}H 90° pulse and ^{1}H decoupling, and $\gamma B_1/2\pi \approx \gamma B_2/2\pi \approx$ 45 kHz for the Hartmann-Hahn match. The ^{31}P MAS and ^{29}Si{^{31}P} CP/MAS NMR experiments acquired at 14.1 T in ^{29}Si – ^{31}P double-tune mode employed a ^{31}P rf field strength of $\gamma B_1/2\pi$ = 60 kHz and matched ^{29}Si, ^{31}P rf field strengths of $\gamma B_1/2\pi \approx \gamma B_2/2\pi \approx$ 40 kHz, respectively.

^{31}P chemical shifts are referenced to 85% H_3PO_4 using a solid sample of $(NH_4)_2HPO_4$ as a secondary reference (δ_{iso} = 1.37 ppm). The chemical shift anisotropy (CSA) parameters (δ_σ and η_σ) are defined from the principal elements (δ_{ii}) of the CSA tensor as $\delta_\sigma = \delta_{iso} - \delta_{33}$ and $\eta_\sigma = (\delta_{11} - \delta_{22})/\delta_\sigma$ where $\delta_{iso} = {}^1/_3 (\delta_{11} + \delta_{22} + \delta_{33})$ following the convention $|\delta_{33} - \delta_{iso}| \geq |\delta_{11} - \delta_{iso}| \geq |\delta_{22} - \delta_{iso}|$.

Results and Discussion

^{31}P MAS NMR of anhydrous cements. Four different Portland cements, including a white Portland cement with a low iron content (cement A) and three ordinary Portland cements (cement B – D, *c.f.*, Table 1), are studied in the present work. The ^{31}P MAS NMR spectra of these cements (Figure 1) all exhibit isotropic resonances in the range 10 ppm to –2 ppm with only low-intensity spinning sidebands (not shown) at the present spinning speed (ν_R = 12.0 kHz) and

magnetic field strength (9.4 T). The isotropic ^{31}P chemical shifts suggest that phosphorus in the anhydrous cements are present as orthophosphate units, following the exploratory ^{31}P NMR study of orthophosphates by Turner *et al.*[15] who found that the isotropic chemical shifts for these PO_4 units primarily depend on next-nearest neighbour interactions and reported linear correlations between $\delta_{iso}(^{31}P)$ and the electronegativity as well as the cation potential (Z/r where Z is the cation charge and r its ionic radius). In agreement with these correlations, δ_{iso} = 3.0 ppm was reported for $Ca_3(PO_4)_2$,[15] which falls in the same spectral range as the chemical shifts observed for the anhydrous Portland cements. In contrast, condensed aluminium orthophosphate ($AlPO_4$) resonates at lower frequency (δ_{iso} = –24.5 ppm)[15] and in the chemical shift range observed for PO_4 tetrahedra in framework aluminophosphates (roughly –5 to –35 ppm).[25-27] These variations in ^{31}P chemical shifts suggest that the phosphorus guest ions are incorporated in the calcium silicate phases alite and belite, which both include orthosilicate SiO_4 units only,[28,29] rather than in tricalcium aluminate, containing 6-rings of AlO_4 tetrahedra,[30] or in the calcium alumino-ferrite phase with a structure of alternating Fe-rich octahedral and Al-rich tetrahedral layers.[31] Obviously, this assignment assumes that the $(PO_4)^{3-}$ ions replace the high-valent $(SiO_4)^{4-}$ ions in alite and belite or $(AlO_4)^{5-}$ and $(AlO_4)^{5-}/(FeO_6)^{9-}$ in tricalcium aluminate and ferrite, respectively.

The crystal structure for belite (β-Ca_2SiO_4)[27] includes a unique Si site whereas 18 distinct Si atoms are reported for the monoclinic M_{III} form of alite.[28] Thus, the replacement of $(SiO_4)^{4-}$ by $(PO_4)^{3-}$ in belite should result in a single ^{31}P resonance whereas a number of overlapping peaks are expected for $(PO_4)^{3-}$ ions incorporated in alite. The spectral effects from these substitutions are similar to those observed in an earlier study on the incorporation of Al^{3+} guest ions in the two calcium silicate phases by ^{27}Al MAS NMR,[32] where a single second-order quadrupolar lineshape was observed for tetrahedrally coordinated aluminium in belite while the spectrum of a synthetic Ca_3SiO_5 sample doped with Al^{3+} revealed a number of overlapping resonances originating from different AlO_4 sites.

The relative intensities of the ^{31}P MAS NMR spectra in Figure 1 agree well with the bulk

contents of P_2O_5 in the cements (Table 1) and it is noted that the characteristic features of the overlapping resonances are clearly observed even for the cement with the lowest quantity of phosphorus (cement D, 0.08 wt.% P_2O_5). Furthermore, a narrow resonance at $\delta(^{31}P) = 1.0$ ppm is clearly observed for cements A and C which can also be identified in the spectra of cements B and D. This resonance is tentatively assigned to $(PO_4)^{3-}$ ions replacing the unique $(SiO_4)^{4-}$ site in belite. Although a distinct resonance is also apparent for cement A and B at $\delta(^{31}P) = 3.0$ ppm, this peak and the underlying resonances in the range from 10 ppm to –2 ppm are all ascribed to $(PO_4)^{3-}$ ions that substitute for the different Si sites in monoclinic M_{III} alite. Obviously, differences in the local environments for the individual SiO_4 tetrahedra may result in a site preference for the $(SiO_4)^{4-} \rightarrow (PO_4)^{3-}$ substitution which may account for the more intense peak at $\delta(^{31}P) = 3.0$ ppm. However, the overall lineshape of the resonances in the range 10 ppm to –2 ppm, beneath the peak from belite at 1.0 ppm, shows some resemblance to the lineshape for the overlapping ^{29}Si resonances in ^{29}Si MAS NMR spectra of alite,[23,33] which further support the assignment. The highest intensity for the ^{31}P resonance from belite is observed for cement A (Figure 1) which also includes the largest belite content of the four studied cements (Table 1). However, the ^{31}P MAS NMR spectra of cement B and C show a significantly larger amount of $(PO_4)^{3-}$ guest ions in the belite phase for cement C as compared to cement B, although these cements contain very similar quantities of belite. This indicates that other factors such as the thermal history, the source of phosphorus in the raw materials/fuels, and the content of other minor elements may influence the degree of $(PO_4)^{3-}$ ion incorporation in the individual phases of alite and belite.

^{31}P chemical shift anisotropy. ^{31}P MAS NMR spectra at a higher magnetic field (14.1 T) and lower spinning speed ($\nu_R = 4.0$ kHz) have also been obtained for the four anhydrous cements (Figure 2). The spectra of cements B – D are rather similar (thus, the spectrum is only shown for cement C) and differ from cement A by a larger number of spinning sidebands (ssbs). The difference in number of ssbs and their intensities for cements A and C reflect the variation in

paramagnetic ions (principally Fe^{3+}) and thereby the higher bulk Fe_2O_3 contents for cements B – D as compared to cement A (Table 1). Following our recent ^{29}Si NMR study of paramagnetic ions in the alite and belite phases of anhydrous cements, the larger number and high-intensity ssbs observed for cement C (Figure 2b) are caused by the dipolar interaction between the unpaired electrons of the Fe^{3+} ions and the ^{31}P nuclear spins which is strongly dependent on the distance between the spins and thereby the concentration of Fe^{3+} species in the anhydrous phases. The significantly smaller Fe_2O_3 content in cement A implies that the few ssbs observed in the ^{31}P MAS NMR spectrum (Figure 2a) mainly result from the ^{31}P chemical shift anisotropy (CSA) interaction. Employing this assumption and the consideration of only the ^{31}P CSA interaction in simulations of the centerband and ssb intensities for ^{31}P in alite and belite, estimated from the spectrum in Figure 2a, indicate that the two different types of ^{31}P environments exhibit shift anisotropies (δ_σ) of magnitudes in the ranges $|\delta_\sigma| = 25 - 30$ ppm and $|\delta_\sigma| = 22 - 25$ ppm for ^{31}P in alite and belite, respectively. Obviously, these values for the anisotropies are upper limits, since Fe^{3+} – ^{31}P electron – nuclear spin dipolar couplings may also contribute slightly to the ssb intensities. The small values for the shift anisotropies further support the presence of ^{31}P in isolated PO_4 tetrahedra since orthophosphate units generally exhibit small shift anisotropies as compared to pyro- and metaphosphates, *i.e.*, magnitudes of δ_σ below 40 ppm are typical for nonprotonated orthophosphates[16] while $\delta_\sigma = -110$ to -50 ppm and $\delta_\sigma = 100 - 170$ ppm are common for pyro- and metaphosphate PO_4 units.[16,34]

Inversion-recovery ^{31}P MAS NMR. A distinction of the ^{31}P resonances from the $(PO_4)^{3-}$ guest ions in alite and belite may be achieved from a difference in spin-lattice relaxation for these species. Thus, the anhydrous cement with the most clear reflection of the resonance from ^{31}P in belite (cement A) has been investigated by inversion-recovery ^{31}P MAS NMR as illustrated in Figure 3. These spectra clearly reveal that the 1.0 ppm resonance exhibits a longer spin-lattice relaxation time than the resonances constituting the broad peak in the range 10 ppm to –2 ppm. The zero-crossings for the resonances from the latter peak are slightly different and observed in

the range from 0.1 to 0.2 s. A subspectrum which mainly includes a single resonance from ^{31}P in belite is obtained for a recovery time of 0.2 s (*c.f.*, Figure 3). The narrow resonance from ^{31}P in belite shows its zero-crossing at approximately 1.0 – 1.5 s, giving a subspectrum for ^{31}P in alite which closely resembles the ^{29}Si MAS NMR spectrum of the M_{III} form for alite.[23,33] Employing a deconvolution of this spectrum as the subspectrum for ^{31}P in alite along with a single resonance at 1.0 ppm for ^{31}P in belite, allows estimation of the relative intensities for these two ^{31}P species at the different recovery times by simulations of the spectra in Figure 3. This approach assumes that the individual ^{31}P sites constituting the alite subspectrum exhibit the same relaxation time which is an acceptable approximation, considering the small dispersion in zero-crossings for these sites. The intensities from the simulations ($M_z(t)$) are shown relative to the equilibrium magnetization (M_0) by a plot of $\ln[1 - M_z(t)/M_0]$ as a function of the recovery time (t) in Figure 4a. The absence of a linear relationship between $\ln[1 - M_z(t)/M_0]$ and t demonstrates that the spin-lattice relaxation is not characterized by a single-exponential relationship. Following our recent analysis of the spin-lattice relaxation for ^{29}Si in alite and belite,[23] the ^{31}P intensities are analyzed using a "stretched exponential" relationship

$$M_z(t) = M_0[1 - (1 + \alpha)\exp(-(t/T_1')^{1/2})] \quad (1)$$

which has been derived for spin relaxation caused by paramagnetic impurities in the absence of spin diffusion.[35] Here, α is a constant related to pulse imperfections (*i.e.*, $\alpha = 1$ for an ideal 180° pulse) and T_1' the time constant for the stretched exponential spin-lattice relaxation. Assuming this relationship, a satisfactory fit to the experimental $M_z(t)$ intensities (Figure 4b) is obtained along with the T_1' spin-lattice relaxation times for ^{31}P in alite and belite listed in Table 2. These data are compared with the corresponding ^{29}Si spin-lattice relaxation times, determined recently for the alite and belite phases in the same cement.[23] For both spin nuclei it is observed that the relaxation times for the belite phase is significantly longer than those for the spins in alite. This

clear resemblance in ^{31}P and ^{29}Si relaxation behaviour strongly support our assignment of the two types of ^{31}P resonances to ^{31}P incorporated in alite and belite by a substitution mechanism where $(PO_4)^{3-}$ ions replace $(SiO_4)^{4-}$ sites.

The simulations of the inversion-recovery ^{31}P MAS NMR spectra also provide the equilibrium magnetization (M_0) for ^{31}P in alite and belite (Eq. 1) and thereby the molar ratio between ^{31}P in these two phases, *i.e.*, M_0(belite)/M_0(alite) = 0.54. This ratio implies that the belite and alite phases in cement A contain 0.16 wt.% and 0.29 wt.% P_2O_5, respectively, where it is assumed that all phosphate ions (0.45 wt.% P_2O_5) are incorporated in the silicate phases only. Combining these quantities with the bulk SiO_2 content (24.68 wt.%) and the belite/alite intensity ratio, I(belite)/I(alite) = 0.345 determined from ^{29}Si NMR,[23] allows calculation of the degree of Si for P substitution. This results in P/Si ratios of 0.021 and 0.013 for belite and alite, respectively. These data indicate that phosphorus is preferentially incorporated in belite rather than alite with a degree of replacement corresponding to roughly 2% of the SiO_4 tetrahedral sites. Futhermore, these P/Si ratios are below the estimated maximum degrees of P for Si replacement in alite and belite (2,3% and 3.3%, respectively), proposed from X-ray microanalysis of laboratory-made clinkers.[7]

Mechanism for incorporation of phosphorus in alite and belite. The ^{31}P isotropic chemical shifts, the magnitudes of the ^{31}P CSAs, and the T_1' relaxation times strongly indicate that phosphorus in anhydrous Portland cements is incorporated in the alite and belite phases. A direct proof for this kind of guest-ion incorporation can potentially be achieved by the detection of the ^{29}Si resonances from alite and belite in a double-resonance ^{31}P – ^{29}Si MAS NMR experiment that utilizes the distance dependence of the ^{31}P – ^{29}Si dipolar interactions ($\propto 1/r^3$) to selectively detect ^{29}Si sites in the near vicinity of the ^{31}P spins. Very recently, a similar approach has proven useful in the detection of fluoride guest ions in the alite phase of anhydrous Portland cement by $^{29}Si\{^{19}F\}$ CP/MAS and CP-REDOR experiments.[36] In this work attempts have been made to characterize phosphorus in cement A by $^{29}Si\{^{31}P\}$ CP/MAS NMR, employing a synthesized

sample of $Si_5O(PO_4)_6$ for the setup experiments with a ramped $^{29}Si\{^{31}P\}$ CP sequence as reported for $^{29}Si\{^{31}P\}$ CP/MAS NMR on this model compound.[37] However, this experiment turned out unsuccessfully for cement A which we ascribe to the very low concentration of $(PO_4)^{3-}$ ions combined with the low natural abundance of ^{29}Si (4.7 %), and considering the fact that only ^{31}P – ^{29}Si spin pairs with an internuclear distance less than approx. 5 Å are detected by this approach.

The observation of orthophosphate $(PO_4)^{3-}$ units in alite and belite by replacement of $(SiO_4)^{4-}$ tetrahedra is in agreement with the commonly suggested substitution mechanism from studies of guest ions in pure phases of alite and belite.[10-14] In cases where phosphorus is considered as the only element of substitution, charge-balance may be achieved by creation of Ca^{2+} ion vacancies,[10,12,13] *i.e.*,

$$2(SiO_4)^{4-} + Ca^{2+} \rightarrow 2(PO_4)^{3-} + \square_{Ca} \quad (2)$$

These vacancies may explain that only a small amount of phosphate can be incorporated in pure Ca_3SiO_5, corresponding to a maximum P/Si ratio of 0.036.[9] However, in commercial cements a number of other guest ions are incorporated in the calcium silicate phases, Mg, Al, Fe, S, Na, K, and F being the most common elements.[24] This opens for coupled substitution mechanisms, where charge-balance for replacement of two $(SiO_4)^{4-}$ ions is achieved by a $(PO_4)^{3-}$ ion and a trivalent cation. For example, it is has been shown that Al^{3+} guest ions in alite and belite are only present in tetrahedral coordination,[32] and thus, the introduction of phosphate may promote the incorporation of aluminium in alite and belite by the substitution mechanism

$$2(SiO_4)^{4-} \rightarrow (PO_4)^{3-} + (AlO_4)^{5-} \quad (3)$$

The formal replacement of Si^{4+} by P^{5+} and Al^{3+} agrees well with the similarity in ionic radii for these ions, *i.e.*, 0.40 Å, 0.31 Å, and 0.53 Å,[38] respectively. However, larger ions such as Fe^{3+} (0.79 Å) may preferentially substitute for the Ca^{2+} ions (1.14 Å), which may lead to a substitution

mechanism of the type

$$(SiO_4)^{4-} + 2Ca^{2+} \rightarrow (PO_4)^{3-} + Fe^{3+} + \square_{Ca} \quad (4)$$

A similar substitution mechanism was proposed in a study of the combined effect of manganese and phosphorus on the formation of monoclinic alite,[10] where electron paramagnetic resonance investigations revealed the presence of divalent Mn^{2+} ions in octahedral sites, suggesting a heterovalent substitution of $(SiO_4)^{4-} + 2½Ca^{2+}$ by $(PO_4)^{3-} + 2Mn^{2+} + ½\square_{Ca}$. It is interesting to note that the paramagnetic Fe^{3+} ions have a significant impact on the ^{31}P MAS NMR spectra, as shown in Figure 2 for cements A and C. Our recent study of these cements by ^{29}Si NMR revealed that alite and belite in cement C contain a higher amount of Fe^{3+} guest ions as compared to the white Portand cement (cement A).[23] Thus, the large number and high-intensity of the spinning sidebands in Figure 2b indicate that the Fe^{3+} ions are in the near vicinity of the $(PO_4)^{3-}$ units, suggesting that the incorporation of phosphate is at least to some extent charge-balanced by a coupled substitution mechanism of the type given in Eq. (4). This may have an potential application for white Portland cement, which generally contains small amounts of Fe_2O_3, since the colour of cement is strongly influenced by the amount of iron, its oxidation state and the nature of its next-nearest neighbours.[39] Thus, a coupling between the $(PO_4)^{3-}$ units and the Fe^{3+} ions may potentially shift the frequency of maximum absorption from the visible region into the UV region of the electromagnetic spectrum, as reported recently for clinkers doped with SO_3, where this shift was ascribed to the location of the $(SO_4)^{2-}$ ions in the region of the Fe^{3+} sites.[39] Thereby, a controlled introduction of these guest ions in the clinkers may potentially be used to modify the colour of white Portland cement.

^{31}P MAS and $^{31}P\{^1H\}$ CP/MAS NMR of hydrated samples. The hydration of cement A is studied by ^{31}P MAS NMR (Figure 5) after 1, 28, and 180 days of hydration. At first sight, the main change in these spectra is the intensity reduction for the narrow resonance from $(PO_4)^{3-}$ in

belite after prolonged hydration. However, phosphate species with ^{1}H in their near vicinity can be selectively detected by $^{31}P\{^{1}H\}$ CP/MAS NMR and the comparison of the ^{31}P MAS and $^{31}P\{^{1}H\}$ CP/MAS NMR spectra for cement A hydrated for 28 days (Figure 6) clearly reveals that the hydrous $(PO_4)^{3-}$ species formed upon consumption of phosphorus in alite and belite have resonances in the same spectral range as observed for ^{31}P in alite. This is supported by a closer examination of the spectra in Figure 5 which shows that the high-frequency shoulder at 7 ppm (Figure 5a) has almost vanished even after one day of hydration, indicating the conversion of the phosphorus guest ions in alite into hydrated phosphate species. Thus, the ^{31}P MAS NMR spectra indicate that the ^{31}P sites in alite are partly consumed during the early hydration (Figure 5b) whereas the main reaction for phosphate in belite is observed after somewhat longer hydration times. This is fully supported by the analysis of ^{29}Si MAS NMR spectra of the same hydrated cement samples which show a degree of reaction of 39% and 85% for alite after one and 28 days of hydration, respectively, whereas the first clear indication of belite hydration is observed after 14 days. The degree of reaction for belite is determined to 24 % and 61% after 28 and 180 days of hydration, respectively.

The close resemblance in ^{31}P chemical shift for the anhydrous and hydrated $(PO_4)^{3-}$ species strongly suggests that the hydrated phosphate units are formed in the near vicinity of the Ca^{2+} ions and potentially also silicate sites. Moreover, the broad peak in the $^{31}P\{^{1}H\}$ CP/MAS NMR spectrum (from 8 ppm to –1 ppm) shows the presence of a range of slightly different $(PO_4)^{3-}$ environments, potentially arising from $(PO_4)^{3-}$ ions in a disordered/amorphous phase. Thus, we assign the resonance at 3 ppm in the $^{31}P\{^{1}H\}$ CP/MAS NMR spectrum to hydrated PO_4 species incorporated in the disordered calcium-silicate-hydrate (C-S-H: $(CaO)_x(SiO_2)_y(H_2O)_z$) phase, the main hydration product resulting from Portland cement hydration. The $(PO_4)^{3-}$ ions are most likely incorporated in the C-S-H interlayers between the defect dreierketten silicate chains sandwiching a calcium-oxide layer with seven-fold coordinated Ca^{2+} ions. This assignment is based on the fact that replacement of either a chain (Q^2) or end-group (Q^1) SiO_4 tetrahedron by a

PO_4 unit would lead to a distinct shift of the ^{31}P resonance towards lower frequency. Furthermore, this kind of SiO_4 substitution would also result in a significant ^{31}P chemical shift anisotropy, as generally found for pyro- and metaphosphates,[16,34] which is not observed in the full $^{31}P\{^1H\}$ CP/MAS spectrum recorded with "slow-speed" spinning (ν_R = 5.0 kHz). Finally, we note that the present analysis can not exclude that a less-ordered calcium phosphate hydrate phase, including orthophosphate units, accounts for the broadened resonance observed with a center at ~3 ppm by $^{31}P\{^1H\}$ CP/MAS NMR.

Conclusions

This work has shown that ^{31}P MAS NMR is a very suitable technique for studying small quantities of phosphorus in anhydrous and hydrated Portland cements, corresponding to bulk P_2O_5 contents below 0.5 wt.%. Two types of $(PO_4)^{3-}$ species have been identified in the ^{31}P MAS NMR spectra of the anhydrous cements. The ^{31}P isotropic chemical shifts, the magnitudes of the chemical shift anisotropies, and the ^{31}P spin-lattice relaxation times determined for these sites strongly indicate that the small amount of phosphorus in anhydrous Portland cement is incorporated in the calcium silicate phases, alite and belite, by substitution of the isolated $(SiO_4)^{4-}$ tetrahedra in these structures by $(PO_4)^{3-}$ ions. This result is in accord with the type of substitution proposed in earlier studies of pure phases of alite and belite[10-14] and of laboratory clinkers.[7] For a white Portland cement including 0.45 wt.% P_2O_5, the simulated intensities of the inversion-recovery ^{31}P MAS NMR spectra combined with the calcium silicate phase analysis from ^{29}Si NMR give replacements of 1.3% and 2.1% of the $(SiO_4)^{4-}$ units by $(PO_4)^{3-}$ ions in alite and belite, respectively, indicating a small preference for phosphorus incorporation in belite as compared to alite, even at low P_2O_5 contents. A coupling between the ^{31}P spins and paramagnetic centers (Fe^{3+}) have been observed for the ordinary Portland cements, which suggests that the incorporation of $(PO_4)^{3-}$ in alite and belite is at least to some extent charge-balanced by a coupled substitution mechnanism where Fe^{3+} ions enters these phases by substitution for Ca^{2+} ions.

The ^{31}P MAS NMR spectra of the hydrated Portland cement have revealed that the

hydrated phosphate species exhibit the same chemical shifts and small chemical shift anisotropies as the ^{31}P sites in alite. Thus, selective detection of these species requires the use of $^{31}P\{^{1}H\}$ CP/MAS NMR. The broad resonance (from 8 ppm to −1 ppm) with maximum intensity at ~3 ppm, observed by this experiment, is assigned to $(PO_4)^{3-}$ ions incorporated in the interlayer region of the calcium-silicate-hydrate (C-S-H) phase, formed upon hydration of alite and belite.

The high sensitivity of ^{31}P MAS NMR, combined with a range of single- and double resonance NMR experiments, show strong promises for the application of this approach in a range of studies focusing on phosphorus guest-ion incorporation in cement phases. Thus, this technique may be conveniently used in investigations of the applicability of alternative phosphorus-containing (bio)fuels in the production of Portland cement.

Acknowledgements

The use of the facilities at the Instrument Centre for Solid-State NMR Spectroscopy, Aarhus University, sponsored by the Danish Natural Science Research Council, the Danish Technical Science Research Council, Teknologistyrelsen, Carlsbergfondet, and Direktør Ib Henriksens Fond, is acknowledged. The Danish Council for Independent Research | Natural Sciences (FNU) is acknowledged for equipment grants. S.L. Poulsen would like to thank NANOCEM, a European industrial/academic partnership for fundamental research on cementitious materials, for financial support.

References

(1) U.S. Department of the Interior, U.S. Geological Survey, *Mineral Commodity Summaries 2009*, United States Government Printing Office, Washington DC, U.S.A., 2009.

(2) Damtoft, J.S.; Lukasik, J.; Herfort, D.; Sorrentino, D.; Gartner, E.M. *Cem. Concr. Res.* **2008**, *38*, 115–127.

(3) Mokrzycki, E.; Uliasz-Bochenczyk, A. *Applied Energy* **2003**, *74*, 95–100.

(4) Kääntee, U.; Zevenhoven, R.; Backman, R.; Hupa, M. *Fuel Processing Technology* **2004**, *85*, 293–301.

(5) Trezza, M.A.; Scian, A.N. *Cem. Concr. Res.* **2005**, *35*, 438–444.

(6) Opoczky, L.; Gavel, V. *Int. J. Miner. Process.* **2004**, *74S*, S129–S136.

(7) Nastac, D.C.; Kääntee, U.; Liimatainen, J.; Hupa, M.; Muntean, M. *Adv. Cem. Res.* **2007**, *19*, 93–100.

(8) Nurse, R.W. *J. Appl. Chem.* **1952**, *2*, 708–716.

(9) Gutt, W. *Proc. 5th Int. Congr. Cem. Chem.* Tokyo, Oct. 7 – 11, 1968, Onogi Shigeharu, Japan, 1968, Vol. I, pp. 93–105.

(10) Diouri, A.; Boukhari, A.; Aride, J.; Puertas, F.; Vazquez, T. *Cem. Concr. Res*. **1997**, *27*, 1203–1212.

(11) Qotaibi, Z.; Diouri, A.; Boukhari, A.; Aride, J.; Rogez, J.; Castanet, R. *World Cem.* **1999**, *30*, 77–80.

(12) Fukuda, K.; Taguchi, H. *Cem. Concr. Res.* **1999**, *29*, 503–506.

(13) Benarchid, My.Y.; Diouri, A.; Boukhari, A.; Aride, J.; Rogez, J.; Castanet, R. *Cem. Concr. Res*. **2004**, *34*, 1873–1879.

(14) Noirfontaine, M.-N.; Tusseau-Nenez, S.; Signes-Frehel, M.; Gasecki, G.; Girod-Labianca, C. *J. Am. Ceram. Soc.* **2009**, *92*, 2337–2344.

(15) Turner, G.L.; Smith, K.A.; Kirkpatrick, R.J.; Oldfield, E. *J. Magn. Reson.* **1986**, *70*, 408–415.

(16) Hartmann, P.; Vogel, J.; Schnabel, B. *J. Magn. Reson. Ser. A.* **1994**, *111*, 110–114.

(17) DeCanio, E.C.; Edwards, J.C.; Scalzo, T.R.; Storm, D.A.; Bruno, J.W. *J. Catal.* **1991**, *132*, 498–511.

(18) Caro, J.; Bülow, M.; Derewinski, M.; Haber, J.; Hunger, M.; Kärger, J.; Pfeifer, H.; Storek, W.; Zibrowius, B. *J. Catal.* **1990**, *124*, 367–375.

(19) Seo, G.; Ryoo, R. *J. Catal.* **1990**, *124*, 224–230.

(20) Stebbins, J.F.; Kim, N.; Brunet, F.; Irifune, T. *Eur. J. Mineral.* **2009**, *21*, 667 – 671.

(21) van Eck, E.R.H.; Kentgens, A.P.M.; Kraus, H.; Prins, R. *J. Phys. Chem.* **1995**, *99*, 16080 –16086.

(22) Damodaran, K.; Wiench, J.W.; Cabral de Menezes, S.M.; Lam, Y.L.; Trebosc, J.; Amoureux, J.-P.; Pruski, M. *Micropor. Mesopor. Mater.* **2006**, *95*, 296–305.

(23) Poulsen, S.L.; Kocaba, V.; Le Saoût, G.; Jakobsen, H.J.; Scrivener, K.L.; Skibsted, J. *Solid State Nucl. Magn. Reson.* **2009**, *36*, 32–44.

(24) Taylor, H.F.W. *Adv. Cem. Res.* **1989**, *2*, 73–77.

(25) Blackwell, C.S.; Patton, R.L. *J. Phys. Chem.* **1984**, *88*, 6135–6139.

(26) Martens, J.A.; Feijen, E.; Lievens, J.L.; Grobet, P.J.; Jacobs, P.A. *J. Phys. Chem.* **1991**, *95*, 10025–10031.

(27) Fyfe, C.A.; Meyer zu Altenschildesche, H.; Wong-Moon, K.C.; Grondey, H.; Chezeau, J.M. *Solid State Nucl. Magn. Reson.* **1997**, *9*, 97–106.

(28) Nishi, F.; Takeuchi, Y.; Maki, I. *Zeit. Kristallogr.* **1985**, *172*, 297–314.

(29) Jost, K.H.; Zeimer, B.; Seydel, R. *Acta Crystallogr.* **1977**, *B33*, 1696–1700.

(30) Mondal, P.; Jeffery, J.W. *Acta Crystallogr.* **1975**, *B31*, 689–697.

(31) Colville, A.A.; Geller, S. *Acta Crystallogr.* **1972**, *B28*, 3196–3200.

(32) Skibsted, J.; Jakobsen, H.J.; Hall, C. *J. Chem. Soc. Faraday Trans.* **1994**, *90*, 2095–2098.

(33) Skibsted, J.; Jakobsen, H.J.; Hall, C. *J. Chem. Soc. Faraday Trans.* **1995**, *91*, 4423–4430.

(34) Fyfe, C.A.; Meyer zu Altenschildesche, H.; Skibsted, J. *Inorg. Chem.* **1999**, *38*, 84–92.

(35) Tse, D.; Hartmann, S.R. *Phys. Rev. Lett.* **1968**, *21*, 511–514.

(36) Tran, T.T.; Herfort, D.; Jakobsen, H.J.; Skibsted, J. *J. Am. Chem. Soc.* **2009**, *131*, 14170–14171.

(37) Lejeune, C.; Coelho, C.; Bonhomme-Coury, L.; Azaïs, T. ; Maquet, J. ; Bonhomme, C. *Solid State Nucl. Magn. Reson.* **2005**, *27*, 242–246.

(38) Shannon, R.D. *Acta Crystallogr.* **1976**, *A32*, 751–767.

(39) Macphee, D.E., Duffy, J.A.; Herfort, D. *Proc. 12th Int. Congr. Cem. Chem.* Montreal, Canada, July 8 – 13, 2007, paper TH1–09.5 (12 pp).

Table 1

Bulk oxide composition (wt.%) for the studied Portland cements from XRF analysis and quantities (wt.%) of alite and belite determined from ^{29}Si MAS NMR spectroscopy[a]

Cement	CaO	SiO_2	Al_2O_3	Fe_2O_3	MgO	SO_3	K_2O	Na_2O	P_2O_5	Alite[b]	Belite[b]
A	68.67	24.68	2.11	0.43	0.58	1.82	0.06	0.17	0.45	72.4	20.0
B	61.29	20.51	5.10	3.33	2.82	2.78	1.40	0.24	0.37	59.1	17.4
C	64.18	21.01	4.63	2.60	1.82	2.78	0.94	0.20	0.40	62.4	16.4
D	63.45	21.03	5.01	2.54	2.05	3.01	1.02	0.26	0.08	70.3	10.2

(a) The cements A – D are identical to cements A – D in a recent ^{29}Si MAS NMR and powder X-ray diffraction investigation focusing on the quantification of alite and belite by different approaches.[23] Cement A is a white Portland cement and cements B – D are ordinary Portland cements. (b) It is assumed that alite and belite have the average compositions proposed by Taylor.[24]

Table 2

Time constants for the ^{31}P and ^{29}Si spin-lattice relaxation (T_1') for alite and belite in cement A from ^{31}P and ^{29}Si inversion-recovery MAS NMR spectra

Observed nucleus	T_1' (alite)[a] (s)	T_1' (belite)[a] (s)
^{31}P	0.26	2.0
^{29}Si[b]	0.24	8.2

(a) Spin-lattice relaxation time corresponding to a stretched exponential relationship (*c.f.*, Eq. 1).

(b) The ^{29}Si relaxation times are from our recent study.[23]

Figure Captions

Figure 1

^{31}P MAS NMR spectra (9.4 T) of the anhydrous Portland cements (A, B, C, and D), obtained with a spinning speed of ν_R = 12.0 kHz, a 60-s relaxation delay, and 1,000 – 4,300 scans. The spectra are shown with the same vertical expansion and thereby the intensities reflect the bulk content of phosphorus in the cements.

Figure 2

^{31}P MAS NMR spectra of (a) cement A and (b) cement C recorded at 14.1 T using a spinning speed of ν_R = 4.0 kHz, a 90^o-excitation pulse, a 15-s relaxation delay, and (a) 10,000 and (b) 5,360 scans. The inset illustrates the isotropic peaks for cement A.

Figure 3

Inversion-recovery ^{31}P MAS NMR spectra (9.4 T, ν_R = 12.0 kHz) for cement A, illustrating the difference in spin-lattice relaxation for the $(PO_4)^{3-}$ guest ions in alite and belite. The expansions above and below the array of spectra correspond to the zero-crossings for ^{31}P in alite and belite at recovery times of 0.2 s and 1.5 s, respectively. The recovery times (in seconds) are indicated for the individual spectra.

Figure 4

Semilog plots of $[1 - M_z(t)/M_0]$ as a function of the recovery time t (a) and $\sqrt{t}$ (b) which should result in linear relationships for single-exponential and stretched-exponential spin-lattice relaxation processes, respectively. The graphs include data for ^{31}P in alite (filled circles) and belite (open circles) obtained from deconvolutions of the inversion-recovery ^{31}P MAS NMR spectra of cement A shown in Figure 3. The dashed curves/lines correspond to a fit of the data to a stretched exponential relationship (Eq. 1), resulting in the ^{31}P relaxation times in Table 2.

Figure 5

^{31}P MAS NMR spectra (9.4 T, ν_R = 12.0 kHz) of cement A before hydration (a) and after one day (b), 28 days (c), and 180 days (d) of hydration. The experiments employed a 45°-excitation pulse, a 60-s relaxation delay, and 1,000 – 1,300 scans.

Figure 6

(a) ^{31}P MAS and (b) ^{31}P{^{1}H} CP/MAS NMR (9.4 T) of cement A after 28 days of hydration, obtained with spinning speeds of ν_R = 12.0 kHz and 5.0 kHz for, respectively. The spectrum in (a) is identical to the spectrum in Figure 5c. The ^{31}P{^{1}H} CP/MAS NMR spectrum employed an optimum CP contact time of 1.0 ms, a 4-s repetition delay, and 16,384 scans.

Figure 1

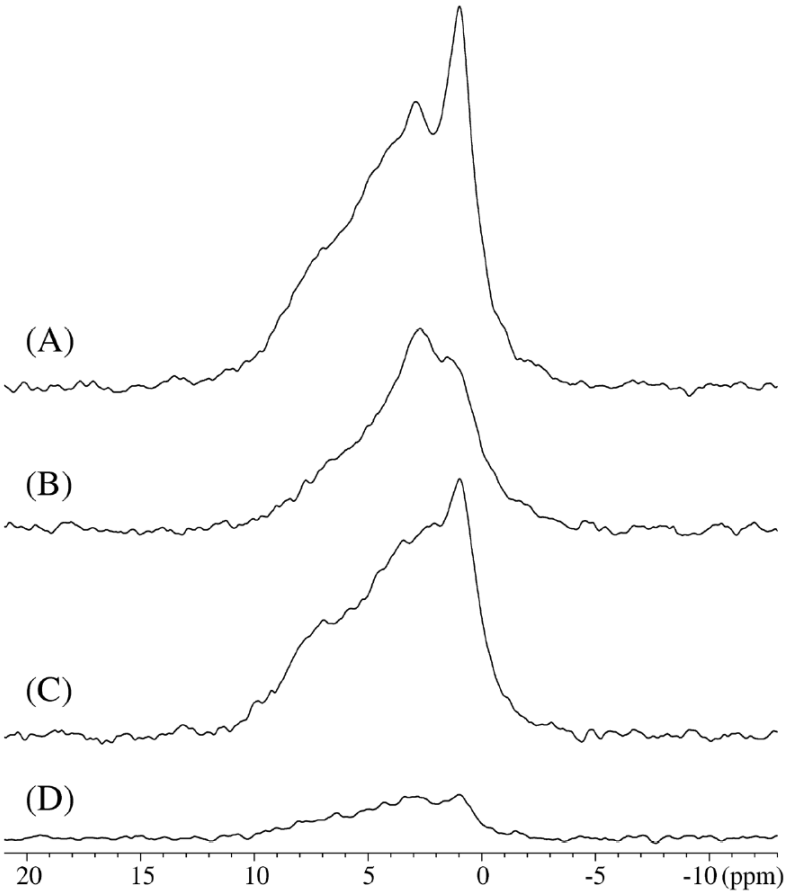

Figure 2

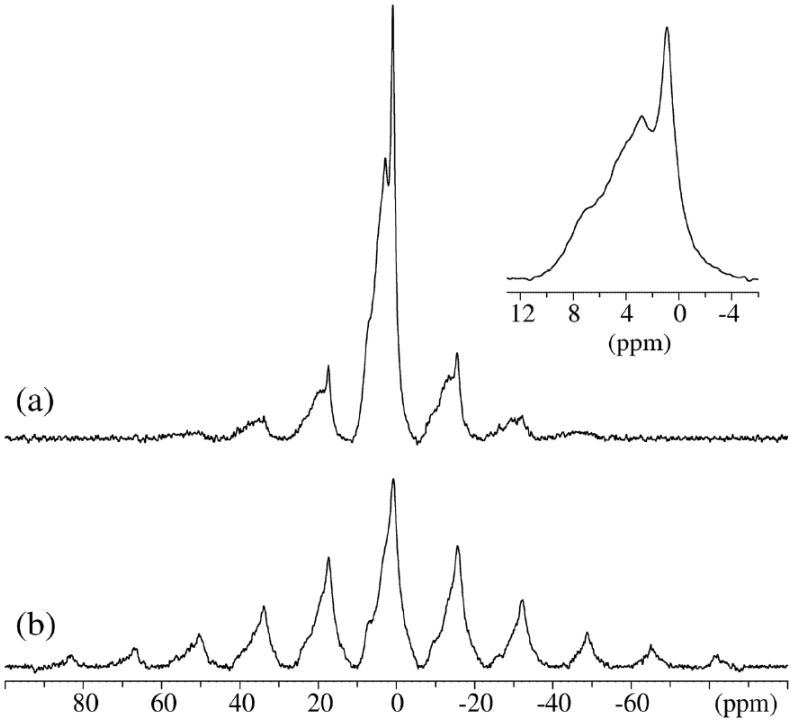

Figure 3

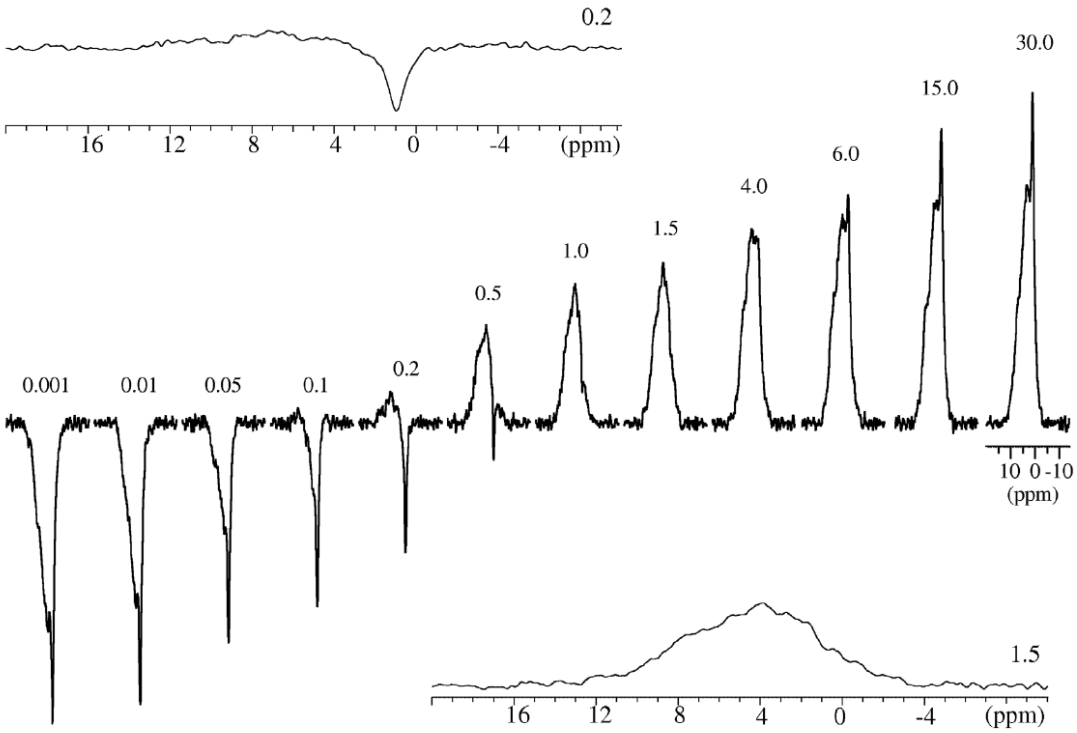
0.2
16
12
8
4
0
-4
(ppm)
30.0
15.0
6.0
4.0
1.5
1.0
0.5
0.2
0.1
0.05
0.01
0.001
10 0 -10
(ppm)
1.5
16
12
8
4
0
-4
(ppm)

Figure 4

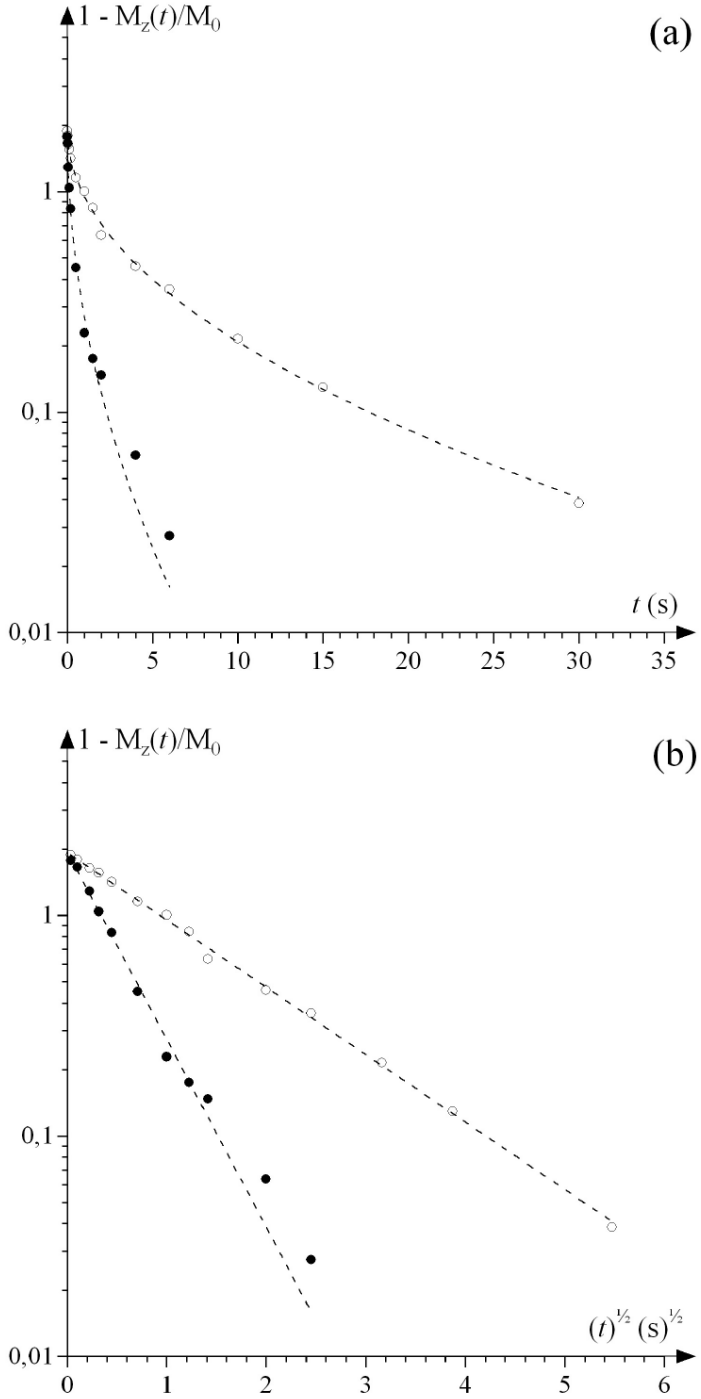
1 - M_Z(t)/M_0
(a)
1
0,1
0,01
t (s)
0
5
10
15
20
25
30
35
1 - M_Z(t)/M_0
(b)
1
0,1
0,01
(t)^½ (s)^½
0
1
2
3
4
5
6

Figure 5

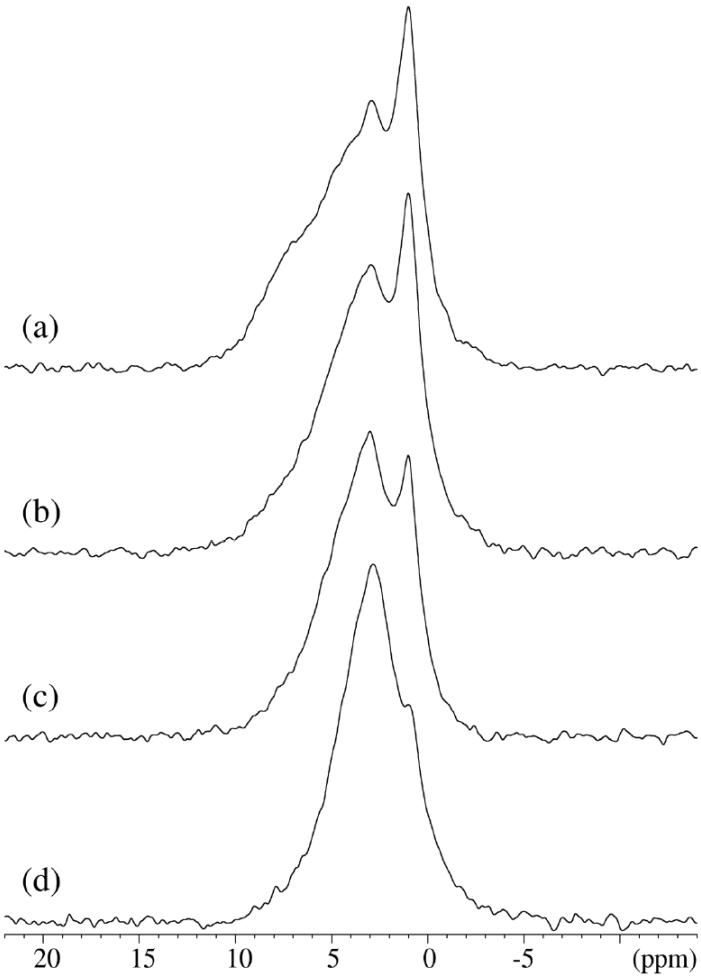

Figure 6

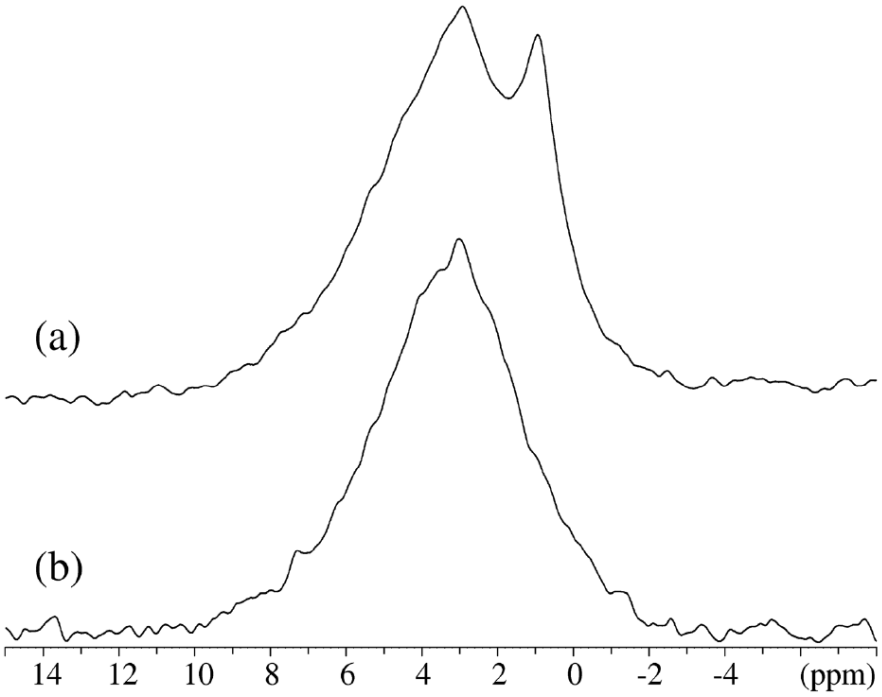

Table of Contents Synopsis

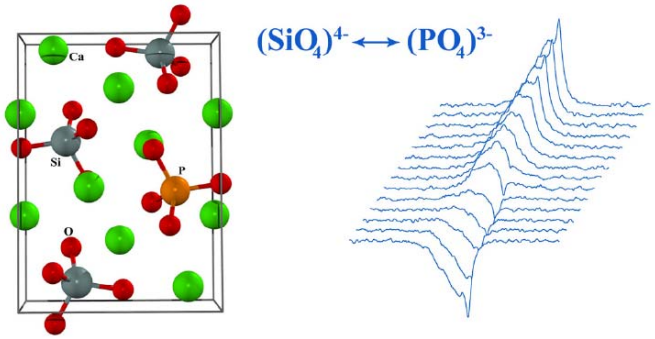

^{31}P MAS NMR is shown to be a convenient technique for studying small quantities of phosphorus in anhydrous and hydrated Portland cements. Phosphate ions are incorporated in the calcium silicates, alite and belite, by substitution for $(SiO_4)^{4-}$ tetrahedra, most likely by a coupled substitution mechanism where Fe^{3+} also replaces Ca^{2+} ions. For a white Portland cement it is found that 1.3% and 2.1% of the Si sites in alite and belite, respectively, are replaced by phosphorus.

Paper III

Methodologies for measuring the degree of reaction in Portland cement blends with supplementary cementitious materials by ^{27}Al and ^{29}Si MAS NMR spectroscopy

Søren L. Poulsen, Hans J. Jakobsen, Jørgen Skibsted

17th IBAUSIL – Internationale Baustofftagung, Weimar, Germany, September 23 – 26, 2009, Vol. 1, p. 177 – 188.

ibausil

S. L. Poulsen, H. J. Jakobsen, J. Skibsted

Methodologies for measuring the degree of reaction in Portland cement blends with supplementary cementitious materials by ^{27}Al and ^{29}Si MAS NMR spectroscopy

Introduction

The global demand for Portland cement has more than doubled during the last two decades, primarily as a result of the increased consumption of concrete in the developing countries, and is approaching three billion tonnes per year /1,2/. Furthermore, it is forecasted that the cement consumption will at least double by the year 2050. For every tonne of cement produced, 650 – 900 kg CO_2 is emitted amounting to more than two billion tonnes worldwide. Thus, cement production accounts for 5 – 8% of the global anthropogenic CO_2 emission and the reduction of CO_2 emission associated with cement production represents probably the most important and urgent challenge for the cement industry.

Roughly 40% of the CO_2 comes from the fuel used to heat the cement kilns and drive the mills whilst 60% originates from the decarbonation of limestone, required to form the main cement clinker phases. Common approaches to reduce the CO_2 emission are the use of biofuels in the cement kilns and a partial replacement of the cement clinkers by supplementary cementitious materials (SCMs). Traditional kiln fuels are gas, oil, and coal but waste materials, such as meat and bone meal, sewage sludge, used oils, waste tyres, solvents, and a range of other industrial by-products, can be employed as alternative fuels, thereby reducing the net CO_2 emission from cement production /3,4/. The largest potential for CO_2 reduction lies in the chemical reaction source ($CaCO_3$ decomposition) by partial replacement of cement with SCMs although these have different chemistries and perform differently in concrete.

SCMs are finely divided materials with pozzolanic or latent hydraulic properties and the most commonly used types include blastfurnace slags from pig iron production, fly ashes from coal burning, silica fume from the production of ferrosilicon, natural pozzolans, calcined shale/clays and rice husk ash /5-7/. These inorganic materials not only act as fillers they also take part in the hydration reactions and thus contribute to the strength development of concrete. Moreover, SCMs can have a positive effect on the workability of fresh concrete and may reduce the heat generation associated with hydration and in this manner diminish the potential risk of thermal cracking in massive construction elements. Anhydrous mixtures of Portland cement and SCMs, referred to as blended cements, are classified as cement types II – V in the European prestandard for common cements (ENV 197-1) and constitute about two-thirds of the produced

The development of new blended cements including either new SCMs or an increased replacement of the Portland cement obviously requires reliable methods to quantify the degree of reaction of the SCMs as well as the principal phase of the Portland cements in the actual blends. Several techniques are employed and currently being improved for measuring the reactivity of the SCMs in blended cement, *e.g.* powder X-ray diffraction, thermal analysis (DTA), solid-state nuclear magnetic resonance (NMR), and microscopy based techniques (optical, SEM or TEM). Each of these techniques can be advantageously used for specific SCMs and blended systems, however, neither of them seem to be appropriate for the whole span of blended cement materials.

This paper focuses on the application of high-resolution magic-angle spinning (MAS) NMR techniques for quantification of the degree of reaction for SCMs and the alite and belite phases in the blended cements. The studied SCMs all include silicate species and the quantitative results are derived from the analysis of ^{29}Si and ^{27}Al MAS NMR spectra. The main advantage of this approach is that the ^{29}Si and ^{27}Al chemical shifts primarily depend on local order, thereby detecting amorphous and crystalline phases in an equal manner. Thus, the degree of reaction can be obtained for several systems from deconvolution or integration of the intensities in the ^{29}Si MAS NMR spectra. The main disadvantage of the technique is the strong interaction of the ^{29}Si and ^{27}Al spins with paramagnetic species, preventing analysis of iron-rich cements or SCMs (roughly $m(Fe_2O_3) > 5$ wt%), and the low sensitivity of the method (e.g. 4.7% natural abundance of ^{29}Si) which implies that only cement – SCM pastes (and not concretes) can be investigated in a reasonably time.

Since the pioneering ^{29}Si MAS NMR studies of Portland cement hydration in the 1980'ies by the NMR groups in Tallinn – East Berlin /8,9/ and Oxford /10,11/, this tool has been used to monitor the reaction for a range of different SCMs in Portland cement mixtures, including silica fume /12,13/, slags /14,15/, clay minerals /16/, and fly ash /17/. This paper includes studies of slags, fly ash, silica fume and a natural pozzolan in Portland cement blends with the main focus on experimental approaches and simulation tools to improve the quantitative analysis of the ^{29}Si and ^{27}Al MAS NMR spectra.

Portland cements and SCMs

The degree of reaction for the SCMs has been studied in two series of hydration using a white Portland cement (WPC) and an ordinary Portland cement (OPC). The mixtures of these cements with the SCMs contained 10 wt% silica fume (SF), 30 wt% fly ash (FA), 30 wt% natural pozzolan (NP) or 40 wt% of slag 1 or slag 2 (S1, S2). Elemental compositions of the anhydrous materials were determined by XRF analysis and are summarized in Table 1.

The hydrated samples were prepared using water/powder ratios in the range 0.40 – 0.45 depending on the density of the anhydrous powder, thus keeping the water/powder

volume ratio constant for all pastes. After mixing with a motorized stirrer for 5 min., the paste was cast in a capped cylindrical plastic container (50 mL) and stored in a temperature-regulated laboratory (21 ± 2 °C). After 24 hours the sample was demoulded and subsequently placed in a closed plastic container (500 mL) filled with tap water. The hydration was stopped after 1, 2, 3, 7, 14, 28, 90, and 180 days by grinding ~5 g of the sample to a fine powder, followed by mixing with 50 mL of isopropyl alcohol (99%) for one hour using a magnetic stirrer. Finally, the suspension was filtered and the sample dried overnight in a desiccator.

Table 1: Bulk metal-oxide composition (wt%) for the studied Portland cements and SCMs determined by XRF analysis.

Sample	CaO	SiO_2	Al_2O_3	Fe_2O_3	MgO	SO_3	K_2O	Na_2O	LOI[a]
WPC[b]	68.67	24.68	2.11	0.43	0.58	1.82	0.06	0.17	0.97
OPC[c]	64.18	21.01	4.63	2.60	1.82	2.78	0.94	0.20	1.26
Silica fume (SF)	0.24	98.51	0.25	0.09	0.09	0.01	0.26	0.05	0.46
Fly ash (FA)	0.10	72.20	24.30	0.43	0.09	0.09	0.32	0.07	-
Nat. pozzolan (NP)	3.35	64.71	13.87	2.48	1.24	0.47	2.20	3.04	-
Slag 1 (S1)	41.59	36.61	12.21	0.85	7.18	0.63	0.28	0.18	0.03
Slag 2 (S2)	32.48	34.60	19.98	0.47	9.17	1.99	0.78	0.16	0.37

[(a)] Loss on ignition (wt%). [(b)] White Portland cement corresponding to cement A in ref. /18/. [(c)] Ordinary Portland cement corresponding to cement C in ref. /18/.

NMR experiments

The ^{29}Si MAS NMR spectra were acquired on a Varian INOVA-400 spectrometer (9.4 T) using a home-built CP/MAS probe for 5 mm o.d. zirconia (PSZ) rotors (120 μL sample volume). The spectra were recorded using a pulse width of 2.2 μs (~45° excitation pulse), a spinning speed of ν_R = 12.0 kHz, a relaxation delay of 30 s, and 2000 – 3000 scans. The ^{27}Al MAS NMR spectra were recorded on a Varian Direct Drive VNMRS-600 spectrometer (14.1 T), employing a home-built CP/MAS probe for 4 mm o.d. zirconia rotors (80 μL), a spinning speed of ν_R = 13.0 kHz, a relaxation delay of 2 s, and typically 2000 scans. The experiments used a pulse width of 0.5 μs for an ^{27}Al rf field strength of $\gamma B_1/2\pi \approx 50$ kHz and ^{1}H decoupling ($\gamma B_2/2\pi \approx 60$ kHz) during acquisition. The ^{29}Si and ^{27}Al NMR spectra and isotropic chemical shifts are referenced to tetramethyl silane (TMS) and a 1.0 M aqueous solution of $AlCl_3 \cdot 6H_2O$, respectively.

Results and Discussion

^{29}Si and ^{27}Al MAS NMR spectra of the anhydrous Portland cements and SCMs are illustrated in Fig. 1. The ^{29}Si MAS NMR spectra have been recorded using "high-speed spinning" (ν_R = 12.0 kHz), following our recent study of anhydrous Portland cements

/18/ which showed that an improved quantification of the alite and belite intensities is achieved from deconvolution of such spectra, mainly as a result of the reduced spinning sideband intensities. The ^{29}Si MAS NMR spectra of the Portland cements are composed of a narrow resonance at –71.3 ppm from belite (Ca_2SiO_4) superimposed on a broader peak originating from the 18 non-equivalent ^{29}Si sites in the M_{III} form of alite (Ca_3SiO_5). Deconvolution of these lineshapes, employing our recent improvement /18/ of an earlier described procedure /19/, results in quantities of 72.4 ± 2.5 wt% alite, 20.0 ± 1.5 wt% belite for the white Portland cement (WPC) and 62.4 ± 2.3 wt% alite, 16.4 ± 1.4 wt% belite for the ordinary Portland cement (OPC), assuming the compositions of alite and belite proposed by Taylor /20/. The ^{29}Si MAS spectrum of silica fume contains a broad resonance from approx. –100 to –125 ppm, in agreement with the amorphous nature of this material, containing fully condensed SiO_4 tetrahedra only (i.e., Q^4 sites). Similar silicate species are also present in the fly ash sample, which includes additional low-intensity resonances from –90 ppm to –102 ppm. These peaks originate most likely from layered or fully condensed SiO_4 tetrahedra with different degrees of Al^{3+} ions in

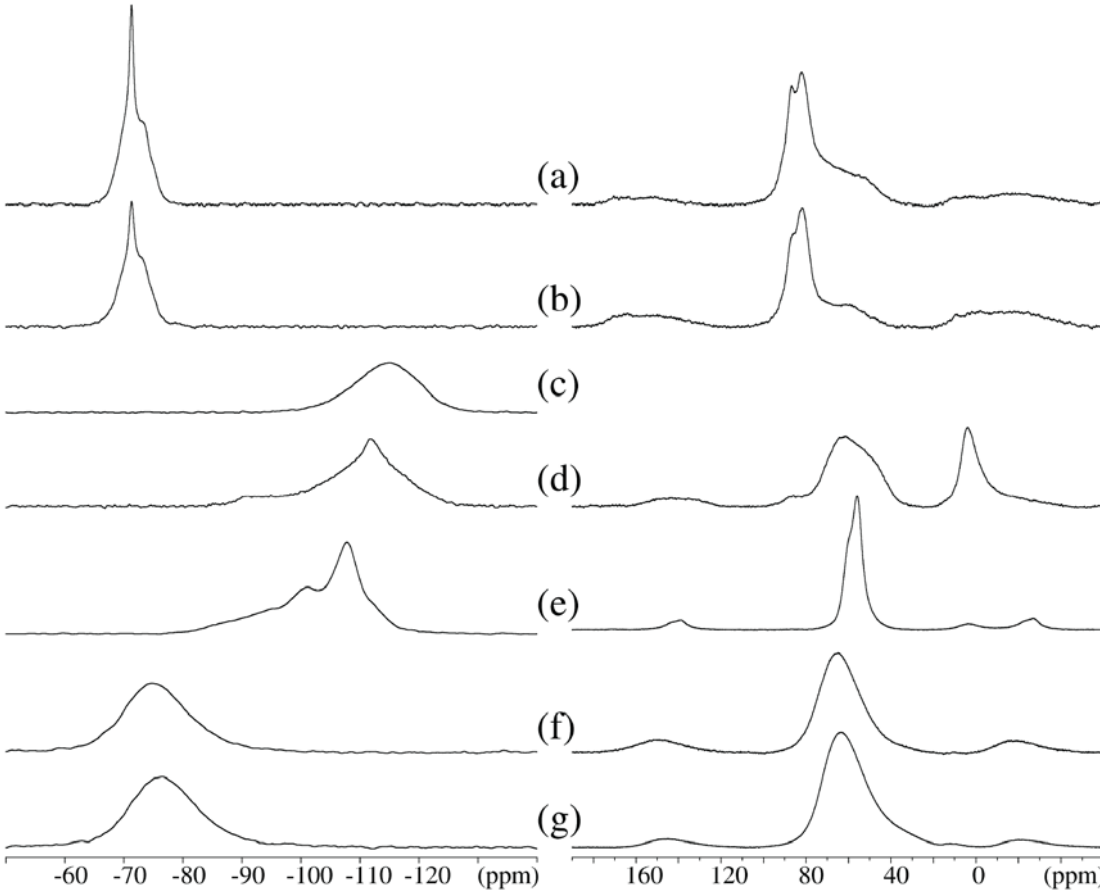

Fig. 1 ^{29}Si MAS NMR spectra (9.4 T, ν_R = 12.0 kHz, left column) and ^{27}Al MAS NMR spectra (14.1 T, ν_R = 13.0 kHz, right column) of the pure anhydrous samples of (a) WPC, (b) OPC, (c) silica fume, (d) fly ash, (e) natural pozzolan, (f) slag 1 (S1), and (g) slag 2 (S2). The spectra are not shown on normalized intensity scales.

the second-coordination spheres, i.e., Q^3(mAl) and Q^4(nAl) sites. The ^{29}Si MAS NMR spectrum of the natural pozzolan allows identification of four overlapping resonances at –95, –101, –108, and –113 ppm and a broadened low-intensity peak ranging from approx. –85 to –95 ppm. An XRD analysis of the pozzolan reveals that it is mixture of several phases including albite ($NaAlSi_3O_8$), clinoptilolite ($(Na,K)_6Al_6(Si_{30}O_{72})\cdot 20H_2O$), sanidine ($(Na,K)(Si,Al)_4O_8$), magnetite ($Fe_3O_4$) and silica ($SiO_2$). From the ^{29}Si chemical shifts reported in the literature for these silicates /21,22/ and similar natural pozzolans /23/, it is apparent that the tallest resonance (–108 ppm) includes contributions from silica, albite, and clinoptilolite and that the weak shoulder at –113 ppm corresponds to a Q^4(0Al) site of clinoptilolite. This phase also contributes to the resonance at –101 ppm which also includes contributions from sanidine and albite. These minerals contain additional peaks in the range –93 to –97 ppm and thus, they account for the weak shoulder at –95 ppm. The ^{29}Si MAS NMR spectra of the two slags are quite similar and exhibit a broad, featureless resonance from –65 to –90 ppm. ^{29}Si MAS NMR spectra of similar slags have been reported in the literature /14,24/ and assigned to a range of different silicate species, i.e., Q^{0-3} sites with different degrees of Al in the second coordination-sphere, present in an amorphous glass-like phase.

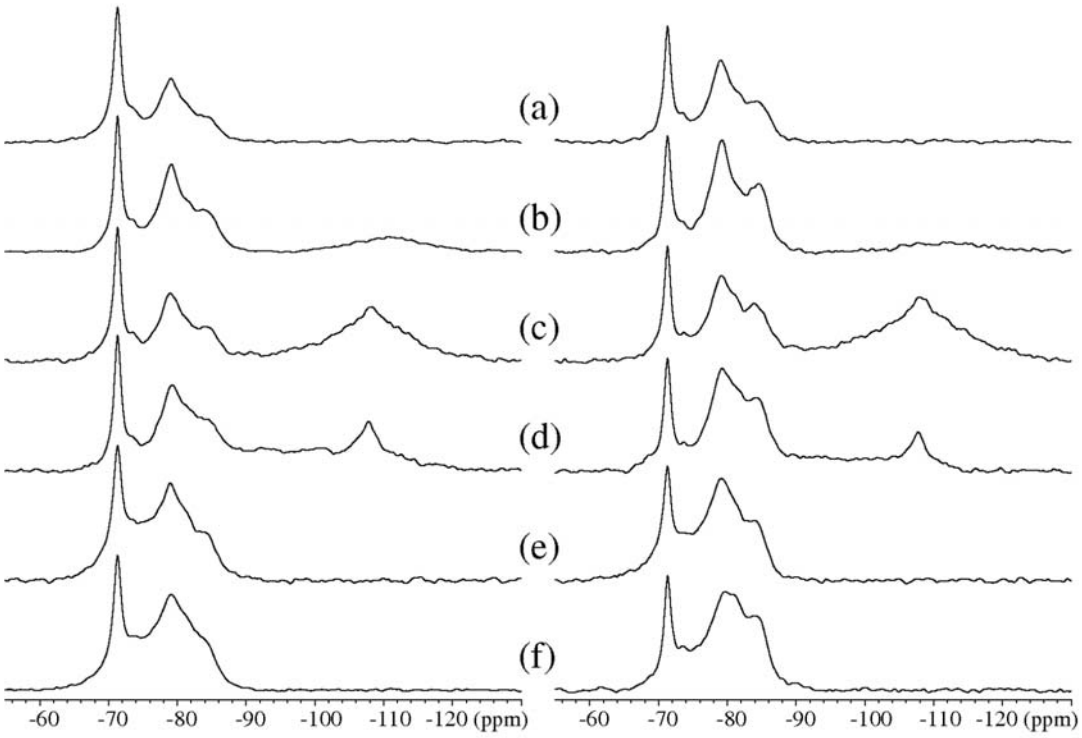

Fig. 2 ^{29}Si MAS NMR spectra (9.4 T, ν_R = 12.0 kHz) of cement (WPC) – SCM pastes after 7 days (left column) and 28 days (right column) of hydration. (a) Pure WPC, (b) 90 wt% WPC + 10 wt.% SF, (c) 70 wt% WPC + 30 wt% FA, (d) 70 wt% WPC + 30 wt% NP, 60 wt% WPC + 40 wt% S1, and (f) 60 wt% WPC + 40 wt% S2.

The hydration of the ordinary (OPC) and white (WPC) Portland cements in blends with the 5 SCMs has been studied by ^{29}Si MAS NMR for hydration times ranging from one

to 180 days. Selected ^{29}Si MAS NMR spectra are illustrated in Fig. 2 for the WP mixtures. The spectra have been recorded using "high-speed" spinning, whic significantly reduces the intensities in the spinning sidebands, providing the basis for a improved determination of the fractions of alite and belite as described in our recer study of anhydrous cements /18/. The reduction in spinning sideband intensities b high-speed MAS is particularly important for SCMs containing a significant amount c iron such as fly ashes, slags, and natural pozzolans. For the SCMs studied in this worl the relatively low iron contents (Table 1) combined with spinning at ν_R = 12.0 kH imply that the spinning sidebands contain less than 10% of the total intensity and thu that the spinning sidebands can be disregarded in the deconvolution procedure (i.e., th spinning sidebands are assumed to have the same intensity distribution as th centerbands). Comparison of the ^{29}Si MAS NMR spectra of the anhydrous SCMs (Fig 1) with those of the cement – SCM mixtures (Fig. 2) reveals that no overlap between th SCM resonances and the peaks from the C-S-H hydration products (–78 ppm to –8 ppm) is only observed for the WPC – SF mixture. In this case the degree of reaction fo SF can be determined simply by spectral integration as illustrated earlier /12/. A sma overlap is observed for the resonances of the FA and NP with the C-S-H peaks whi the resonances from the slags overlap severely with the peaks from alite, belite, and th C-S-H phase.

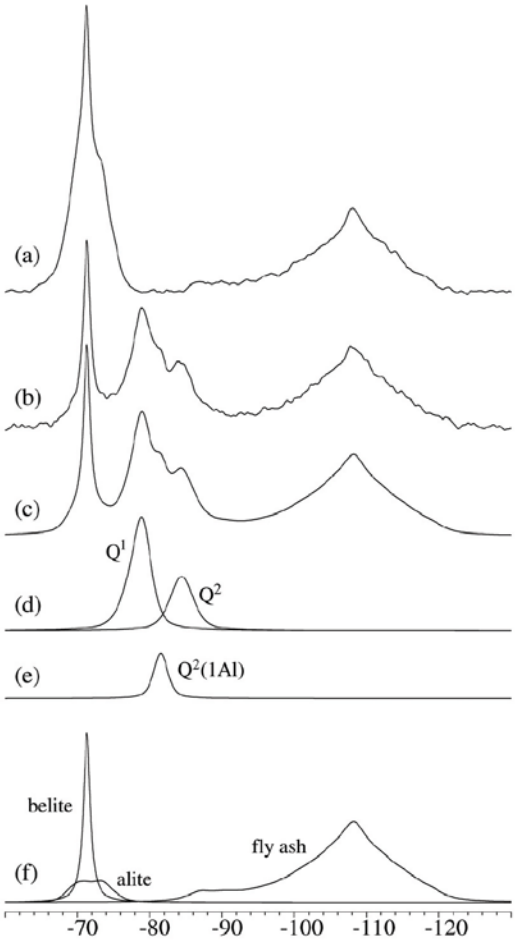

Fig. 3 ^{29}Si MAS NMR spectra (9.4 T, ν_R = 12.0 kHz) of the WPC – FA blend before hydration (a) and after 14 days of hydration (b). (c) Optimized deconvolution of the experimental spectrum in (b) obtained using distinct resonances for the Q^1, Q^2 and Q^2(1Al) sites of the C-S-H phase (d and e) and subspectra for alite, belite and the fly ash (e).

The degree of hydration for alite, belite, and the SCMs is obtained by deconvolution of the experimental ^{29}Si MAS NMR spectra using a slightly modified version of the method outlined earlier for anhydrous /19/ and hydrated Portland cements /25/. This method is illustrated in Fig. 3 by the deconvolution of the ^{29}Si MAS NMR spectrum of a hydrated WPC – FA sample. An examination of the resonances from FA in the series of hydrated samples reveals no indications of any changes in the lineshape for this SCM. Thus, it is assumed that no preferential hydration of parts of the FA material occurs during hydration, implying that the resonances from FA can be considered by a fixed subspectrum (Fig. 3f) in the deconvolutions. In addition to this spectrum, subspectra of alite, belite and the Q^1, Q^2(1Al) and Q^2 resonances of the C-S-H phase are considered in a least-squares refinement of the ^{29}Si MAS NMR spectra. The relative intensities (I(t)) from these deconvolutions allow a straightforward calculation of the degree of hydration for alite, belite, and the SCM, i.e., $H(t) = [1 - I(t)/I(t=0)]$, while the intensities for the C-S-H peaks provide quantitative information about the Al/Si ratio and average chain length of alumino-silicate tetrahedra in the C-S-H phase /26,27/.

Fig. 4 shows the degree of hydration for alite, belite, and the SCMs SF, FA, and NP in mixtures with the WPC and OPC. Generally, the addition of the SCMs results in a higher degree of hydration for alite in the WPC – SCM blends as compared to the degree of hydration for alite in pure WPC. This effect is most pronounced for the blends with NP and SF where the degree of reaction for alite is significantly accelerated during the first week of hydration. For example, after one day of hydration about 40 wt% of alite has reacted in the pure WPC paste, whereas more than 60 wt% of alite has been consumed in the blend with NP. After one week of hydration the differences in the degree of alite hydration levels off, and more than 80% of alite has reacted in all mixtures after 90 days of hydration. A similar effect on the degree of hydration is observed for the OPC mixtures, however, the accelerating effect seems to be less pronounced and the overall degree of hydration is slightly lower after 90 days. The higher reactivity of alite in the WPC mixtures may reflect the smaller average grain size of this cement (d_{50} = 9.4 μm) as compared to the OPC (d_{50} = 20.1 μm), determined by laser granulometric measurements. Furthermore, the increased reactivity in the presence of SF and NP may reflect that these particles act as nucleation agents for the C-S-H phase. A similar explanation has been proposed for the increased reactivity of alite in WPC – kaolinite mixtures where, on the other hand, the clay mineral itself did not react during cement hydration /16/.

The results for belite are in accordance with the fact that this phase does not contribute significantly to the early strength development. For the pure cements, almost no reaction of belite is observed for the first week and only about 50% of belite has reacted after 180 days of hydration. However, the slow reaction of belite is somewhat affected by the SCMs in particular SF and NP for the WPC while belite in the WPC – FA blend reacts very similar to belite in the pure WPC. Similar trends are observed for belite in the OPC with and without NP or FA added. The increased reactivity of belite may be associated with the reaction of the SCMs themselves, since the reaction of these silicate-rich phases may reduce the amount of calcium ions available and thereby result in an

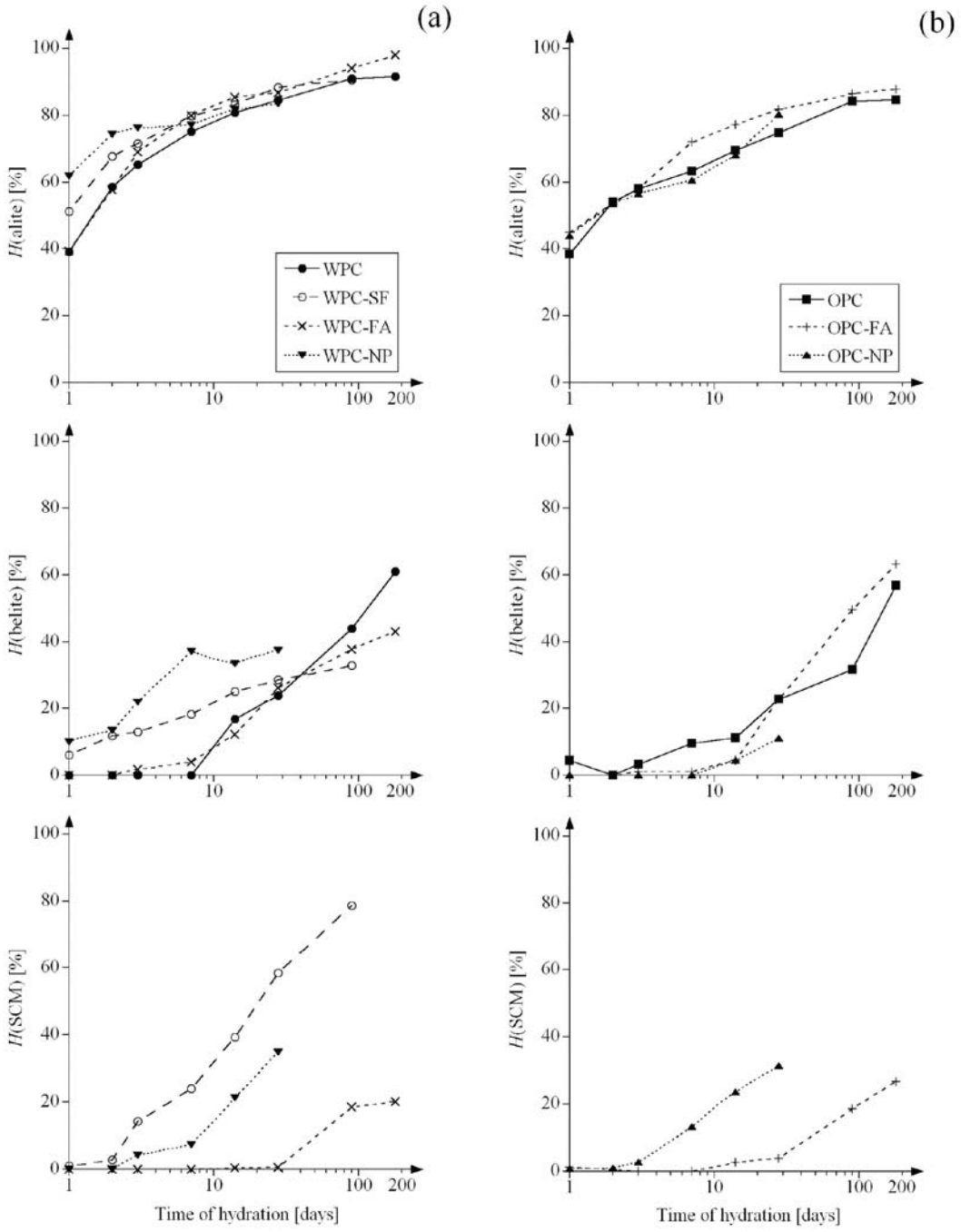

Fig. 4 The degree of hydration (H(t)) for alite, belite and SCMs (SF,FA, and NP) as a function of hydration time (logarithmic scale). Data for the SCMs in WPC blends are displayed in part (a) while the right column (b) includes data for similar mixtures of OPC with FA and NP. The determination of the degrees of hydration is based on deconvolutions of ^{29}Si MAS NMR spectra (9.4 T, ν_R = 12.0 kHz). For the blends including NP and SF, data beyond 28 and 90 days of hydration, respectively, are not included since these hydration experiments are still in progress.

As a principal goal of the present work, Fig. 4 includes the degree of reaction for th SCMs, SF, FA, and NP. The degree of reaction for NP and FA is very similar for th two cements and it is apparent that FA only reacts after prolonged hydration and only t a small degree. This agrees well with reported results for high-volume (45 – 55%) fl ash cement pastes where selective dissolution experiments indicated that more than 80% of the fly ash remained unreacted after 90 days of hydration /28/. The largest degree c reaction is observed for SF where about 80% has reacted after 90 days of hydratio This high degree of reactivity for SF is in accord with earlier studies /12,25/ and als reflect that the WPC – SF blend only includes 10 wt% SF while 30 wt% SCM was use in the FA and NP mixtures. Furthermore, the SF includes the smallest particles (d_{50} 0.25 μm) which is significantly smaller than those of the FA (d_{50} = 7 μm) and NP (d_{50} 9 μm) additives. It is noted that in the evaluation of the degree of reaction for the NI we have at the moment not been able to distinguish the individual mineral componen of this SCM. However, an independent evaluation of the degree of reaction for th alumina-containing phases of the NP (i.e., albite, clinoptilolite, and sanidine) ma potentially be obtained from the corresponding ^{27}Al MAS NMR spectra since th anhydrous material is dominated by a rather narrow resonances at 56 ppm (14.1 T originating from Al(OSi)$_4$ sites in a silicate network. This region of the ^{27}Al MAS NM spectrum does not overlap with other ^{27}Al resonances from the hydrating cement /27 which may form the basis for an independent measure of the reactivity for the NP.

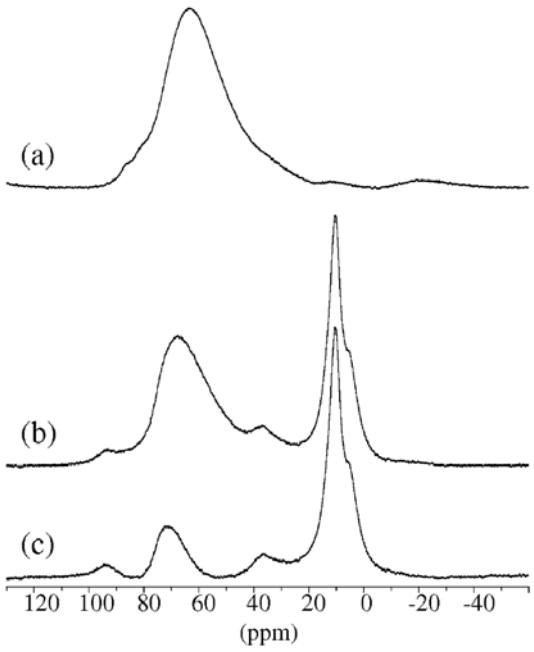

Fig. 5 ^{27}Al MAS NMR spectra (14.1 T, ν_R = 13.0 kHz) of (a) the anhydrous slag (S1) – WPC mixture, (b) the mixture after hydration for 28 days, and (c) a difference plot

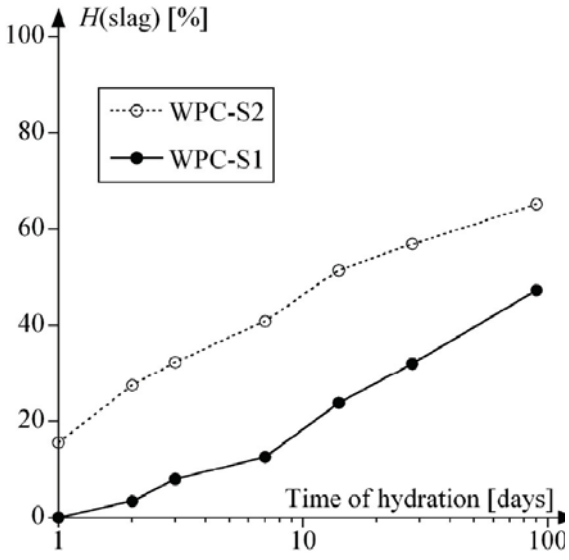

Fig. 6 Degrees of hydration (H(t)) for slags S1 and S2 (40 wt%) in blends with the WPC (60 wt%) determined from ^{27}Al MAS NMR spectra (14.1 T, ν_R = 13.0 kHz).

The degree of hydration for the slags cannot be determined from the ^{29}Si MAS NMR spectra due to the severe overlap of resonances from the slags and the alite, belite and C-S-H phase of the hydrating cement (c.f., Fig. 1). However, a valuable estimate of the degree of slag reaction can be achieved from the ^{27}Al MAS NMR spectra, utilizing that the cement – slag mixtures (60:40 wt%) are dominated by aluminum from the slag (c.f., Table 1). Furthermore, it is assumed that no preferential hydration occurs for specific aluminate sites in the slag, which is justified by SEM micrographs of hydrated cement – slag pastes that show a clear boundary between the reacting slag and the formed hydration products. The approach employs ^{27}Al MAS NMR spectra of weighed samples of the anhydrous cement – slag mixture and the corresponding hydrated sample. The spectrum of the anhydrous mixture is subtracted from the hydrated cement (before baseline correction) in an interactive manner where the difference between the two spectra is displayed. Thereby, the intensity of the spectrum for the anhydrous material can be adjusted to precisely remove the contribution from the slag in the spectrum of the partially hydrated material. This procedure is illustrated in Fig. 5 by the ^{27}Al MAS NMR spectra of the WPC – S1 mixture before and after 28 days of hydration. The relative intensity of the anhydrous mixture subtracted from the hydrated material can be related to the quantity of unreacted slag in the sample by consideration of the amount of water bound in the sample during hydration. This quantity is determined from loss of ignition measurements for the individual hydrated samples. The difference spectrum in Fig. 5 includes resonances from tetrahedral (~72 ppm) and penta-coordinated (~38 ppm) aluminum incorporated in the C-S-H phase, in addition to overlapping peaks from AFm/hydrotalcite (~10 ppm) and the so-called third aluminate hydrate phase (~5 ppm) /29/. It is noted that the intensity for tetrahedrally coordinated Al in the C-S-H is observed at higher frequency as compared to the dominating peak of the slags (~64 ppm) which ensures a reliable subtraction of the two experimental spectra. Furthermore, the difference spectrum (Fig. 5c) indicates that the hydrated WPC – S1 mixture includes a C-S-H phase with a higher degree of Al incorporation as compared to the other cement – SCM mixtures, in agreement with the high Al content of the slag.

The ^{27}Al MAS NMR method for estimating the degree of slag reaction has so far been employed for the WPC – S1 and WPC – S2 mixtures (Fig. 6). These results show that S2 exhibits a higher degree of reaction as compared to S1, in agreement with DTA studies of the same mixtures. The degree of reaction for S2 is similar to the results from an earlier study of a cement-slag blend (70:30 wt%) using a selective dissolution method where it was estimated that about 40% of the slag had reacted after one month of hydration /30/. More recently, a Portland cement – slag blend (75:25 wt%) has been studied using a combination of ^{29}Si MAS NMR and selective dissolution techniques for removal of all silicate species from both the anhydrous cement and the C-S-H hydration products /15/. Subsequently, the ^{29}Si MAS NMR spectrum of the residue was used as a subspectrum in the analysis of the hydrated cement – slag which provided the basis for a determination of the degree of slag reaction. By this approach it was estimated that ~30% of the slag had reacted after one month of hydration /15/. However, this approach is very sensitive to the accuracy of the selective dissolution method, as also evidenced by TEM and ^{29}Si MAS NMR of the dissolution residues in the abovementioned study which indicated that the residues included a small amount of aluminosilicate gel. The presence of this phase would result in an underestimation of the degree of slag reaction.

Acknowledgements

The present research is a part of Core project 4 in the NANOCEM network which focuses on methods for measuring the degree of reaction in cements including SCMs. We thank NANOCEM for financial support and V. Kocaba and K. L. Scrivener, Ecole Polytechnique Fédérale de Lausanne, Switzerland, for providing the bulk chemical analyses of the cements and SCMs. The use of the facilities at the Instrument Centre for Solid-State NMR spectroscopy, Aarhus University, is also acknowledged.

References

/1/ Damtoft, J.S.; Lukasik, J.; Herfort, D.; Sorrentino, D.; Gartner, E.M.: Sustainable development and climate change initiatives. – In: Cement and Concrete Research. – 38 (2008) 2. – p. 115-127.

/2/ Humphreys, K.; Mahasenan, M.: Toward a sustainable cement industry. Sub-study 8: climate change, An Independent Study Commissioned to Battelle by World Business Council for Sustainable Development, March 2002.

/3/ Mokrzycki, E.; Uliasz-Bochenczyk, A.: Alternative fuels for the cement industry. – In: Applied Energy. – 74 (2003). – p. 95-100.

/4/ Kääntee, U.; Zevenhoven, R.; Blackman, R.; Hupa, M.: Cement manufacturing using alternative fuels and the advantages of process modeling. – In: Fuel Processing Technology. – 85 (2004). – p. 293-301.

/5/ Taylor, H.F.W.: Cement Chemistry. 2nd ed., Thomas Telford, London, 1997.

/6/ Hewlett, P.: Lea's chemistry of cement and concrete. 4th ed., Elsevier Butterworth-Heinemann, Oxford, 2008.

/7/ Worrell, E.; Price, L.; Martin, N.; Hendriks, C.; Meida, L.O.: Carbon Dioxide Emission from the Global Cement Industry. – In: Annual Review of Energy and Environment. – 26 (2001). – p. 303-329.

/8/ Lippmaa, E.; Mägi, M.; Tarmak, M.; Wieker, M.; Grimmer, A.R.: A high resolution ^{29}Si NMR study of the hydration of tricalciumsilicate. – In: Cement and Concrete Research. – 12 (1982) 5. – p. 597-602.

/9/ Mägi, M.; Lippmaa, E.; Samoson, A.; Engelhardt, G.; Grimmer, A.-R.: Solid-state high-resolution silicon-29 chemical shifts in silicates. – In: Journal of Physical Chemistry. – 88 (1984). – p. 1518-1522.

/10/ Clayden, N.J.; Dobson, C.M.; Hayes, C.J.; Rodger, S.A.: Hydration of tricalcium silicate followed by solid-state ^{29}Si NMR spectroscopy. – In: Journal of the Chemical Society Chemical Communications. – (1984). – p. 1396-1397.

/11/ Clayden, N.J.; Dobson, C.M.; Growes, G.W.; Hayes, C.J.; Rodger, S.A.: Solid-state NMR studies of cement hydration. – In: Proceedings of the British Ceramic Society. – 35 (1984). – p. 55-65.

/12/ Hjorth, J.; Skibsted. J.; Jakobsen, H.J.: ^{29}Si MAS NMR studies of Portland cement components and effects of microsilica on the hydration reaction. – In: Cement and Concrete Research. – 18 (1988) 5. – p. 789-798.

/13/ Dobson, C.M.; Goberdhan, D.G.C.; Ramsay, J.D.F.; Rodger, S.A.: ^{29}Si MAS NMR study of the hydration of tricalcium in the presence of finely divided silica. – In: Journal of Materials Science. – 23 (1988). – p. 4108-4114.

/14/ Pietersen, H.S.; Kentgens, A.P.M.; Nachtegaal, G.H.; Veeman, W.S.; Bijen, J.M.: The reaction mechanism of blended cements: A ^{29}Si NMR study. – In: 4th Canmet/ACI Conference on Fly Ash, Silica Fume, Slag, and Natural Pozzolans in Concrete. – 1 (1992). – p. 797-812 .

/15/ Dyson, H.M..; Richardson, I.G.; Brough, A.R.: A Combined ^{29}Si MAS NMR and Dissolution Technique for the Quantitative Evaluation of Hydrated Blast Furnace Slag Cement Blends. – In: Journal of the American Ceramic Society. – 90 (2007) 2. – p. 598-602.

/16/ Krøyer, H.; Lindgreen, H.; Jakobsen, H.J.; Skibsted, J.: Hydration of Portland cement in the presence of clay minerals studied by ^{29}Si and ^{27}Al MAS NMR spectroscopy. – In: Advances in

/17/ Al-Zahrani, M.M.; Al-Tayyib, A.-H.J.; Al-Dulaijan, S.U.; Osei-Twum, E.: ^{29}Si MAS-NMR study of hydrated cement paste and mortar with varying content of fly ash. – In: Advances in Cement Research. – 18 (2006) 1. – p. 27-34.

/18/ Poulsen, S.L.; Kocaba, V.; Le Saoût, G.; Jakobsen, H.J.; Scrivener, K.L.; Skibsted, J.: Improved quantification of alite and belite in anhydrous Portland cements by ^{29}Si MAS NMR: Effects of paramagnetic ions. – In: Solid-state Nuclear Magnetic Resonance. – (2009) 6. – doi:10.1016/j.ssnmr.2009.05.001

/19/ Skibsted, J.; Jakobsen, H.J.; Hall, C.: Quantification of Calcium Silicate Phases in Portland Cements by ^{29}Si MAS NMR Spectroscopy. – In: Journal of the Chemical Society. Faraday Transactions. – 91 (1995). – p. 4423-4430.

/20/ Taylor, H.F.W.: Modification of the Bogue calculation. – In: Advances in Cement Research. – 2 (1989). – p. 73-77.

/21/ Klinowski, J.: Nuclear magnetic resonance studies of zeolites. – In: Progress in NMR Spectrsoscopy. – 16 (1989). – p. 237-309.

/22/ Kirkpatrick, J.R.; Kinsey, R.A.; Smith, K.A.; Henderson, D.M.; Oldfield, E.: High resolution solid-state sodium-23, aluminium-27, and silican-29 nuclear magnetic resonance spectroscopic reconnaissance of alkali and plagioclase feldspars. – In: American Mineralogist. – 70 (1985). – p. 106-123.

/23/ Blanco Varela, M.T.; Martínez Ramírez, S.; Ereña, I.; Gener, M.; Carmona, P.: Characterization and pozzolanicity of zeolitic rocks from two Cuban deposits. – In: Applied Clay Science. – 33 (2006). – p. 149-159.

/24/ Richardson, I.G.; Brough, A.R.; Groves, G.W.; Dobson, C.M.: The characterization of hardened alkali-activated blast-furnace slag pastes and the nature of the calcium silicate hydrate (C-S-H) phase. – In: Cement and Concrete Research. – 24 (1994) 5. – p. 813-829.

/25/ Skibsted, J.; Jensen, O.M.; Jakobsen, H.J.: Hydration kinetics for the alite, belite, and calcium aluminate phases in Portland cements from ^{27}Al and ^{29}Si MAS NMR spectroscopy. – In: Proc. 10th Int. Congr. Chem. Cem., Gothenburg, Sweden. – 2 (1997), paper (2ii56).

/26/ Richardson, I.G.; Brough, A.R.; Brydson, R.; Groves, G.W.; Dobson, C.M.: Location of aluminium in substituted calcium silicate hydrate (C-S-H) gels as determined by ^{29}Si and ^{27}Al NMR and EELS. – In: Journal of the American Ceramic Society. – 76 (1993). – p. 2285-2288.

/27/ Andersen, M.D.; Jakobsen, H.J.; Skibsted, J.: Incorporation of aluminium in the calcium silicate hydrate (C-S-H) of hydrated Portland cements: a high-field ^{27}Al and ^{29}Si MAS NMR investigation. – In: Inorganic Chemistry. – 43 (2003). – p. 2280-2287.

/28/ Lam, L.; Wong, Y.L.; Poon, C.S.: Degree of hydration and gel/space ratio of high volume fly ash/cement systems. – In: Cement and Concrete Research. – 30 (2000) 5. – p. 747-456.

/29/ Andersen, M.D.; Jakobsen; H.J.; Skibsted, J.: A new aluminium-hydrate species in hydrated Portland cements characterized by ^{27}Al and ^{29}Si MAS NMR spectroscopy. – In: Cement and Concrete Research. – 36 (2006) 1. – p. 3-17.

/30/ Luke, L.; Glasser, F.P.: Internal Chemical Evolution of the Constitution of Blended Cements. – In: Cement and Concrete Research. – 18 (1988) 4. – p. 495-502.

Authors

Søren L. Poulsen
PhD student, MSc
Instrument Centre for Solid-State NMR Spectroscopy
Department of Chemistry
Aarhus University
8000 Aarhus C, Denmark

Hans J. Jakobsen
Professor
Instrument Centre for Solid-State NMR Spectroscopy
Department of Chemistry
Aarhus University
8000 Aarhus C, Denmark

Jørgen Skibsted
Associate Professor, PhD
Instrument Centre for Solid-State NMR Spectroscopy
Department of Chemistry
Aarhus University
8000 Aarhus C, Denmark